REPUBLIQUE DU CAMEROUN
Paix – Travail – Patrie
****
UNIVERSITE DE YAOUNDE I
FACULTE DES SCIENCES
DEPARTEMENT DE PHYSIQUE
****
CENTRE DE RECHERCHE ET DE FORMATION DOCTORALE EN SCIENCES, TECHNOLOGIES ET GEOSCIENCES
LABORATOIRE DE MECANIQUE, MATERIAUX ET STRUCTURES

REPUBLIC OF CAMEROUN
Peace – Work – Fatherland
****
UNIVERSITY OF YAOUNDE I
FACULTY OF SCIENCE
DEPARTMENT OF PHYSICS
****
POSTGRADUATE SCHOOL OF SCIENCES, TECHNOLOGY AND GEOSCIENCES
LABORATORY OF MECHANICS, MATERIALS AND STRUCTURES

Dynamics and vibration isolation of two multi-span continuous beam bridges coupled by their close environment

Thesis submitted and defended in partial fulfillment of the requirements for the degree of Doctorate/PhD in Physics

Par : **SONFACK BOUNA Hervé**
Master of Science in Physics

Sous la direction de
NANA NBENDJO Blaise Roméo
Professor
University of Yaoundé I
WOAFO Paul
Professor
University of Yaoundé I

Année Académique : 2020

UNIVERSITÉ DE YAOUNDÉ I
UNIVERSITY OF YAOUNDE I

FACULTÉ DES SCIENCES
FACULTY OF SCIENCE

DÉPARTEMENT DE PHYSIQUE
DEPARTMENT OF PHYSICS

ATTESTATION DE CORRECTION DE LA THÈSE DE DOCTORAT/Ph.D

Nous, Professeur **KENFACK JIOTSA Aurélien** et Professeur **NDJAKA Jean Marie Bienvenu**, respectivement Examinateur et Président du jury de la Thèse de Doctorat/Ph.D de Monsieur **SONFACK BOUNA Hervé**, Matricule **08W1103**, préparée sous la supervision conjointe du Professeur **WOAFO Paul** et du Professeur **NANA NBENDJO Blaise Roméo**, intitulée : « **DYNAMICS AND VIBRATION ISOLATION OF TWO MULTI-SPAN CONTINUOUS BEAM BRIDGES COUPLED BY THEIR CLOSE ENVIRONMENT** », soutenue le **Mercredi 31 Mars 2021**, en vue de l'obtention du grade de Docteur/Ph.D en Physique, Spécialité **Mécanique, Matériaux et Structures,** Option **Mécanique Fondamentale et Systèmes Complexes,** attestons que toutes les corrections demandées par le jury de soutenance ont été effectuées.

En foi de quoi, la présente attestation lui est délivrée pour servir et valoir ce que de droit.

Fait à Yaoundé le ..15 APR 2021.....

Examinateur	Le Chef de Département de Physique	Le Président du jury
Pr. KENFACK JIOTSA Aurélien	Pr. NDJAKA Jean Marie Bienvenu	Pr. NDJAKA Jean Marie Bienvenu

Dedications

This work is gratefully dedicated to:

♠ My late father **BOUNA Etienne** who would have liked to physically witness the outcome of this thesis that he was impatiently waiting for. Wherever you are right now, know that I am proud of you and the man you made me.

♠ My mother **NGUIMFACK Christine**: your sincere care was beyond any measure,

♠ My brothers and sisters **Anicet**, **Eric**, **Gertrude**, **Serge**, **Sophie**, **Stève**, **Léonel** and **Romaric**: your trust is unbelievable,

♠ My wife **Pascaline Laure**: your support is incredible,

♠ And my son **Akim** and daughter **Anaïs**: your love is fantastic.

Acknowledgements

Successful completion of this thesis will never be one man's task. It requires hard work in right direction. There are many who have helped to make my experience as a student a rewarding one. Therefore I would like to thank and pay a tribute to :

- **Pr. NANA NBENDJO Blaise Roméo** the Director of this thesis who guided me into the area of structural vibration with great patience and encouraged me to explore the edge of this area. I acknowledge his invaluable comments and constructive suggestions during the performance of this work. I really feel fortunate to have had such a wonderful person as Director who has contributed largely to my academic life.

- **Pr. WOAFO Paul** for his constructive supervision, his experienced guidance, unfailing advices, and directing this research with sincere interest and patience.

- **Pr. NDJAKA Jean Marie Bienvenu** the Head of the Department of Physics, Faculty of Science, University of Yaoundé I, for his advices during the Master's courses.

- **Pr. KOFANE Timoléon Crépin** for the wide advices during courses in nonlinear physics and whose research has been very beneficial for me in my work.

- **Pr. TCHAWOUA Clément** for his courses in vibration and elasticity and the large number of advices during the Bachelor and Master's courses.

- All the teaching staff and personnel of the Department of Physics, Faculty of Science, University of Yaoundé I, for their teachings and help since my first year in this institution.

- All the jury members for all their remarks to render this work : the President **Pr. NDJAKA Jean Marie Bienvenu** of University of Yaoundé I; the members namely **Pr. NJANDJOCK NOUCK Philippe**, **Pr. KENFACK JIOTSA Aurélien**,

Pr. SIEWE SIEWE Martin of University of Yaoundé I and **Pr. TALLA Pierre Kisito** of University of Dschang.

- **Dr. NGUEUTEU MBOUNA Serge Gervais**, receive my gratitude for your helpful and precious advices.

- **Dr. NANA Bonaventure**, **Dr. TALLA MBE**, **Dr. TAKOUGANG SIFEU**, **Dr. ABOBDA Lejuste**, **Dr. TCHEUTCHOUA Omer**, **Dr. SIMO Hervé** and **Dr. NANHA Armand**, receive my gratitude for your inspiring life experiences.

- My pairs and labmates **Dr. CHAMGOUE André**, **Dr. TALLA Francis**, **Dr. NOTUE Arnaud**, **Dr. TCHAWOU Eder Batista**, **Dr. METSEBO Jules**, **Dr. NDEMANOU Borus**, **Dr. TSAPLA Rolande**, **Dr. TOKOUE Dianoré**, **Dr. OUMBE Gabin**, **Dr. ANAGUE leonel**, **MBA Stève**, **FANKEM Raïssa** and all the others, thank for your trust.

- My Family, especially my late father **BOUNA Etienne**, my mother **NGUIMFACK Christine**, my sisters and brothers **TEMGOUA Anicet**, **ASSAATSA Eric**, **TONG-NANG Gertrude**, **TSOPFACK Sophie**, **TSOBENG Stève**, **SAATSA Léonel** and **TEUGO Romaric**, for their full love.

- My Wife **NANTCHOUANG Pascaline** who has always made me feel her unconditional love wherever I am, whatever I do; and who has always believed in my dreams no matter the circumstances.

- All my friends for their constant encouragement.

- All my parents, uncles, aunts, nephews, nieces, brothers, sisters, those whose names have not been mentioned here, those reading this work for their active support.

Contents

Résumé

L'étude expérimentale des caractéristiques vibratoires des ponts est un élément important dans les efforts pour comprendre et contrôler de nombreux phénomènes vibratoires rencontrés lors de la conception de ces derniers. À cet effet, une étude expérimentale a été réalisée dans cette thèse sur un modèle réalisé en laboratoire simulant la dynamique de deux ponts de poutres indirectement couplés par leur environnement proche constitué du sol sous les piles des ponts. L'objectif de cette recherche étant le développement d'un modèle théorique valide de ponts indirectement couplés et la mise en évidence des influences mutuelles de la dynamique de ces ponts couplés, l'un sur l'autre. Une modélisation de la dynamique du système est proposée puis validée par les résultats expérimentaux. Les influences mutuelles des vibrations des ponts de poutres soumis à diverses excitations extérieures sont explorées expérimentalement puis théoriquement. Par suite, les performances des mécanismes d'isolement non linéaires avec une caractéristique de rigidité quasi-nulle sont étudiées pour l'isolation vibratoire de ces deux ponts de poutres couplés afin de réduire leurs vibrations.

Tout au long de cette thèse, tous les ponts ont été modélisés avec des poutres d'Euler-Bernoulli continues à travées multiples sur appuis simples. L'environnement proche de couplage des ponts a été modélisé comme une fondation de type Winkler viscoélastique linéaire. L'isolation des vibrations des ponts de poutres couplées a été réalisée grâce aux isolateurs de vibrations non linéaires à rigidité quasi-nulle qui se sont avérés plus efficaces que leurs homologues linéaires. La principale contribution scientifique de cette thèse est le développement d'un modèle théorique valide de ponts couplés par leur environnement proche et la proposition d'un modèle d'isolement efficace basé sur un mécanisme à rigidité quasi-nulle.

Mots-clés: Vibration, Ponts couplés, Isolateur de vibrations à raideur quasi-nulle, Poutres d'Euler-Bernoulli continue à travées multiples, Fondation de type Winkler.

Abstract

The experimental study of the vibration characteristics of bridges is an important element in the efforts to understand and control many vibration phenomena encountered in design. For this purpose, an experimental study was carried out in this thesis on a laboratory-mounted model simulating the dynamics of two beam bridges indirectly coupled by their close environment consisting of the ground under the piers of the bridges. The objective of this research being the development of a valid theoretical model of indirectly coupled bridges and the highlighting of the mutual influences of the dynamics of these coupled bridges, one on the other. A modeling of the system dynamics is proposed and then validated by experimental results. The mutual influences of the vibrations of beam bridges subjected to various external excitations are explored experimentally and then theoretically. Consequently, the performance of nonlinear isolation mechanisms with a quasi-zero stiffness characteristic are investigated for vibration isolation of these two coupled beam bridges in order to reduce their vibrations.

Throughout this thesis, all the bridges have been modelled with elastically simply supported multi-span continuous Euler-Bernoulli beams. The coupling close environment of the bridges has been modelled as a linear viscoelastic Winkler foundation. The vibration isolation of the coupled beam bridges has been achieved by nonlinear quasi-zero stiffness vibration isolators which have been proven to be more effective than their linear counterparts. The main scientific contribution of this thesis is the development of a valid theoretical model of bridges coupled by their close environment and the proposal of an efficient isolation model based on a quasi-zero stiffness mechanism.

Keywords: Vibration, Coupled bridges, Quasi-zero stiffness vibration isolator, Multi-span continuous Euler-Bernoulli beam, Winkler foundation.

List of Abbreviations

DAF: Dynamic Amplitude Factor

DOF: Degree Of Freedom

HB: Harmonic Balance

MDOF: Multi-Degree Of Freedom

MS: Modal Superposition

NSD: Negative Stiffness Device

ODE(s): Ordinary Differential Equation(s)

PDE(s): Partial Differential Equation(s)

QZS: Quasi-Zero Stiffness

RK4: Fourth-Order Runge-Kutta

SDOF: Single-Degree Of Freedom

TMD: Tuned Mass Damper

List of Figures

List of Tables

General Introduction

Very often in practical engineering, the experimental tests are performed on a complex structure with the objective of obtaining an empirical description of its dynamical behavior, or providing verification for an analytical or a numerical structural model [1–5]. To quantify the dynamical response of a given structure, the determination of its intrinsic dynamic properties such as natural frequencies, vibration modes and damping, etc., is of a particular importance. Over the years, dynamic tests of highway bridges have been performed by many researchers and engineers. However, most of the tests are in-field dynamic tests [6]. Lab-based dynamic tests of full assemblage bridge models under a controlled environment are rather scanty. Looking at the way the tests were performed on the field or in laboratory, these tests were focused essentially on single bridges [7]. Despite the existence of many coupled bridges on beds of multiple rivers over the world, dynamic tests on bridges indirectly coupled by their close environment are rarely performed. As an example, we can cite in Cameroon, the two bridges built on the Wouri river about ten meters apart [8] (see Fig. 1) which have inspired the work of this thesis. It is therefore of interest to investigate these coupled bridges from a dynamic test setting. In addition, the dynamical response and the vibration isolation of single span bridges subjected to different kinds of dynamic loads have drawn much research attention, but relatively small amount of research work has been devoted to dynamics and vibration isolation of multi-span continuous bridges and coupled bridges.

In most of the cases, vibrations are undesirable because of their detrimental effects on bridges and on the human body. Excessive levels of noise from factories and vehicles engines as well as vibrations transmitted through bridges can cause discomfort in humans, and high amplitude vibrations can cause fatigue and damage in machinery and in bridges. Structure damages often occur at a low excitation frequency in practical engineering [9, 10]. Due to their structural easiness and as the fundamental vibrational period of most bridges ranges from 0.2 to 1.2 second [11], bridges are particularly vulnerable to damages and sometimes

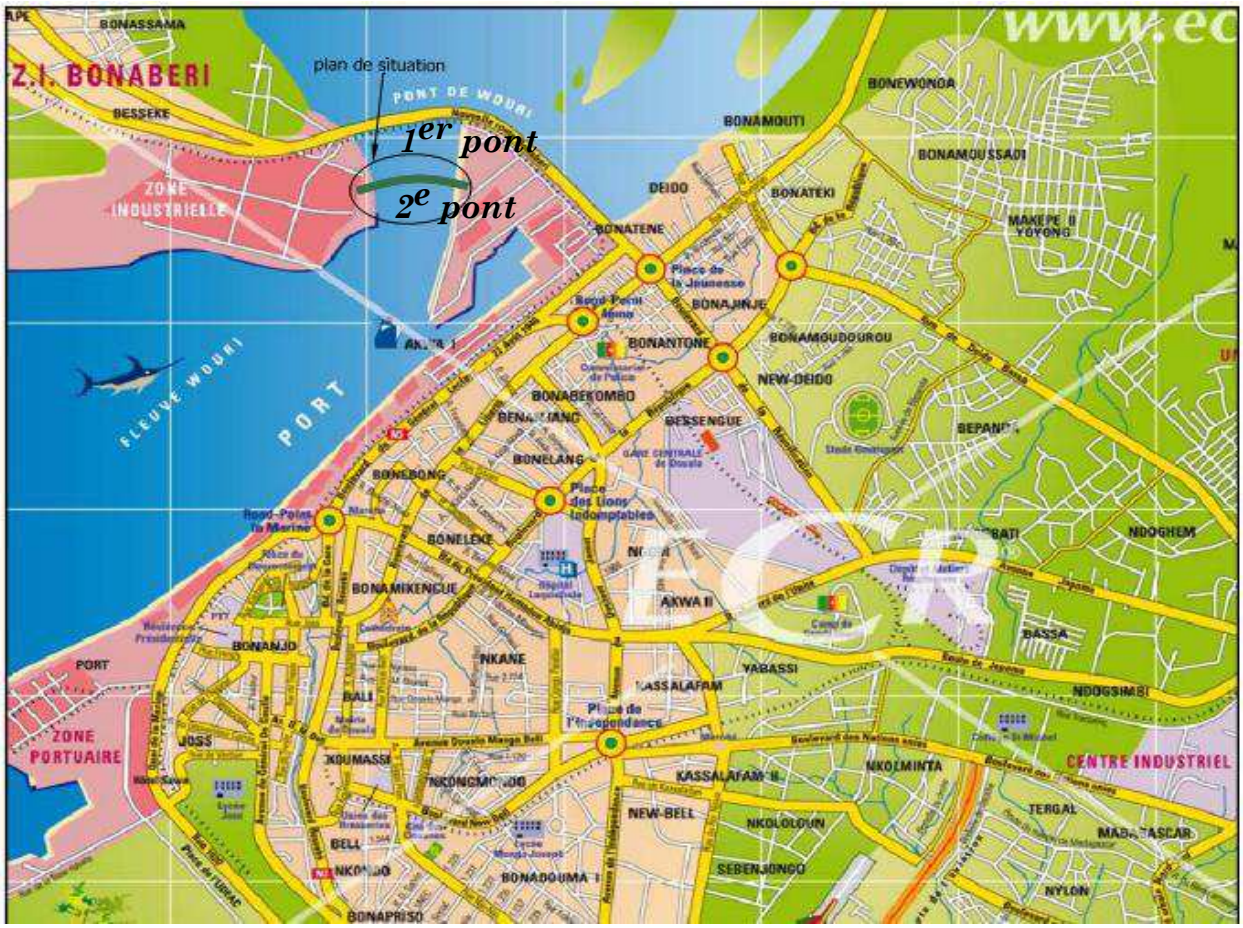

Figure 1: Location map of the second bridge over the Wouri river in Cameroon [8]

collapse when subjected to earthquakes and other external excitation such as moving and wind loads. Since the collapse of Stephenson's bridge at Chester in England in 1847 [12], more than a century of research has been devoted to vibration control of bridges under different kinds of loads such as moving loads and earthquakes. Nowadays there is still a pressing demand for the protection of structural installations, nuclear reactors, mechanical components, and sensitive instruments from earthquake ground motion, shocks, and impact loads. These detrimental effects have motivated diverse approaches to vibration control which can be divided mainly into three areas. The first is the reduction of the vibrational excitation at source, which is often unrealizable because of economic and practical reasons. The second is the modification of the physical properties of the receiver, which is the part of the system

which receives the transmitted vibration. The third is called vibration isolation. In this approach, the vibration is reduced by employing vibration isolators between the vibration source and the receiver [13, 14].

In recent years, base vibration isolation has become an increasingly applied structural design technique to protect bridges from severe loads. The main goal of base vibration isolation is to produce a substantial decoupling of the superstructure from the substructure resting on the vibrating ground, therefore minimizing the internal state of stress during an earthquake by increasing the period of the structure and acting as an energy dissipation device [15, 16]. It can be achieved by means of active, semi active and passive vibration isolators placed between the source and the receiver. Active isolators usually perform well, reducing vibration to desirable levels over a wide range of excitation frequencies. However, computers and actuators are employed to modify the system response and they require a continuous supply of energy and have high costs. Semi active isolators modify the properties of the system. They use small quantities of energy and have good performance at high excitation frequencies, but usually they have a complicated engineering design. A passive vibration isolator is composed of a spring and a damper located in parallel between the source and the receiver. Passive vibration isolation systems can be linear or nonlinear depending on the form of the forces in the system. Vibration isolation is still an important problem, especially the low-frequency vibration isolation. The most important characteristics of a vibration isolator are its natural frequency and load bearing capacity. As it is well known, a linear passive vibration isolator often faces a difficult choice situation that arises between these two characteristics. For traditional passive linear vibration isolators, a smaller stiffness is needed to achieve a smaller natural frequency so that it can reduce low frequency vibrations [17]. In this case, a larger static deflection is unavoidable in practical applications. To overcome the limitation between the isolation frequency range and the load bearing capac-

ity of linear vibration isolators, many nonlinear vibration isolators using quasi-zero stiffness (QZS) mechanisms have been proposed to obtain a high static stiffness resulting in a small static deflection and a low dynamic stiffness resulting in a small natural frequency [18–21]. QZS vibration isolators have been proven to offer a unique passive approach for achieving low vibration environments [22]. In recent years, several types of vibration isolators using QZS mechanisms have been developed and applied to improve working environment for users in many engineering fields, such as vibration resonance test of aircrafts, vibration isolation of precision instruments, sensor, energy harvest, suspensions and seats of vehicles and protection of motors. However, there are not many research on vibration isolation of beam bridges. The main goal of this thesis is to gain knowledge on the subjects of Structural Control of beam-like structures by comparing theoretically, the performance of a nonlinear QZS isolator with that of a linear isolator on the reduction of vibrations of two coupled beam bridges. But the dynamics of these coupled beam bridges is first investigated experimentally on a model built in lab.

The aim of this thesis is to study the dynamic interaction between two indirectly coupled seven-span continuous beam bridges in lab by theories and experiments in order to gain further understanding of the dynamic interaction of two beam bridges coupled by their close environment and to propose an efficient isolation technique based on a QZS mechanism to reduce their vibrations. To this end, there are several interesting aspects that are worth investigated:

(1) To describe the mode shapes of a continuous beam bridge approximately by one equation for the whole length of the beam bridge and to derive the analytical solution of the equation of motion of the two seven-span continuous beam bridges subjected to sinusoidal and impulsive loads in two coupled equations.

(2) To assess the vibration behavior of two coupled beam bridges model excited by sinusoidal

and impulsive loads theoretically and experimentally.

(3) To implement the Mode Superposition (MS) method and an iterative algorithm for analysing the problem of the dynamics of beam bridges.

(4) To build a complete enough descriptive theoretical model for experimental indirect coupled beam bridges dynamic system and determine their dynamical responses efficiently.

(5) To study the influences of distance between the two coupled bridges, the nature of the close environment on the dynamic responses of the coupled bridges theoretically and experimentally in the lab.

(6) To use QZS vibration isolators to control the vibrations of the coupled beam bridges under pier base vibrating excitation on one hand and subjected to a moving mass on the other hand.

(7) To study the performance of a nonlinear QZS vibration isolator with that of a linear isolator on the reduction of vibrations of the two coupled beam bridges theoretically.

(8) To study the effects of each control parameter on the absolute motion transmissibility of steady-state responses of the two coupled beam bridges for a better isolation performance.

This thesis has made several contributions by:

(1) Developing a complete enough descriptive theoretical model of indirect coupled bridges validated experimentally. We have analyzed analytically and numerically the effectiveness of this modelling.

(2) Making a brief review of existing structural control systems and utilizing the QZS vibration isolation in vibration control of beam bridges.

(3) Establishing the benefit of using such QZS mechanisms as vibration isolators in vibration control of beam bridges under pier base vibrating excitation and subjected to a moving mass.

Chapter 1 presents a brief literature review of the most important aspects related to the dynamical behavior and vibration isolation of bridges under several kinds of external

excitations. This includes an overview of generalities on bridges, coupled bridges and their dynamical behavior, soil-bridge interaction, and a state-of-the-art review of structural vibration control systems. Chapter 2 focuses on the different methods used along the thesis to solve the problems presented in Chapter 1. It presents the mathematical, numerical and experimental methods used in this thesis. In Chapter 3, the results of the mathematical analysis, numerical and experimental simulations are presented. Discussion and extension to applications are made. The thesis ends with a general conclusion where the main results obtained are reminded in summary and perspectives for future investigations are suggested.

Chapter I

State of the art

1.1 Introduction

Bridge vibrations due to their close environment are a source of nuisance that affects the longevity of bridges and the comfort of their users. Vibration isolators are therefore widely used to subdue vibrations in order to lengthen the service life of equipments and structures, also to provide a more comfortable and safe condition for human beings. Due to their structural easiness, bridges are particularly vulnerable to damages and sometimes collapse when subjected to earthquakes and other external excitation such as moving and wind loads. In recent years, vibration isolation has become an increasingly applied structural design technique to protect bridges from severe loads. Its main goal is to produce a substantial decoupling of the superstructure from the substructure resting on the ground. Despite the decades of previous studies, vibration isolation remains an important problem, especially the low-frequency vibration isolation.

This chapter presents a brief literature review of the most important aspects related to the dynamical behavior and vibration isolation of bridges under several kinds of external excitations. This includes the formulation of the equation of motion, the soil-bridge interaction, and a state-of-the-art review of structural vibration control systems.

1.2 Generalities on bridges and coupled bridges

A bridge is a structure that crosses over a river, bay, or other obstruction, permitting the smooth and safe passage of vehicles, trains, and pedestrians. It acts as an important link in surface transportation network. An elevation view of a typical bridge is shown in Fig. 1.1. A bridge structure is divided into an upper part (the superstructure), which consists of the slab, the floor system, and the main truss or girders, and a lower part (the substructure), which are piers, footings, piles and abutments. The superstructure provides horizontal spans

such as deck and girders and carries traffic loads directly. The substructure supports the horizontal spans, elevating above the ground surface.

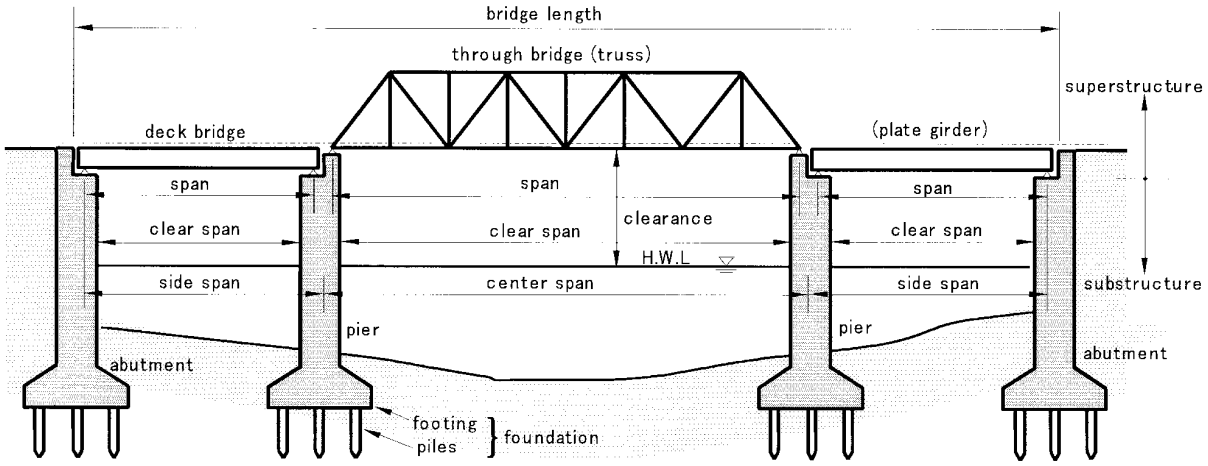

Figure 1.1: Elevation view of a typical bridge [23]

1.2.1 Classification

a) Classification by Materials

• **Steel bridges**: A steel bridge may use a wide variety of structural steel components and systems: girders, frames, trusses, arches, and suspension cables.

• **Concrete bridges**: There are two primary types of concrete bridges: reinforced and prestressed.

• **Timber bridges**: Wooden bridges are used when the span is relatively short.

• **Metal alloy bridges**: Metal alloys such as aluminium alloy and stainless steel are also used in bridge construction.

b) Classification by Objectives

• **Highway bridges**: bridges on highways.

• **Railway bridges**: bridges on railroads.

- **Combined bridges**: bridges carrying vehicles and trains.
- **Pedestrian bridges**: bridges carrying pedestrian traffic.
- **Aqueduct bridges**: bridges supporting pipes with channeled waterflow.

c) Classification by Structural System (Superstructures)

- **Plate girder bridges**: The main girders consist of a plate assemblage of upper and lower flanges and a web. H- or I-cross-sections effectively resist bending and shear.
- **Box girder bridges**: The single (or multiple) main girder consists of a box beam fabricated from steel plates or formed from concrete, which resists not only bending and shear but also torsion effectively.
- **T-beam bridges**: A number of reinforced concrete T-beams are placed side by side to support the live load.
- **Arch bridges**: The arch is a structure that resists load mainly in axial compression. In ancient times stone was the most common material used to construct magnificent arch bridges.
- **Cable-stayed bridges**: The girders are supported by highly strengthened cables (often composed of tightly bound steel strands) which stem directly from the tower. These are most suited to bridge long distances.
- **Suspension bridges**: The girders are suspended by hangers tied to the main cables which hang from the towers. The load is transmitted mainly by tension in cable. This design is suitable for very long span bridges.

d) Classification by Support Condition

Fig. 1.2 shows three different support conditions for girder bridges.

- **Simply supported bridges**: The main girders or trusses are supported by a

movable hinge at one end and a fixed hinge at the other (simple support); thus they can be analyzed using only the conditions of equilibrium.

• **Continuously supported bridges**: Girders or trusses are supported continuously by more than three supports, resulting in a structurally indeterminate system. These tend to be more economical since fewer expansion joints, which have a common cause of service and maintenance problems, are needed. Sinkage at the supports must be avoided.

• **Gerber bridges (cantilever bridge)**: A continuous bridge is rendered determinate by placing intermediate hinges between the supports.

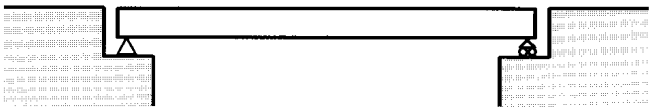

(a) Simple girder

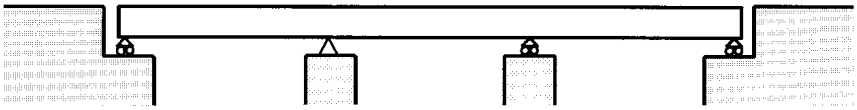

(b) Continuous girder

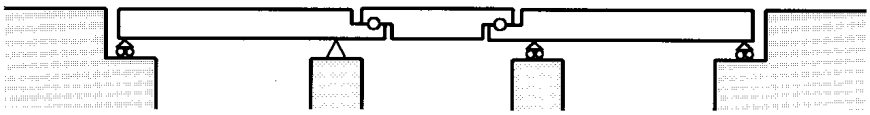

(c) Gerber girder

Figure 1.2: Supporting conditions

1.2.2 Loads

Designers should consider the following loads in bridge design:

a) Primary loads exert constantly or continuously on the bridge

• **Dead load**: weight of the bridge.

• **Live or imposed load**: vehicles, trains, or pedestrians, including the effect of impact. Other primary loads may be generated by prestressing forces, the creep of concrete, the shrinkage of concrete, soil pressure, water pressure, buoyancy, snow, and centrifugal actions or waves.

b) Secondary loads occur at infrequent intervals

• **Wind load**: a typhoon or hurricane.

• **Earthquake load**: especially critical in its effect on the substructure.

• Other secondary loads come about with changes in temperature, acceleration, collision forces, and so forth.

1.2.3 Bridges and beams coupling

Directly coupled bridges are very scarce in practical engineering. However, there are several types of coupling between bridge-like structures consider as beams or plates. These couplings are generally carried out in order to control the vibrations of one of the structures involved. Nana and Woafo [24] have presented a sandwich control comprise of a nonlinear beam coupled in a sandwich manner with a linear beam as shown in Fig. 1.3. The linear beam serves as a control element used to reduce the amplitude of vibration of the nonlinear beam. The range of coupling or control parameters that can produce an effective control (reduction of amplitude) is determined. Zhang *et al.* [25] have proposed to stabilize an elastic plate using

viscoelastic boundary condition as feedback control. Hongpan *et al.* [26] have investigated vibrations control of plate through electromagnetic constrained layer damping which consists of, electromagnet layer, permanent layer and viscoelastic damping layer. Moreover, Aida *et al.* [27, 28] have modelled the dynamics and optimized control by sandwich of a plate (and beam) under sinusoidal periodic excitation. They have shown that the effectiveness of this control is more effective as the number of springs and shock absorbers becomes higher. Sonfack and Nana [29] have modelled the dynamics of a plate by plate type dynamics vibration absorber subjected to a localized periodic impulsive excitation. as shown in Fig. 1.4. Another approach is the use of coupling beams between the structures to be controlled. Coupling beams are essential for transmitting shear forces from a shear wall to another in order to create a coupled-wall system [30]. This system is used to resist both monotonic and cyclic lateral loads due to wind or earthquake. The aim of coupling beams in high-rise buildings is to connect shear walls which resist, in addition to gravity loads, lateral loads induced by seismic events or wind loading. When subjected to lateral ground acceleration the loads need to be transferred to the foundation system through the coupled-wall system. The deformation of coupled wall systems is shown in Fig. 1.5. It can be seen that the coupling beams suffer from double curvature due to lateral loading (seismic loading in this example). Coupling beams are used typically in high-rise buildings to connect shear walls which usually surround elevator shafts.

1.3 Dynamics of bridges

As seen in previous subsection, bridges can be modelled as single span or multi-spans continuous elastic beams as shown in Fig. 1.2. Beams are the most common type of structural component, particularly in Civil and Mechanical Engineering. A beam is a bar-like structural

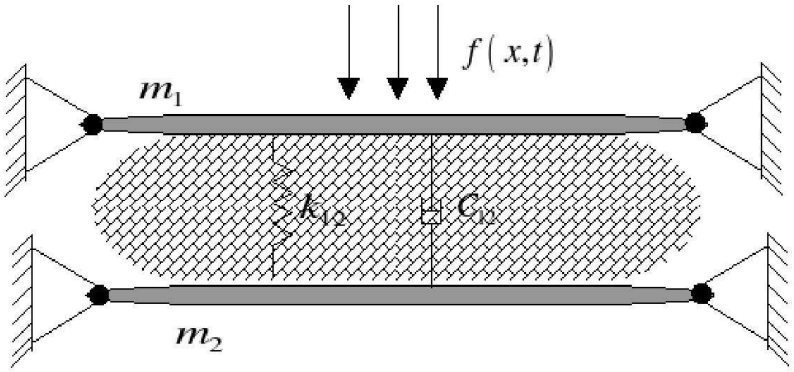

Figure 1.3: Beams with sandwich coupling [24]

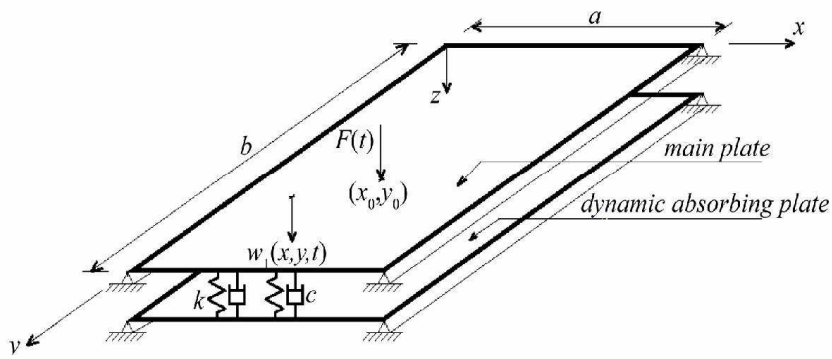

Figure 1.4: Main plate and dynamic absorbing plate with uniformly distributed connecting springs and dampers [29]

member whose primary function is to support transverse loading and carry it to the supports as seen in Fig. 1.6. By "bar-like" it is meant that one of the dimensions is considerably larger than the other two. This dimension is called the longitudinal dimension or beam axis. The intersection of planes normal to the longitudinal dimension with the beam member are called cross sections. A longitudinal plane is one that passes through the beam axis.

A beam resists transverse loads mainly through bending action, bending produces compressive longitudinal stresses in one side of the beam and tensile stresses in the other. The two regions are separated by a neutral surface of zero stress. The combination of tensile and compressive stresses produces an internal bending moment. This moment is the primary

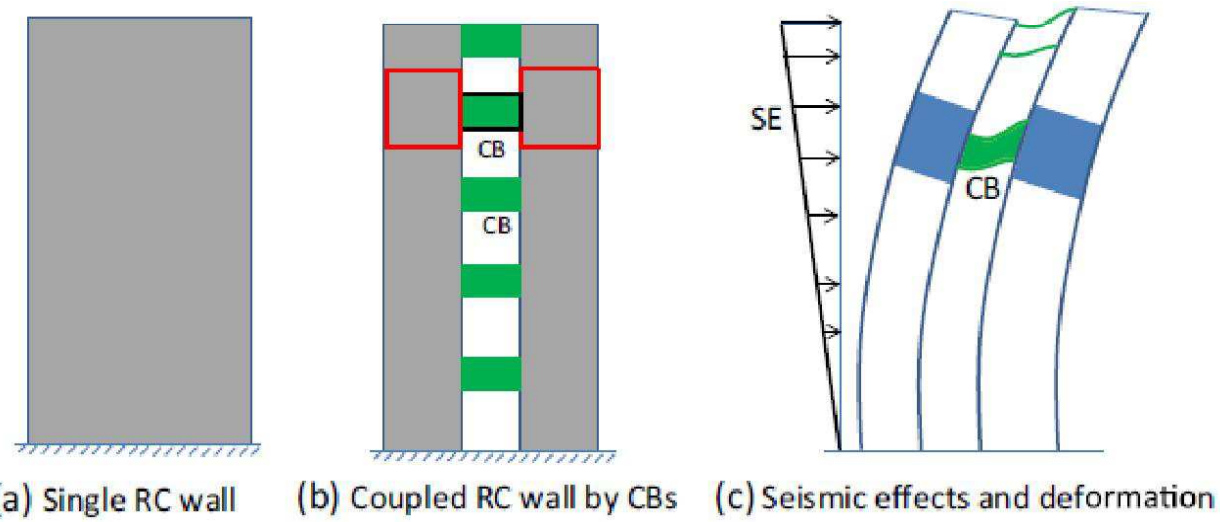

Figure 1.5: Reinforce concrete (RC) wall, Coupled RC wall by coupling beams (CB) and deformation due to seismic effects (SE) [30]

mechanism that transports loads to the supports. The mechanism is illustrated in Fig. 1.7. Here, the mathematical modelling of bending vibration of a free bridge will be treated. For bending vibration of a bridge in the vertical plane, beam theories can be used.

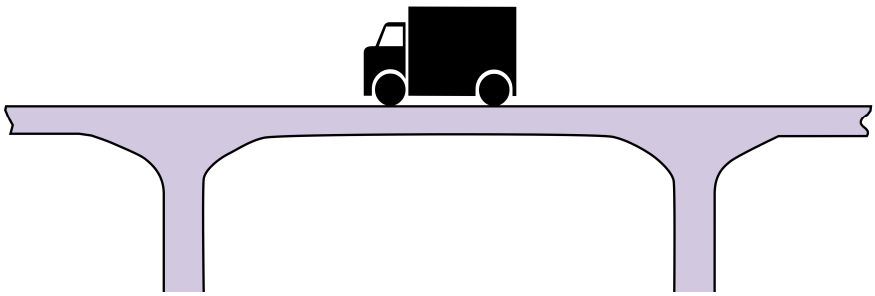

Figure 1.6: A beam is a structural member designed to resist transverse loads

1.3.1 Mechanical model of beam bridges

One-dimensional mathematical models of structural beams are constructed based on beam theories. Because beams are three-dimensional bodies, all models necessarily involve

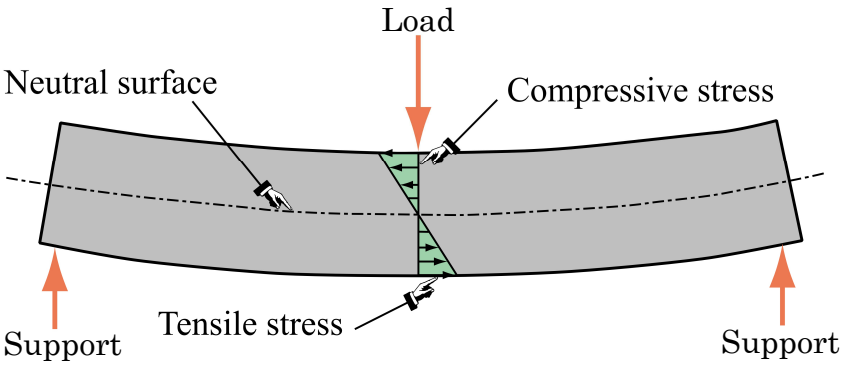

Figure 1.7: Beam transverse loads are primarily resisted by bending action

some form of approximation to the underlying physics. There are four main theories about beams modelling [31]. In Table 1.1, we present these different beam theories:

Table 1.1: Four beam theories

Beam models	**Bending moment**	**Lateral displacement**	**Shear deformation**	**Rotary inertia**
Euler - Bernoulli	√	√	×	×
Rayleigh	√	√	×	√
Shear	√	√	√	×
Timoshenko	√	√	√	√

Bridges are usually modelled as beam-type structures with Euler-Bernoulli or Timoshenko beam models. Euler-Bernoulli beam theory is the oldest, the simplest classical theory for beam bending. It is used in typical hand calculations of beam deflection. It assumes that the cross-section of the beam is always perpendicular to the neutral axis (also after the deformation). Deflection is calculated only using the bending moment, without taking shear forces into account. On the other hand, Timoshenko beam theory is the extended version of Euler-Bernoulli theory that takes into consideration deformations caused by shear. It assumes that the cross-section after deformation doesn't have to be perpendicular to the neu-

tral axis. In general, Timoshenko beam theory is used for thick beams while Euler-Bernoulli theory is used for thin beams for which the length L is much larger than the thickness h_b of the cross-section (at least 10 times i.e. $L/h_b \geq 10$) and the deflections are small compared to the thickness h_b of the cross-section.

The choice of the Euler-Bernoulli beam model in this thesis is justified because this theory describes more simply the real situation of common bridge structures than other theories.

1.3.2 Governing equation of transverse vibration of Euler-Bernoulli beams

Basically, a real bridge vibrates in three directions. These three vibrations influence each other through the wheel/rail contact, but the influence is sometimes small and could be ignored depending on the situation and the purpose of the study. The vertical vibration of a bridge is one of the major concerns in design. The lateral vibration of the train-bridge system is important in studying train derailment [32]. The longitudinal vibration of the rail is a big factor affecting the wheel and rail wear. In this thesis, the vertical vibration of the bridge is the only concern. The influences of the lateral vibration and longitudinal vibration on the vertical vibration of the bridge are small for the experimental rig in the lab and thus ignored. The transverse vibration of beams is governed by the well-known Euler-Bernoulli equation. To develop the governing equation, let us consider a free-clamped cantilever beam according to Fig. 1.8. The Cartesian axes for plane beam analysis are chosen as shown in Fig. 1.9. Axis x lies along the beam longitudinal axis, at neutral axis height. Axis y lies in the symmetry plane and points downwards. The origin is placed at the left most section.

The beam is vibrates in a transversal fashion, up and down in the y direction. The vibration is predominant in the y direction and we will neglect vibration in the x direction.

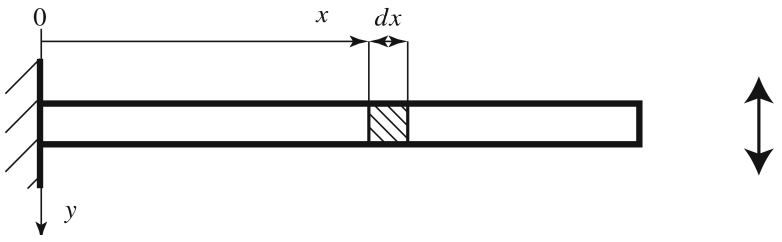

Figure 1.8: Schematic representation of a clamped beam under transversal vibration

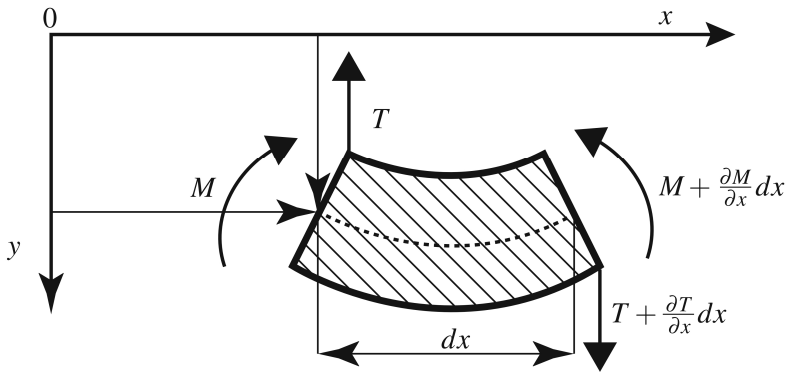

Figure 1.9: Forces and moments acting on the infinitesimally small portion of the clamped beam under transversal vibration

The vibration in the direction perpendicular to the beam length is commonly referred to as flexural or transverse vibration. We may separate the beam to create infinitesimal slices dx. The position of this element is denoted by the coordinate x. The beam is made of the homogeneous material with the density ρ, its constant cross section is given by S, Young's modulus by E and its second moment of area by I. The total length (or span) of the beam member is called L. Fig. 1.9 shows a free body diagram of a beam element in bending. In this figure, $M(x,t)$ is the bending moment, $T(x,t)$ is the shear force, and $f(x,t)$ is the external force per unit length acting on the beam.

Equilibrium condition of moments leads to the following equation

$$M + T\delta x - \left(M + \frac{\partial M}{\partial x}\right) = 0, \tag{1.1}$$

or

$$T = \frac{\partial M}{\partial x} = \frac{\partial}{\partial x}\left(EI\frac{\partial^2 y}{\partial x^2}\right). \tag{1.2}$$

Since a uniform beam is not assumed in the formulation, $I(x)$ will be variable along the beam length. The equation of motion in the transverse direction for the beam element is

$$(\rho S\delta x)\frac{\partial^2 y}{\partial t^2} = f(x,t)\,\delta x + T - \left(T + \frac{\partial T}{\partial x}\right). \tag{1.3}$$

In Eq. (1.3), ρ is the mass density of the beam material. After simplifications, this equation can be rewritten as follows

$$\rho S\frac{\partial^2 y}{\partial t^2} + \frac{\partial T}{\partial x} = f(x,t). \tag{1.4}$$

Considering Eq. (1.2), Eq. (1.4) can be rewritten as

$$\frac{\partial^2}{\partial x^2}\left(EI\frac{\partial^2 y}{\partial x^2}\right) + \rho S\frac{\partial^2 y}{\partial t^2} = f(x,t), \tag{1.5}$$

which is the well-known Euler-Bernoulli equation descibing the forced transverse vibrations of a beam.

For a uniform beam, EI is constant. therefore, Eq. (1.5) reduces to

$$EI\frac{\partial^4 y}{\partial x^4} + \rho S\frac{\partial^2 y}{\partial t^2} = f(x,t). \tag{1.6}$$

Consequently, the equation of motion of a uniform beam for free vibrations where $f(x,t) = 0$ is given by

$$EI\frac{\partial^4 y}{\partial x^4} + \rho S\frac{\partial^2 y}{\partial t^2} = 0. \tag{1.7}$$

Transverse vibration of beams is an initial-boundary value problem. Hence, both initial and boundary conditions are required to obtain a unique solution $y(x,t)$. Since the equation involves a second-order derivative with respect to time and a fourth-order derivative with respect to a space coordinate, two initial conditions and four boundary conditions are needed.

1.3.3 Boundary and initial conditions

The boundary conditions express the deflection position of the beam (and its derivatives with respect to beam longitudinal coordinate x) at any given time. In more practical terms, the zeroth derivation with respect to beam longitudinal coordinate x is a deflection position, while the first is the angle of the tangent line to the neutral axis. Moreover, If the beam is uniform, i.e. EI is constant, the second and third derivatives can be expressed using the moment and shear force as

$$\frac{\partial^2 y}{\partial x^2} = \frac{M}{EI}, \tag{1.8}$$

$$\frac{\partial^3 y}{\partial x^3} = \frac{T}{EI}. \tag{1.9}$$

The common boundary conditions related to beam's ends are given in Table 1.2 below.

Table 1.2: The common boundary conditions related to beam's ends

Boundary condition	**Deflection**	**Slope**	**Bending Moment**	**Shear Force**
at $x_b = 0$ **and** $x_b = L$	$y(x_b, t) = 0$	$\frac{\partial y}{\partial x}\big\vert_{x=x_b} = 0$	$EI\frac{\partial^2 y}{\partial x^2}\Big\vert_{x=x_b} = 0$	$EI\frac{\partial^3 y}{\partial x^3}\Big\vert_{x=x_b} = 0$
Simply supported (Pinned) end/ Hinged end	$\surd$	$\times$	$\surd$	$\times$
Fixed (Clamped) end	$\surd$	$\surd$	$\times$	$\times$
Free end	$\times$	$\times$	$\surd$	$\surd$
Sliding end	$\times$	$\surd$	$\times$	$\surd$

The boundary conditions for beams are very varied, but as seen in previous subsection, only one canonical case is most often encountered in practical bridge engineering: the simple support, as illustrated in Fig. 1.10. This justifies the choice of this type of boundary condition in this thesis. In addition to the boundary condition, there is also the initial conditions,

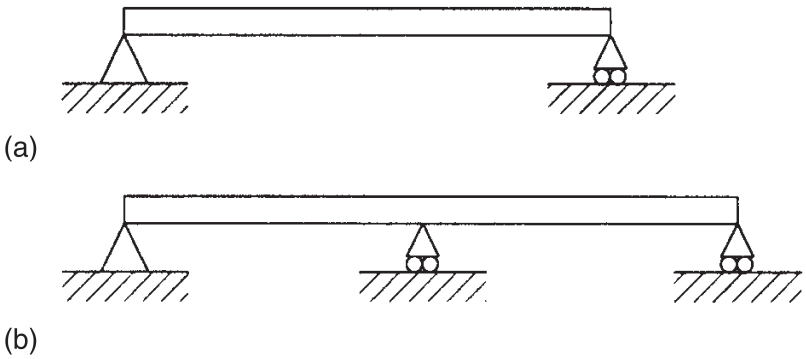

Figure 1.10: Simply supported beam: (a) single span; (b) continuous multi-span

expressing geometrical configuration at zero time as

$$y\left(x,0\right)=\psi_1\left(x\right), \tag{1.10}$$

$$\left.\frac{\partial y}{\partial t}\right|_{t=0}=\psi_2\left(x\right). \tag{1.11}$$

1.4 Bridge-soil interaction model

The role of the soil-structure interaction (SSI) in the field of bridge dynamics is a relatively unexplored topic. One reason for this could be that researchers within the field of bridges have limited knowledges of soil materials. However, during the last decade, the interest in SSI has increased due to the development of new highspeed lines.

The following subsections describe some fundamentals of soil dynamics. Dynamic loading is characterized by short duration, but repeated loading. The soil behavior in dynamic situations will differ from that under static circumstances. Soil dynamics include the understanding of soil properties influencing its dynamic behavior, how the waves propagate through the material and also the mechanisms behind attenuation of the waves motions as the distance to the source increases.

1.4.1 Elastic foundations models of soil

The key aspect in the design of flexible structural elements in contact with bearing soils is the way in which soil reaction, referred qualitatively as soil's reactive pressure (p), is assumed or accounted for in analysis.

Generally, the analysis of bending of flexible structural elements on an elastic foundation is developed on the assumption that the reaction forces of the foundation are proportional at every point to the deflection of the beam at that point. The vertical deformation characteristics of the foundation are defined by means of identical, independent, closely spaced, discrete and linearly elastic springs. The constant of proportionality of these springs is known as the foundation stiffness (the bed modulus), $k_s(\mathrm{N/m^2})$. This simple and relatively crude mechanical representation of soil foundation was firstly introduced by Winkler, in 1867 [33, 34].

The Winkler model, which had been originally developed for the analysis of railroad tracks, is very simple but does not accurately represents the characteristics of many practical foundations. One of the most important deficiencies of the Winkler model is that a displacement discontinuity appears between the loaded and the unloaded part of the foundation surface. In reality, the soil surface does not show any discontinuity (Fig. 1.11).

Figure 1.11: Deflections of elastic foundations under uniform pressure: (a) Winkler foundation; (b) practical soil foundation

Historically, the traditional way to overcome the deficiency of Winkler model is by

introducing some kind of interaction between the independent springs by visualizing various types of interconnections such as flexural elements (beams in one-dimension (1-D), plates in 2-D), shear-only layers and deformed, pretensioned membranes [33]. The foundation model proposed by Filonenko and Borodich in 1940 [33] acquires continuity between the individual spring elements in the Winkler model by connecting them to a thin elastic membrane under a constant tension. In the model proposed by Hetényi in 1950 [33], interaction between the independent spring elements is accomplished by incorporating an elastic plate in 3-D problems, or an elastic beam in 2-D problems, that can deform only in bending. Another foundation model, proposed by Pasternak in 1954, acquires shear interaction between springs by connecting the ends of the springs to a layer consisting of incompressible vertical elements which deform only by transverse shearing [33]. This class of mathematical models have another constant parameter which characterizes the interaction between springs and hence are called two-parameter models (Fig. 1.12).

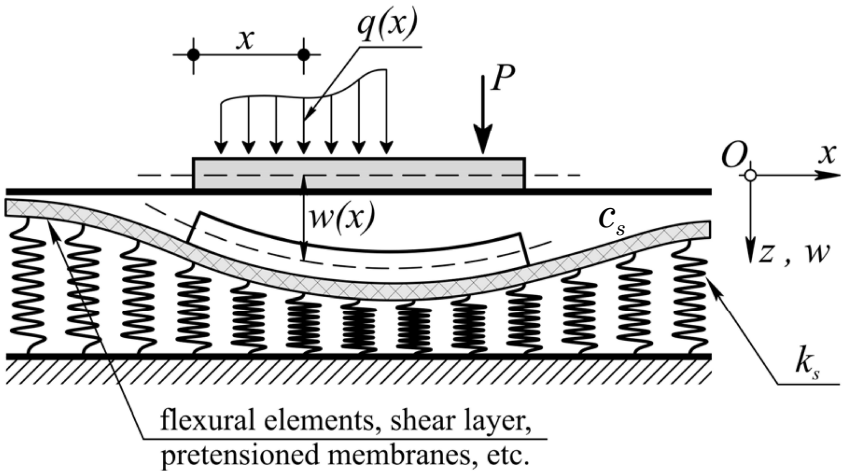

Figure 1.12: Beam resting on two-parameter elastic foundation

In this thesis, the soil foundation is modelled as a linear viscoelastic Winkler foundation ([35, 36]) known as Kelvin-Voigt model of soil [3]. In this model, the elastic behavior of the soil is represented by a stiffness spring (k_s) placed in parallel with a viscosity damping (C_s)

representing the viscous behavior of the soil (Fig. 1.13). Thus, external restoring forces of a linear viscoelastic Winkler foundation are given as follows

$$F(x,t) = -k_s w(x,t) - C_s \frac{\partial w(x,t)}{\partial t}, \tag{1.12}$$

where k_s and C_s are the two coupling parameters characterizing the strength and the damping of the soil, respectively.

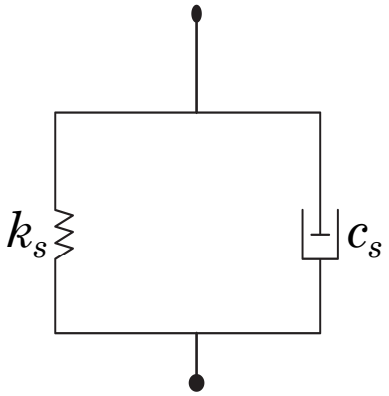

Figure 1.13: Kelvin-Voigt model of soil

1.4.2 Modelling the propagation of vibration in the soil

It is well-known that ground borne vibrations are transmitted as shown in Fig. 1.14, through soil material as compression (P), shear (S), and Rayleigh (R) waves whose propagation velocities are given by [37] as

$$V_P = \sqrt{\frac{E(1-\nu)}{\rho(1+\nu)(1-2\nu)}}, \tag{1.13}$$

$$V_S = \sqrt{\frac{G}{\rho}}, \tag{1.14}$$

$$V_R \approx \frac{v_S(0.86+1.14\nu)}{1+\nu}, \tag{1.15}$$

where the modulus of elasticity E, the density ρ, the Poisson's ratio ν, and the shear modulus G are assumed to be known. From Eqs. (1.13) to (1.15) it is easy to show that $V_R < V_S < V_P$.

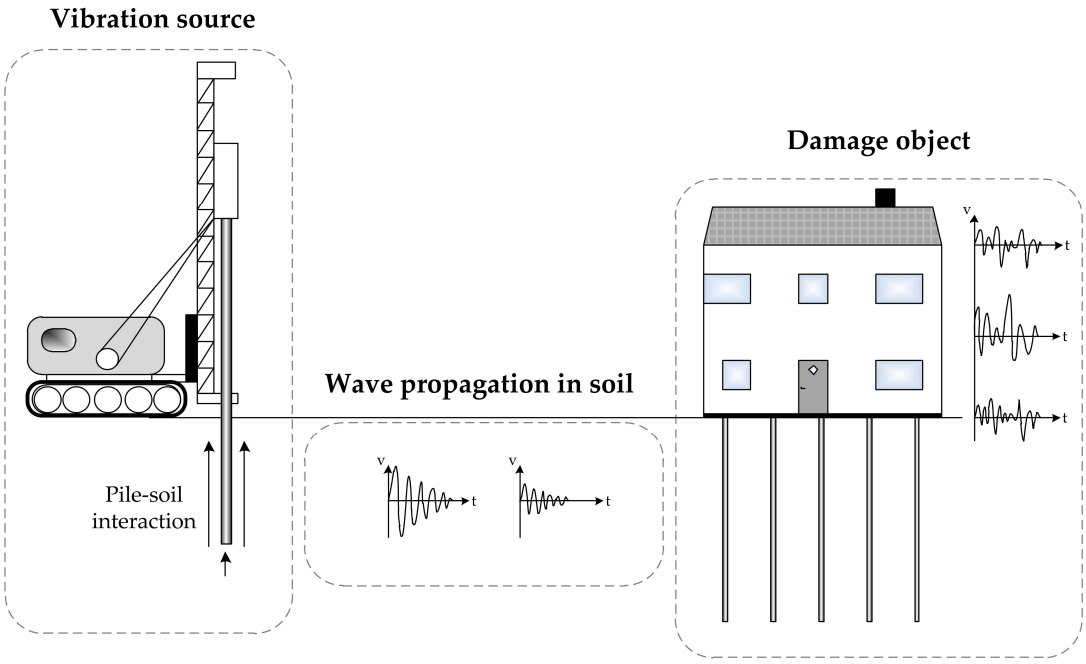

Figure 1.14: Illustration of vibration transfer during vibratory sheet pile driving [38]

The intensity of vibrations decreases as the wave propagates away from the source. The attenuation of the vibration depends mainly on two damping factors: the geometry of the propagation and the material in which the waves propagate [39]. Considering both the material and geometrical damping, Eq. (1.16) can be used to describe the total damping effect on the wave amplitude [39, 40].

$$A_2 = A_1 \left(\frac{r_1}{r_2}\right)^n e^{-\alpha(r_2 - r_1)}, \tag{1.16}$$

where A_1 is vibration amplitude at distance r_1 from the source, A_2 is vibration amplitude at distance r_2 from the source, α is an absorption coefficient describing material damping and n is $1/2$ for surface waves (Rayleigh waves), 1 for body waves and 2 for body waves along the surface.

The origin of Eq. (1.16) dates back to 1912 when Golitsin derived it specifically for Rayleigh waves generated by earthquakes, but it has later been adjusted for application on different kinds of waves [41]. Furthermore, the acceleration at the distant points is estimated in the frequency domain in Refs. [42, 43].

Other types of loads to which bridges can be subjected are modeled in the next subsection.

1.5 Modelling of the dynamic loading acting on bridge structures

There is a growing interest nowadays in the process of designing civil engineering structures to withstand dynamic loads [44–46]. As examples, we can mention (i) structures with house moving or vibrating equipment, (ii) bridges under traffic, (iii) multistory structures subject to wind and (iv) the case of earthquake induced loads [47, 48]. Essentially, the dynamic analyses focus on the evaluation of time dependent displacements, from which the stress state of the structure in question can be computed [49–51]. The most basic pieces of information needed for this are the natural period, which is a function of the structure's mass and stiffness, and the amount of available damping (or, equivalently , the amount of energy that can be absorbed by the structure).

Generally, loads on bridges structures fall into two categories: dead loads and live or imposed loads. Dead loads are loads that act on a structure all the time. Live or imposed loads are dynamic loads; these include vehicles and people crossing a bridge, and dynamic effects produced, for example, by vibrating machinery, wind gusts, wave action or even earthquake action in some parts of the world. These dynamic loads can be modeled by sinusoidal loads, impulsive loads, moving loads, random loads or a combination of these different loads as

developed in the following subsections.

1.5.1 Sinusoidal loads

A sinusoidal load on a bridge can model for example to the actions of pedestrian and certain vibrating machinery. Ravindra and Mallik [52] have investigated isolation systems having nonlinearity in the stiffness and the damping under both harmonic force excitation and harmonic base excitation. Moreover, Ding *et al.* [53] present a nonlinear isolation of transverse vibration of pre-pressure beams subjected to a uniformly distributed sinusoidal load. In this thesis, Sonfack *et al.* develop and examine an experimental model of two coupled beam bridges, which on one is exerted a localized combination of sinusoidal load and periodic impulsive load.

1.5.2 Impulsive loads

Commonly, impulsive loads (e.g., impact and blast loads) are of subsecond duration and magnitude tens of times larger than any other loads in the design life of the structure. This type of load on a bridge can model for example to the actions of pedestrian, certain vibrating machinery, wave action or even earthquake action and explosive load. In general, the impact load is modelled as a rectangular pulse or as a Gaussian function whose integral over the duration of the impact is equal to the impulse of impact. The duration of the impact depends on the nature of contact between the exciter and the structure, the material they are made of and their dimensions. Therefore, minimizing the impact load is equivalent to minimizing the impulse of impact [54]. In this thesis, the impact load is used to model the external excitation produce by the vibration source.

1.5.3 Moving loads

The dynamic analysis of beam structure with moving load is a fundamental problem in structural dynamics. In comparison to other dynamic loads, the moving load varies in position as well as time and that is why the moving load problem is a special topic in structural dynamics. Since the 19th century, the moving load problem has become more dynamic in nature due to the increasing of vehicle speed and structural flexibility. The problem of dynamic response of Euler-Bernoulli beam subjected to a moving mass has been studied by many authors and the importance of this problem is demonstrated in several ways by many authors. The dynamic effects of moving loads were not recognized until mid-19th century. It was believed that it was the collapse of Stephenson's bridge across Dee river at Chester in England in 1847 that triggered the research into moving-load problems [55]. Stokes was credited to be the first researcher who formally analysed a moving-load problem (it is actually a moving-force problem). This history was chronicled by Timoshenko [56]. The dynamic behavior of beam structures, such as bridges on railways, subjected to moving loads has been investigated for over a century. There are numerous reports available in the book by Fryba [57], and most of them treat a uniform simply supported beam of single span. Various kinds of problems associated with moving loads have been presented in the same book. Vehicles crossing a bridge can be treated as a moving force, a moving mass, a moving oscillator or a more complicated moving vehicle model consisting of springs, dashpot and rigid bodies in theoretical models as shown in Fig. 1.15.

If the moving load was treated as a moving force, it would not be hard to solve the problem. Taking a constant force moving at a constant velocity on a simply supported beam bridge for example, the equation of motion of the beam after applying MS method has the same form as a single degree of freedom (SDOF) system excited by a harmonic force, which can be solved analytically [58]. On the other hand, if the mass of the moving vehicle is

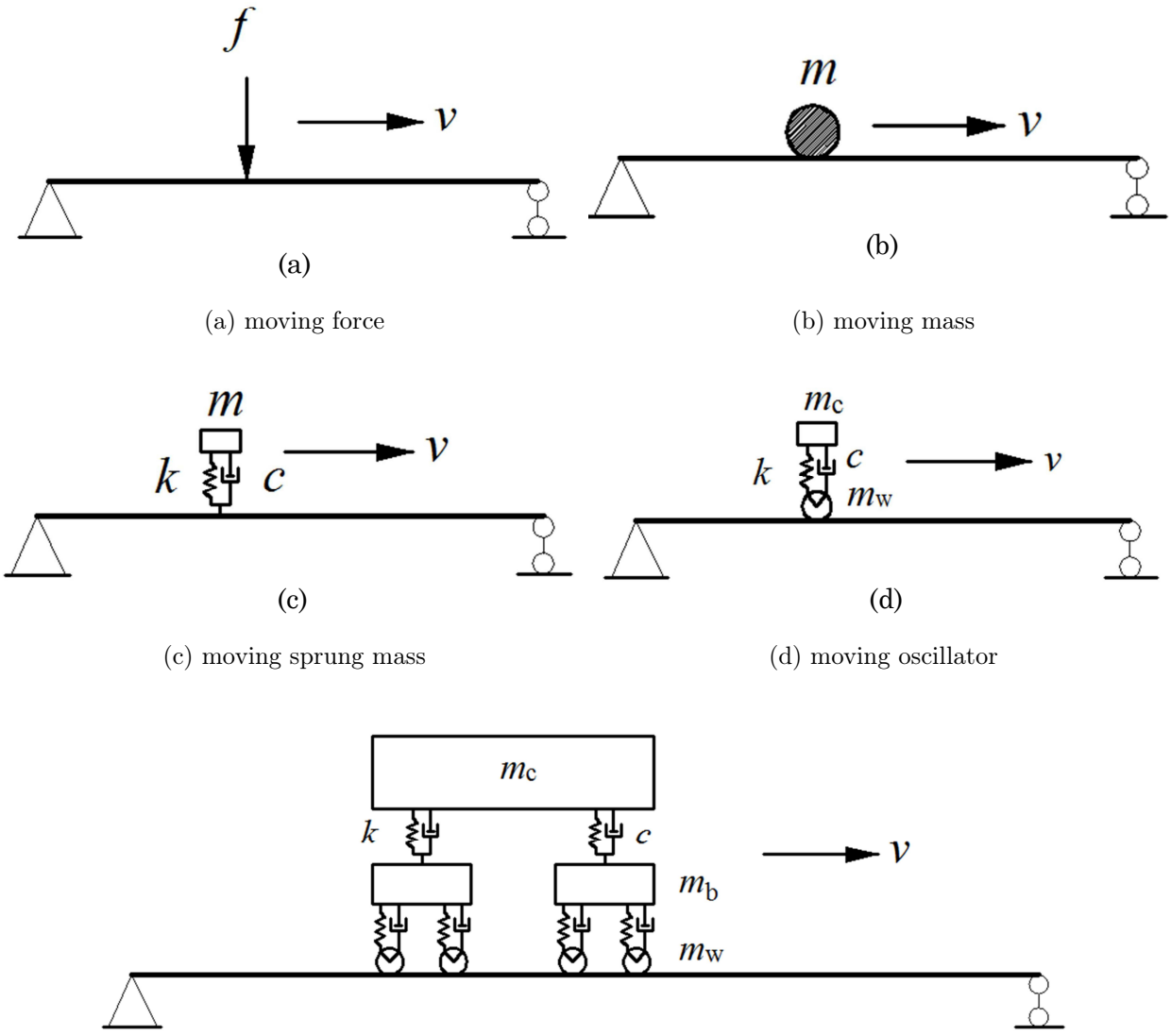

(a) moving force

(b) moving mass

(c) moving sprung mass

(d) moving oscillator

(e) moving vehicle

Figure 1.15: Different models of moving loads

considered (moving mass, moving oscillator and moving vehicle models), the contact force between the vehicle and the bridge would change with time, as the contact force includes an inertial force of the vehicle. The inertial force depends on the motion of the vehicle, which is influenced by the motion of the bridge, so the contact force actually is an interaction force varying with time. In this case, the equation of motion of the bridge cannot be solved analytically. In order to determine the dynamic response of the bridge under moving vehicles,

MS method can be used to separate the space component from the time component in the whole solution. The whole solution is equal to the sum of different modes multiplied by their corresponding modal coordinates.

The simplest type of moving loads is a constant or harmonic, pure force. But several researches have shown that a structure under a moving pure force is equivalent to a nonmoving-load vibration problem and does not reveal most properties specific to moving-load dynamics and hence does not qualify as a proper moving-load problem [55]. When the inertial effect of moving vehicles cannot be ignored, it is essential to use more complicated models for the vehicles. As the moving mass model (Fig. 1.15(b)) is the simplest model including the inertial effect of a moving vehicle, that model will be used in this thesis.

1.6 State of the art review of structural vibration control systems

Structural vibration control systems, which are also referred to as Motion Control Systems, can be utilized to reduce structure's responses to different types of dynamic loads such as earthquakes, winds, traffic and other kinds of service loads. In general, these devices can be classified into four main groups (passive, active, semi-active, and hybrid) based on their operating mechanisms, as shown in Fig. 1.16 [59–66]. The following subsections describe the main groups and subgroups of structural vibration control systems in used nowaday.

A passive control system (Fig. 1.17(a)) does not require an external power supply. Such devices respond as per the structural response, dissipate the energy in the form of heat and eventually reduce the structural response. Friction dampers, yielding elastoplastic dampers, viscous dampers etc. fall into this category. Passive devices, such as base isolators, modify the free vibration characteristics of the structure and brings it to a lower frequency, where

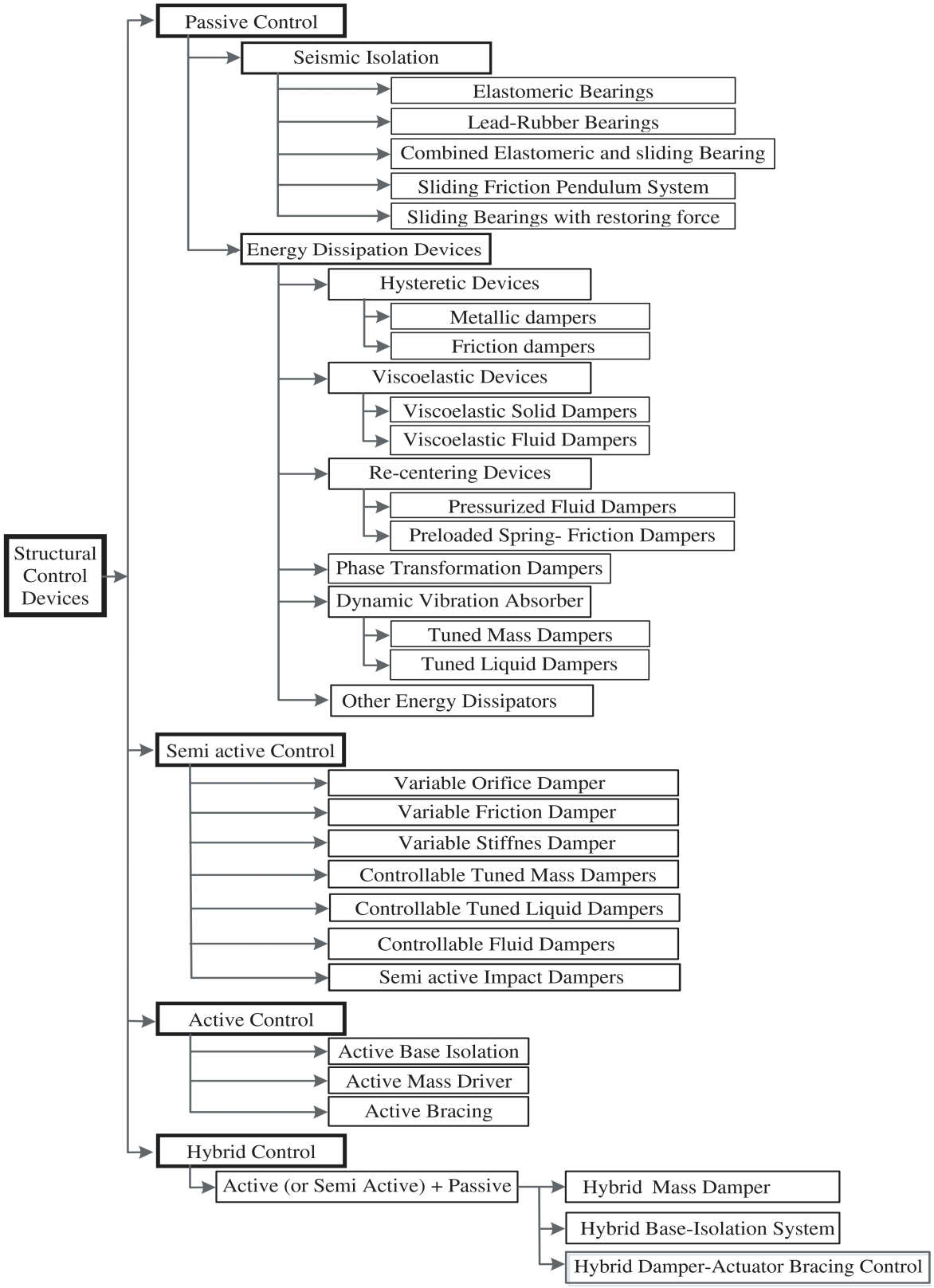

Figure 1.16: Categorization of structural control systems

the amplitude of earthquake excitation is smaller.

An active control system (Fig. 1.17(b)) is one in which external source power control actuators require large power sources on the order of tens of kilowatts for small structures and several megawatts for large structures. These actuators apply forces to the structure in a prescribed manner, which can be used to both add and dissipate energy in the structure. In the active feedback control system, the signals sent to the control actuators are a function of the response of the system measures with physical sensors. Active tuned mass dampers, active variable stiffness systems and active pulse generators are some of the active dampers. An overview of active response control has been provided by Soong *et al.* [67].

A semi-active control system (Fig. 1.17(c)) is a combination of active and passive systems. This facilitates less supply power on the order of tens of watts input to the systems. The advantage is that in case of power failure the passive component of the control will still offer some protection. Among the dampers of this type are mechatro dampers, variable friction dampers and controllable tuned liquid dampers. Semi-active control systems have been reviewed by Symans *et al.* [68].

Hybrid control systems consist of combined passive and semi-active devices [69,70] and of combined passive and active devices [71,72] are described in the literature. Passive hybrid control systems, mentioned by Makris *et al.* [73] and Soneji *et al.* [74], consist of passive supplemental energy dissipation devices in association with base isolation systems.

Table 1.3 presents a general comparison of the different kinds of structural vibration control systems presented above.

In most of engineering applications, passive vibration isolators are usually the first solution to the problem of vibration transmission. This is mainly due to the fact that they provide high performance and stability, they are rather simple, do not require any external power source or computer control and therefore are also not expensive. In fact, active and

Table 1.3: Comparison among the different kinds of structural control systems

structural control systems	**Passive control systems**	**Semi-active control systems**	**Active control systems**	**Hybrid control systems**
How they work?	Absorb or diverge part of the input energy	Natural extension of passive devices	Automatically apply a force to the structure	Mixture
How they act on structural response?	- Dependent on relative movement - Related only to the local structure response - No structural response measurements	Include adaptive systems	- Depend on the global response - Ability to sense excitation and automatically adjust control efforts	Mixture
Optimal condition of use	Optimally tuned to a specified dynamic loading	Broader applicability than passive systems but more than active system	Superior efficiency compared to passive control systems	Suitable for all types of structures
Efficiency	- No optimal for other types of dynamic loadings - Unable to adapt to the excitation and global structural response - Limited control capacity	- Capable of acting better than passive systems - Limited control capacity	- Designed for different objectives - No theoretical limits on efficiency - Wide frequency range	- Greater capacity than a passive system - Greater efficiency than a passive system
Stability	Inherently stable	- Fail-safe - Reliable	Detuning may occur	More reliable
Energy supply	No energy requirement	Little power requirement	Significant energy consumption	Costs less than active system
Manufacturing	Simpler to design and construct	Easy to manufacture	Complicated	

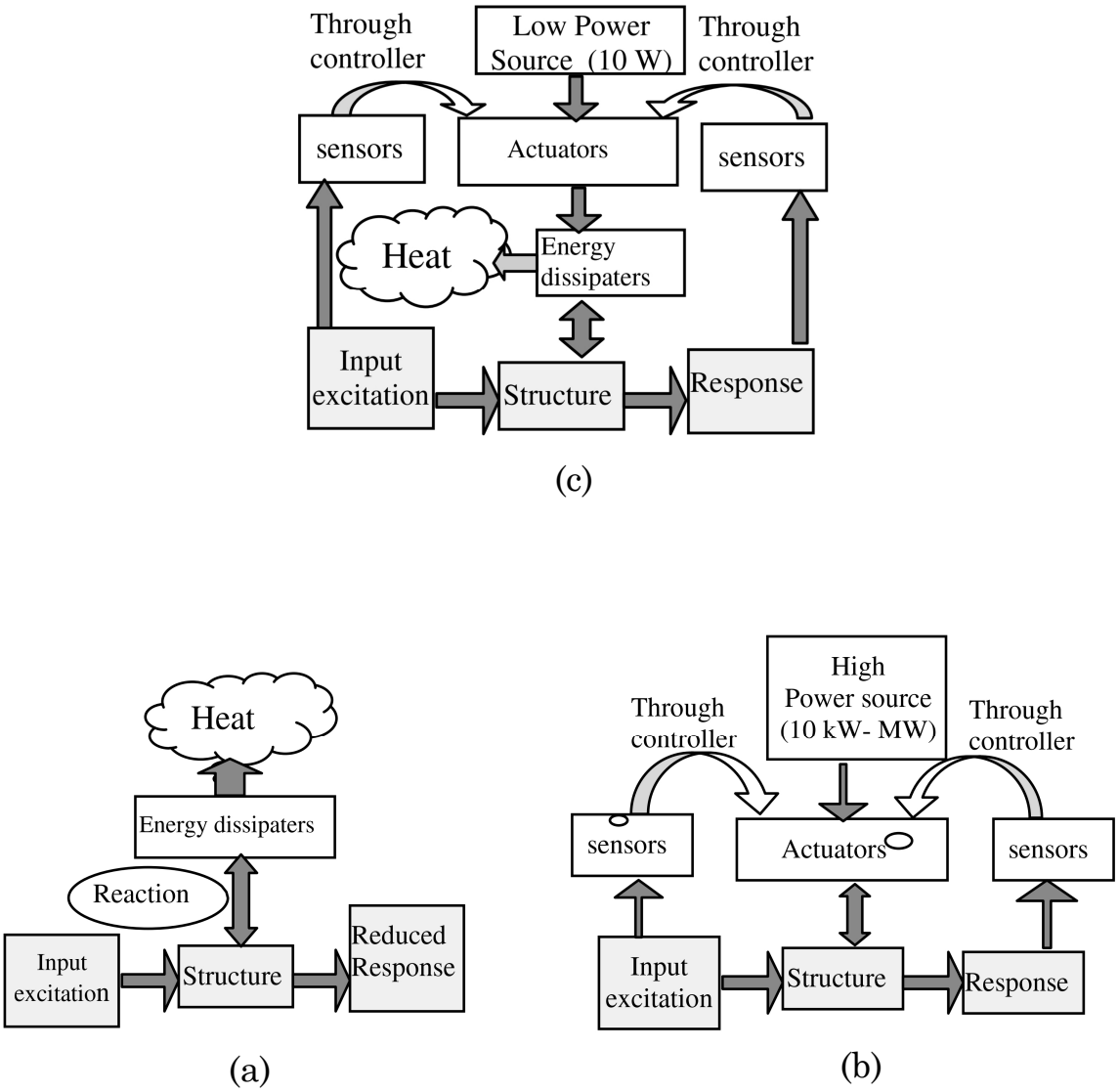

Figure 1.17: Different kinds of structural vibration control systems: (a) Structure with passive control device, (b) Structure with active control device, (c) Structure with semi-active control device

semi-active devices have the main disadvantage of the use of power, and hence they are not that attractive for example in seismic response control. In a severe earthquake, power failure often occurs and the power required to operate active and semi-active devices may not be available. Hence there is always a requirement to reduce the number of active systems and semi-active systems, and it is usually recommended to go for passive devices and the fail-safe

design approach. For the above reasons, it is felt to be necessary to carry out a wide-ranging literature review of passive dampers and mention the advantages and limitations of each along with their applications in real life structures.

1.6.1 Passive vibration control (PVC)

PVC systems does not operated with the help of any external force or source. In the passive control approach, control devices are embedded or connected to the structural members (Fig. 1.17) to improve the structural damping or increase the stiffness without any use of external force.

There are a great number of passive vibration isolators that are used extensively in engineering applications. The common aspects to these isolator designs are that they all employ a resilient structure to support the payload, and a damping component to absorb the residual vibration energy on the payload. The current state of passive control systems and their characteristics is summarized in Table 1.4 and common passive vibration control systems used in bridges are discussed in more details below.

The applications of passive control systems in bridge engineering has attracted many attentions in terms of proposing innovative control devices. Passive control systems have proven to be effective in reducing the cable vibrations as the control system can be adjusted for maximum damping ratio. Yan *et al.* [75] showed the usefulness of tuned particle dampers on a scaled model of a continuous viaduct subjected to ground motions. Miguel *et al.* [76] suggested concurrent optimization of placement and force of friction dampers (FDs) using the Firefly Algorithm [77]. They evaluated the proposal on two footbridges under human-induced vibrations where locations and forces of FDs were the design variables. Takeya *et al.* [78] introduced an energy harvester device known as Tuned Mass Generator (TMG) consisting of a tuned dual-mass damper system for vibration control of bridges. An electromagnetic-

Table 1.4: State of the art in passive control systems

Control System	**Key Features**	**Applications**
Seismic isolation devices	- Low-Damping natural and synthetic Rubber Bearing (LDRB), Lead-plug bearing (LRB), High-Damping Natural Rubber (HDNR), Teflon Articulated Stainless Steel (TASS) System, Friction Pendulum System (FPS), Sleeved-Pile Isolation System - More safe and economic than the traditional structural systems	Many buildings and bridges have been built with these devices
Hysteretic devices	- Metallic dampers, Friction dampers - Energy dissipation is independent of loading rate - Have long term reliability - Fabrication details can significantly affect the overall performance of the friction dampers	They are mostly used in structures
Viscoelastic devices	- Viscoelastic solid dampers, Viscoelastic fluid dampers - Their displacement characteristics depend on the frequency of the motion and relative velocity between the ends of the damper	They are mostly used in structures
Re-centering devices	Possess an inherent re-centering capability	Many buildings have been built with these devices
Phase transformation dampers	- Use Shape Memory Alloys - Self-centering mechanism - Insensitivity to environmental temperature changes - Excellent fatigue resistance - Corrosion resistance - Capable of producing large control forces	Still in the stage of research
Dynamic vibration absorber	- Tuned Mass Damper (TMD), Tuned Liquid Damper (TLD), Tuned Liquid Column Damper (TLCD) - Dissipation is achieved by transferring some of the vibrational energy to the absorber - The dynamic properties should be tuned to those of the primary structure - Detuning may occur - No need for any activation mechanism - Less maintenance cost	Successfully applied in mitigation of wind loads in a number of buildings and bridges

transducer was applied to use the unused energy reserve of the damper. Moreover, TMG was tuned through multi-domain parameter design approach for both the power generation and energy storage. Miguel *et al.* [79] presented an application of robust optimal design of Tuned Mass Damper (TMD) and Multiple-TMD for vehicle-induced vibration of bridges by the implementation of a parallel-processing Monte Carlo simulation to carry out the high computational complexity. Camara *et al.* [80] proposed an approach to design optimum yielding dampers employing Triangular Added Damping and Stiffness (TADAS) dampers placed between the deck and supports, based on the equivalent SDOF approximation for short to medium span cablestayed bridges in the transverse direction. Attary *et al.* [81, 82] evaluated the performance of Negative Stiffness Devices (NSD) for seismic response control of scaled highway bridge structures experimentally on a shake table. The proposed NSD is shown in Fig. 1.18.

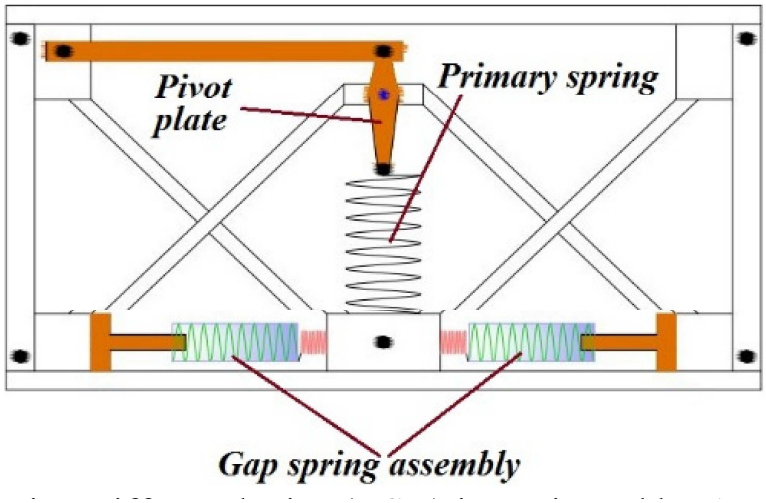

Figure 1.18: Negative stiffness device (NSD) investigated by Attary *et al.* [81, 82]

1.6.2 Linear and nonlinear viscoelastic vibration isolation

According to Rivin [83], "vibration isolation is one of the vibration control techniques whereby the source of vibration excitation and the object to be protected are separated by an auxiliary system comprising special devices called vibration isolators or vibration isolation mounts". The purpose of an isolator may differ depending on the situation. Despite different purposes, the same principles apply in each case. Viscoelastic vibration isolators normally use a resilient structure to support the payload. According to the elastic behavior of the supporting structure, passive vibration isolators can be categorized into linear and nonlinear types.

a) Linear vibration isolation

The structural stiffness of a linear vibration isolator remains constant regardless of either isolator static deflection (caused by the payload weight) or dynamic deflection (caused by the dynamic load exerted from external disturbances). A typical example is the coil spring isolator, where the spring force is a linear function of the spring deformation. In these isolators, the payload sensitivity to external disturbance is fixed, and is dependent on the stiffness of the supporting structure. A complete review of linear vibration isolation can be found in numerous undergraduate texts, for example, "Passive Vibration Isolation" [83], which contains both theories and extensive examples of the applications of linear vibration isolators. Several studies and applications concern the TMD, which consists in adding to a primary structure and tuning to one resonant mode, a linear device.

Early studies were conducted in [84–86], and the main parameter optimisation criteria are based on the minimization either of the transfer function maximum or of the energy [87, 88], as well as on the pole location [89, 90]. The effectiveness of one or multiple-TMD added on single or multi degree of freedom systems subjected to harmonic, random, and seismic

excitations has been studied in [91–95]. Among the experimental devices, recent studies deal with TMD based on the eddy currents damping effect, [96–98]. The performance of the TMD is very effective in the case of linear systems and has been proven to be a very reliable passive mitigation device in many contexts. However, it is known to bear some limitations, as e.g. its tuning to only one resonant frequency and its sensitivity to the primary structure uncertainty [99–101]. To overcome these drawbacks, the use of nonlinear vibration absorbers is studied as an alternative to the TMD in order to enhance the range of effectiveness in terms of frequency or vibration amplitude.

b) Nonlinear vibration isolation

Nonlinear vibration isolation theories have witnessed significant developments due to pressing demands for high performance vibration isolation. The stiffness and/or damping of the resilient structures used in these designs behave in a nonlinear fashion so that, by combining multiple nonlinear supporting structures, the overall stiffness of the isolator can be more flexibly tuned to suit different applications [102]. Some common applications of nonlinear vibration isolators include: isolation of diesel engines in marine vessels, isolation of space craft, isolation of vehicle passengers from road disturbances, isolation of vibration generated by hand-held tools, and isolation of buildings, bridges, storage tanks and oil pipelines from destructive impacts from earthquakes. The literature reports a considerable number of studies on nonlinear vibration isolators. Ibrahim [102] published a comprehensive review on nonlinear passive vibration isolators. This covers a wide range of mechanisms and mounts. Ravindra and Mallik [52] investigated isolation systems having nonlinearity in the stiffness and the damping under both harmonic force excitation and harmonic base excitation. They showed that for such nonlinear systems, when excited by a harmonic force, the effect of increasing the damping results in a decrease in the transmitted force at resonance and that the

attenuation of forces at high frequencies decreases, in agreement with the results presented by Ruzicka and Derby [103]. Therefore, the effects of the damping in such a system are similar to those of a linear system. Moreover, Ding *et al.* [104] present a nonlinear isolation of transverse vibration of pre-pressure beams.

As seen, the most important characteristics of an isolator are its natural frequency and load bearing capacity. As it is well known, a linear vibration isolator often faces a difficult choice situation that arises between these two characteristics. For traditional passive linear isolators, a smaller stiffness is needed to achieve a smaller natural frequency so that it can reduce low frequency vibrations [17,105]. In this case, a larger static deflection is unavoidable in practical applications. To overcome the limitation between isolation performance and static deflection, passive nonlinear isolators have been used to obtain a high static stiffness resulting in a small static deflection and a low dynamic stiffness resulting in a small natural frequency [14, 18, 106]. By choosing the appropriate configurative and geometric parameters of nonlinear isolators, a QZS vibration isolator possessing zero dynamic stiffness at the static equilibrium position is chosen in this thesis for bridge vibration isolation. Its mechanism is presented in the following subsection.

1.6.3 Passive vibration isolation with QZS mechanism

QZS mechanism is presented to design nonlinear stiffness vibration isolators with large static stiffness but very small dynamic stiffness, which can provide zero stiffness at the static equilibrium position by connecting positive stiffness elements in parallel with negative stiffness elements [107–112]. Since the 1980's, the work in nonlinear vibration isolation has resulted in development of several designs that can achieve quasi-zero payload supporting stiffness. A simple QZS configuration design proposed by Carella *et al.* [107, 108] in 2007 consists of three linear springs with one vertical spring connected with two inclined springs

as shown in Fig. 1.19. The negative stiffness effect can be obtained by installing springs in the horizontal direction as shown, which can counteract the effect of positive stiffness due to the springs in the vertical direction. With the mass loaded on the vertical spring, the static equilibrium position with the oblique springs in the horizontal direction can be determined by the geometry configuration. The zero stiffness at the static equilibrium position can be obtained as shown in Fig. 1.20 by the optimum geometry configuration design. As the disturbance is applied in the vertical direction, the system dynamic stiffness will vary nearby the zero stiffness except for some ill conditions.

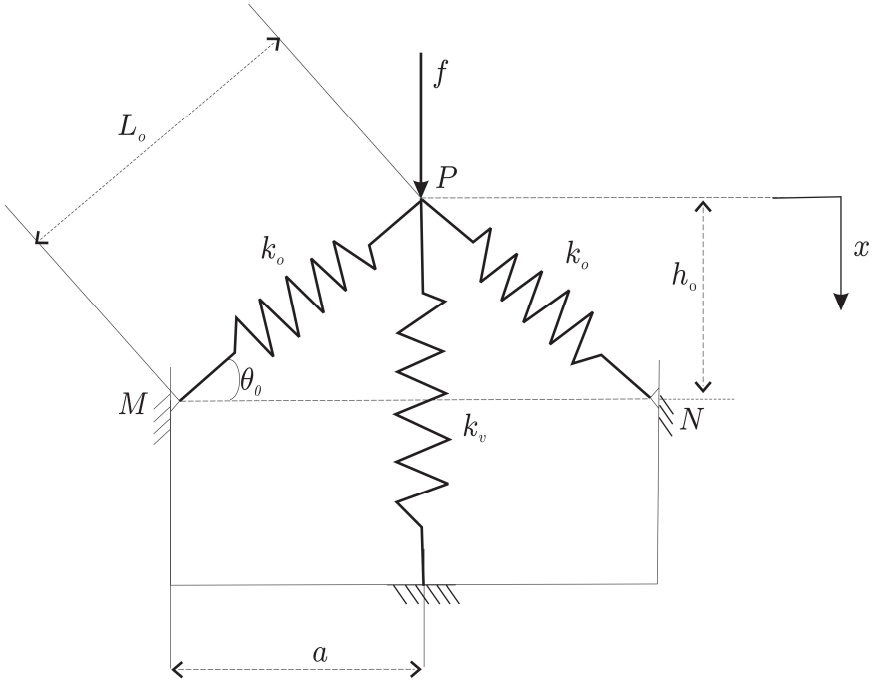

Figure 1.19: Schematic representation of the simplest system with QZS mechanism by Carella *et al.* [107, 108]

By rightly selecting the geometry and stiffness parameters of the negative stiffness, the vibration isolation system can resist a large load statically while having low-frequency vibration isolation performance. Vibration isolation with the QZS stiffness is often used in practice to improve comfort or safety of the systems under study. To overcome disadvantages

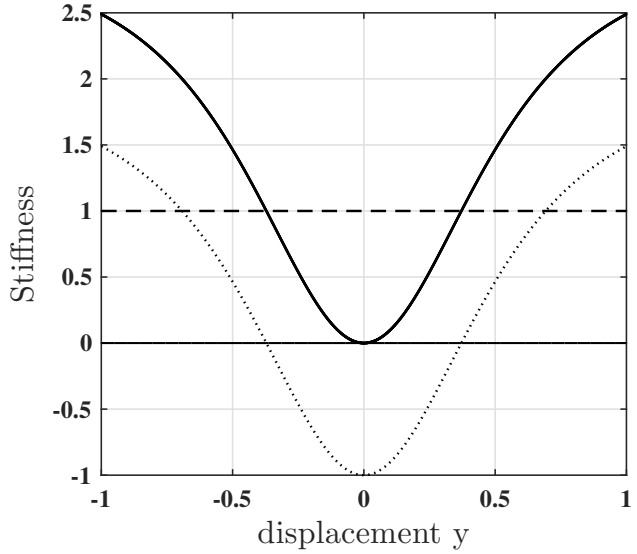

Figure 1.20: Stiffness-displacement characteristic of a QZS mount: by connecting in parallel (summing the stiffness) a linear spring (with positive stiffness, dashed line) with 2 oblique springs (negative stiffness, dotted line); the total stiffness (solid line) at the static equilibrium position can be set to zero

such as large value of natural frequency and large static deflection of traditional mass-spring isolators with linear springs and dampers, oblique or horizontal springs are added as shown in Fig. 1.19. Due to the nonlinearity introduced by oblique springs with/without pre-deformation, the system can obtain a high static stiffness, and low natural frequency induced by the small dynamic stiffness. Although the advantages of the QZS vibration isolator are well recognized above, the resonance peak of the system is often considerably large and the inherent nonlinearity could induce jump phenomenon at around the resonant frequency, which may not be expected in practice due to safety and stability.

Because they can meet the needs of isolating low frequency vibration, even ultralow frequency vibration, various forms of negative stiffness mechanisms have been designed to obtain negative stiffness and combined with the positive stiffness structures to construct QZS vibration isolators. In recent years, several types of vibration isolators using QZS mech-

anisms have been developed and applied to improve working environment for users in many engineering fields, such as vibration resonance test of aircraft, vibration isolation of precision instruments, sensor, energy harvest, suspensions and seats of vehicles and protection of motors.

Many different prototypes of QZS vibration isolators were proposed by Alabuzhev *et al.* [96] and more detailed information about their technical design methods and their applications was recapitulated by Ibrahim [102]. A vehicle suspension using the negative stiffness mechanism combined with a positive stiffness support was designed by Arafat *et al.* [114]. A prototype of QZS vibration isolator composed of a pair of bars linked with a pair of horizontal linear springs to improve the vibration isolation performance of vehicle seats under low excitation frequencies was studied theoretically and experimentally by Le and Ahn [115,116]. Liu *et al.*, Huang *et al.* and Fulcher *et al.* [117–119] built a QZS vibration isolator by using Euler buckled beams as negative stiffness correctors and explored the isolation performance theoretically and experimentally. In these studies, the starting frequency of isolation of the nonlinear isolator were found to be lower than that of the linear one with the same support capacity. Platus [120] developed a nonlinear vibration isolator using two axially loaded beams to achieve the QZS property for horizontal vibration isolation. Carrella *et al.* [107, 108] built a QZS vibration isolator made of a vertical spring acting in parallel with two inclined linear springs used as negative stiffness correctors, and investigated the force and motion transmissibilities theoretically. The results showed that the QZS vibration isolator outperforms the linear counterpart in some aspects. Meng *et al.* [105] proposed a QZS vibration isolator using a disc spring as negative stiffness corrector and investigated its isolation performance considering a mistuned mass. All the works mentioned above indicate that the effectiveness of the QZS vibration isolator is superior to its linear counterpart when the excitation amplitude is relatively small. However, increasing the excitation amplitude

leads to the increase in response and deteriorates the isolation performance of the QZS vibration isolator due to the existence of cubic nonlinear stiffness. The transmissibility of vibration isolators with high dimensional QZS has also been studied by Li *et al.* and Wang *et al.* [122–124]. The results show that quasi-zero stiffness vibration isolators have the low force transmissibility and the low frequency band for vibration isolation.

From this literature review, it emerges that both academic and industrial organizations show a particular interest in vibration isolators with a QZS characteristic. However, in all the abovementioned works related to nonlinear vibration isolation using QZS mechanism, isolated structures have usually been treated as discrete systems of concentrated masses. The bending vibration of the isolated main structure itself has been neglected. Therefore, it is not understood how multimode bending vibration of isolated structures changes the isolation efficiency of a nonlinear QZS vibration isolator. In order to study the performance of a nonlinear QZS vibration isolator on the multimodal elastic vibration of a continuous structure, dynamics and nonlinear isolation of the transverse vibration of a multi-span continuous beam bridge subjected to pier base vibrating excitation and moving mass are investigated in this thesis. It should be noted that although there are many works on bending vibrations and vibration isolation of beams containing linear elastic boundaries and supports [125–127], to the best of our knowledge, there are not many research papers on beams with nonlinear boundaries and supports [128–131]. Presently, there is a lack of methods for studying the bending vibration of beams with nonlinear supports. In addition, the dynamic response and the vibration isolation of a single span beam subjected to different kind of dynamic loads has drawn much research attention, but relatively little research has been done on the dynamics and vibration isolation of multi-span beams under base vibrating excitation. In order to study the performance of the nonlinear QZS vibration isolator on the multimodal elastic vibration of a continuous structure, the dynamics and nonlinear vibration isolation

of a multi-span continuous beam bridge are studied in this thesis.

1.7 Experimental studies of vehicle-excited bridge vibration

Experimental work is important for validating theoretical models and assessing the condition of real systems. Experimental results are often different from the results predicted by theoretical models. Model updating is usually adopted to tackle this problem [132]. The material properties and modal properties of a vehicle-bridge dynamic system are significant values to be determined by experiments in many cases. It is ideal to have the complete information of the whole system. However, this is hard to achieve in reality. In most cases, only partial information about a bridge or vehicles is available or can be measured. Therefore, it is necessary to study the identification problem from partial information of the whole system.

To assess the real structural or vehicular properties, field tests are to be carried out. However, field tests are expensive in terms of labour and equipment, and traffic control is often needed. These drawbacks can be overcome by doing laboratory experiments. It is ideal to carry out laboratory experiments especially when the main purpose of the experiments is to check a model or identification methods. In addition, the experimental conditions can be adjusted or controlled by experimental staff depending on the experimental purposes. The experimental work in the area of vehicle-bridge interaction is reviewed based on field tests and laboratory experiments in the following two subsections.

1.7.1 Field Experiments

To predict accurately the dynamical responses of a real vehicle-bridge system, it is of great significance to determine the actual geometric and material parameters of the system and to validate the theoretical models by experiments. In spite of the large amount of work dedicated to the theoretical study of the vehicle-bridge dynamic problem, much less experimental works have been reported in the literature.

Green and Cebon [133] identified the modal properties of a three-span highway bridge by impact tests on the bridge with an instrumented hammer. The wheel loads of a vehicle and the dynamic response of the bridge were measured simultaneously when the vehicle was travelling on the bridge by Green [134]. Kwark *et al.* [135] compared simulation results with experimental results of the dynamic response of a bridge crossed by a Korean high-speed train. Lee and Yhim [136] adopted the FE method to analyse the dynamic response of a two-span continuous box girder bridge subjected to moving forces. Liu *et al.* [3] measured the ambient vibration and high-speed train-induced vibration of a composite railway bridge with seven-spans to validate their train-bridge interaction model. Koziol [137] validated experimentally the wavelet-based approach of solving the infinite Euler-Bernoulli beam resting on a nonlinear foundation subjected to a set of moving forces for the train-track interaction problem.

To assess the bridge or the vehicle condition, various works have been done in order to identify the bridge or vehicle parameters by using different signal processing techniques or algorithms. Paultre *et al.* [138] evaluated the Dynamic Amplitude Factor (DAF) of three highway bridges in Canada by measuring the forced vibrations of the bridges excited by one or two trucks. Huang *et al.* [139] identified the modal properties of a three-span continuous bridge by impulse testing with impulsive forces generated from a loaded truck. The recorded data was processed by applying the Ibrahim time-domain identification technique.

The identified results were compared with those by ambient test. Gonzalez *et al.* [140] used the moving force model to estimate the critical speed and the DAF of the bridge by doing the field experiment of a truck passing over a simply supported bridge. Lee *et al.* [141] developed a moving cart system instrumented with an accelerometer, a microphone and an impact hammer to indirectly measure the Frequency Response Function (FRF) of structures. The cart system moves at a speed of 0.4 m/s and stops to measure the FRF of a foot bridge with the impact hammer as excitation in a field test.

1.7.2 Laboratory Experiments

Another way to study the train-bridge dynamics experimentally is conducting laboratory tests, which allow researchers a greater control of experimental conditions. Bilello *et al.* [142] validated the theoretical model of a beam subjected to a moving mass by experimental results. Stancioiu *et al.* [143] investigated the vibration of a fourspan continuous beam subjected to one or two rolling balls travelling at various speeds experimentally and theoretically (as a one-dimensional moving mass-beam model). Bian *et al.* [144] developed a computer-controlled sequential loading system to generate equivalent vertical loading on a ballastless high-speed railway sample by using actuators for simulating the dynamic excitation due to moving trains. One advantage of this method is that high train speeds, like a 360 km/h train speed, can be modelled in the lab.

Chan and Ashebo [145] identified the moving force between a travelling vehicle and a multi-span continuous beam by using the measured bending moment of the beam. Cerda *et al.* in 2012 compared an indirect approach of identifying the bridge damage (using the measured vehicular response) with a direct approach (using the measured bridge response) based on laboratory tests. McGetrick *et al.* [146] experimentally investigated the feasibility of identifying the global stiffness of a beam by using a passing vehicular response. Kim *et*

al. [147] utilized the subtracted responses of two connected travelling vehicles on a simply supported beam to reduce the effect of the surface roughness of the beam on identifying the beam's frequencies. A laboratory experiment was conducted to verify this approach and examine its feasibility.

1.8 Problems of the thesis

As seen above in literature review, over the years, dynamic and vibration isolation tests on highway bridges have been performed by many researchers and engineers. However, most of these tests are in-field tests. Lab-based dynamic and vibration isolation tests of full assemblage bridge models under a controlled environment are rather scanty. Regardless of whether the tests were performed on the field or in the laboratory, these tests were focused essentially on single bridges. Despite the existence of many bridges coupled on beds of several rivers, dynamic and vibration isolation tests on bridges coupled by their close environment are rarely performed. It is therefore of interest to investigate these coupled bridges from a dynamic test setting for a better understanding of the dynamics of coupled bridges on the one hand and to propose an effective vibration isolator to reduce their vibrations on the other hand. Furthermore, since the fundamental vibrational period of most bridges ranges from 0.2 to 1.2 second [11] and as failure induced by vibrations, often occur at a low excitation frequency, the need for low frequency isolators is imperative in the field of vibration isolation of bridges. The literature review above has shown that it is in the interest of both academia and industry to improve the performance of isolation mounts by using nonlinear stiffness elements.

The present thesis propose a dynamic test which aims at developing an enough complete descriptive theoretical model of indirect coupled bridges. After several dynamic tests

performed on a scale model built in the laboratory, a mathematical model of the device is then proposed. We analyze analytically and numerically the effectiveness of this model setting up. Because they can meet the needs of isolating low frequency vibration, even ultralow frequency vibration, nonlinear vibration isolators base on QZS mechanism have been used in this thesis for vibration isolation of two coupled bridges summited to different external excitations: firstly, to pier base vibrating excitation, and secondly to moving mass excitation.

1.9 Conclusion

This chapter has provided an overview of the dynamics and generalities, on beams bridges, soil-bridge interaction, and structural vibration control systems. We have also presented some essential works related to these topics. To analyse and to solve the problems of the thesis, one needs the use of some analytical and numerical methods, and experimental investigations. The next chapter will be devoted to these methods.

Chapter II

Methodology

2.1 Introduction

This chapter focuses on the different methods used along the thesis to solve the problems stated in the precedent chapter. Theoretical methods concerning both analytical and numerical methods are presented: Galerkin method for modal approximation of partial differential equations, Harmonic Balance (HB) method and method of multiple scales for analytical resolution of ordinary differential equations (ODEs), and fourth-order Runge- Kutta (RK4) method for numerical resolution. The experimental procedure is also presented for lab experiment.

2.2 Analytical and numerical methods

In general, exact analytical solutions of nonlinear differential equations rarely exist. Results are obtained either by numerical integration or with mathematical techniques that yield approximate closed-form expressions. However, the mathematical techniques needed for obtaining the approximate solution of nonlinear differential equations are not always straightforward and can be complex in nature. These analytical methods are presented in reference textbooks [148, 149] and Refs. [150–154] which contain sections dedicated to the topic. In this section, a brief recall of the most used techniques is provided, placing emphasis on the Galerkin method for modal approximation, HB method, method of multiple scales and RK4 method for numerical solutions of ODEs.

2.2.1 Galerkin method for modal approximation

In most engineering problems and bridge vibration problem in particular, a set of partial differential equations (PDEs) with boundary conditions are often derived as equations of motion. To solve the problem, one must find the solution function which satisfies the given

PDEs and boundary conditions. In reality, it is a difficult task, even impossible to solve the problem analytically. But in practical cases we often apply approximation methods. One of these approximation methods is the Galerkin method, proposed firstly by the russian mathematician Boris Grigoryevic Galerkin while working on the numerical solutions of the equations of the elastic equilibrium of rods and plates [155]. In this procedure, the solution of a partial derivative equation is assumed to be separable into amplitude and mode shapes (the mode shapes must satisfy the geometry and natural boundary conditions). As an example, the transverse displacement of a beam described by Eq. (1.6) with a given set of boundary conditions, can be written as

$$y\left(x,t\right)=\sum_{n=1}^{N_{\max}}\phi_{n}\left(x\right)q_{n}\left(t\right), \tag{2.1}$$

where $N_{\max}$ is an integer greater than 1, $q_n\left(t\right)$ is the amplitude of the nth mode of vibration and $\phi_n\left(x\right)$ are the mode shapes. These mode shape functions depend of the boundary conditions and are eigenfunctions of the governing equations, of uniform Euler-Bernoulli beam in absence of external excitation, obtained from Eq. (1.7) as follows

$$c^{2}\frac{\partial^{4}y}{\partial x^{4}}+\frac{\partial^{2}y}{\partial t^{2}}=0, \tag{2.2}$$

where

$$c=\sqrt{\frac{EI}{\rho S}}. \tag{2.3}$$

The free vibration solution can be obtained by inserting Eq. (2.1) into Eq. (2.2) and rearranging it as

$$\frac{c^{2}}{\phi_{n}\left(x\right)}\frac{\partial^{4}\phi_{n}\left(x\right)}{\partial x^{4}}=-\frac{1}{q_{n}\left(t\right)}\frac{\partial^{2}q_{n}\left(t\right)}{\partial t^{2}}=\omega_{n}^{2}, \tag{2.4}$$

where c is defined in Eq. (2.3) and ω_n^2 is defined as constant. Eq. (2.4) can be rearranged as two ordinary differential equations (ODEs) as

$$\frac{d^{4}\phi_{n}\left(x\right)}{dx^{4}}-\lambda_{n}^{4}\phi_{n}\left(x\right)=0, \tag{2.5}$$

$$\frac{d^2 q_n(t)}{dt^2} + \omega_n^2 q_n(t) = 0, \tag{2.6}$$

where

$$\lambda_n^4 = \frac{\omega_n^2}{c^2}. \tag{2.7}$$

The general solution of Eq. (2.5) is a mode shape, given by

$$\phi_n(x) = C_1 \cosh \lambda_n x + C_2 \sinh \lambda_n x + C_3 \cos \lambda_n x + C_4 \sin \lambda_n x. \tag{2.8}$$

The constants C_1, C_2, C_3 and C_4 can be found from the boundary conditions of the beam. Then, the natural frequencies of the beam are obtained from Eq. (2.7) as

$$\omega_n = \lambda_n^2 c. \tag{2.9}$$

Inserting Eq. (2.3) into Eq. (2.9) leads to

$$\omega_n = (\lambda_n L)^2 \sqrt{\frac{EI}{\rho S L^4}}. \tag{2.10}$$

For the simply-supported beam, the deflection and bending moment at both beam ends have to be zero, thus the boundary conditions are expressed as follows

$$y(0,t) = 0, y(L,t) = 0, y''(0,t) = 0, y''(L,t) = 0. \tag{2.11}$$

Substituting these boundary conditions into Eq. (2.8), we get the constants $C_1 = 0$, $C_2 = 0$, $C_3 = 0$ and $C_4 = 1$, and the eigenvalues given by

$$\lambda_n = \frac{n\pi}{L}. \tag{2.12}$$

Therefore, the eigenfunctions for a simply supported beam are obtained as

$$\phi_n(x) = \sin \frac{n\pi x}{L}, n = 1, 2, 3, ... \tag{2.13}$$

Then, the natural resonant frequencies of the beam are derived as

$$\omega_n = \left(\frac{n\pi}{L}\right)^2 \sqrt{\frac{EI}{\rho S}}. \tag{2.14}$$

The orthogonality condition of the mode shape functions can be written as

$$\int_0^L \phi_n(x)\,\phi_m(x)\,dx = \frac{L}{2}\delta_{nm}, \tag{2.15}$$

where δ_{nm} is the Heaviside function defined as

$$\delta_{nm} = \begin{cases} 1 & \text{for } n = m, \\ 0 & \text{for } n \neq m. \end{cases} \tag{2.16}$$

As previously stated, using Galerkin method, the transverse displacement of the beam (Eq. (2.1)) can be rewritten as

$$y(x,t) = \sum_{n=1}^{N_{\max}} q_n(t) \sin\frac{n\pi x}{L}. \tag{2.17}$$

In this approximative solution, the time functions $q_n(t)$ are determined by the modal equations which are obtained by substituting the transverse displacements (Eq. (2.17)) into the governing partial differential equations (PDEs) of the system. By applying the orthogonality property of the mode shape functions and with some mathematical calculations and arrangements, the modal equations can be obtained.

2.2.2 Harmonic Balance method

HB method is used to determine oscillatory solution of a linear or nonlinear ODE with a sinusoidal excitation. Indeed, let us consider the following equation

$$\ddot{y} + \Omega_0^2 y + f(t, y, \dot{y}) = F_0 \cos(\Omega t), \tag{2.18}$$

where y is the displacement, Ω_0 is the natural frequency of the system, F_0 and Ω are respectively the magnitude and frequency of the excitation force. The dot over y denotes differentiation with respect to time t and the function $f(t, y, \dot{y})$ depends explicitly on time.

The general approach when solving a differential equation using HB method is to assume that the solution has the form

$$y(t) = A\cos(\Omega t + \varphi), \tag{2.19}$$

where A and φ are unknowns amplitude and initial phase difference, respectively. Substituting Eq. (2.19) into Eq. (2.18) and equating the coefficients of equivalent harmonics, it is possible to obtain a system of two algebraic equations. The resolution of the obtained algebraic equations allows to deduce the characteristics A and φ of the oscillatory approximate solutions.

2.2.3 Method of multiple scales for ordinary differential equations

Let's Consider a nonlinear oscillator described by the equation of motion

$$\ddot{y} + \Omega_0^2 y = \varepsilon f\left(t, y, \dot{y}\right), \tag{2.20}$$

where ε is a dimensionless parameter, assumed to be small. The dot over y denotes differentiation with respect to time t and $f\left(t, y, \dot{y}\right)$ is a nonlinear function which can depends explicitly on time.

With the method of multiple scales, it is assumed that the solution of Eq. (2.20) depends on multiple independent variables (two in its simplest form). Accordingly, this solution is expressed in terms of different time scales as

$$y\left(t\right) = \sum_{m=0}^{\infty} \varepsilon^m y_m\left(t_0, t_1, ...\right) = y_0\left(t_0, t_1, ...\right) + \varepsilon y_1\left(t_0, t_1, ...\right) + ..., \tag{2.21}$$

where t_m represents different independent time scales given by

$$t_m = \varepsilon^m t, m = 0, 1, ... \tag{2.22}$$

There is a normal time scale $t_0 = t$, slow time scale $t_1 = \varepsilon t$, a super slow time scale $t_2 = \varepsilon^2 t$, etc. Thus,

$$\frac{d}{dt} = D_0 + \varepsilon D_1 + \ldots, \tag{2.23a}$$

$$\frac{d^2}{dt^2} = D_0^2 + 2\varepsilon D_0 D_1 + \ldots, \tag{2.23b}$$

where

$$D_m = \frac{\partial}{\partial t_m}, \text{ i.e. } \mathrm{D}_0 = \frac{\partial}{\partial \mathrm{t}_0} \text{ and } \mathrm{D}_1 = \frac{\partial}{\partial \mathrm{t}_1} \tag{2.24}$$

Substituting Eq. (2.21) into Eq. (2.20) and taking into account Eqs. (2.23) and (2.24), the following set of linear ordinary differential equations result

$$\varepsilon^0 : D_0^2 y_0 + \Omega_0^2 y_0 = 0, \tag{2.25a}$$

$$\varepsilon^1 : D_0^2 y_1 + \Omega_0^2 y_1 = -2 D_0 D_1 y_0 + f\left(y_0, D_0 y_0, t_0\right), \tag{2.25b}$$

et cetera.

The expansion gets more and more tedious with increasing order in ε. Let's carry this procedure out to first order in ε. At order ε^0,

$$y_0 = A\cos\left(\Omega_0 t_0 + \varphi\right), \tag{2.26}$$

where A and φ are arbitrary (at this point) functions of $\{t_1, t_2, ...\}$. Now we solve the next equation in the hierarchy, for y_1.

Let $\theta = \Omega_0 t_0 + \varphi$. Then $D_0 = \frac{\partial}{\partial t_0} = \Omega_0 \frac{\partial}{\partial \theta}$ and we have

$$D_0^2 y_1 + \Omega_0^2 y_1 = 2\Omega_0 \sin\theta D_1 A + 2A\Omega_0 \cos\theta D_1 \varphi + f\left(A\cos\theta, -A\sin\theta, t_0\right). \tag{2.27}$$

Since the arguments of f are periodic under $\theta \to \theta + 2\pi$, we may expand f in a Fourier series as

$$f(\theta) = f\left(A\cos\theta, -A\sin\theta, t_0\right) = \sum_{k=1}^{\infty} \alpha_k(A)\sin(k\theta) + \sum_{k=1}^{\infty} \beta_k(A)\cos(k\theta). \tag{2.28}$$

The inverse of this relation is

$$\alpha_k(A) = \frac{1}{\pi}\int_0^{2\pi} f(\theta)\sin(k\theta)\, d\theta \qquad (k > 0), \tag{2.29a}$$

$$\beta_0(A) = \frac{1}{2\pi}\int_0^{2\pi} f(\theta)\, d\theta, \tag{2.29b}$$

$$\beta_k(A) = \frac{1}{\pi}\int_0^{2\pi} f(\theta)\cos(k\theta)\, d\theta \qquad (k > 0). \tag{2.29c}$$

We now demand that the secular terms on the right-hand side (Eq. (2.27)) – those terms proportional to $\cos\theta$ and $\sin\theta$ – must vanish. This means

$$2\Omega_0 D_1 A + \alpha_1(A) = 0, \tag{2.30a}$$

$$2A\Omega_0 D_1\varphi + \beta_1(A) = 0. \tag{2.30b}$$

These two first order equations require two initial conditions, which is sensible since our initial equation $\ddot{y} + \Omega_0^2 y = \varepsilon f(y, \dot{y}, t)$ is second order in time. With the secular terms eliminated, we may obtain y_1 as follows

$$y_1 = \sum_{k\neq 1}^{\infty} \left\{ \frac{\alpha_k(A)}{1-k^2}\sin(k\theta) + \frac{\beta_k(A)}{1-k^2}\cos(k\theta) \right\} + B_0\cos\theta + C_0\sin\theta, \tag{2.31}$$

the constants B_0 and C_0 are arbitrary functions of t_1, t_2, etc..

The equations for A and φ (Eqs. (2.30)) are both first-order in t_1. They will therefore involve two constants of integration – call them A_0 and φ_0. At second order, these constants are taken as dependent upon the super slow time scale t_2. The method itself may break down at this order.

2.2.4 Numerical methods: fourth-order Runge-Kutta method

An ODE is solved analytically considering some assumption to obtain approximate solutions. In contrast, a numerical method proposes solutions which are closed with the experiment. In this thesis, RK4 is used for numerical resolution of ODEs. Fortran 90, with Matlab software language are also used as programming languages. RK4 method has been elaborated for the first time in 1894 by Carle Runge and has been improved by Martin W. Kutta in 1901. This method is widely used because of its stability. It combines trapezium numerical integration and Simpson methods. Let us consider the first-order ODE as

$$\frac{dy}{dt} = f(t, y), \tag{2.32}$$

with the initial condition $y(t_0) = y_0$.

The aim of the RK4 method is to find solutions after each time step h i.e. to determine the point $(t+h; y(t+h))$ knowing the point $(t; y(t))$. This method establishes the following relations:

$$y(t+h) = y(t) + \frac{1}{6}(L_1 + 2L_2 + 2L_3 + L_4), \tag{2.33}$$

where

$L_1 = hf(t, y(t))$,

$L_2 = hf\left(t + \frac{h}{2}, y(t) + \frac{L_1}{2}\right)$,

$L_3 = hf\left(t + \frac{h}{2}, y(t) + \frac{L_2}{2}\right)$ and

$L_4 = hf(t + h, y(t) + L_3)$.

This procedure needs in its iteration only the initial value y_0, to calculate all the other values taken by the function y at other times separated by the time step h.

In the case of second-order differential equation

$$\begin{cases} \frac{d^2y}{dt^2} = f\left(t, y, \frac{dy}{dt}\right) \\ y(t_0) = y_0, \quad \frac{dy}{dt}\big|_{t=t_0} = y_0^{(1)} \end{cases}, \tag{2.34}$$

it can be divided in order to obtain two first order equations. With variables change, let's consider Eq. (2.34) under the following form

$$\begin{cases} \frac{dy}{dt} = z \\ \frac{dz}{dt} = f(t, y, z) \\ y(t_0) = y_0, \quad z(t_0) = z_0 \end{cases}, \tag{2.35}$$

The RK4 iterations are given by the following equation

$$\begin{cases} y(t+h) = y(t) + \frac{1}{6}(L_1 + 2L_2 + 2L_3 + L_4) \\ z(t+h) = z(t) + \frac{1}{6}(K_1 + 2K_2 + 2K_3 + K_4) \end{cases}, \tag{2.36}$$

where $L_1 = hz(t)$,

$K_1 = hf(t, y, z)$,

$L_2 = h\left(z\left(t\right) + \frac{K_1}{2}\right),$

$K_2 = hf\left(t + \frac{h}{2}, y\left(t\right) + \frac{L_1}{2}, z\left(t\right) + \frac{K_1}{2}\right),$

$L_3 = h\left(z\left(t\right) + \frac{K_2}{2}\right),$

$K_3 = hf\left(t + \frac{h}{2}, y\left(t\right) + \frac{L_2}{2}, z\left(t\right) + \frac{K_2}{2}\right),$

$L_4 = h\left(z\left(t\right) + K_3\right)$ and

$K_4 = hf\left(t + \frac{h}{2}, y\left(t\right) + L_3, z\left(t\right) + K_3\right).$

This generalized form can also serve to solve numerically second-order coupled ODEs.

2.3 Method for an experimental test in lab

An experimental work is important for validating theoretical models and assessing the condition of real systems. Experimental results are often different from predicted results by theoretical models. The experimental method, applied to a model of two coupled beam bridges subjected to a vibrating universal motor is presented in this section. Firstly, the techniques of measuring transverse vibrations of each beam bridge are given. Then, the method of analyzing vibrating data is also presented. The transverse vibrations of coupled beam bridges are sensed by DE-ACCM2G accelerometers incorporated to the structure and then processed by Matlab software. Let's note that the DE-ACCM2G Buffered ±2g Accelerometer shown in Fig. 2.1 is an off the shelf 2 axis 2g accelerometer solution with analog outputs. It features integrated op amp buffers for direct connection to a microcontroller's analog inputs, or for driving heavier loads.

Some applications of DE-ACCM2G accelerometer concern motion, tilt and slope measurement, shock sensing and vehicle acceleration logging. To measure acceleration, the accelerometer can be mounted in one of the configurations shown in Fig. 2.2 and the procedure for determining the value of the acceleration is described below. The voltage outputs on the

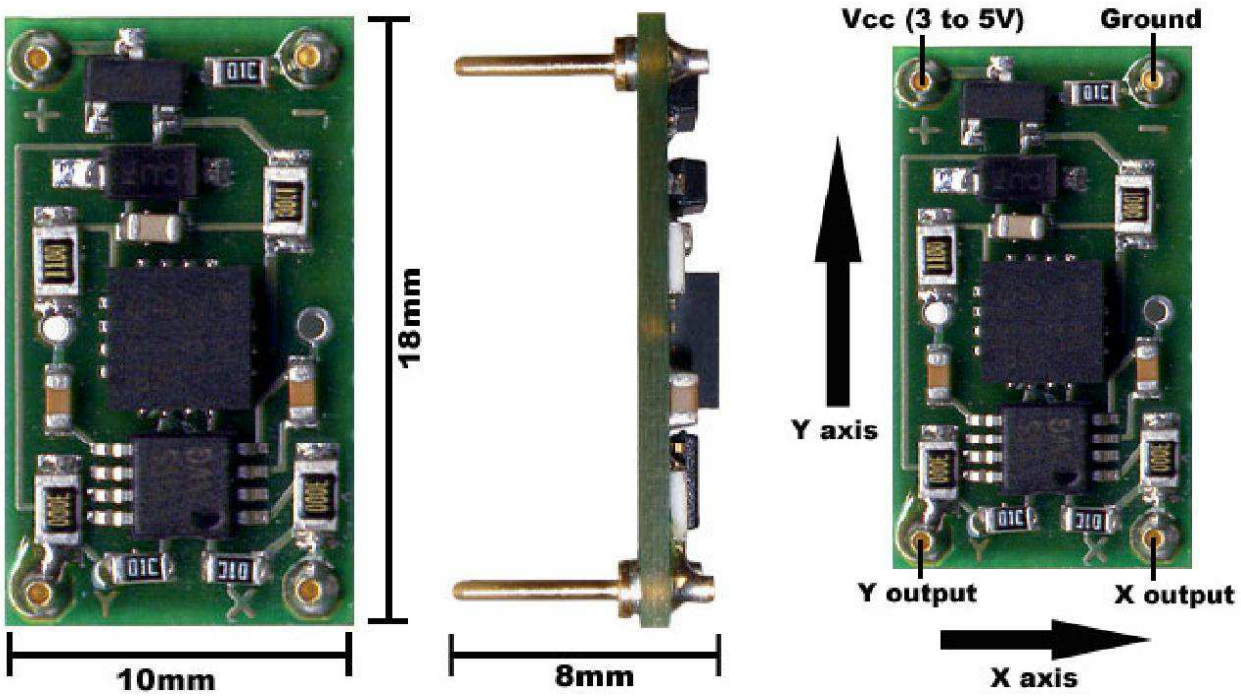

Figure 2.1: Different views of DE-ACCM2G accelerometer

DE-ACCM2G correspond to acceleration being experienced in the X and Y directions. The output is ratiometric, so the output sensitivity (in mV/g) will depend on the supply voltage. When supplied with 5 V, sensitivity is typically 750 mV/g. At 3 V, sensitivity drops to 420 mV/g. Zero acceleration (0 g) will result in an output of $V_{CC}/2$ regardless of the voltage supplied to the unit.

For example, with a 3 V supply, if the X output reads 1.92 V as obtained in the last configuration of Fig. 2.2, the corresponding value of acceleration is obtain as follows.

At 3 V, the 0 g point is approximately $V_{CC}/2 = 3.00/2 = 1.50$ V

1.92 V − 1.50 V = +0.42 V with respect to the 0 g point.

At 3 V, as the sensitivity is 420 mV/g, so the corresponding acceleration is $0.42/0.420 = 1.00$ g. Therefore, the acceleration in the X direction is +1 g i.e. +9.8 m/s^2 if g = 9.8 m/s^2 for example.

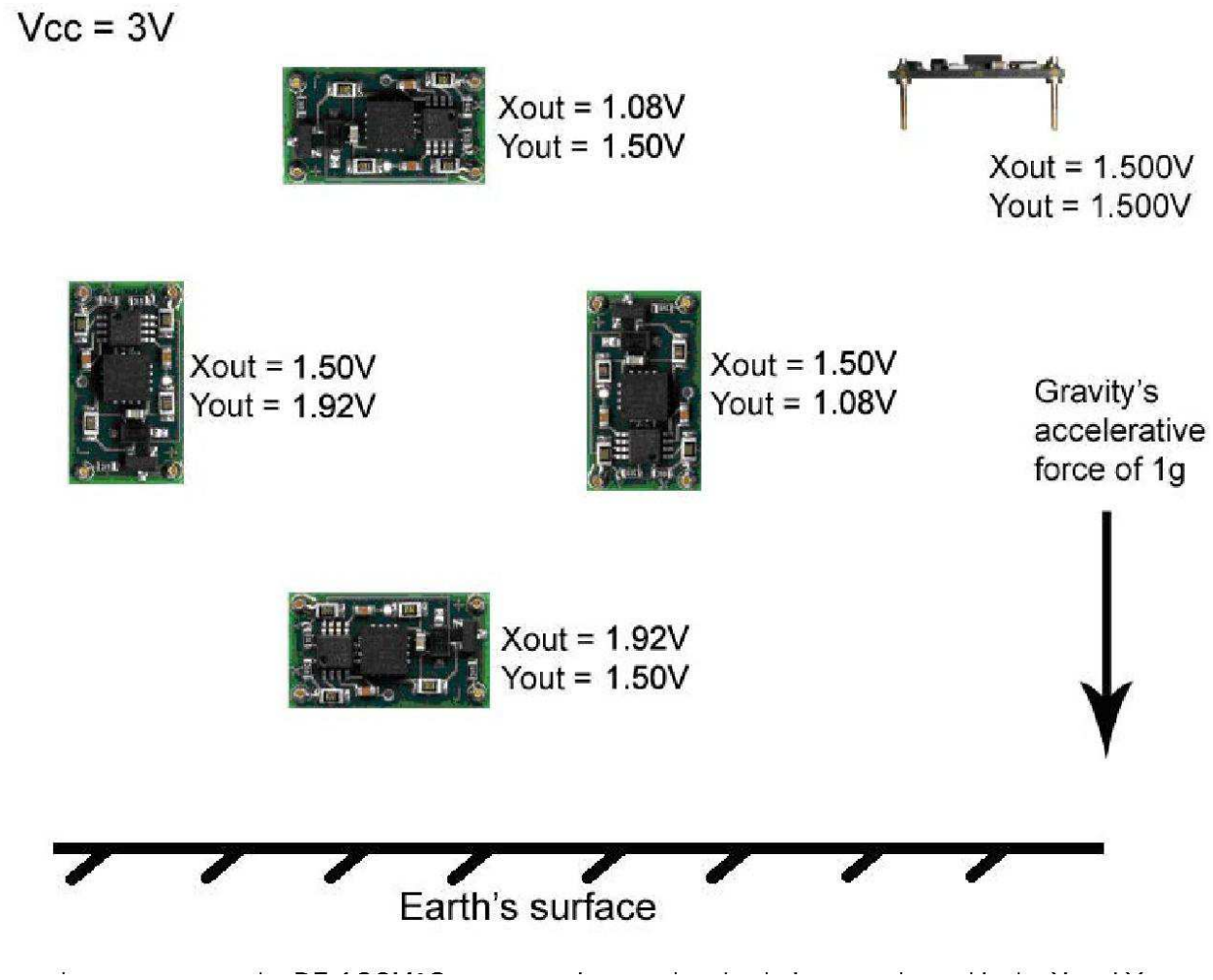

Figure 2.2: Use of DE-ACCM2G accelerometer for the measurement of accelerations

The higher the sensitivity, the greater the change in the output signal. Reading such a signal is easier and more precise. It is for this reason that during our laboratory experiment, the sensitivity selected was 750 mV/g, corresponding to the supply voltage of 5 V. An example of the analog outputs obtained by the digital oscilloscope is given in Fig. 2.3. Time/div and Volt/div controls of the digital oscilloscope are set as 10 ms/div and 30 mV/div, respectively.

The output voltage curves are obtained, one in the absence of vibrations making it possible to determine the 0 g point which is located in the middle of the oscillogram (Fig. 2.3(a)) and the other in the presence of vibrations making it possible to determine the

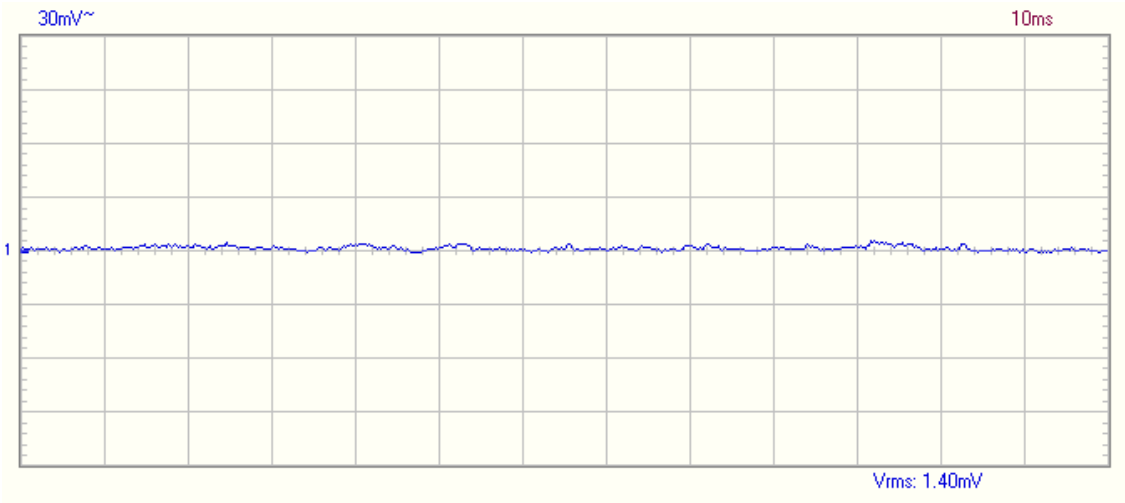

(a) motor supplied at the voltage $U = 0$ V

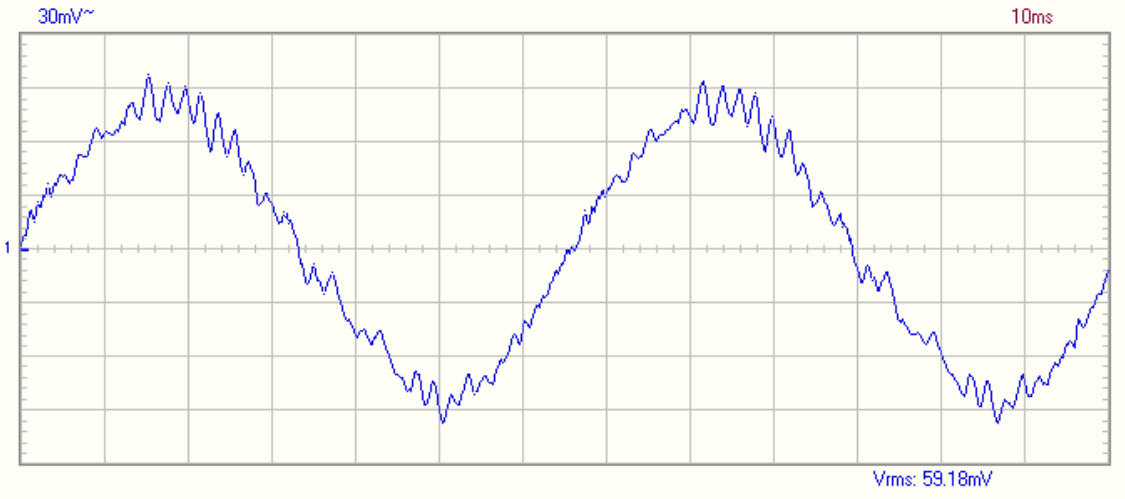

(b) motor supplied at the voltage $U = 23$ V

Figure 2.3: Digital oscilloscope screenshots of transversal acceleration of a beam bridge subjected to motor excitation

transverse acceleration of the beam bridge at any time (Fig. 2.3(b)). The experimental data collected and viewed using a digital oscilloscope through the curves in Fig. 2.3 can also be processed in Matlab software. The curves obtained are shown in Fig. 2.4.

The curves of Fig. 2.4 are plotted with the calibrations below, given by the digital oscilloscope.

Time step: 125 pt. = 10 ms

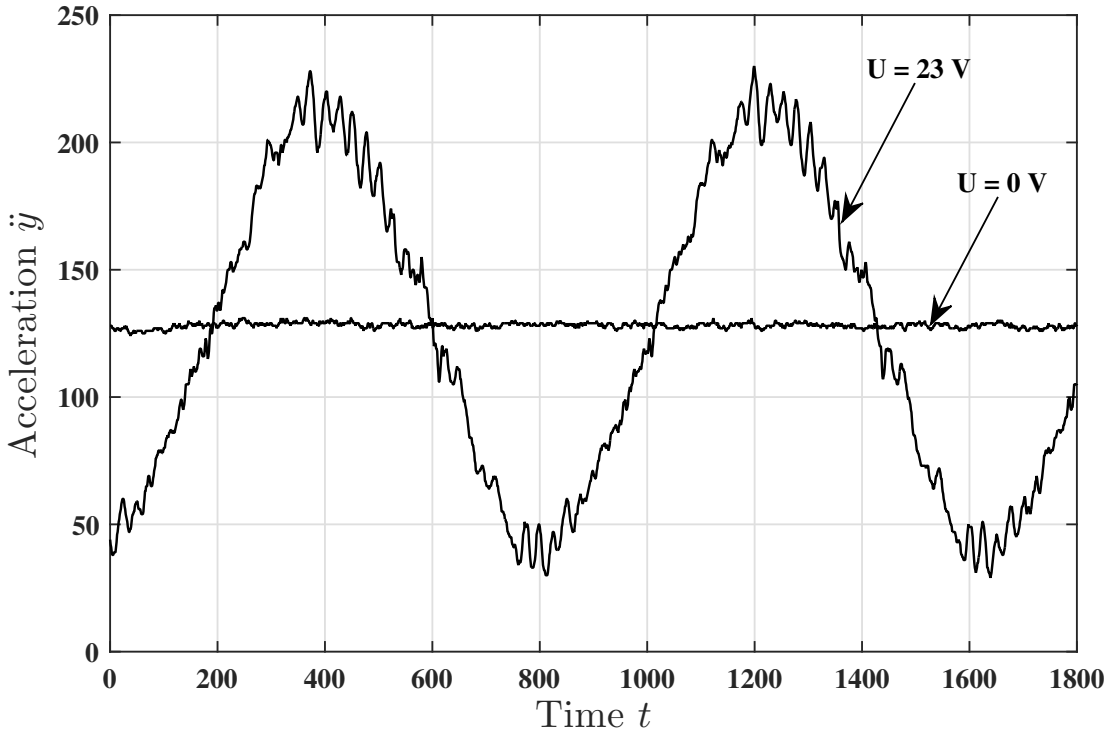

Figure 2.4: Transversal acceleration of a beam bridge subjected to motor excitation supplied at the voltage $U = 0$ V and $U = 23$ V, plotted in Matlab software

Voltage step:

CH1: 32 pt. = 30 mV

GND: 128 pt.

CH1 Y-position low: 32 pt.

CH1 Y-position mid: 127 pt.

CH1 Y-position high: 224 pt.

All these calibrations then make it possible to determine the true values of the physical quantities on each axis as follows:

- **For accelerations**

  The 0 g point is CH1 Y-position mid i.e. 127 pt.

  If the Matlab plot output voltage is N_a pt., the voltage corresponding to acceleration

is $(N_a - 127)$ pt. with respect to the 0 g point. As the voltage step is such that 32 pt. = 30 mV, the voltage corresponding to acceleration is $(N_a - 127) \times \frac{30}{32}$ mV. As the sensitivity is 750 mV/g, so the corresponding acceleration is $(N_a - 127) \times \frac{30}{32 \times 750}$ g. Therefore, the acceleration is $\ddot{y} = (N_a - 127) \times 1.25 \times 10^{-3}$ g.

- **For times**

The time step is such that 125 pt. = 10 ms.

If the Matlab plot output time is N_t pt., the corresponding time is $N_t \times \frac{10 \times 10^{-3}}{125}$ s. Therefore, the time is $t = N_t \times 8.00 \times 10^{-5}$ s.

Since the vibrations of the beam bridge are almost sinusoidal with regard to the different curves obtained, the transverse displacement of the beam would be proportional to its acceleration as follows $\ddot{y} = -\omega y$, where ω is the vibration frequency of the beam bridge.

2.4 Mechanical model of QZS vibration isolator and transmissibility of vibrations

2.4.1 Mathematical modelling of the QZS mechanism

The QZS mechanism under consideration is schematically shown in Figs. 1.19 and 2.5, where the device to be isolated is not included. The system comprises a vertical spring with linear stiffness k_v which is connected at point P with two linear springs with identical stiffness k_0 and initial length L_0 mounted obliquely. The two springs are initially inclined with a slope of an angle θ_0 from the horizontal plane and hinged at points M and N respectively. Consider a loading force f at point P downwards. The loading point P is initially located at height h_0 above the points M, N and a horizontal distance a_0 apart from these points respectively. It is assumed that $L_0 \geq a_0$. The application of the force f causes a vertical displacement Y_0 and

when the system is loaded with a suitably force, the springs are compressed from the initial unloaded position P to the equilibrium position O where the oblique springs are compressed in the horizontal position and the static load is only supported by the vertical spring as shown in Fig. 2.6. When k_v and k_0 match, the positive stiffness of the vertical spring and negative stiffness formed by the oblique springs will cancel with each other to achieve zero stiffness at the equilibrium position. In this way the system is developed into a QZS system.

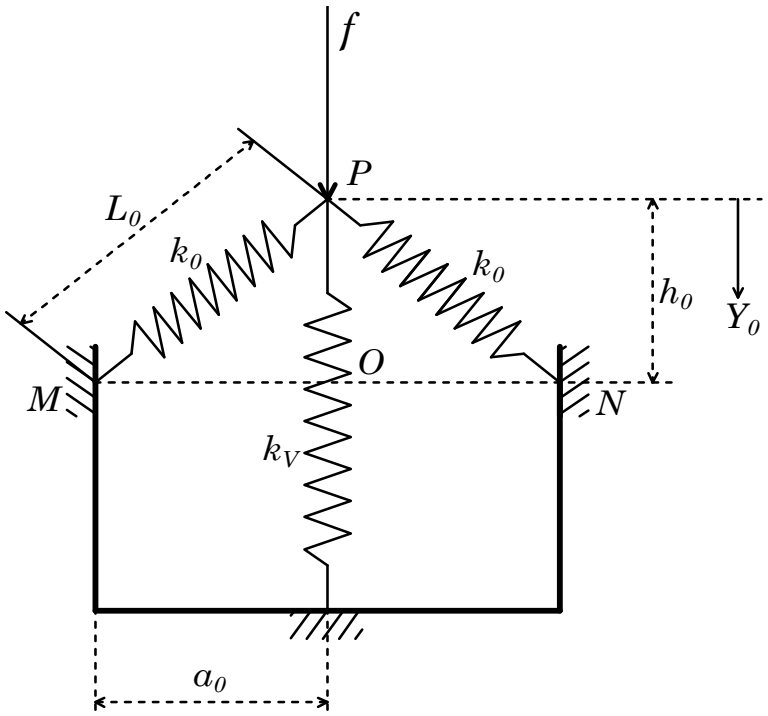

Figure 2.5: Schematic representation of an isolator with QZS characteristic

The geometry of the system is defined by the parameters a_0 and h_0. Provided the coordinate Y_0 defines the displacement from the initial unloaded position, a loading force f given by the following equation, leads to a resulting displacement Y_0 [14, 108, 156]

$$f = f_v + f_0, \tag{2.37}$$

where the term f_v denotes the contribution from the vertical spring and the term f_0 denotes

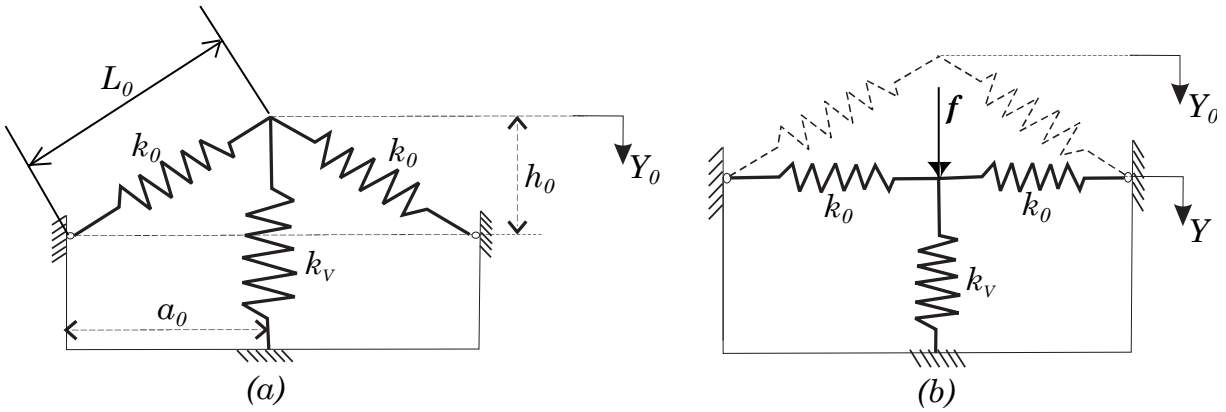

Figure 2.6: QZS system with 3 springs: (a) unloaded condition; (b) loaded with a tuned mass m so that at the static equilibrium position the oblique springs lie horizontal

the contribution from the two oblique springs given as follows

$$f_v = k_v Y_0, \tag{2.38}$$

and

$$f_0 = 2k_0 \left(L_0 - L\right) \sin\theta_0, \tag{2.39}$$

where $\sin\theta_0 = \frac{(h_0 - Y_0)}{L}$. It should be noticed that when $\theta_0 = 0$ the springs lie horizontally and do not exert any vertical force, i.e. $f_0 = 0$. Thus, the force-displacement relationship can be rewritten as

$$f_0 = 2k_0 \left(h_0 - Y_0\right) \left(\frac{L_0}{L} - 1\right). \tag{2.40}$$

From Fig. 2.5 it can also be seen that

$$L = \sqrt{a_0^2 + \left(h_0 - Y_0\right)^2}. \tag{2.41}$$

Combining Eq. (2.40) with Eq. (2.41) gives

$$f_0 = 2k_0 \left(h_0 - Y_0\right) \left(\frac{L_0}{\sqrt{a_0^2 + \left(h_0 - Y_0\right)^2}} - 1\right). \tag{2.42}$$

If the variable Y defines the downward displacement of the slider from the equilibrium position, when the oblique springs are placed horizontally after applying the loading force

f, Eq. (2.37) can be rewritten as

$$f = k_v Y - 2k_0 Y\left(\frac{L_0}{\sqrt{a_0^2 + Y^2}} - 1\right) + k_v h_0. \tag{2.43}$$

For clarity of analysis, the following non-dimensional parameters are introduced

$$y = Y/L_0, a = a_0/L_0 = \cos\theta_0, h = h_0/L_0, \alpha = k_0/k_v, F = \frac{f}{k_v L_0} - h = \left(\frac{f}{k_v} - h_0\right)\Big/ L_0. \tag{2.44}$$

so that Eq. (2.43) can be recast in its non-dimensional form as

$$F = y - 2\alpha y\left(\frac{1}{\sqrt{a^2 + y^2}} - 1\right). \tag{2.45}$$

According to the definition of stiffness, differentiating Eq. (2.45) with respect to y gives the non-dimensional stiffness of the QZS system as

$$K = 1 + 2\alpha\left(1 - \frac{a^2}{\left(a^2 + y^2\right)^{3/2}}\right). \tag{2.46}$$

Substituting zero for y and setting Eq. (2.46) equal to zero, we derive the condition for zero stiffness as

$$\alpha_{QZS} = \frac{a}{2\left(1 - a\right)} = \frac{\cos\theta_0}{2\left(1 - \cos\theta_0\right)}. \tag{2.47}$$

The parameter α denotes the stiffness ratio and α_{QZS} denotes the geometric ratio. When α_{QZS} and α are equal, zero stiffness is achieved [156].

The non-dimensional force and the non-dimensional stiffness as functions of the non-dimensional displacement respectively are plotted in Fig.2.7 for different values of the stiffness ratio α and when $a = 0.67$.

From Fig. 2.7, it can be seen that if the stiffness ratio and the geometric ratio are equal ($\alpha = \alpha_{QZS}$), zero stiffness can be achieved at the static equilibrium position. In this case, the negative stiffness provided by the oblique springs exactly counteracts the positive stiffness of the vertical spring in the vertical direction, and as a result, the system is developed into

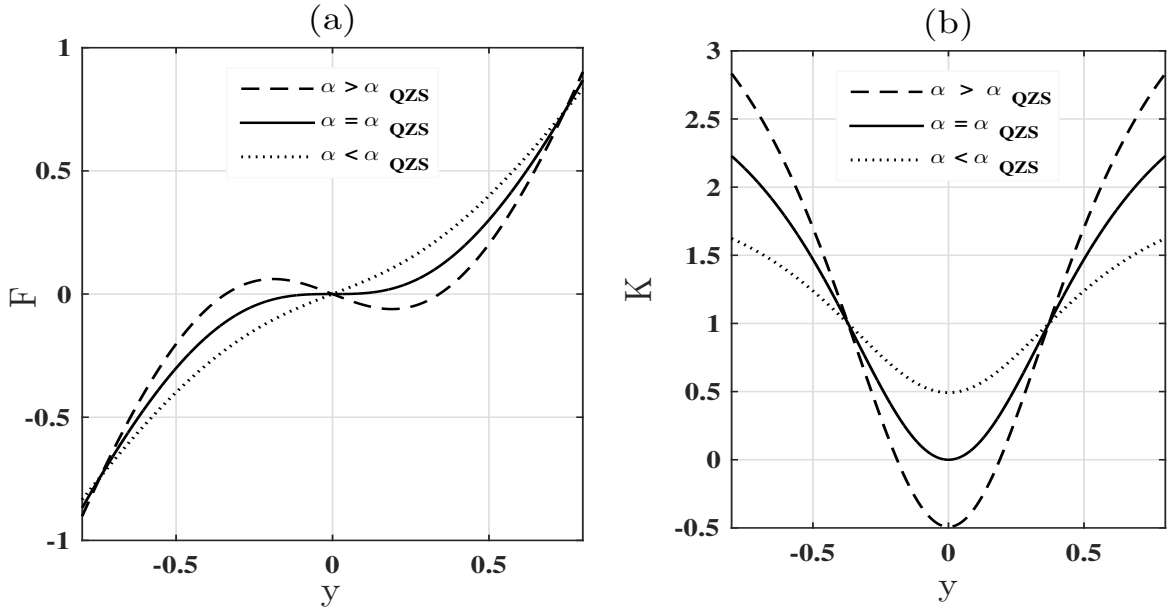

Figure 2.7: (a) Force-displacement characteristic and (b) non-dimensional stiffness of the system when $a = 0.67$

a QZS system. When $\alpha < \alpha_{QZS}$, the system has a weakly nonlinear characteristic and its combined stiffness is positive; otherwise when $\alpha > \alpha_{QZS}$, the stiffness of the oblique springs dominates and as a result the combined stiffness of the system is always negative in the neighborhood of the static equilibrium position.

From Fig. 2.7(a), it can also be seen that the relationship between force and displacement given in Eq. (2.45) is similar to that of a cubic function [14,156]. Therefore, to simplify subsequent dynamic analysis of the QZS system, an approximate cubic expression of the force is sought using a Taylor series expansion at the static equilibrium position $y = 0$ as

$$F(y) \approx F(0) + \sum_{n=1}^{3} \frac{F^n(0)}{n!} y^n = \frac{\alpha_{QZS}}{a^3} y^3. \tag{2.48}$$

Differentiating Eq. (2.48) with respect to y gives an approximate expression for the stiffness as

$$K \approx \frac{3\alpha_{QZS}}{a^3} y^2. \tag{2.49}$$

The approximations defined by Eqs. (2.48) and (2.49) are plotted in Fig. 2.8 in comparison

with the exact expressions. It can be seen (Fig. 2.8(b)) that the QZS system has a very small stiffness in the neighborhood of the static equilibrium position. Furthermore, there is a very good correlation between the exact curves and the approximate curves for relatively small displacements from the equilibrium position ($\pm$ 0.2 excursion range). Clearly, higher amplitudes of oscillation would invalidate the approximation of the cubic force and the quadratic stiffness [14].

Let's consider this approximation of a QZS system modelling in motion modelling of the dynamics of a beam bridge under QZS vibration isolators driven by a pier base harmonic vibrating displacement.

2.4.2 Experimental set up of the QZS vibration isolator

Based on QZS mechanism, QZS isolator is built up as shown in Fig. 2.9, where the QZS system is parallel connected with a viscous damper with damping coefficient C and used for vibration isolation of a beam bridge.

The approximate expression of the external force due to a QZS vibration isolator is obtained from Eqs. (2.48) and (2.44) as follows

$$F_{QZS} = -C\frac{\partial Y}{\partial T} - \frac{\alpha_{QZS}}{a_0^3}k_v L_0 Y^3. \tag{2.50}$$

where α_{QZS} is the geometric ratio of the QZS vibration isolator defined as

$$\alpha_{QZS} = \frac{a_0}{2\left(L_0 - a_0\right)}. \tag{2.51}$$

2.4.3 Transmissibility of vibrations

The vibration isolation performance of an isolation system is often quantified by the vibration transmissibility of the isolator. It is the function characterizing the transmissibility in the frequency domain, and is sometimes referred to as isolator transfer function in some

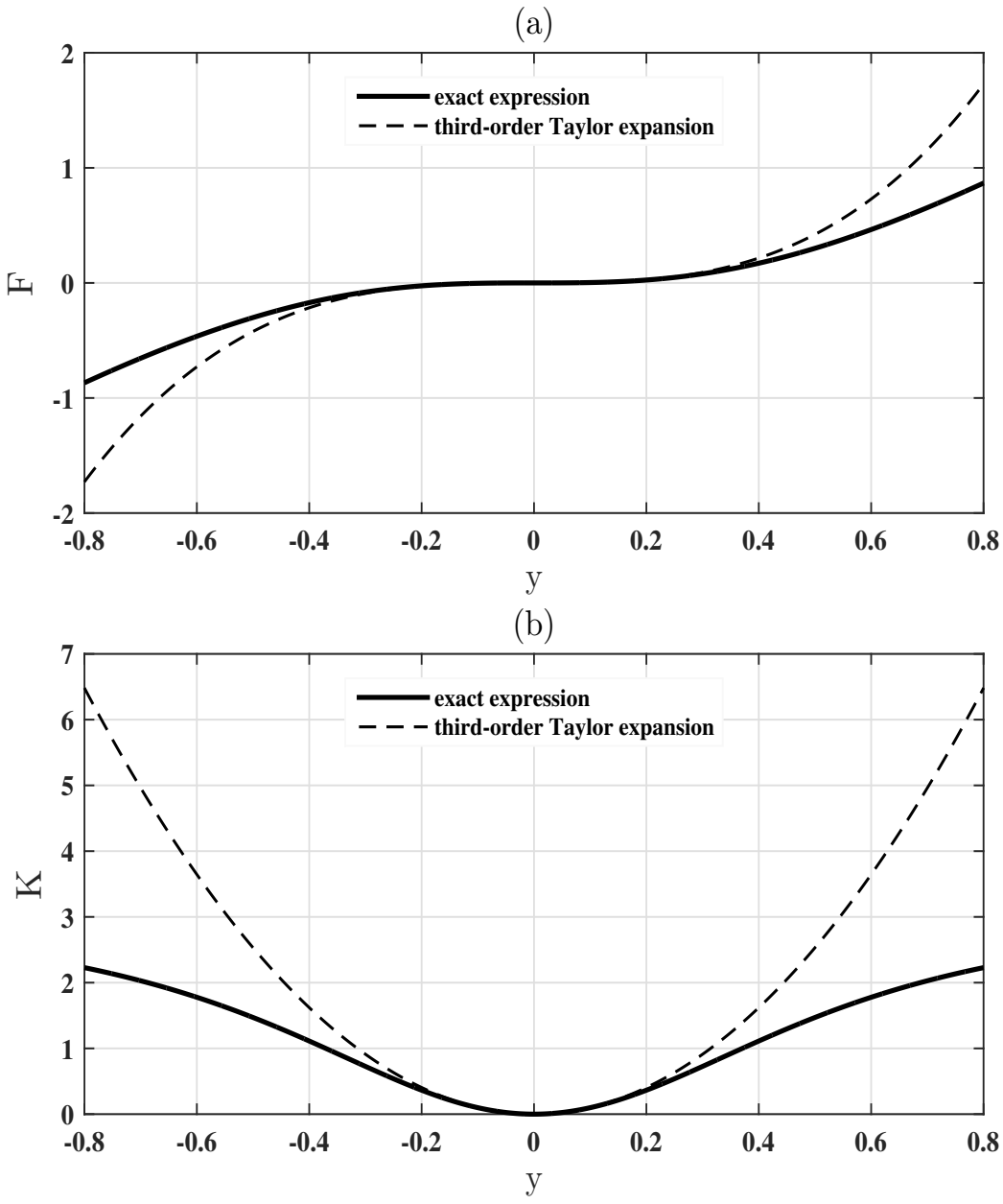

Figure 2.8: Non-dimensional (a) force-displacement characteristic and (b) stiffness of the quasi-zero-stiffness system when $a = 0.67$

contexts. In general, the vibration transmissibility is the ratio between the input and output of a vibration isolation system. It can be categorized into two types, force transmissibility and motion transmissibility. The force transmissibility is defined as the absolute value of the ratio of the excitation force to the transmitted force. The absolute motion transmissibility is

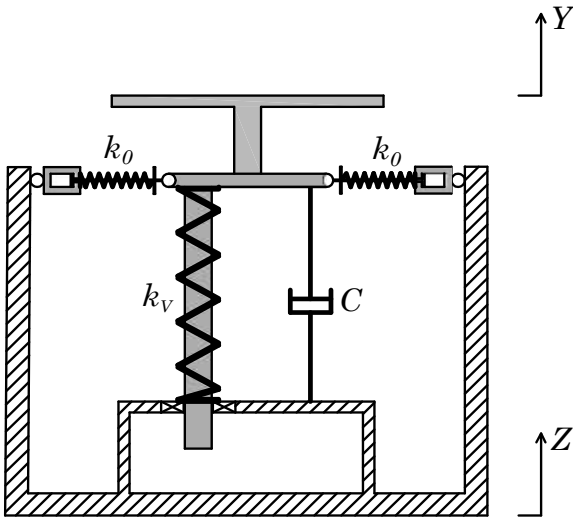

Figure 2.9: Schematic of the dynamic model of the QZS vibration isolator

defined as the absolute value of the ratio of the excitation displacement to the transmitted displacement.

The concept can better be described by a SDOF system in Fig. 2.10. A mass m is suspended on a parallel combination of a spring of coefficient k_l and a dashpot c (which are both considered massless). There are two different problems related to the transmission of vibration from a source to a receiver. In one case, the mass is directly excited by a force f_e, and therefore acts as the source of the disturbance. The objective of a vibration isolator is then to reduce the force f_t transmitted to the base, which is the receiver. In the other situation, the disturbance comes from the motion z of the base (source), in which case the purpose of the isolator is to reduce the motion x of the mass (receiver), attached to the vibrating base. Either way, the vibration isolator that separates the source and the receiver can be schematised with a spring and a dashpot connected in parallel. In order to minimise the level of the transmitted vibrations without the intervention of external forces (i.e. passive isolation), these two elements should be opportunely chosen.

The expressions for the absolute force and motion transmissibilities are given by Eqs.

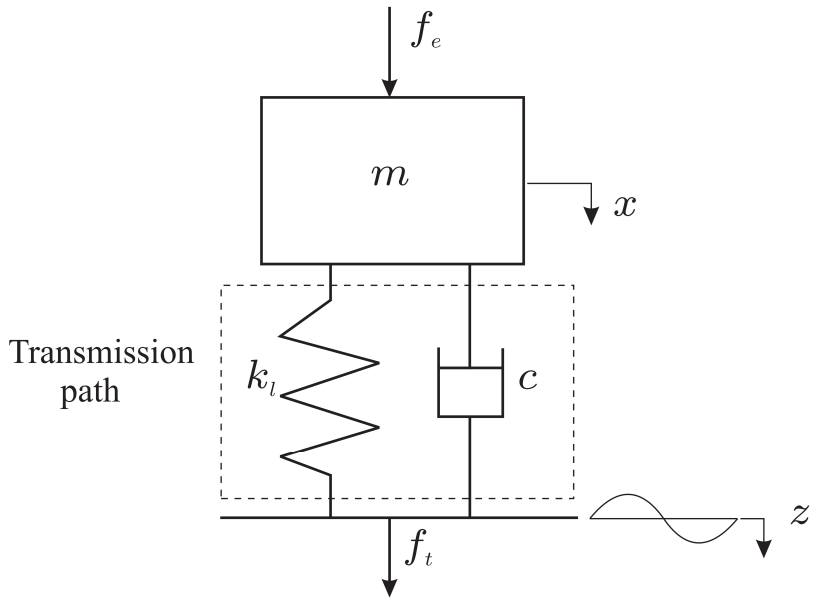

Figure 2.10: SDOF vibration isolator model: the transmission of vibration from a source to a receiver through the spring k_l and the dashpot c which constitute the transmission path

(2.52) and (2.53), respectively

$$T_F = \frac{|f_e|}{|f_t|}, \tag{2.52}$$

$$T_M = \frac{|x|}{|z|}. \tag{2.53}$$

The transmissibilities in decibels can also be defined as

$$T_F\,(\mathrm{dB}) = 20 \cdot \log\left(\frac{|f_e|}{|f_t|}\right), \tag{2.54}$$

$$T_M\,(\mathrm{dB}) = 20 \cdot \log\left(\frac{|x|}{|z|}\right). \tag{2.55}$$

For example, in the case of an isolator dedicated to the attenuation of ground vibration, the force transmissibility is described as the ratio between the magnitude of the transmitted and the base excitation forces at a given frequency, and the motion transmissibility is defined as the ratio between the motion intensity of the payload vibration and the ground vibration. Clarence [157] has demonstrated that for a linear system, both the forces and the motion transmissibilities are equivalent due to the reciprocity characteristics in linear systems and

therefore it is sufficient to consider only one of them. However, this is not the case for a nonlinear system. In the work presented in this thesis, due to the relative simplicity of measuring payload motions, the performance of a QZS isolator is characterized using motion transmissibility.

The evaluation of the vibration isolation performance normally includes (but is not limited to) assessing the three key aspects of the transmissibility curve which are the resonance frequency, the 0 dB cross over and the peak response. The resonance frequency represents the frequency at which the maximum displacement (the peak response $x_{\max}$ or the peak transmissibility $T_{F\max}$) of the payload occurs. For a linear system, this resonance frequency occurs approximatively at the natural frequency. The 0 dB cross over frequency is the marginal frequency where the payload and the base have the same motion amplitudes. In other words, it is the frequency at which the isolation begins, the frequency above which $T_M < 1$ (or $T_M\,(\text{dB}) < 0$ dB). The isolation system starts to attenuate vibration beyond this frequency and the attenuation increases at certain rates depending of the characteristics of the isolator. The value of the 0 dB cross over frequency is directly related to the resonance frequency. An increase in the resonance frequency will result in an increase in the 0 dB cross over frequency, and vice versa. Since vibration attenuation is only achieved beyond the 0 dB cross over frequency, it is generally desirable to have low isolator resonance frequency (and thus 0 dB cross over frequency) so that vibration attenuation is achieved from the lowest possible frequency.

2.5 Conclusion

The present chapter has been devoted to the presentation of mathematical, numerical and experimental methods used for the analysis of the problem of this thesis. These solving

methods and experimental techniques will be used in chapter 3 to:

- transform the partial differential equations to ordinary differential equations;
- validate our modelling by comparing some results by both methods;
- predict the behaviour of the system while varying some parameters of the system.

Chapter III

Results and Discussion

3.1 Introduction

This chapter is devoted to the results and discussions on the work carried out in this thesis. It is therefore organized as follows. In the second section, theoretical and experimental investigations of the dynamics of a model of two multi-span continuous beam bridges model coupled by their close environment and subjected to different external excitations are carried out. The third section focusses on the isolation performance of QZS vibration isolators in vibration isolation of a multi-span continuous beam bridge under pier base vibrating excitation. The fourth section deals with the vibration isolation of a multi-span continuous beam bridge under a moving mass using QZS vibration isolators. The last section concludes the chapter.

3.2 Dynamics of two multi-span continuous beam bridges model coupled by their close environment

3.2.1 Experimental set up

The real structure whose model is mounted in laboratory is the one from the two bridges built on the Wouri river in Cameroon. For simplifying reasons, the two bridges have been considered identical in this study and to the dimensions of the second newly built. This newly built bridge is a five-lane road seven-span continuous bridge of 820 m long and 25.6 m wide [8] as shown in Fig. 3.1. The experimental device simulating the dynamics of the two bridges indirectly coupled by their close environment via their piers is shown in Fig. 3.2. On one of these bridge call bridge 1 is exerted a localized combination of sinusoidal and periodic impulsive loads. The coupled bridges model of the experimental device consists of two wooden beams designed to scale E = 1: 546.6 of the real second bridge over the Wouri

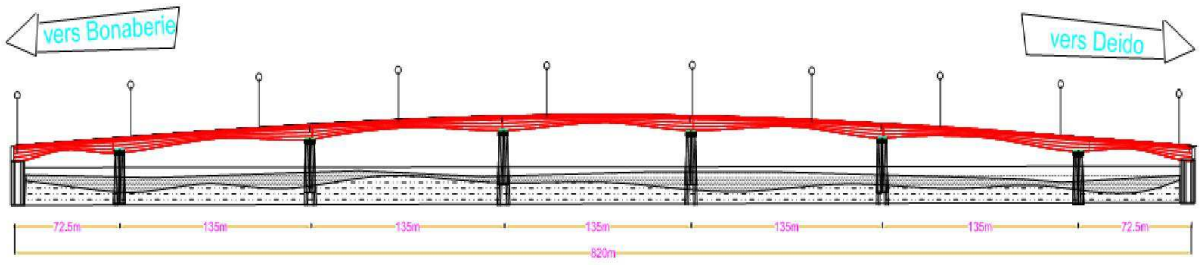

Figure 3.1: A long view of the second bridge over the Wouri river [8]

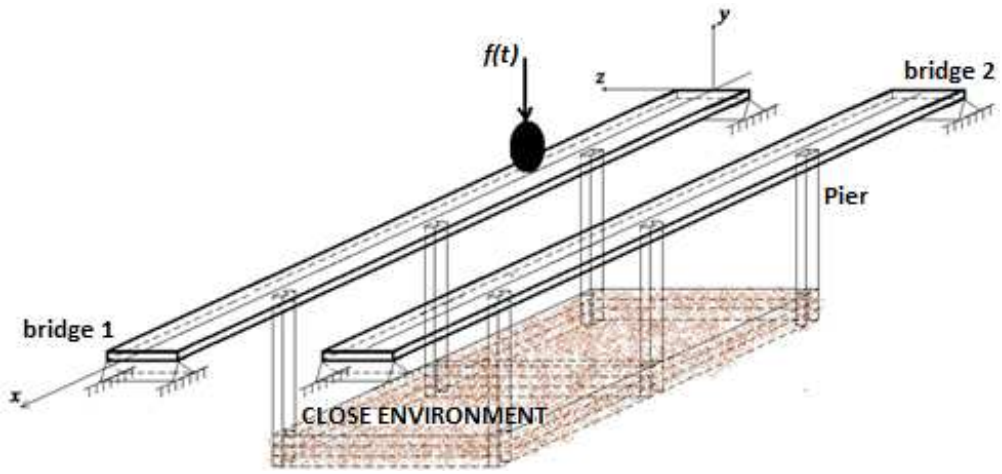

Figure 3.2: Schematic of the experimental device

river. Their dimensions are compiled in the Table 3.1 and the photographs of the model and the model structural elements are given in Figs. 3.3 and Fig. 3.4, respectively.

In the scale model, the two bridges are represented by two wooden beam bridges of dimensions specified in the Table 3.1. In addition, a polyurethane (PU) mattress (see Fig. 3.4) is the most available material we could find to play the role of the close environment, given its good viscoelastic properties; and an universal motor attached to one of the beam bridges (bridge 1) imposes its vibrations on it in the form of both sinusoidal and periodic impulsive loads. Vibrations are sensed by DE-ACCM2G accelerometers incorporated to the

Table 3.1: Dimensions of the experimental set up elements

	Real bridge	Model
Length	820 m	1,5 m
Height	25,6 m	45 mm
Width	4 - 7,5 m	12 mm
Thickness	25 - 50 cm	1 mm
Pier length	32 m	60 mm
Span length	72,5 m and 135 m	13,25 cm and 24,7 cm

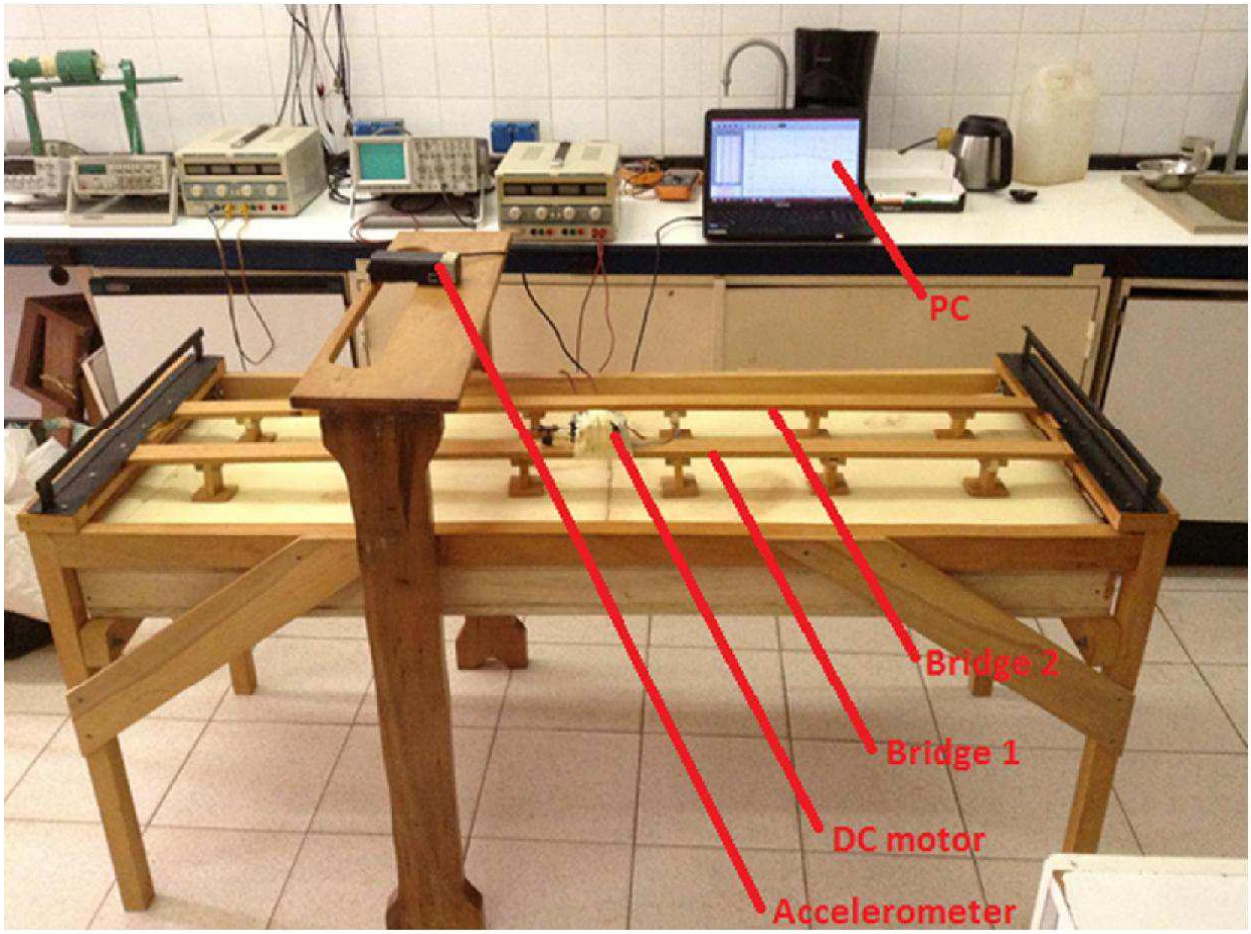

Figure 3.3: Photograph of the experimental set up

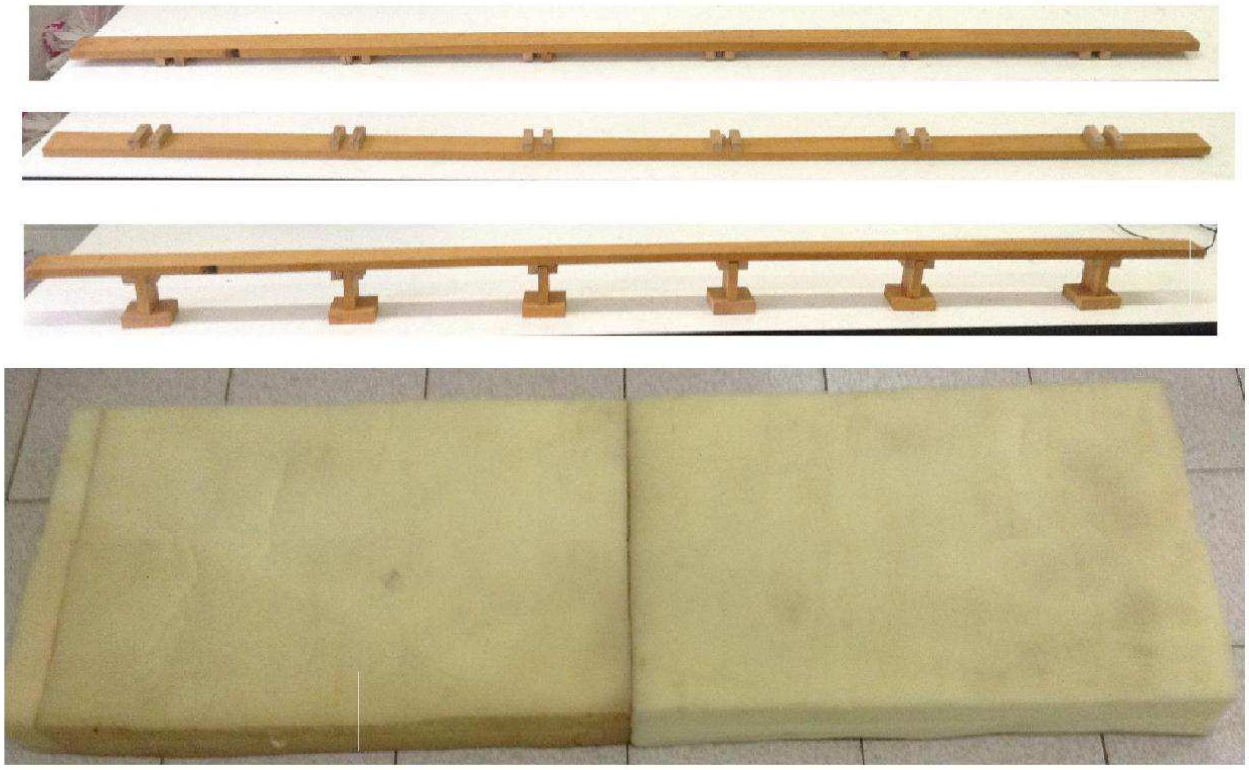

Figure 3.4: Photograph of the model structural elements

structure and then processed by a digital oscilloscope and an appropriate computer software. Let us recall that the DE-ACCM2G accelerometer is an off the shelf 2 axis 2g accelerometer solution with analog outputs. It features integrated op amp buffers for direct connection to a micro controller's analog inputs, or for driving heavier loads.

3.2.2 Modelling the coupled bridges system

a) Model of the bridge and soil support

The transverse equation of motion for a homogeneous, isotropic and uniform elastic beam subjected to a time-varying load is taken as the governing Euler-Bernoulli equation as

$$\rho S\frac{\partial^2 Y}{\partial T^2}+C_b\frac{\partial Y}{\partial T}+EI\frac{\partial^4 Y}{\partial X^4}=f\left(X,T\right), \tag{3.1}$$

where $Y = Y(X,T)$ is the transverse deflection of the beam, ρ and E are the density and the Young's modulus of the beam, S and I are the area and the second moment of area of the beam cross section, respectively. C_b the vertical viscous damping coefficient and $f(X,T)$ represents all the external loads per unit of length.

The external excitation brought by the motor is supposed to be both sinusoidal and impulsive, localized at the point X_0 of bridge 1. So, it can be described as follows

$$f(X,T) = [f_{\sin}(X,T) + f_{imp}(X,T)]\,\delta(X - X_0), \tag{3.2}$$

where $\delta(X)$ is the Dirac delta function which reflects the local nature of the excitation on the bridge, $f_{\sin}(X,T)$ is the sinusoidal load and $f_{imp}(X,T)$ is the periodic impulsive force occurring at regular intervals of time ${T_0}^*$ [29]. $f_{\sin}(X,T)$ and $f_{imp}(X,T)$ are given as follows

$$f_{\sin}(X,T) = f_0 \cos \Omega T, \tag{3.3}$$

$$f_{imp}(X,T) = I_0 \sum_{i=1}^{N} \{H(T - i{T_0}^*) - H[T - (i{T_0}^* + \Delta {T_0}^*)]\}, \tag{3.4}$$

where f_0 is the amplitude of the sinusoidal load and Ω its frequency. I_0 is the amplitude of each impulsion, N stands for the total number of impulsions while $\Delta {T_0}^*$ represents the duration of the impact. $H(X)$ is the Heaviside function defined as follows

$$H(X) = \begin{cases} 1 & \text{if } X \geq 0 \\ 0 & \text{if } X < 0 \end{cases} \tag{3.5}$$

The coupling between the two bridges is an indirect coupling via an environment that is primarily the ground under their piers that can be modelled as a linear viscoelastic Winkler foundation (Kelvin-Voigt model of soil [3]). Thus, for this system, each bridge suffers from environmental coupling (soil support), external restoring forces $F_j(X,T)$ located under the piers and given as follows

$$F_j(X,T) = -\left[k_s Y(X,T) + C_s \frac{\partial Y(X,T)}{\partial T}\right] \delta(X - X_j), \tag{3.6}$$

where k_s and C_s are the two coupling parameters characterizing the strength and the damping of the soil, respectively. X_j are the positions of the piers under the considered bridge and $\delta(X)$ is the Dirac delta function which reflects the local nature of piers positions.

b) Modelling the propagation of vibration in the soil

Let $a(Z_\alpha, \omega)$ the acceleration in the soil at the distance Z_α from the source. It was shown that the acceleration $a(Z_\beta, \omega)$ at the distance Z_β can be estimated in the frequency domain as a function of $a(Z_\alpha, \omega)$ [42, 43] as follows

$$a(Z_\beta, \omega) = a(Z_\alpha, \omega) \exp\left[ik^*(\omega) d_{\alpha\beta}\right], \tag{3.7}$$

where $d_{\alpha\beta} = Z_\beta - Z_\alpha$ and can be the distance between the two points Z_α and Z_β if $Z_\beta > Z_\alpha$ and $k^*(\omega)$ is the complex wave number defined by

$$k^*(\omega) = k(\omega) + i\lambda(\omega), \tag{3.8}$$

where $k(\omega) = \frac{2\pi V}{\omega}$ is the real wave number; with V the wave velocity in the ground. $\lambda(\omega)$ is the vibration attenuation factor defined by the viscoelastic model considered to model the close environment.

But a simpler model used to describe the propagation of the vibration into the soil is given by [165] as follows

$$a(Z_\beta, \omega) = a(Z_\alpha, \omega) \exp\left[-\lambda(\omega) d_{\alpha\beta}\right]. \tag{3.9}$$

Let's set $\gamma_{\alpha\beta} = exp\left[-\lambda(\omega) d_{\alpha\beta}\right]$ the coefficient reflecting the vibration transfer from point Z_α to point Z_β; which decreases with the distance $d_{\alpha\beta}$. This coefficient reflects the vibration propagation from one to another point. Thus, the expression (3.9) can be rewritten as follows

$$a(Z_\beta, \omega) = \gamma_{\alpha\beta} a(Z_\alpha, \omega). \tag{3.10}$$

It comes out that a pier of index-number α and with an acceleration $a(Z_\alpha, \omega)$ induces on each neighboring pier of index-number β, some vibration translated by the inertia force given by the following equation

$$f_\beta(T) = -m_\beta a(Z_\beta, \omega) = -m_\beta \gamma_{\alpha\beta} a(Z_\alpha, \omega), \tag{3.11}$$

where m_β is the mass of the neighbouring pier of index-number β.

c) Modelling the coupled bridges system

Taking into account the above considerations, the system which consists of a bridge under localized universal motor excitation coupled to a second one by their close environment is governed by the following set of equations

$$\begin{cases} \rho_1 S_1 \frac{\partial^2 Y_1}{\partial T^2} + C_{b1} \frac{\partial Y_1}{\partial T} + E_1 I_1 \frac{\partial^4 Y_1}{\partial X^4} + \sum\limits_{\alpha=1}^{N_1} \left[C_s \frac{\partial Y_1}{\partial T} + k_s Y_1 \right] \delta(X - X_{1\alpha}) + \\ \quad \sum\limits_{\alpha=1}^{N_1} m_{1\alpha} \sum\limits_{\beta=1}^{N_2} \gamma_{\alpha\beta} \frac{\partial^2 Y_2}{\partial T^2} \delta(X - X_{2\beta}) = \left[f_{\sin}(X,T) + f_{imp}(X,T) \right] \delta(X - X_0), \\ \rho_2 S_2 \frac{\partial^2 Y_2}{\partial T^2} + C_{b2} \frac{\partial Y_2}{\partial T} + E_2 I_2 \frac{\partial^4 Y_2}{\partial X^4} + \sum\limits_{\alpha=1}^{N_2} \left[C_s \frac{\partial Y_2}{\partial T} + k_s Y_2 \right] \delta(X - X_{2\alpha}) + \\ \quad \sum\limits_{\alpha=1}^{N_2} m_{2\alpha} \sum\limits_{\beta=1}^{N_1} \gamma_{\alpha\beta} \frac{\partial^2 Y_1}{\partial T^2} \delta(X - X_{1\beta}) = 0, \end{cases} \tag{3.12}$$

where $Y_j = Y_j(X,T)$ is the transverse displacement of the bridge of index-number j, N_1 and N_2, $m_{1\alpha}$ and $m_{2\alpha}$, and $X_{1\alpha}$ and $X_{2\alpha}$ are the numbers of piers, masses and positions of the piers under the main bridge and the coupled bridge, respectively. As the two beam bridges are hinged-hinged, the boundary conditions of the problem are given by

$$Y_1(X,T)|_{X=0,X=L} = 0, \qquad Y_2(X,T)|_{X=0,X=L} = 0,$$
$$\left.\frac{\partial^2 Y_1(X,T)}{\partial^2 X}\right|_{X=0,X=L} = 0, \qquad \left.\frac{\partial^2 Y_2(X,T)}{\partial^2 X}\right|_{X=0,X=L} = 0.$$

Let's consider the dimensionless variables defined as $x = \frac{X}{L}$, $y_1 = \frac{Y_1}{L}$, $y_2 = \frac{Y_2}{L}$, $t = T\omega_0$; where $\omega_0 = \frac{1}{L^2}\sqrt{\frac{E_1 I_1}{\rho_1 S_1}}$. Then, the dimensionless problem is given by the following set of

equations

$$\begin{cases} \frac{\partial^2 y_1}{\partial t^2} + \delta_1 \frac{\partial y_1}{\partial t} + \omega_1^2 \frac{\partial^4 y_1}{\partial x^4} + \sum\limits_{\alpha=1}^{N_1} \left[c_{s1} \frac{\partial y_1}{\partial t} + k_{s1} y_1 \right] \delta (x - x_{1\alpha}) + \\ \qquad \sum\limits_{\alpha=1}^{N_1} \sum\limits_{\beta=1}^{N_2} \gamma_{\alpha\beta 1} \frac{\partial^2 y_2}{\partial t^2} \delta (x - x_{2\beta}) = F(t)\, \delta (x - x_0) \\ \frac{\partial^2 y_2}{\partial t^2} + \delta_2 \frac{\partial y_2}{\partial t} + \omega_2^2 \frac{\partial^4 y_2}{\partial x^4} + \sum\limits_{\alpha=1}^{N_2} \left[c_{s2} \frac{\partial y_2}{\partial t} + k_{s2} y_2 \right] \delta (x - x_{2\alpha}) + \\ \qquad \sum\limits_{\alpha=1}^{N_2} \sum\limits_{\beta=1}^{N_1} \gamma_{\alpha\beta 2} \frac{\partial^2 y_1}{\partial t^2} \delta (x - x_{1\beta}) = 0, \end{cases} \tag{3.13}$$

where

$$M_1 = \rho_1 S_1,\ M_2 = \rho_2 S_2,\ \mu = \frac{M_1}{M_2},\ \varepsilon = \frac{E_1 I_1}{E_2 I_2}$$

$$\omega_1^2 = \frac{1}{L^4} \frac{E_1 I_1}{M_1 \omega_0^2} = 1,\ \omega_2^2 = \frac{1}{L^4} \frac{E_2 I_2}{M_2 \omega_0^2} = \frac{\mu}{\varepsilon} \omega_1^2 = \frac{\mu}{\varepsilon},\ \omega = \frac{\Omega}{\omega_0}$$

$$\delta_1 = \frac{C_{b1}}{M_1 \omega_0},\ \delta_2 = \frac{C_{b2}}{M_2 \omega_0},\ c_{s1} = \frac{C_s}{M_1 \omega_0},\ c_{s2} = \frac{C_s}{M_2 \omega_0} = \mu c_{s1}$$

$$k_{s1} = \frac{k_s}{M_1 \omega_0^2},\ k_{s2} = \frac{k_s}{M_2 \omega_0^2} = \mu k_{s1}$$

$$\gamma_{\alpha\beta 1} = \frac{m_{1\alpha}}{M_1} \gamma_{\alpha\beta},\ \gamma_{\alpha\beta 2} = \frac{m_{2\alpha}}{M_2} \gamma_{\alpha\beta},\ F(t) = \frac{L^3}{E_1 I_1} \left[f_{\sin}(x,t) + f_{imp}(x,t) \right]$$

The set of Eqs. (3.13) are the dimensionless equations of coupled bridges resting on a linear viscoelastic Winkler foundation. In index notation, this set of equations can be rewritten in the following combined form

$$\begin{aligned} &\frac{\partial^2 y_j}{\partial t^2} + \delta_j \frac{\partial y_j}{\partial t} + \omega_j^2 \frac{\partial^4 y_j}{\partial x^4} + \sum_{\alpha=1}^{N_j} \left[c_{si} \frac{\partial y_j}{\partial t} + k_{si} y_j \right] \delta (x - x_{j\alpha}) + \\ &\sum_{\alpha=1}^{N_j} \sum_{\beta=1}^{N_k} \gamma_{\alpha\beta j} \frac{\partial^2 y_k}{\partial t^2} \delta (x - x_{k\beta}) = F_j(t)\, \delta (x - x_0), \quad j,k = 1,2 \text{ and } k \neq j, \end{aligned} \tag{3.14}$$

with

$$F_j(t) = \begin{cases} F(t) & \text{if } j = 1, \\ 0 & \text{if } j = 2. \end{cases} \tag{3.15}$$

In the following sections we will deal with Eq. (3.14).

3.2.3 Analytical explanation of the model

The MS method suggest the solutions of Eq. (3.14) into the following form

$$y_j(x,t) = \sum_{n=1}^{\infty} \phi_n(x)\, q_{jn}(t), \tag{3.16}$$

where $\phi_n(x)$ are the mode shapes, given in accordance with the boundary conditions of the problem by the following expression

$$\phi_n(x) = \sin(n\pi x) \tag{3.17}$$

$q_{in}(t)$ are time functions determined by the modal equations which are obtained by substituting the transverse displacements (Eq. (3.16)) in Eq. (3.14) governing the dynamics of the coupled bridges. By multiplying by $\phi_m(x)$, integrating over the length of the beam bridge and applying the orthogonality property of spatial functions, the modal equations are obtained below

$$\ddot{q}_{jn} + 2\lambda_{jn}\dot{q}_{jn} + \omega_{jn}^2 q_{jn} + C_{kj}\ddot{q}_{kn} = 2F_j(t)\sin(n\pi x_0), \tag{3.18}$$

where $j,k = 1,2$ and $k \neq j$, $n = 1,...,\infty$ characterizing the different modes of vibration and

$$2\lambda_{jn} = \delta_j + 2c_{sj}\sum_{\alpha=1}^{N_j} \sin^2(n\pi x_{j\alpha}), \tag{3.19}$$

$$\omega_{jn}^2 = \omega_j^2 (n\pi)^4 + 2k_{sj}\sum_{\alpha=1}^{N_j} \sin^2(n\pi x_{j\alpha}), \tag{3.20}$$

$$C_{kj} = 2\sum_{\alpha=1}^{N_j}\sum_{\beta=1}^{N_k} \gamma_{\alpha\beta j}\sin^2(n\pi x_{k\beta}). \tag{3.21}$$

For the bridge of index-number j, ω_{jn} is the frequency of the vibration mode n. The term C_{kj} given by Eq. (3.21) is the coupling term reflecting the impact of the bridge of index-number k on the bridge of index-number j. It depends on the vibration transfer coefficient $\gamma_{\alpha\beta}$; and

therefore on the distance between the two bridges with respect of which it decreases. Eq. (3.18) can be rewritten as follows

$$\begin{cases} \ddot{q}_{1n} + 2\lambda_{1n}\dot{q}_{1n} + \omega_{1n}^2 q_{1n} + C_{21}\ddot{q}_{2n} = 2F(t)\sin(n\pi x_0) \\ \ddot{q}_{2n} + 2\lambda_{2n}\dot{q}_{2n} + \omega_{2n}^2 q_{2n} + C_{12}\ddot{q}_{1n} = 0, \end{cases} \tag{3.22}$$

An analytical solution of this set of modal equations is given in the following subsections in the cases of a sinusoidal excitation and a periodic impulsive load.

a) Analytical solution of the modal equations for sinusoidal excitation

In this case, Eq. (3.22) can be rewritten as follow

$$\begin{cases} \ddot{q}_{1n} + 2\lambda_{1n}\dot{q}_{1n} + \omega_{1n}^2 q_{1n} + C_{21}\ddot{q}_{2n} = F_{0n}\cos\omega t, \\ \ddot{q}_{2n} + 2\lambda_{2n}\dot{q}_{2n} + \omega_{2n}^2 q_{2n} + C_{12}\ddot{q}_{1n} = 0, \end{cases} \tag{3.23}$$

where $F_{0n} = \frac{2L^3}{E_1 I_1} f_0 \sin(n\pi x_0)$.

To solve this set of ODEs, let us use the HB method. Let set

$$\begin{cases} q_{1n} = A_n \cos(\omega t + \varphi_1), \\ q_{2n} = B_n \cos(\omega t + \varphi_2). \end{cases} \tag{3.24}$$

Substituting Eq. (3.24) into Eq. (3.23), we obtain the following amplitude equations after some mathematical calculations

$$\begin{cases} A_n = F_{0n}\sqrt{\frac{\eta_1^2+\eta_2^2}{\eta^2}} \\ B_n = F_{0n}\sqrt{\frac{\eta_3^2+\eta_4^2}{\eta^2}}, \end{cases} \tag{3.25}$$

where

$$\begin{cases} \eta = (\omega_{1n}^2-\omega^2)^2(\omega_{2n}^2-\omega^2)^2 - 2\omega^4 C_{12}C_{21}\left(\omega_{1n}^2-\omega^2\right)\left(\omega_{2n}^2-\omega^2\right) - 4\omega^2\lambda_{1n}^2(\omega_{2n}^2-\omega^2)^2 \\ -4\omega^2\lambda_{2n}^2(\omega_{1n}^2-\omega^2)^2 + 16\omega^4\lambda_{1n}^2\lambda_{2n}^2 - 8\omega^6 C_{12}C_{21}\lambda_{1n}\lambda_{2n} + \omega^8 C_{12}^2C_{21}^2 \\ \eta_1 = \left(\omega_{1n}^2-\omega^2\right)^2\left(\omega_{2n}^2-\omega^2\right) - \omega^4 C_{12}C_{21}\left(\omega_{2n}^2-\omega^2\right) - 2\omega^2\lambda_{2n}\left(\omega_{1n}^2-\omega^2\right) \\ \eta_2 = 2\omega\lambda_{1n}(\omega_{2n}^2-\omega^2)^2 + 2\omega^5 C_{12}C_{21}\lambda_{2n} - 8\omega^3\lambda_{1n}\lambda_{2n}^2 \\ \eta_3 = \omega^2 C_{12}\left[\left(\omega_{1n}^2-\omega^2\right)\left(\omega_{2n}^2-\omega^2\right) + 4\omega^2\lambda_{1n}\lambda_{2n} + \omega^4 C_{21}\right] \\ \eta_4 = 2\omega^3 C_{12}\left[\lambda_{1n}\left(\omega_{2n}^2-\omega^2\right) + \lambda_{2n}\left(\omega_{1n}^2-\omega^2\right)\right], \end{cases} \tag{3.26}$$

The two last expressions of Eq. (3.26) show, as might be expected, that the vibrations of the unexcited coupled bridge (bridge 2) strongly depend on the vibration transfer coefficient C_{12} from the main bridge 1 to the second one.

b) Analytical solution of the modal equations for periodic impulsive excitation

In this case, Eq. (3.22) can be rewritten as follows

$$\begin{cases} \ddot{q}_{1n} + 2\lambda_{1n}\dot{q}_{1n} + \omega_{1n}^2 q_{1n} + C_{21}\ddot{q}_{2n} = F_{0n}\sum_{i=1}^{N}\left\{H\left(t-iT_0\right) - H\left[t-(iT_0+\tau)\right]\right\}, \\ \ddot{q}_{2n} + 2\lambda_{2n}\dot{q}_{2n} + \omega_{2n}^2 q_{2n} + C_{12}\ddot{q}_{1n} = 0, \end{cases} \tag{3.27}$$

where $F_{0n} = \frac{2L^3}{E_1 I_1} I_0 \sin\left(n\pi x_0\right)$, T_0 and τ are non-dimensional period and duration of the impact of the periodic impulsive excitation, respectively. T_0 and τ are define as $T_0 = {T_0}^*\omega_0$ and $\tau = \Delta {T_0}^*\omega_0$.

As the analytical resolution of the set of Eqs. (3.27) is not quite evident, let us look at the case of two identical beam bridges whose modal equations are given as follows

$$\begin{cases} \ddot{q}_{1n} + 2\lambda_n\dot{q}_{1n} + \omega_n^2 q_{1n} + C\ddot{q}_{2n} = F_{0n}\sum_{i=1}^{N}\left\{H\left(t-iT_0\right) - H\left[t-(iT_0+\tau)\right]\right\}, \\ \ddot{q}_{2n} + 2\lambda_n\dot{q}_{2n} + \omega_n^2 q_{2n} + C\ddot{q}_{1n} = 0, \end{cases} \tag{3.28}$$

where $\lambda_n = \lambda_{1n} = \lambda_{2n},\ \omega_n^2 = \omega_{1n}^2 = \omega_{2n}^2,\ C = C_{12} = C_{21}$.

To solve these new equations, it is useful to assume new variables as follows

$$q_+ = q_{1n} + q_{2n}, \tag{3.29}$$

$$q_- = q_{1n} - q_{2n}. \tag{3.30}$$

Each of them is solution of the following differential equation

$$\ddot{q}_\pm + 2\lambda_\pm \dot{q}_\pm + \omega_\pm^2 q_\pm = F_{0\pm} \sum_{i=1}^{N} \{H\left(t - iT_0\right) - H\left[t - (iT_0 + \tau)\right]\}, \tag{3.31}$$

obtained by adding and subtracting the two sets of Eqs. (3.28) and where $\lambda_\pm = \frac{\lambda_n}{1\pm C}$, $\omega_\pm^2 = \frac{\omega_n^2}{1\pm C}$, $F_{0\pm} = \frac{F_{0n}}{1\pm C}$.

The solutions of Eq. (3.28) are then obtained from new variable parameters as follows

$$\begin{cases} q_{1n} = \frac{q_+ + q_-}{2}, \\ q_{2n} = \frac{q_+ - q_-}{2}. \end{cases} \tag{3.32}$$

For each modes ($n = 1, 2, ...\infty$), the solutions of Eq. (3.31) can be expressed as the sum of a homogeneous solution $q_\pm^H(t)$ and a particular solution $q_\pm^P(t)$, i.e.

$$q_\pm(t) = q_\pm^H(t) + q_\pm^P(t), \tag{3.33}$$

where

$$q_\pm^H(t) = \left[A_\pm \cos\Omega_\pm t + B_\pm \sin\Omega_\pm t\right] e^{-\lambda_\pm t}, \tag{3.34}$$

with $\Omega_\pm = \sqrt{\omega_\pm^2 - \lambda_\pm^2}$.

The form of the external excitation in Eq. (3.31) suggests a treatment per intervals in order to determine its particular solutions $q_\pm^P(t)$. For instance, let us subdivide time in two great time domains according to instant where the impacts occur. One of these two great time domains correspond to intervals of time before the impact sequence i and after the last impact sequence of index N and the other correspond to the intervals of time during the impact sequence i.

• Before the impact sequence i i.e. $\forall t \in [(i-1)\,T_0+\tau; iT_0[\,; i=1,...,N$ and after the last impact sequence N i.e. $\forall t \in [NT_0+\tau; +\infty[,\ H\left(t-iT_0\right)-H\left[t-(iT_0+\tau)\right]=0$ and therefore a particular solution can be $q_{\pm}^{P}\left(t\right)=0$.

• During the impact sequence i i.e. $\forall t \in [iT_0;\ iT_0+\tau[\,;\ i=1,...,N,\ H\left(t-iT_0\right)-H\left[t-(iT_0+\tau)\right]=1$ and therefore a particular solution can be $q_{\pm}^{P}\left(t\right)=\frac{F_{0\pm}}{\omega_{\pm}^{2}}$.

So, the general solution of the problem can be written as

$$q_{\pm}\left(t\right)=\begin{cases} q_{\pm}^{(i)}\left(t_1\right)=\left[A_{\pm}^{(i)}\cos\Omega_{\pm}t_1+B_{\pm}^{(i)}\sin\Omega_{\pm}t_1\right]e^{-\lambda_{\pm}t_1} \\ \qquad\qquad \text{For}\ \ (i-1)\,T_0+\tau\leq t<\ iT_0\ \ \text{ or }\ t>NT_0, \\ \tilde{q}_{\pm}^{(i)}\left(t_2\right)=\left[C_{\pm}^{(i)}\cos\Omega_{\pm}t_2+D_{\pm}^{(i)}\sin\Omega_{\pm}t_2\right]e^{-\lambda_{\pm}t_1}+\frac{F_{0\pm}}{\omega_{\pm}^{2}} \\ \qquad\qquad \text{For}\ \ iT_0\leq t<\ iT_0+\tau, \end{cases} \tag{3.35}$$

where $i=1,...,N$, $t_1=t-\left[(i-1)\,T_0+\tau\right]$ the initial instant just after the impact sequence $i-1$ and $t_2=t-iT_0$ the initial instant of the impact sequence i. Taking into account Eqs. (3.29) and (3.30), the final solutions of the modal equations (3.28) are given per intervals as follows.

• Before the impact sequence i i.e. $\forall t \in [(i-1)\,T_0+\tau; iT_0[\,; i=1,...,N$ and after the last impact sequence of index N i.e. $\forall t \in [NT_0+\tau; +\infty[$

$$\begin{cases} q_{1n}\left(t\right)=q_{1n}^{(i)}\left(t_1\right)=\dfrac{1}{2}\left\{\left[A_{+}^{(i)}\cos\Omega_{+}t_1+B_{+}^{(i)}\sin\Omega_{+}t_1\right]e^{-\lambda_{+}t_1}+\right. \\ \qquad\qquad \left.\left[A_{-}^{(i)}\cos\Omega_{-}t_1+B_{-}^{(i)}\sin\Omega_{-}t_1\right]e^{-\lambda_{-}t_1}\right\} \\ q_{2n}\left(t\right)=q_{2n}^{(i)}\left(t_1\right)=\dfrac{1}{2}\left\{\left[A_{+}^{(i)}\cos\Omega_{+}t_1+B_{+}^{(i)}\sin\Omega_{+}t_1\right]e^{-\lambda_{+}t_1}-\right. \\ \qquad\qquad \left.\left[A_{-}^{(i)}\cos\Omega_{-}t_1+B_{-}^{(i)}\sin\Omega_{-}t_1\right]e^{-\lambda_{-}t_1}\right\}, \end{cases} \tag{3.36}$$

- During the impact sequence i i.e. $\forall t \in [iT_0;\ iT_0 + \tau[\ ;\ i = 1, ..., N$

$$\begin{cases} q_{1n}(t) = \tilde{q}_{1n}^{(i)}(t_2) = \dfrac{1}{2}\left\{\left[C_+^{(i)}\cos\Omega_+ t_2 + D_+^{(i)}\sin\Omega_+ t_2\right]e^{-\lambda_+ t_2} + \right. \\ \qquad\qquad \left.\left[C_-^{(i)}\cos\Omega_- t_2 + D_-^{(i)}\sin\Omega_- t_2\right]e^{-\lambda_- t_2}\right\} + \dfrac{F_{0n}}{\omega_n^2}, \\ q_{2n}(t) = \tilde{q}_{2n}^{(i)}(t_2) = \dfrac{1}{2}\left\{\left[C_+^{(i)}\cos\Omega_+ t_2 + D_+^{(i)}\sin\Omega_+ t_2\right]e^{-\lambda_+ t_2} - \right. \\ \qquad\qquad \left.\left[C_-^{(i)}\cos\Omega_- t_2 + D_-^{(i)}\sin\Omega_- t_2\right]e^{-\lambda_- t_2}\right\}, \end{cases} \tag{3.37}$$

where the unknown integration constants $A_\pm^{(i)}$, $B_\pm^{(i)}$, $C_\pm^{(i)}$ and $D_\pm^{(i)}$ are determined from the initial conditions of the problem which correspond to the final conditions of the previous phases of the movement.

3.2.4 Numerical simulations and discussion

In this section, we present the results of numerical simulations of the proposed model of coupled bridges. Subsequently, we compare the theoretical results with experimental results obtained on the scale model built in the laboratory to assess the efficiency of the proposed theoretical model. In our simulations, we limit only on the first mode of vibration ($n = 1$) and the numerical method used is the RK4 method.

Numerical solutions of the coupled beam bridges subjected to each kind of excitation (sinusoidal and impulsive) whose dynamics is described by Eqs. (3.23) and (3.28) are found and compare with the corresponding analytical solutions given by Eqs. (3.24), (3.36) and (3.37).

a) Dynamic response of coupled bridges: validation of the analytical study

For the validation of the analytical study, the numerical solutions of the coupled beam bridges are found and displayed in the same graph with the corresponding analytical solutions. The curves of Figs. 3.5 and 3.6 are obtained for the following sets of non-dimensional

parameters.

- **For sinusoidal excitation** :

$\lambda_1 = \lambda_2 = 0.05,\ \omega_1 = \omega_2 = 10,\ C_{12} = C_{21} = 0.5,\ \omega = 1,\ F_0 = 0.5$

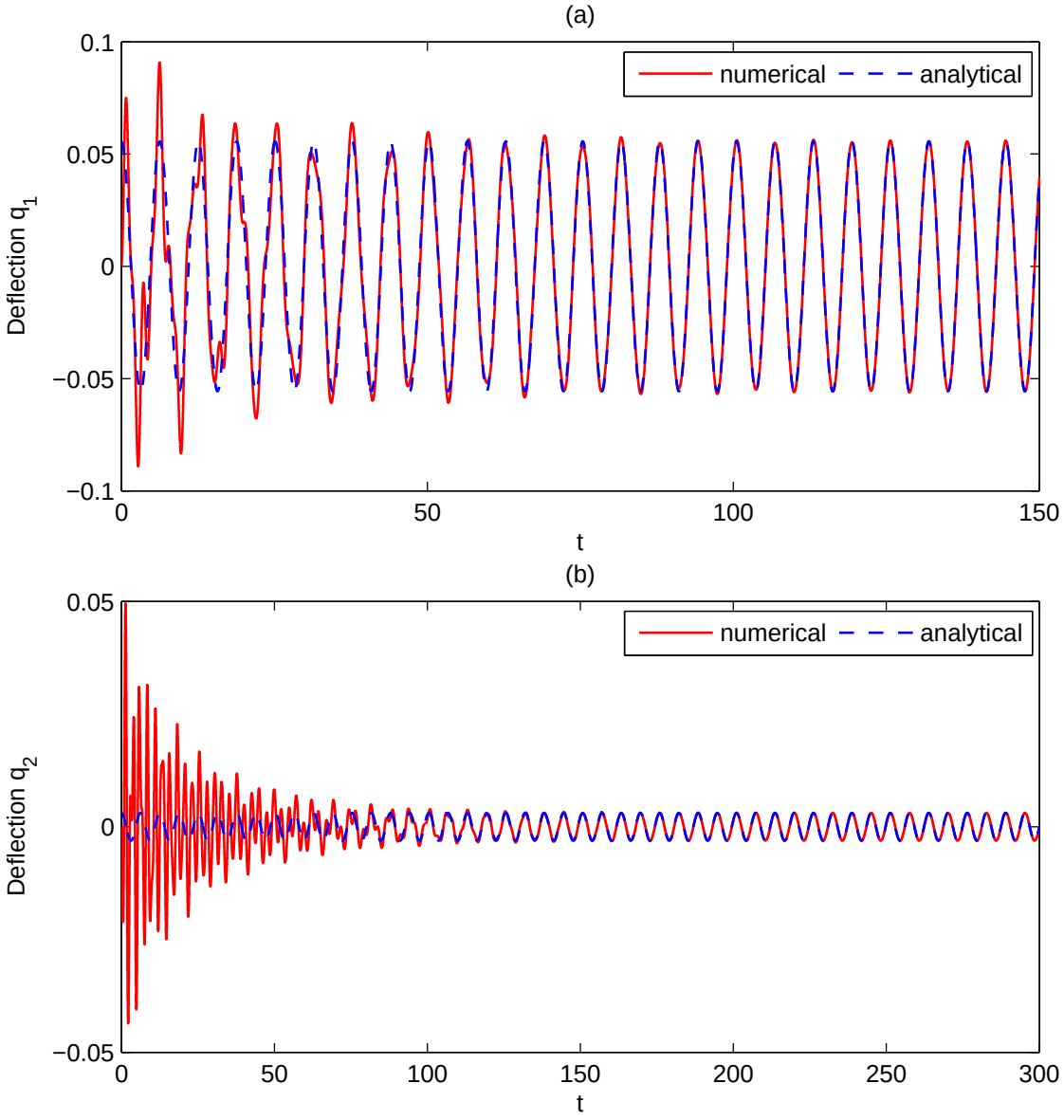

Figure 3.5: Comparison of numerically and analytically deflections obtained for sinusoidal excitation: (a) bridge 1; (b) bridge 2

- **For train of 3 impulsions** :

$\lambda_1 = \lambda_2 = 0.05,\ \omega_1 = \omega_2 = 1,\ C_{12} = C_{21} = 0.5,\ T_0 = 50;\ \tau = 0.1,\ F_0 = 0.5$

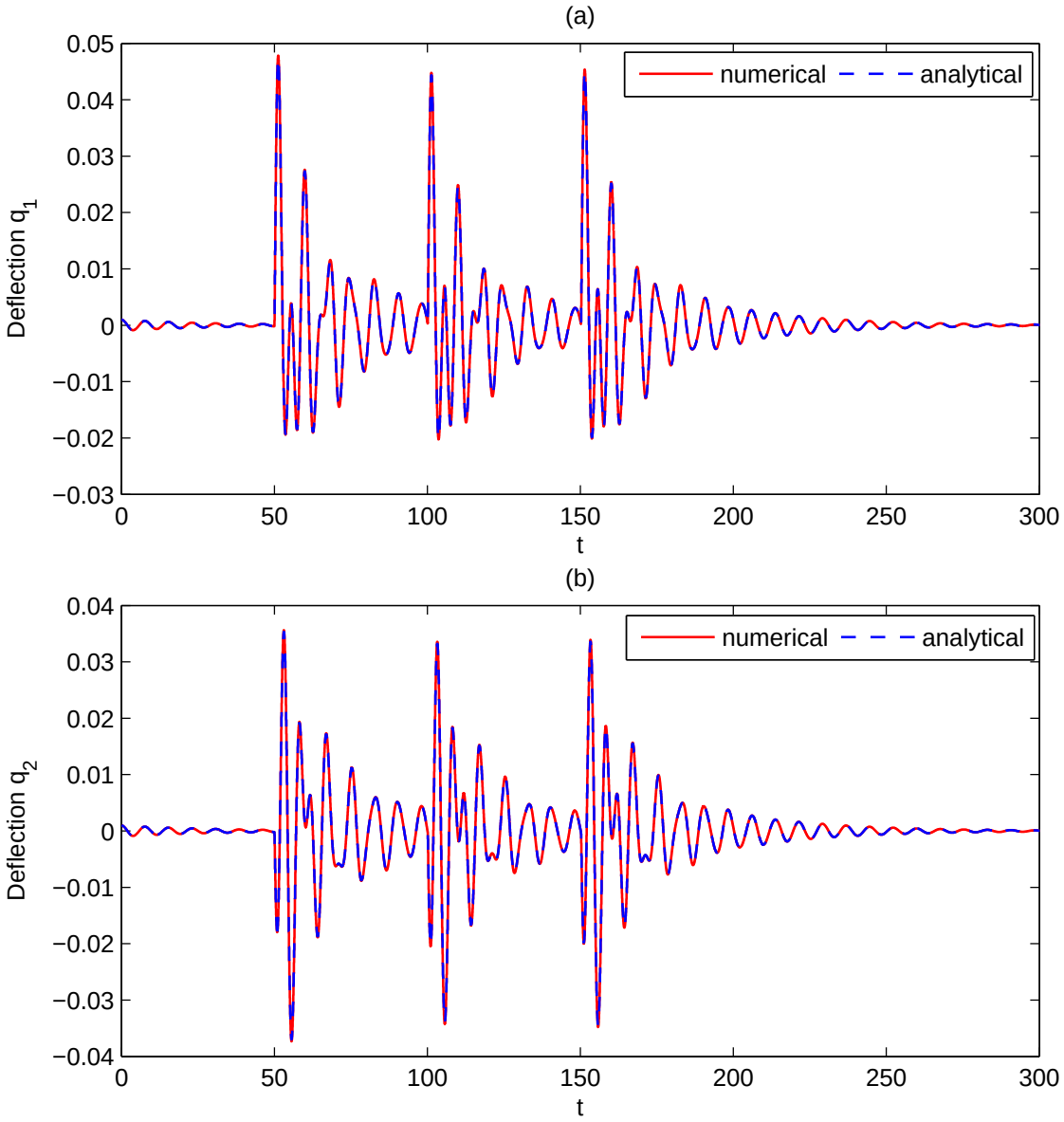

Figure 3.6: Comparison of numerically and analytically deflections obtained for periodic impulsive excitation: (a) bridge 1; (b) bridge 2

The coincidence between the curves obtained by numerical and analytical treatment after the initial transient regime for the two bridges in Figs. 3.5 and 3.6 shows that the proposed analytical solutions are quite good.

b) Resonant response

The amplitude curves are plotted versus the excitation frequency ω of the sinusoidal excitation on the one hand and the period T_0 of the periodic impulsive excitation on the other hand. The different curves obtained are presented and discussed below for the following sets of non-dimensional parameters $\lambda_1 = \lambda_2 = 0.05,\ C_{12} = C_{21} = 0.5,\ F_0 = 0.5$.

- **For sinusoidal excitation**

Each of the amplitude curves corresponding to the dynamical response of the two coupled bridges for a sinusoidal excitation presents four resonances in two pairs with very close peaks as shown in Figs. 3.7 and 3.8. These two pairs are separated by many antiresonances, with the most significant antiresonance located around the frequency ω_2 of bridge 2 (Fig. 3.7). As shown in Figs. 3.7 and 3.8, the two coupled bridges present their resonance pairs approximately at the same positions on either side of the antiresonance frequency ω_2. However, these positions vary depending on the frequencies ω_1 and ω_2 of the bridges 1 and 2 respectively; one gradually comes closer to the antiresonance frequency ω_2 while the other moves away when ω_1 increases (Fig. 3.8).

The antiresonance frequency ω_2 pointed out here for which the vibration amplitudes of bridge 1 become almost zero can be an interesting result in vibration control of the dynamics of beams. It will be then a good issue to consider the control of the vibration of a beam by another beam dimensioned at the excitation frequency range of this later.

- **For periodic impulsive excitation**

In this case, all the amplitude curves of bridges present an infinite number of resonances of least importance as shown in Figs. 3.9 and 3.10. As shown in Figs. 3.9 and 3.10, the intensities of these resonances decrease with respect to the period T_0 of the impulsive

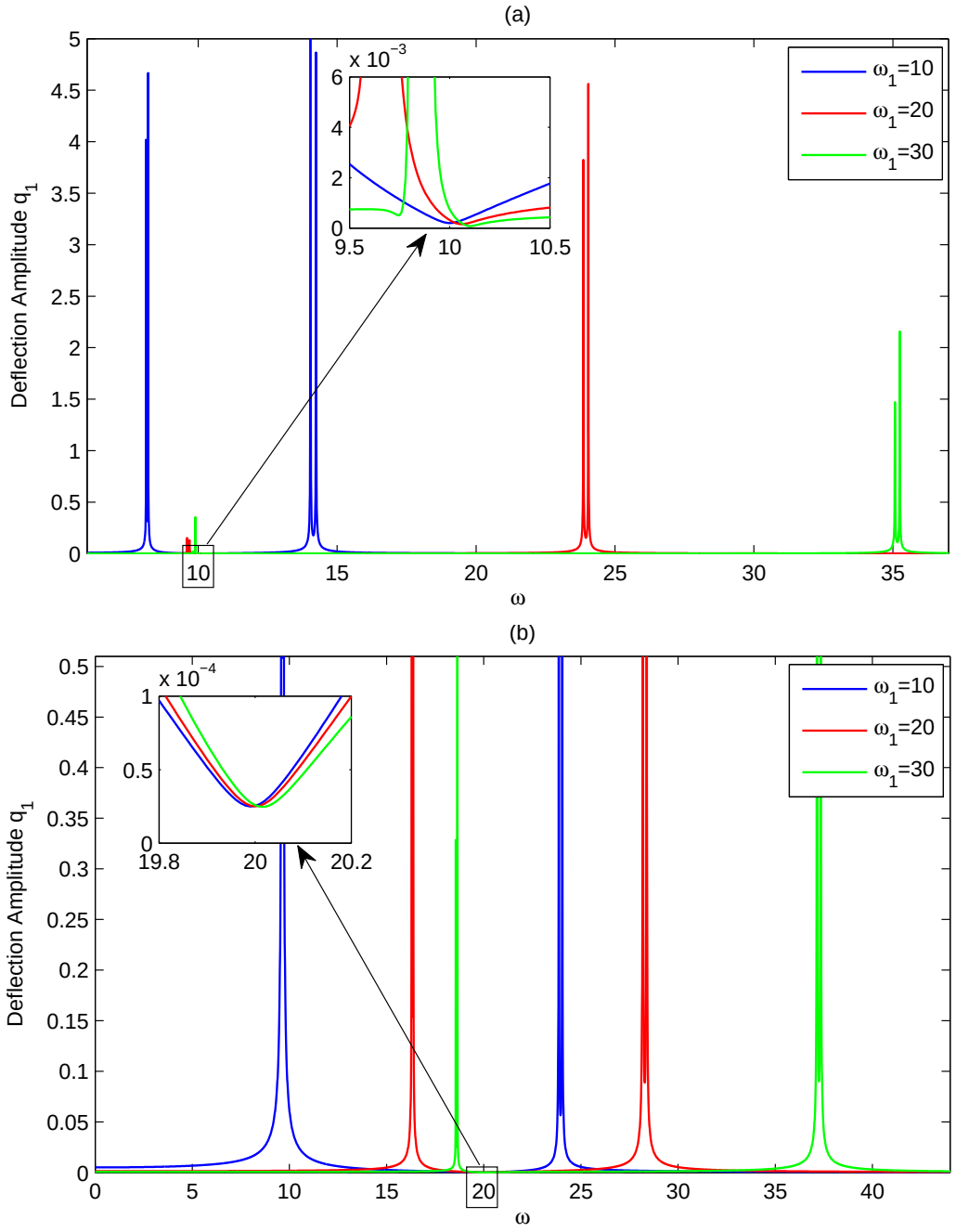

Figure 3.7: Amplitude curves of bridge 1 versus the frequency ω of the sinusoidal excitation for (a) $\omega_2 = 10$; (b) $\omega_2 = 20$

excitation (i.e. increase with respect to its frequency) and with respect to the frequencies ω_1 and ω_2 of the two bridges; and their values tend asymptotically to a given limit. But we can notice from Fig. 3.10(a) that the change in the frequency ω_2 of bridge 2 does not have

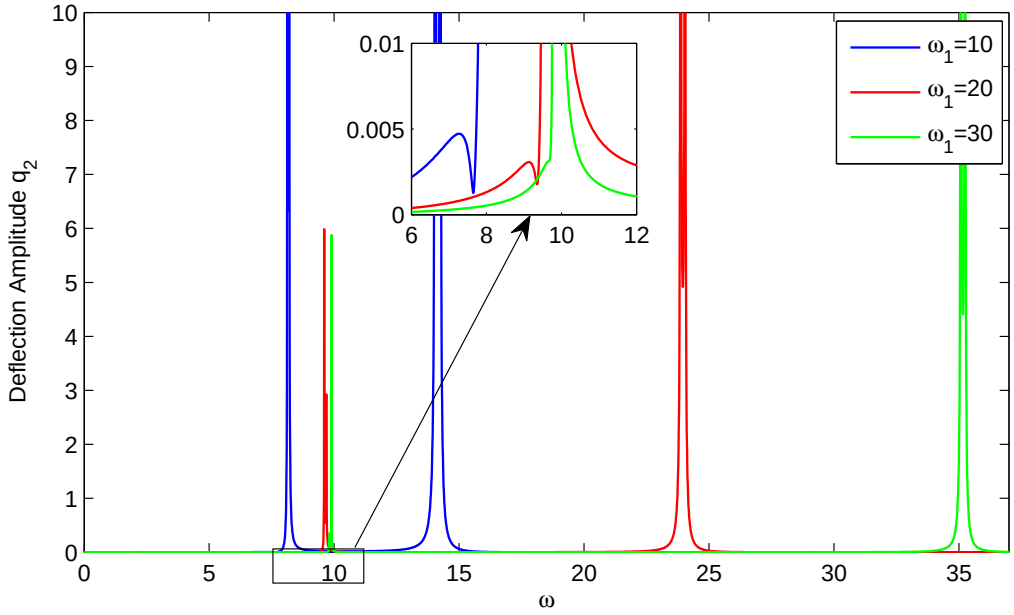

Figure 3.8: Amplitude curves of bridge 2 versus the frequency ω of the sinusoidal excitation for $\omega_2 = 10$

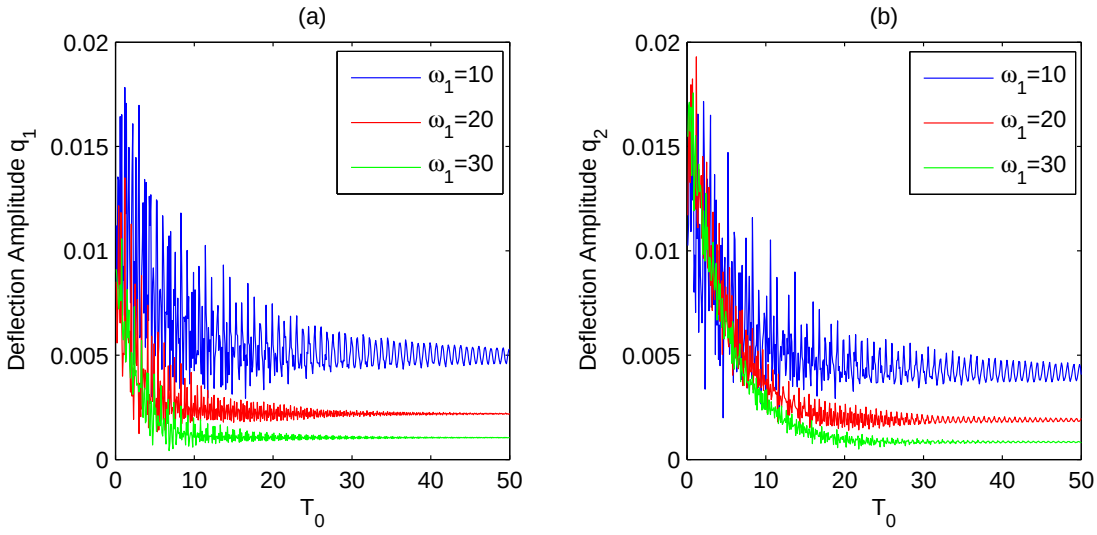

Figure 3.9: Amplitude curves versus the period T_0 of the periodical impulsive excitation for several values of ω_1 (a) bridge 1; (b) bridge 2

a significant effect on the dynamics of bridge 1.

It is therefore clear from this study that it would be more beneficial to the structure

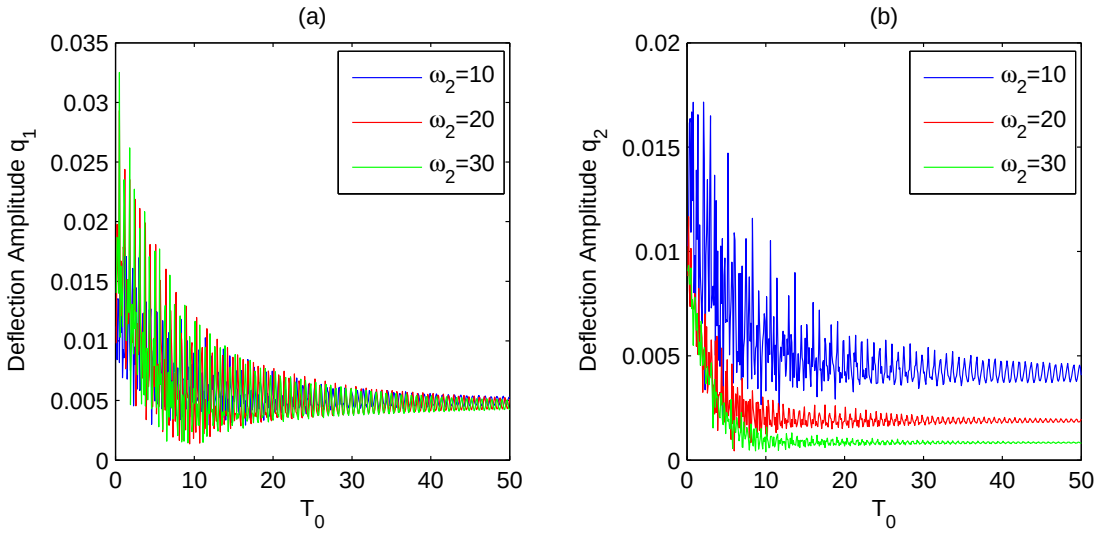

Figure 3.10: Amplitude curves versus the period T_0 of the periodical impulsive excitation for several values of ω_2 (a) bridge 1; (b) bridge 2

to have great natural frequencies of vibration in order to present small amplitude responses.

c) Effects of some parameters on the dynamics of coupled bridges

In this section we present the influence of various parameters on the dynamic responses of the two coupled bridges. This is done in order to point out the influences of the viscoelastic coupling of the soil and the effect of the distance between the two bridges. Figs. 3.11, 3.12 and 3.13 show the amplitude of the two bridges versus the non-dimensional parameters involving the viscoelastic coupling and the distance between the coupled bridges.

- **Effects of viscoelastic coupling of the Winkler foundation**

The non-dimensional parameters reflecting the effects of the viscoelastic coupling are the frequencies ω_1 and ω_2 of the two coupled bridges and the damping coefficients λ_1 and λ_2. The frequencies ω_1 and ω_2 include the stiffness of the soil through the terms k_{si} in Eq. (3.20) while λ_1 and λ_2 include its viscosity through the terms c_{si} in Eq. (3.19). So, the study

of the effects of viscoelastic coupling on the dynamic responses of the two coupled bridges amounts to the study of the effects of these four parameters.

The study of the effect of the frequencies ω_1 and ω_2 was made in the previous paragraph. For periodic impulsive excitation, Figs. 3.9 and 3.10 show that the amplitudes of vibration of the two bridges decrease with these frequencies, therefore with the rigidity k_s of the Winkler foundation, according to the definition of the non-dimensional parameters of Eq. (3.13). In the case of a sinusoidal excitation, the effects of viscoelastic coupling of the Winkler foundation is reflected in the resonances and antiresonances observed in Figs. 3.7 and 3.8.

As regards the effect of the damping coefficients λ_1 and λ_2, for the non-dimensional quantities $\omega_1 = \omega_2 = 10,\ \omega = 1,\ C_{12} = C_{21} = 0.5,\ T_0 = 50;\ \tau = 0.1,\ F_0 = 0.5$, one obtains the amplitude curves of Figs. 3.11 and 3.12.

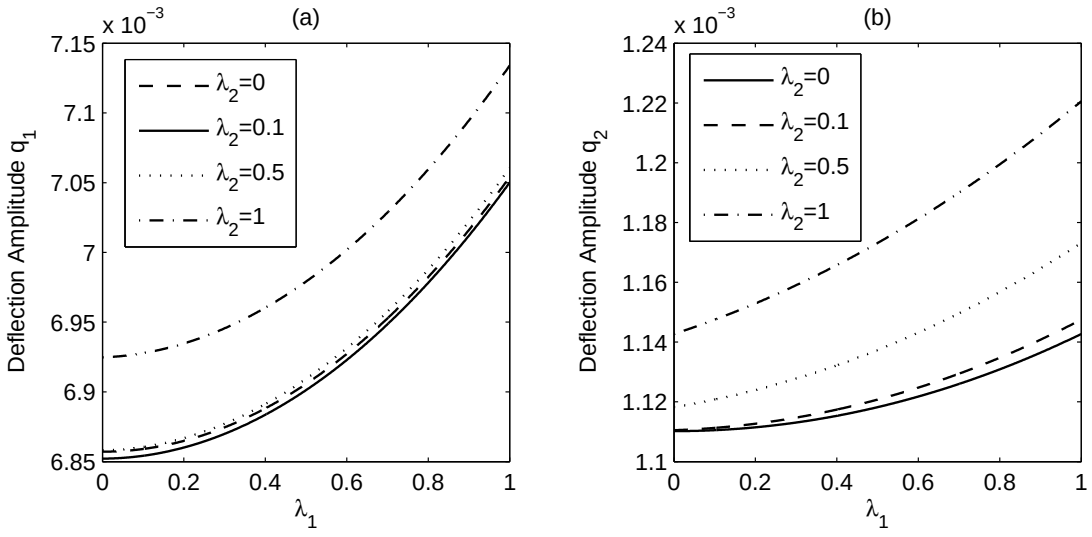

Figure 3.11: Amplitude curves versus the damping coefficient λ_1 for sinusoidal excitation: (a) bridge 1; (b) bridge 2.

Fig. 3.11 shows that the deflection amplitudes of the two coupled bridges increase with respect to the damping coefficients λ_1 and λ_2 in the case of sinusoidal excitation. However, the behavior vary in the case of periodic impulsive excitation as shown in Fig. 3.12.

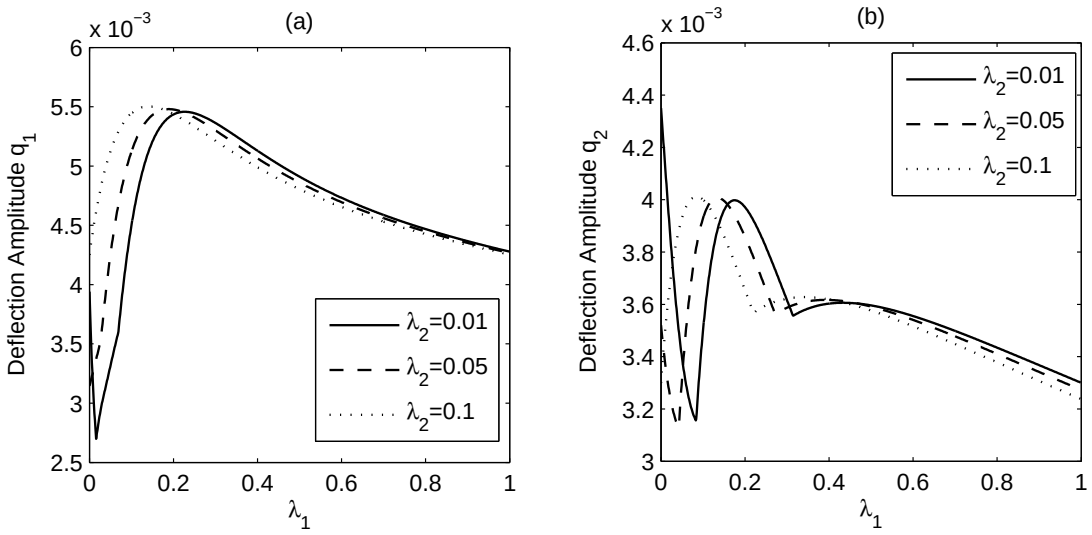

Figure 3.12: Amplitude curves versus the damping coefficient λ_1 for periodical impulsive excitation: (a) bridge 1; (b) bridge 2.

It comes out from this study that the viscoelastic coupling of the soil presents various effects on the dynamics of the two coupled beams bridges.

- **Effects of the distance between the two beam bridges**

The non-dimensional parameters that include the effect of distance on the dynamics of the coupled beam bridges are the coupling coefficients C_{12} and C_{21} between the two modal equations in Eq. (3.22). According to Eqs.(3.9) and (3.21), C_{12} and C_{21} are decreasing function of the distance between the bridges. Studying the effects of the distance between the two bridges comes down now to study the effect of the parameters C_{12} and C_{21} on their dynamic responses. For this purpose, the curves of Figs. 3.13 have been plotted for the given values of non-dimensional parameters $\lambda_1 = \lambda_2 = 0.05$, $\omega_1 = \omega_2 = 10$, $\omega = 1$, $T_0 = 50$, $\tau = 0.1$ and $F_0 = 0.5$.

Fig. 3.13 shows that, for a sinusoidal excitation, the deflection amplitudes of the two coupled bridges increase with the coupling parameters C_{12} and C_{21}; i.e. when the distance

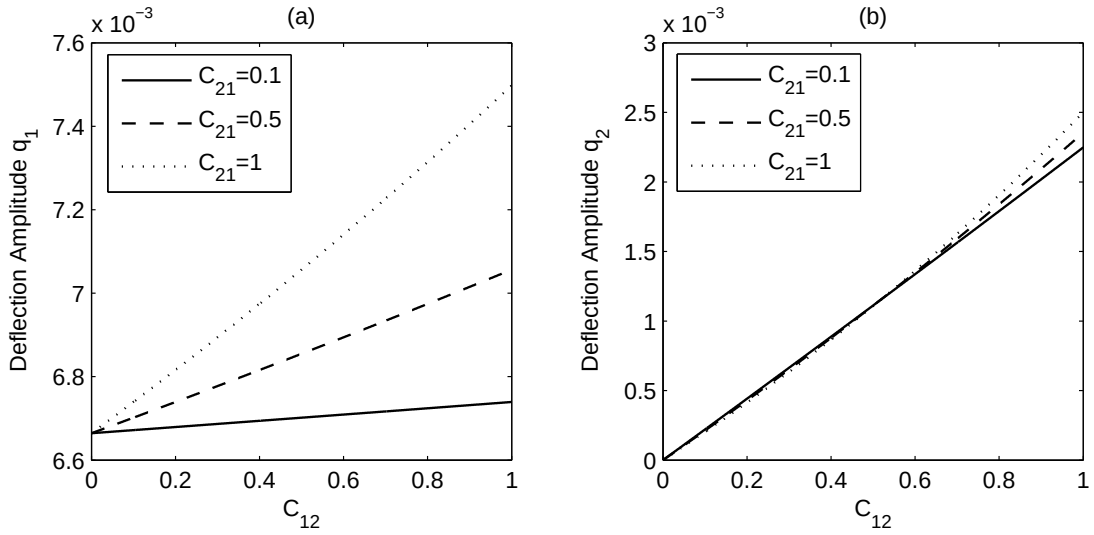

Figure 3.13: Amplitude curves versus the coupling coefficient C_{12} for sinusoidal excitation : (a) bridge 1; (b) bridge 2.

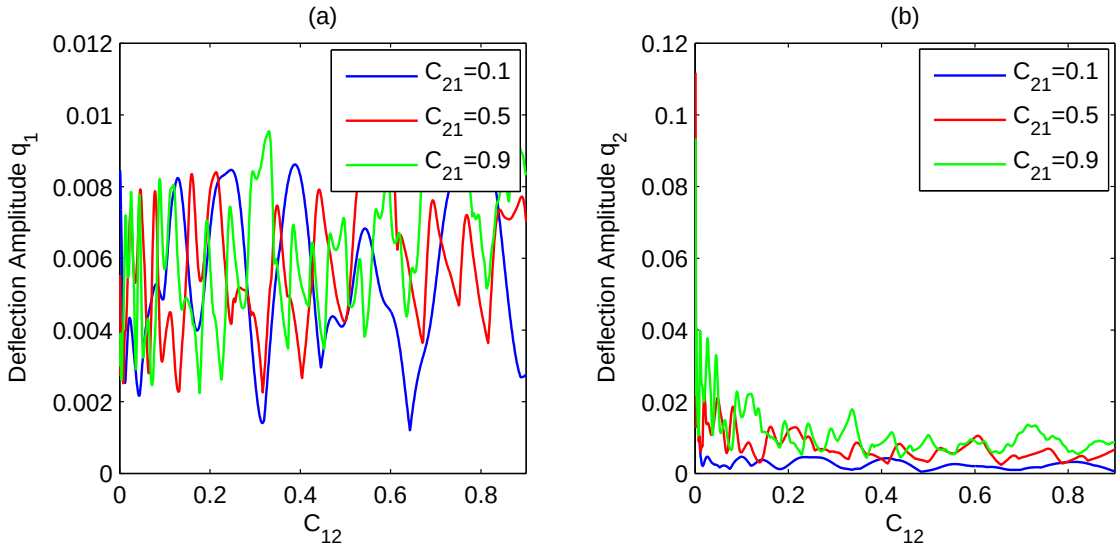

Figure 3.14: Amplitude curves versus the coupling coefficient C_{12} for periodical impulsive excitation : (a) bridge 1; (b) bridge 2.

between the two bridges decreases. This is however not checked for bridge 2 for certain values of C_{12} below 0.5. Before this value, the amplitudes of bridge 2 increase with C_{12} but decrease with C_{21} as shown in Fig. 3.13(b).

For a periodic impulsive excitation, complex behaviors are observed with variation of amplitudes around a given values. Bridge 2 nevertheless has a lesser disordered response than bridge 1 with the amplitudes that tend to decrease while C_{12} and C_{21} increase as shown in Fig. 3.14.

d) Experimental validation of the theoretical analysis

In this subsection, comparison of the experimental results obtained from the model built in lab is done with some results of previous theoretical study.

- **Transverse displacements of the coupled beam bridges**

The transverse displacements of bridge 1 in the presence of the outer exciter universal motor are captured using the miniaturized DE-ACCM2G accelerometer incorporated into the structure and the results are shown in the Figs. 3.15.

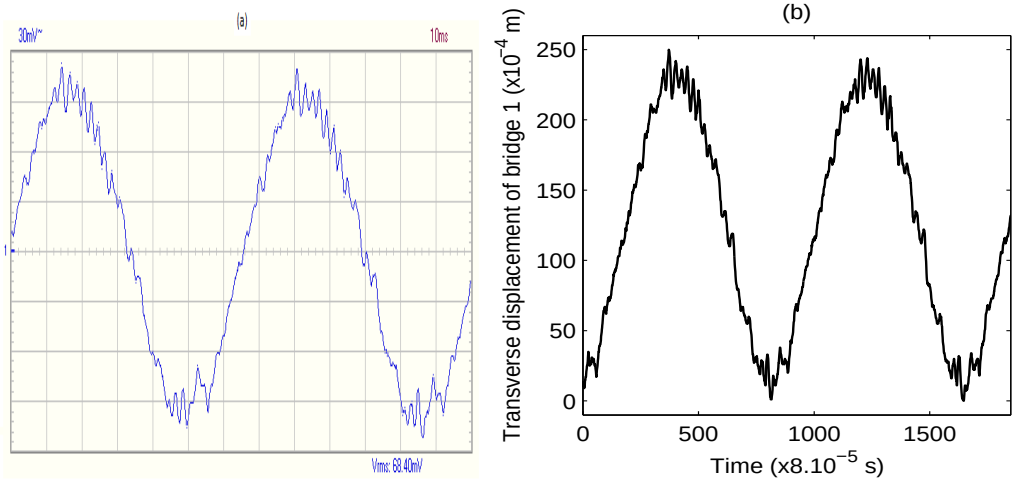

Figure 3.15: Transversal displacements of bridge 1 for excitation motor excite at the voltage $U = 23$ V: (a) screen of the digital oscilloscope; (b) plotted in Matlab software

Fig. 3.15 shows a perfect similarity between the curves displayed in the portable digital oscilloscope and those drawn in Matlab software from the experimental data file.

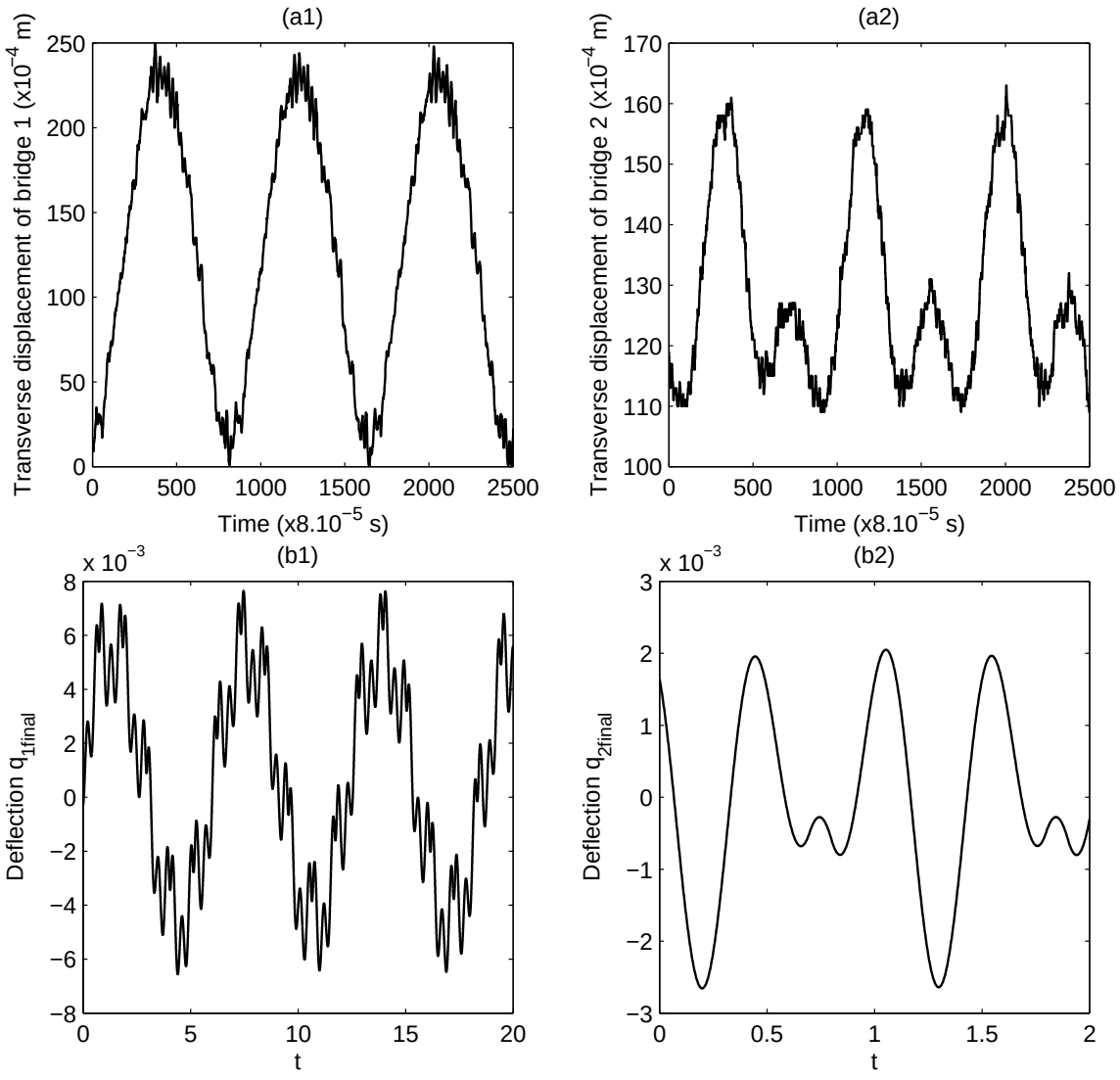

Figure 3.16: Comparison of the transverse displacements of the bridges 1 and 2: (a) Experimental data plotted in Matlab software: bridge 1 (a1) and bridge 2 (a2); (b) numerical simulation of the model: bridge 1 (b1) and bridge 2 (b2)

The curves of Fig. 3.16 shows a fairly good quantitative correlation between the experimental results and those obtained from numerical simulations of the developed model. Let us notice that the numerical results are obtained by adding the dynamical responses of the coupled beam bridges obtained from the two forms of excitation studied i.e. sinusoidal excitation and periodic impulsive excitation as shown in Fig. 3.17.

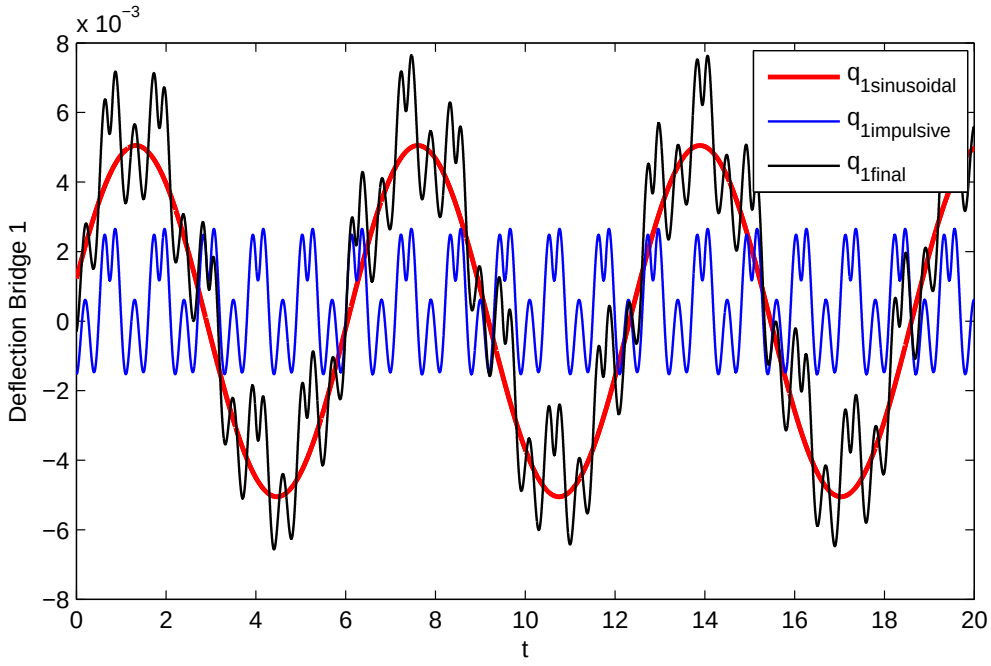

Figure 3.17: Transverse displacement of bridge 1 subjected simultaneously to sinusoidal excitation and periodic impulsive excitation for $\lambda_1 = \lambda_2 = 0.05;\ \omega_1 = \omega_2 = 10;\ C_{12} = C_{21} = 0.5;\ \omega = 1;\ T_0 = 1;\ \tau = 0.1;\ F_0 = 0.5$

- **Effect of the environmental coupling**

To experimentally highlight the effects of coupling, the transverse displacements are captured for different distances between the two coupled bridges. The data obtained are then plotted in Fig. 3.18 and compared to the results of numerical simulations of the developed model.

The experimental results in Fig. 3.18 show that the transverse displacements of bridge 1 (subject to universal motor excitation) and the bridge 2 (free of excitation) increases when the distance between them decrease. This result has indeed been obtained theoretically on the curve of the Fig. 3.13 for which the deflection amplitudes of the bridges increase with coupling parameters C_{12} and C_{21}; i.e. when the distance between the two bridges decreases.

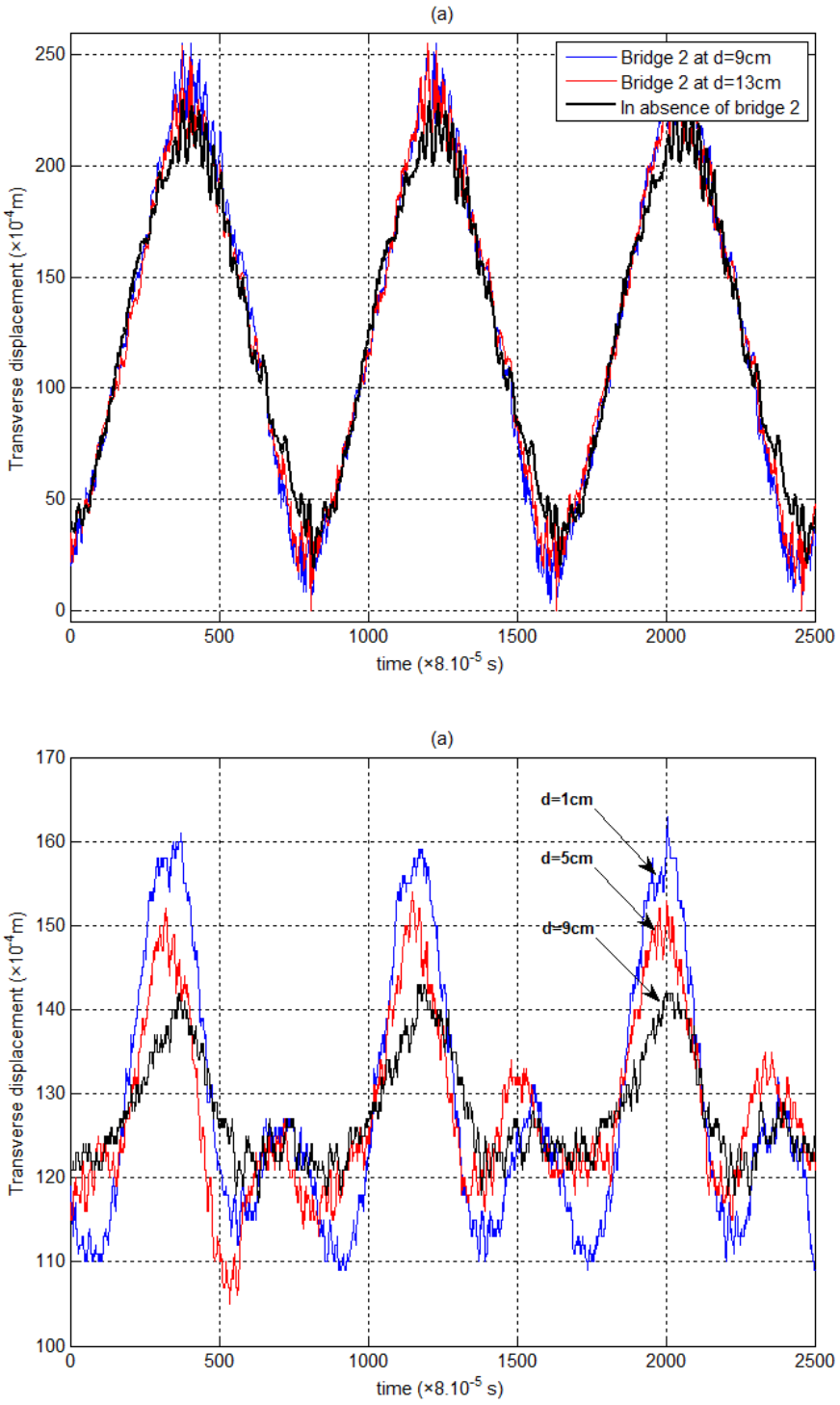

Figure 3.18: Experimental transverse displacement for several distances between the two bridges: (a) bridge 1; (b) bridge 2.

We can therefore conclude once again that the mathematical model we have developed is qualitatively valid.

We have shown in these previous two paragraphs that the proposed mathematical model of two coupled beam bridges is qualitatively satisfactory. To investigate the performance of the QZS vibration isolation on vibration isolation of these two coupled bridges, let us explore the dynamic behavior of a multi-span continuous beam bridge under QZS vibration isolation in the next two sections.

3.3 Isolation performance of a quasi-zero stiffness isolator in vibration isolation of a multi-span continuous beam bridge under pier base vibrating excitation

3.3.1 Model description, modelling and modal equations of a beam bridge under base vibrating excitation

a) Model description

The mechanical model of transverse vibration of a multi-span continuous beam bridge under QZS vibration isolators is shown in Fig. 3.19 where each QZS vibration isolator is made up of a QZS system connected in parallel with a viscous damper of damping coefficient C as shown in Fig. 2.9. Both boundaries of the bridge are simply supported and isolation is achieved by including the QZS vibration isolators under each pier of the bridge located at the positions X_j. L represents the length of the bridge, T and X are the time and the axial coordinate of the bridge, respectively.

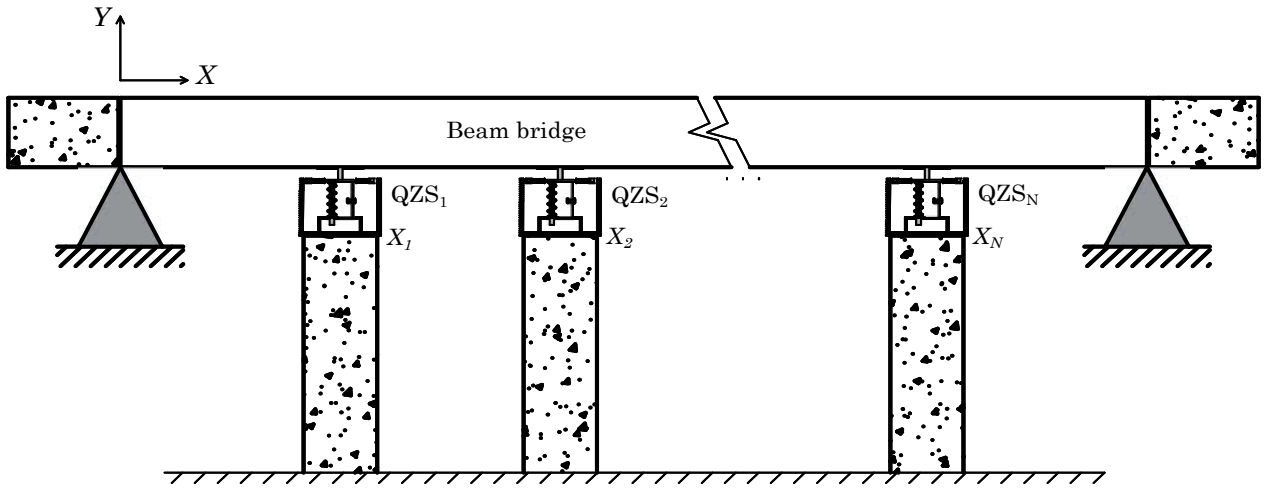

Figure 3.19: Mechanical model of the beam bridge with the QZS vibration isolators

b) Governing equation of a beam bridge with and without control

The transverse displacement of a homogeneous, isotropic and uniform elastic beam bridge subjected to a time varying load is described by the well-known Euler-Bernoulli equation as follows

$$\rho S\frac{\partial^2 Y}{\partial T^2}+C_b\frac{\partial Y}{\partial T}+EI\frac{\partial^4 Y}{\partial X^4}=F\left(X,T\right), \tag{3.38}$$

where $Y\left(X,T\right)$ is the transverse deflection of the beam bridge, ρ and E are the density of the beam and Young's modulus of the beam, respectively; S and I are the area and second moment of area of beam's cross section, respectively; C_b is the external viscous damping coefficient of the beam and $F\left(X,T\right)$ represents all the external loads including the external forces F_{QZS} due to the QZS vibration isolators under each pier of the beam bridge and defined by Eq. (2.50). Given that the beam bridge is simply supported, the boundary conditions of the problem are given by

$$Y\left(X,T\right)|_{X=0,X=L}=0 \quad \text{and} \quad \left.\frac{\partial^2 Y\left(X,T\right)}{\partial X^2}\right|_{X=0,X=L}=0. \tag{3.39}$$

To investigate the performance of the QZS vibration isolation on bridge vibration, let's consider a sinusoidal base vibrating excitation $Z=Z_0\cos\Omega T$, so the dynamical equations

of the beam bridge can be derived as following, where $\delta(\cdot)$ is the Dirac function, N and X_j are the number and the positions of the QZS vibration isolators located under the piers of the beam bridge, respectively.

• **with QZS vibration isolators**

The dynamical equation of a beam bridge with the N QZS vibration isolators can be obtained as

$$\rho S\frac{\partial^2 Y}{\partial T^2}+C_b\frac{\partial Y}{\partial T}+EI\frac{\partial^4 Y}{\partial X^4}+\sum_{j=1}^{N}\left(C\frac{\partial\left(Y-Z\right)}{\partial T}+\frac{\alpha_{QZS}}{a_0^3}k_vL_0\left(Y-Z\right)^3\right)\delta\left(X-X_j\right)=0. \tag{3.40}$$

• **without QZS control**

The dynamical equation of a beam bridge without QZS control can be obtained as

$$\rho S\frac{\partial^2 Y}{\partial T^2}+C_b\frac{\partial Y}{\partial T}+EI\frac{\partial^4 Y}{\partial X^4}=-\frac{\rho S}{N}\ddot{Z}\sum_{j=1}^{N}\delta\left(X-X_j\right), \tag{3.41}$$

where $\ddot{Z}=-\Omega^2 Z_0\cos\Omega T$. So, Eq. (3.41) can be rewritten as

$$\rho S\frac{\partial^2 Y}{\partial T^2}+C_b\frac{\partial Y}{\partial T}+EI\frac{\partial^4 Y}{\partial X^4}=\frac{\rho S\Omega^2 Z_0}{N}\sum_{j=1}^{N}\delta\left(X-X_j\right)\cos\Omega T. \tag{3.42}$$

• **with linear viscoelastic isolators**

For a linear viscoelastic isolator obtained from the corresponding QZS vibration isolator without the horizontal auxiliary springs, Eq. (2.50) giving the external force due to the nonlinear QZS vibration isolator can be rewritten as

$$F_{Linear}=-C\frac{\partial Y}{\partial T}-k_vY. \tag{3.43}$$

So, the dynamical equation of a beam bridge with the N linear viscoelastic isolators can be obtained as

$$\rho S\frac{\partial^2 Y}{\partial T^2}+C_b\frac{\partial Y}{\partial T}+EI\frac{\partial^4 Y}{\partial X^4}+\sum_{j=1}^{N}\left(C\frac{\partial\left(Y-Z\right)}{\partial T}+k_v\left(Y-Z\right)\right)\delta\left(X-X_j\right)=0. \tag{3.44}$$

c) Modal analysis

Let's introduce the following non-dimensional parameters

$$y = \frac{Y}{L_0}, z = \frac{Z}{L_0}, z_0 = \frac{Z_0}{L_0}, x = \frac{X}{L}, x_j = \frac{X_j}{L}, \tag{3.45}$$

$$a = \frac{a_0}{L_0}, \alpha_{QZS} = \frac{a}{2\left(1-a\right)}, \gamma_{QZS} = \frac{\alpha_{QZS}}{a^3} = \frac{1}{2a^2\left(1-a\right)}, \tag{3.46}$$

$$t = T\omega_0, \omega_0 = \frac{\pi^2}{L^2}\sqrt{\frac{EI}{\rho S}}, c_b = \frac{C_b}{\rho S\omega_0}, c = \frac{2C}{\rho SL\omega_0}, k = \frac{2k_v}{\rho SL\omega_0^2}, \omega = \frac{\Omega}{\omega_0}, \tag{3.47}$$

so that the motion equations, Eqs. (3.40), (3.42) and (3.44) can be rewritten in their non-dimensional form given by Eqs. (3.48), (3.49) and (3.50), respectively.

$$\frac{\partial^2 y}{\partial t^2} + c_b\frac{\partial y}{\partial t} + \frac{1}{\pi^4}\frac{\partial^4 y}{\partial x^4} + \frac{L}{2}\sum_{j=1}^{N}\left[c\left(\frac{\partial y}{\partial t} - \frac{dz}{dt}\right) + \gamma_{QZS}k\left(y-z\right)^3\right]\delta\left(x-x_j\right) = 0, \tag{3.48}$$

$$\frac{\partial^2 y}{\partial t^2} + c_b\frac{\partial y}{\partial t} + \frac{1}{\pi^4}\frac{\partial^4 y}{\partial x^4} = \frac{z_0\omega^2}{N}\sum_{j=1}^{N}\delta\left(x-x_j\right)\cos\omega t, \tag{3.49}$$

$$\frac{\partial^2 y}{\partial t^2} + c_b\frac{\partial y}{\partial t} + \frac{1}{\pi^4}\frac{\partial^4 y}{\partial x^4} + \frac{L}{2}\sum_{j=1}^{N}\left[c\left(\frac{\partial y}{\partial t} - \frac{dz}{dt}\right) + k\left(y-z\right)\right]\delta\left(x-x_j\right) = 0, \tag{3.50}$$

with boundary conditions

$$y\left(x,t\right)\big|_{x=0,x=1} = 0 \ \text{ and } \ \left.\frac{\partial^2 y\left(x,t\right)}{\partial x^2}\right|_{x=0,x=1} = 0. \tag{3.51}$$

3.3.2 Resonance responses

In ordre to obtain the modal equations, the Galerkin method is applied. This method of separation of variables suggests the solutions of the equations of motion (Eqs. (3.48), (3.49) and (3.50)) into the following form

$$y\left(x,t\right) = \sum_{n=1}^{N_{\max}}\phi_n\left(x\right)q_n\left(t\right), \tag{3.52}$$

where $N_{\max}$ is an integer greater than 1, $q_n(t)$ the amplitude of the nth mode of vibration and $\phi_n(x)$ the mode shapes, given in accordance with the boundaries conditions of the problem by

$$\phi_n(x) = \sin(n\pi x). \tag{3.53}$$

By applying the Galerkin method, the modal ordinary differential equations (3.54), (3.55) and (3.56) can be derived for the motion partial differential equations (3.48), (3.49) and (3.50), respectively as

$$\begin{aligned}\ddot{q}_m + c_b\dot{q}_m + \omega_m^2 q_m + c\sum_{j=1}^{N}\sin(m\pi x_j)\left[\sum_{n=1}^{N_{\max}}\dot{q}_n\sin(n\pi x_j) + z_0\omega\sin\omega t\right] \\ + \gamma_{QZS}k\sum_{j=1}^{N}\sin(m\pi x_j)\left[\sum_{n=1}^{N_{\max}}q_n\sin(n\pi x_j) - z_0\cos\omega t\right]^3 = 0,\end{aligned} \tag{3.54}$$

$$\ddot{q}_m + c_b\dot{q}_m + \omega_m^2 q_m = \frac{2z_0\omega^2}{NL}\sum_{j=1}^{N}\sin(m\pi x_j)\cos\omega t, \tag{3.55}$$

$$\begin{aligned}\ddot{q}_m + c_b\dot{q}_m + \omega_m^2 q_m + c\sum_{j=1}^{N}\sin(m\pi x_j)\left[\sum_{n=1}^{N_{\max}}\dot{q}_n\sin(n\pi x_j) + z_0\omega\sin\omega t\right] \\ + k\sum_{j=1}^{N}\sin(m\pi x_j)\left[\sum_{n=1}^{N_{\max}}q_n\sin(n\pi x_j) - z_0\cos\omega t\right] = 0,\end{aligned} \tag{3.56}$$

where $\omega_m = m^2$ is the non-dimensional natural frequency of the mth mode of the beam bridge, with $m = 1, 2, ..., N_{\max}$.

3.3.3 Absolute motion transmissibility

A more valuable parameter for the assessment of the isolation properties of the QZS vibration isolators is the absolute motion transmissibility which is defined as the ratio between the displacement of the beam bridge at a given point and that of the pier base. So, when the steady-state response occurs for the mth mode, the absolute motion transmissibility of

the QZS vibration isolators can be defined as follow

$$T_{am} = \frac{|y_m|_{\max}}{|z|_{\max}} = \frac{|q_m|_{\max} \sin(m\pi x)}{z_0} = \frac{A_{\mathrm{m}} \sin(m\pi x)}{z_0}, \tag{3.57}$$

where A_{m} is the response amplitude of the mth shape mode of the beam bridge, z_0 is the magnitude of the base excitation and $\sin(m\pi x)$ is the shape function of the mth mode of vibration. This expression of absolute motion transmissibility (Eq. (3.32)) have the same forms as the linear viscoelastic isolators. The next section aims to show the benefits of employing a QZS isolation mount. This is done by comparing the absolute motion transmissibility of the QZS vibration isolators with that of the equivalent linear viscoelastic supports.

3.3.4 Dynamical explanation

In this work, the number of vibration modes is set as $N_{\max} = 4$. Eqs. (3.54), (3.55) and (3.56) are numerically solved by using the RK4 method in other to generate the transverse response of the beam bridge in the presence of QZS vibration isolators, without a QZS control and in the presence of linear vicoelastic isolators, respectively. The initial values for the first calculations are set as $q_1 = 0.01$ (i.e. $Y_1 = 0.01L_0$), $\dot{q}_1 = 0$, $q_n = 0$, $\dot{q}_n = 0$ for $n = 2, 3, 4$ and the non-dimensional magnitude of the base excitation is $z_0 = 0.05$ (i.e. $Z_0 = 0.05L_0$). Table 3.2 presents the physical and geometrical parameters values of the QZS vibration isolators used under a seven-span beam bridge with wood material [**?**, 29, 104]. In the following study, the parameter values are assigned as listed in Table 3.2 if there is no special mention.

The non-dimensional parameters are obtained by calculation on the basis of Eqs. (3.46), (3.47) and $I = \frac{bh^3}{3} = 2,59 \times 10^{-8}$ m^4 as follows

$a = 0.67$, $\gamma_{QZS} = 3.375$, $\omega_0 = 79.69$ rad/s, $c_b = 0.290$, $c = 0.019$, $k = 2.43$.

So, the first four natural frequencies of the beam bridge are determined as $\Omega_1 = 79.69$ rad/s

Table 3.2: Physical and geometric parameters of the wooden beam bridge and the QZS vibration isolators

Item	**Notation**	**Value**
Young's modulus of the beam	E	5.5 GPa
Density of the beam	ρ	800 Kg/m^3
Length of the beam	L	1.5 m
Width of the beam	b	0.045 m
Height of the beam	h_b	0.012 m
External damping of the beam	C_b	10 N.s/m^2
Viscosity damping of the spring	C	0.5 N.s/m
Initial length of the horizontal spring	L_0	0.1 m
Horizontal length of the horizontal spring	a_0	0.067 m
Horizontal spring linear stiffness	k_0	5000 N/m
Vertical spring stiffness	k_v	5000 N/m
Number of piers	N	6
positions of the piers	X_j	$X_j = 0.133 + 0.247 \times (j-1)$ m

($f_1 = 12.68$ Hz), $\Omega_2 = 318.74$ rad/s ($f_2 = 50.73$ Hz), $\Omega_3 = 717.16$ rad/s ($f_3 = 114.14$ Hz) and $\Omega_4 = 1274.95$ rad/s ($f_4 = 202.92$ Hz). Moreover, the corresponding mode functions of the transverse vibration can be obtained. The RK4 algorithm is used to compute the numerical solutions of Eqs. (3.54), (3.55) and (3.56) for the above non-dimensional parameters.

a) Resonant vibration without and with control

In this subsection, amplitude and motion transmissibility curves are plotted versus the excitation frequencies ω of the sinusoidal base excitation. The steady-state amplitude A_m and the absolute motion transmissibility T_{am} are plotted in Figs. 3.20, 3.21, 3.22 and 3.23 for the first four modal primary resonances (m=1,2,3 and 4) of the beam bridge in the following cases: firstly in the presence of QZS vibration isolators, then without QZS control and finally in the presence of linear viscoelastic isolators.

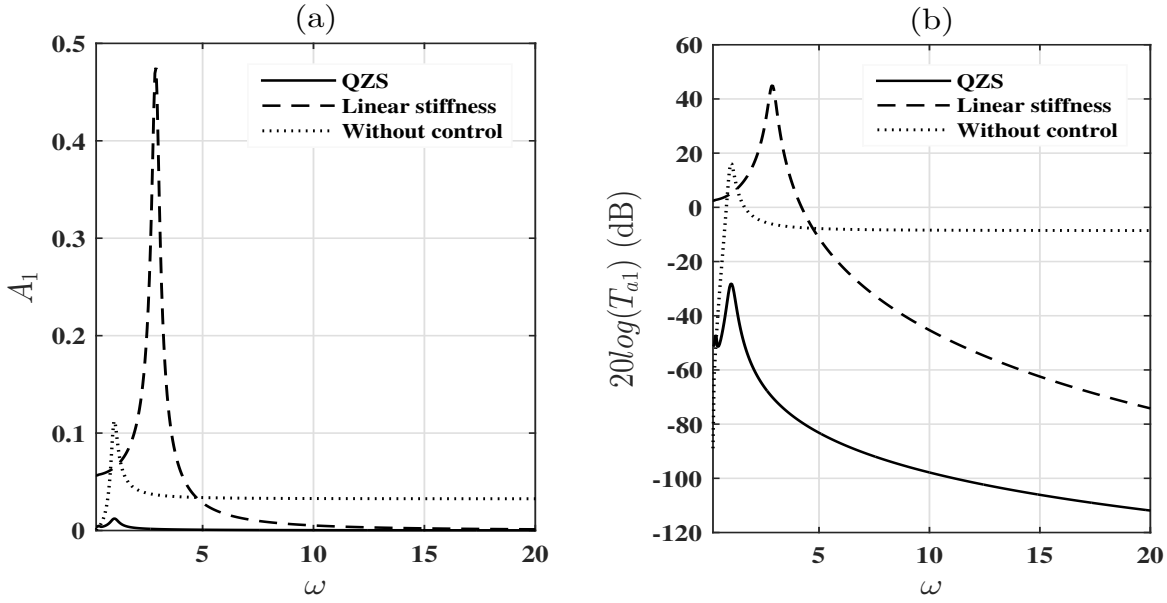

Figure 3.20: The steady-state amplitude (a) and the absolute motion transmissibility (b) for first-order primary resonance of the beam bridge without and with control (QZS and linear viscoelastic controls)

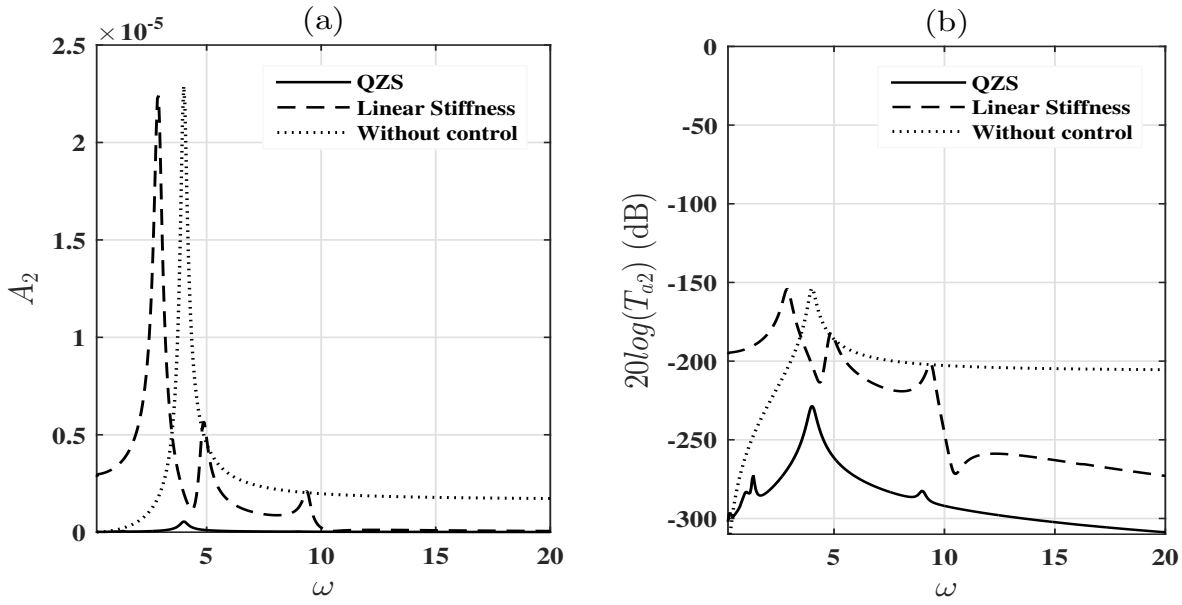

Figure 3.21: The steady-state amplitude (a) and the absolute motion transmissibility (b) for second-order primary resonance of the beam bridge without and with control (QZS and linear viscoelastic controls)

It can be argued that there are two indices that allow measuring the effectiveness of a vibration isolator: the first one is the bandwidth of the isolation region, which is the frequency region within which the transmitted motion amplitude becomes smaller than the base excitation amplitude, that is when $T_{am} < 1$ (i.e. $20log\,(T_{am}) < 0$ dB); the other is the peak-transmissibility, which is the maximum amplitude of the transmitted motion for a given amplitude of the base excitation. Figs. 3.20, 3.21, 3.22 and 3.23 show that for all the first four modes of vibration,

(a) both linear and QZS vibration control methods are effective for high frequencies after the resonance region but only the QZS vibration isolators are able of attenuating low frequency vibrations;

(b) the linear viscoelastic isolators modifie the natural frequencies of the beam bridge while the QZS vibration isolators keeps them constant;

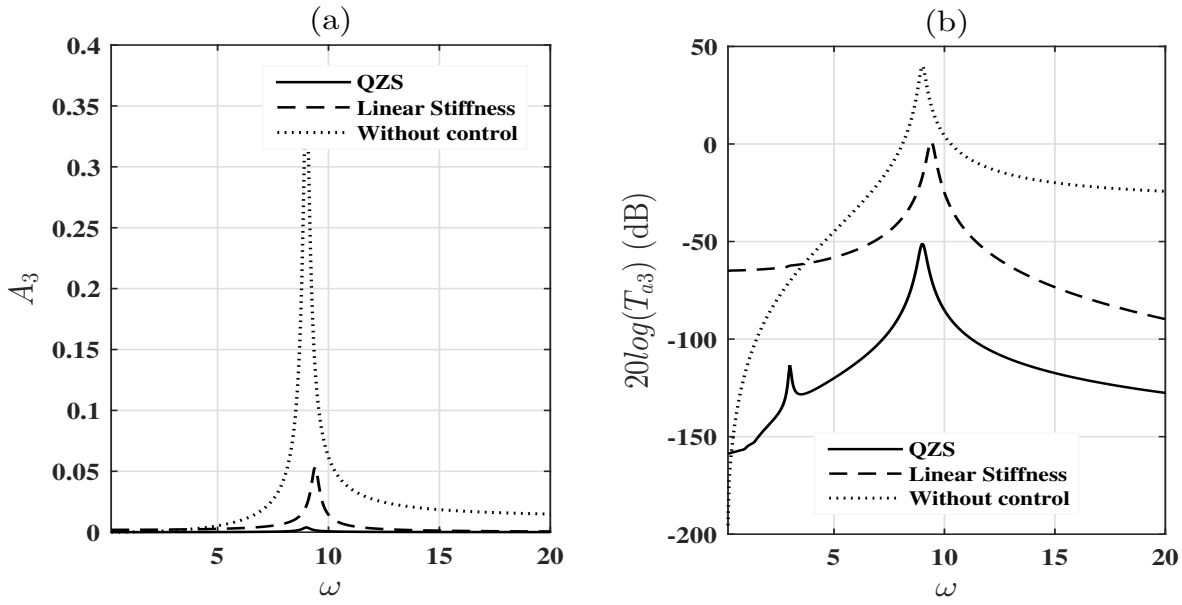

Figure 3.22: The steady-state amplitude (a) and the absolute motion transmissibility (b) for third-order primary resonance of the beam bridge without and with control (QZS and linear viscoelastic controls)

(c) in the presence of the control, the vibration amplitudes of the first-order mode are very large compared to those of the other three modes, confirming that most of the energy of the beam bridge is concentrated in the first mode [29, 166].

In order to confirm the effectiveness of the two control methods, the dynamical responses of the first four modes of vibration of the beam bridge when the exciter vibrates at their resonance frequencies have been plotted in Fig. 3.24. This figure clearly shows that the QZS control method is more efficient than the linear viscoelastic control method for the first four modes of vibration.

b) Evaluation of the vibration isolation performance of the QZS control

The vibration isolators are sometimes used to isolate the displacement excitation transmitted from the base to the working equipment. In this subsection, the effects of some

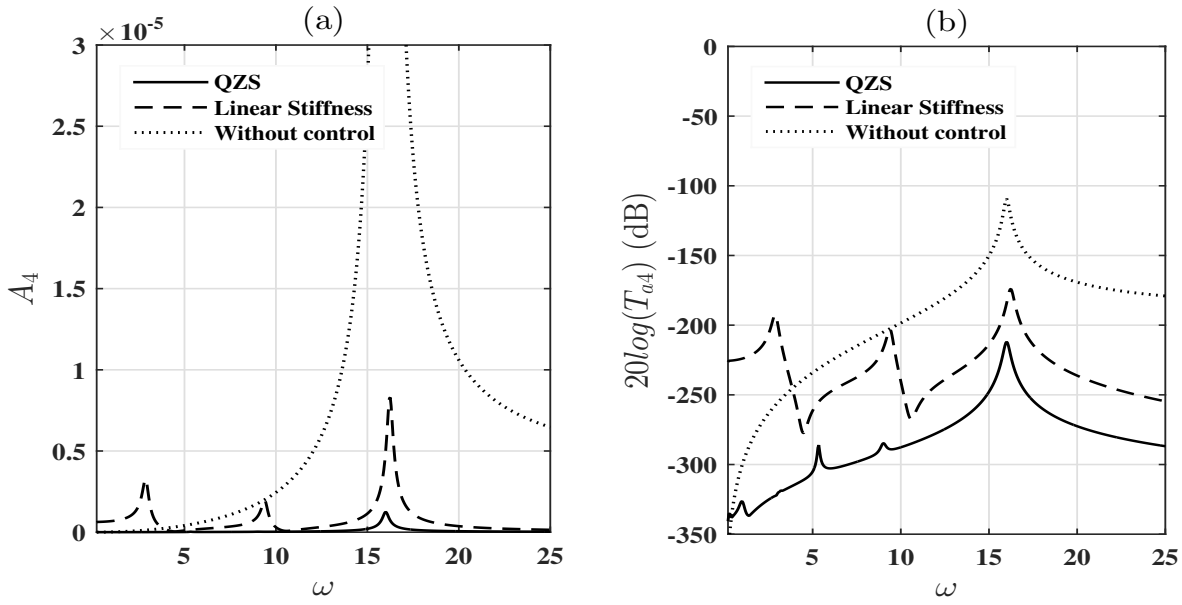

Figure 3.23: The steady-state amplitude (a) and the absolute motion transmissibility (b) for fourth-order primary resonance of the beam bridge without and with control (QZS and linear viscoelastic controls)

parameters on the absolute transmissibility of steady-state behaviors are investigated, including geometrical arrangement ratio γ_{QZS}, vertical spring stiffness k of the QZS vibration isolators and for the corresponding linear viscoelastic isolators, damping coefficient c and excitation magnitude z_0. The absolute motion transmissibility curves of the system for these different parameters are plotted in Figs. 3.28, 3.29 and 3.30 for the beam bridge, (a) under QZS control and (b) under linear viscoelastic control. Then, the benefit of QZS isolators is verified when some conditions are satisfied, by comparing the absolute motion transmissibility of the QZS vibration isolators with that of the corresponding linear viscoelastic isolators. The analysis is limited to the first mode of vibration of the midspan of the beam bridge where $\sin(m\pi x) = 1$, insofar as the first mode is expected to carry most of the energy, and therefore one hopes that it could suffice to obtain a first estimate of the system behavior.

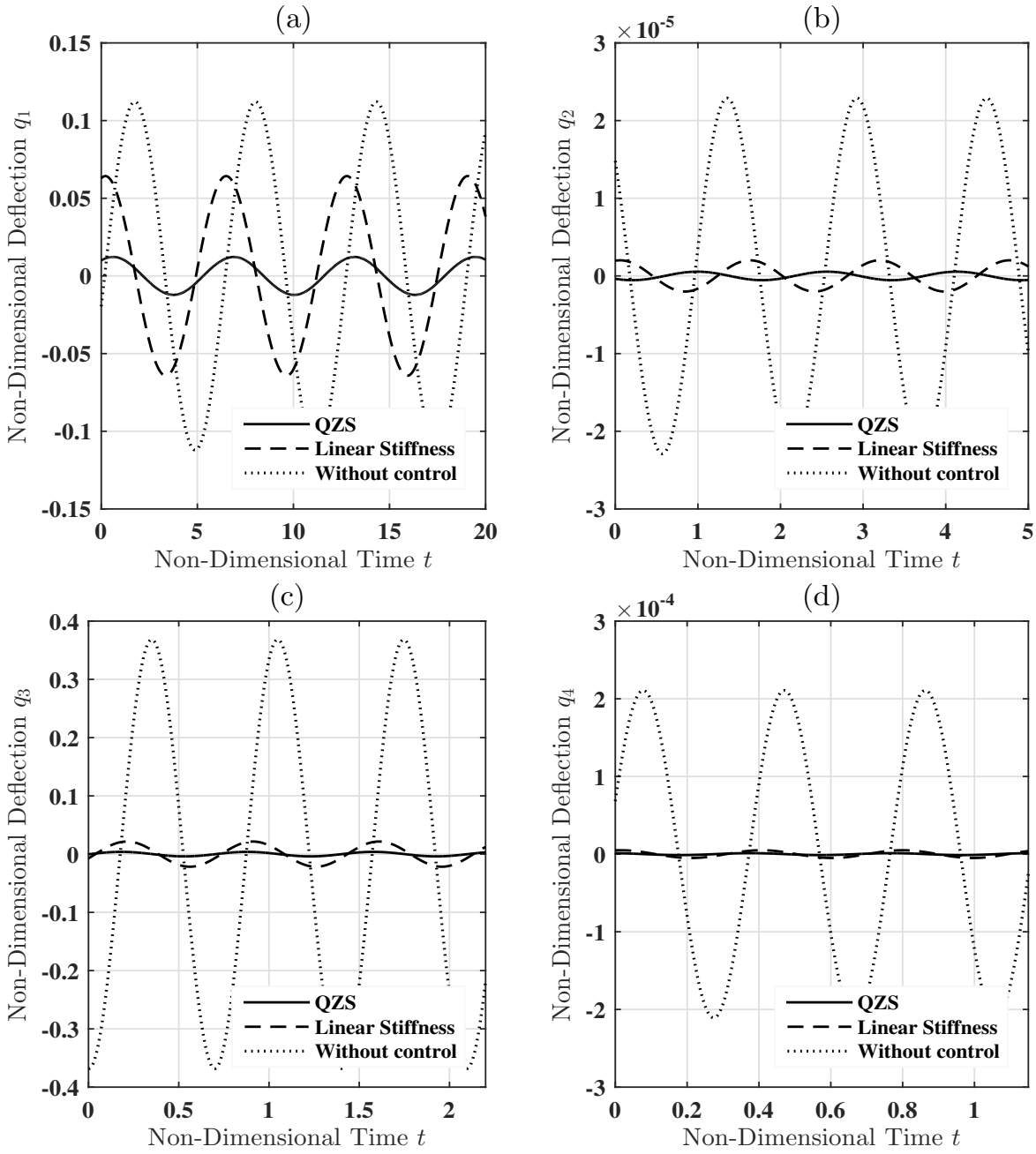

Figure 3.24: Times histories of the first four primary resonance of the beam bridge: (a) first-order with $\omega = \omega_1 = 1$, (b) second-order with $\omega = \omega_2 = 4$, (c) third-order with $\omega = \omega_3 = 9$ and (d) fourth-order with $\omega = \omega_4 = 16$

- **Effect of the nonlinear term of the QZS vibration isolator**

Let us recall the geometric ratio α_{QZS} is given from Eq. (2.47) as follows

$$\alpha_{QZS} = \frac{a}{2\,(1-a)}. \tag{3.58}$$

So, for a given value of a, there is only one value of the stiffness ratio α that ensures zer stiffness behavior. Equivalently, the value a_{QZS} that gives quasi-zero stiffness for a given value of the stiffness ratio α is

$$a_{QZS} = \frac{2\alpha}{2\alpha+1}. \tag{3.59}$$

The subscript QZS on either α or a is used to denote that the other parameter is not independent, but has been chosen in accordance with Eqs. (3.58) and (3.59) so as to achieve stable QZS behavior. The combinations of stiffness ratio α and geometric ratio a that give rise to stable QZS are shown in graphical form in Fig. 3.25. This figure shows that for small initial angles ($a \approx 1$, i.e. $\theta_0 \approx 0°$) and according to the expression of the parameter α given in Eq. (2.44), the order of magnitude of the stiffness of the inclined springs needs to be larger than this of the vertical spring. Furthermore, for moderate initial inclination angle of is a moderate ($0.4 < a < 0.8$, i.e. $\theta_0 \approx 36° - 66°$), vertical and inclined springs of similar stiffnesses can be used. The combinations of nonlinear geometric parameter γ_{QZS} and geometric ratio a that give rise to stable QZS have been plotted in Fig. 3.26. This figure shows that for great initial inclination angle ($a < 0.2$, i.e. $\theta_0 \approx 78° - 90°$), the nonlinear geometric parameter γ_{QZS} presents very large values, which means that the isolation system involves a strong nonlinearity. The smallest values of control parameter γ_{QZS} ($\gamma_{QZS} = 3.375$) is obtained for $a = 0.67$, corresponding to the initial inclination angle $\theta_0 = 48°$. Then, the steady-state amplitude and the absolute motion transmissibility for the first mode of the beam bridge for different values of the nonlinear geometric parameter γ_{QZS} are studied and plotted in Fig. 3.27. This figure shows that the vibration amplitude and the absolute motion

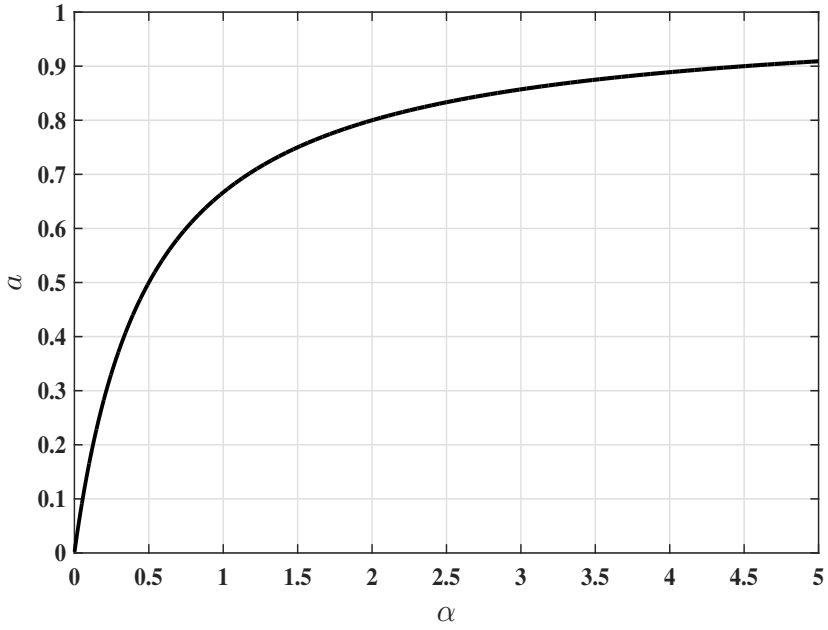

Figure 3.25: Combinations of geometric ratio a and stiffness ratio α that yield QZS

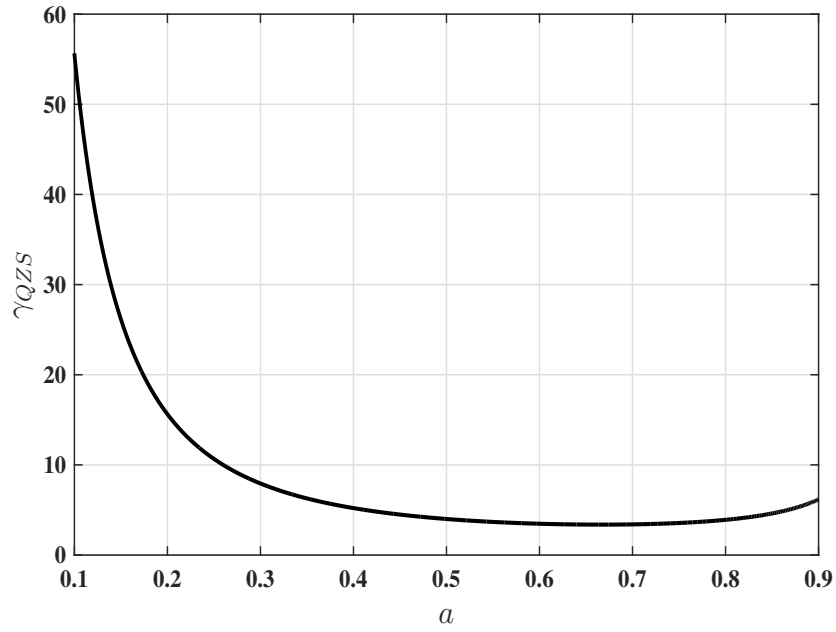

Figure 3.26: Combinations of geometric ratio a and nonlinear geometric parameter γ_{QZS} that yield QZS

transmissibility increase gradually with the nonlinear term of the system, and the bend of the curve is more and more obvious. Furthermore, for strong nonlinearities ($\gamma_{QZS} = 26.1$ and $\gamma_{QZS} = 55.6$), the frequency of resonance is shifted to the high frequency region and jump phenomenon occur. Therefore, geometric nonlinearity is not beneficial for the vibration isolation.

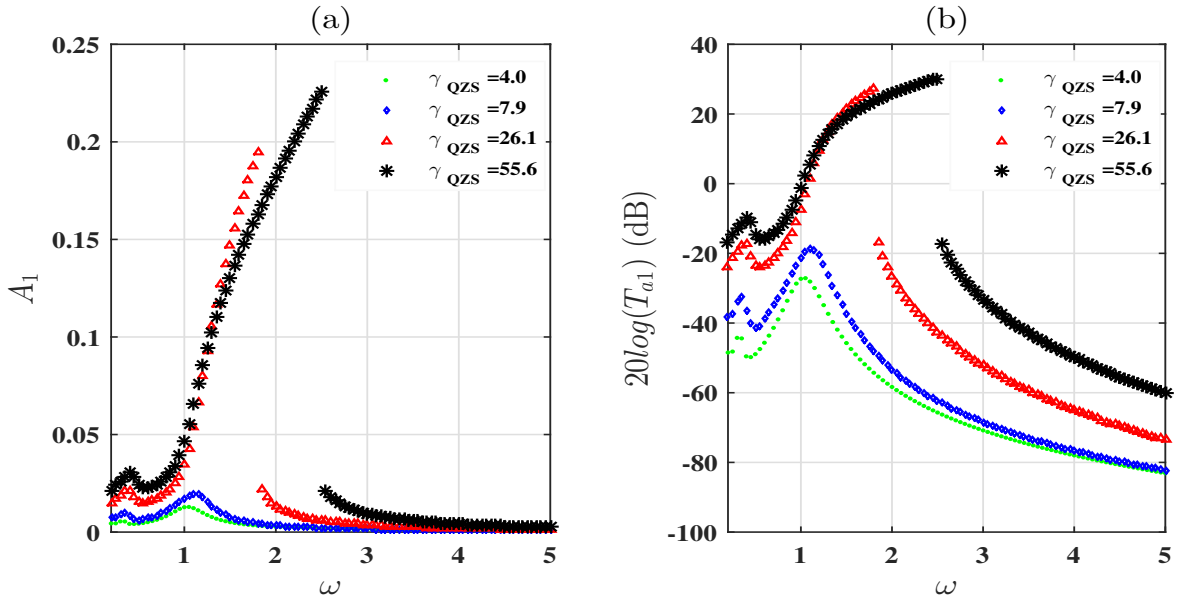

Figure 3.27: Effect of the nonlinear geometric parameter γ_{QZS} on (a) the steady-state amplitude and (b) the absolute transmissibility of the beam bridge for $\gamma_{QZS} = 4.0$ ($a = 0.50$), $\gamma_{QZS} = 7.9$ ($a = 0.30$), $\gamma_{QZS} = 26.1$ ($a = 0.15$) and $\gamma_{QZS} = 55.6$ ($a = 0.10$)

- **Effect of the vertical spring stiffness**

The absolute motion transmissibility of the first mode of vibration of the beam bridge for different values of the vertical spring stiffness (a) under QZS control and (b) under linear viscoelastic control are plotted in Fig. 3.28 in order to study the effect of the vertical spring stiffness on the performance of the two types vibration isolators. Fig. 3.28(a) shows that the vertical spring stiffness presents similar effects on the dynamics of the beam bridge as those

observed with the nonlinear term of the QZS vibration isolators. It can be seen that smaller stiffness yields smaller motion transmissibility, i.e. better isolation performance of the QZS vibration isolators. On the other hand, Fig. 3.28(b) shows that the motion transmissibility depends strongly on the value of the vertical spring stiffness k of the linear viscoelastic isolators with which it increases, as well as the isolation frequency band. In addition, the frequency of resonance is also shifted to the high frequency region while k increases. Therefore, vertical spring stiffness is not beneficial for the vibration isolation both for QZS vibration isolator and its equivalent linear viscoelastic isolator. But it can be seen that, QZS vibration isolator could have a remarkable benefit in isolation performance compared to the linear one.

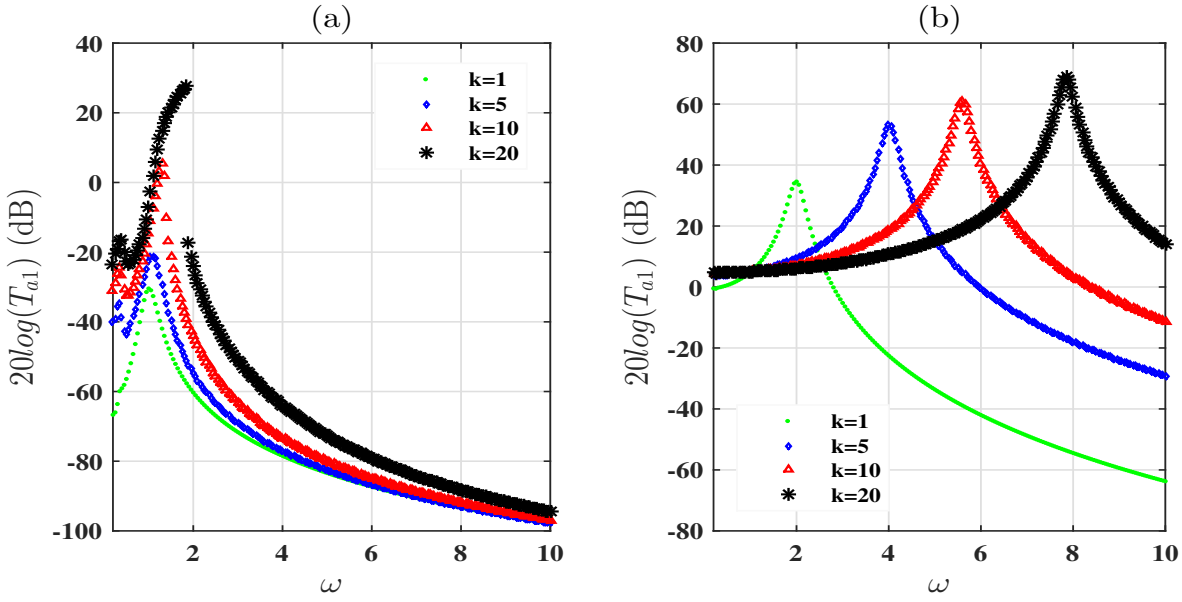

Figure 3.28: Effect of the vertical spring stiffness on the absolute transmissibility of the beam bridge (a) under QZS control and (b) under linear viscoelastic control for $k = 1$, $k = 5$, $k = 10$ and $k = 20$

- **Effect of the viscosity damping of the QZS vibration isolator**

Fig. 3.29 shows the absolute motion transmissibility of the QZS vibration isolators and

linear viscoelastic isolators for various values of the damping coefficient c. Fig. 3.29(a) shows that the absolute motion transmissibility of the QZS vibration isolators increase with the viscous damping, with sacrificing the performance of the nonlinear isolators. This result is too original in this case of base vibration control of a beam bridge with QZS vibration isolators. Since in most of the cases where QZS vibration isolator is applied for discrete structures, the absolute transmissibility undergoes a reduction as the damping increases [111, 156, 167], similarly to the case of damping effect on linear viscoelastic isolator an shown in Fig. 3.29(b). From the above analysis, it can be concluded that, QZS vibration isolator could have a remarkable benefit in isolation performance for relatively low damping or without damping. Fig. 3.29(b) shows that the increase of viscous damping lowers the absolute transmissibility at resonance frequency but deteriorates the higher frequency vibration attenuation rate.

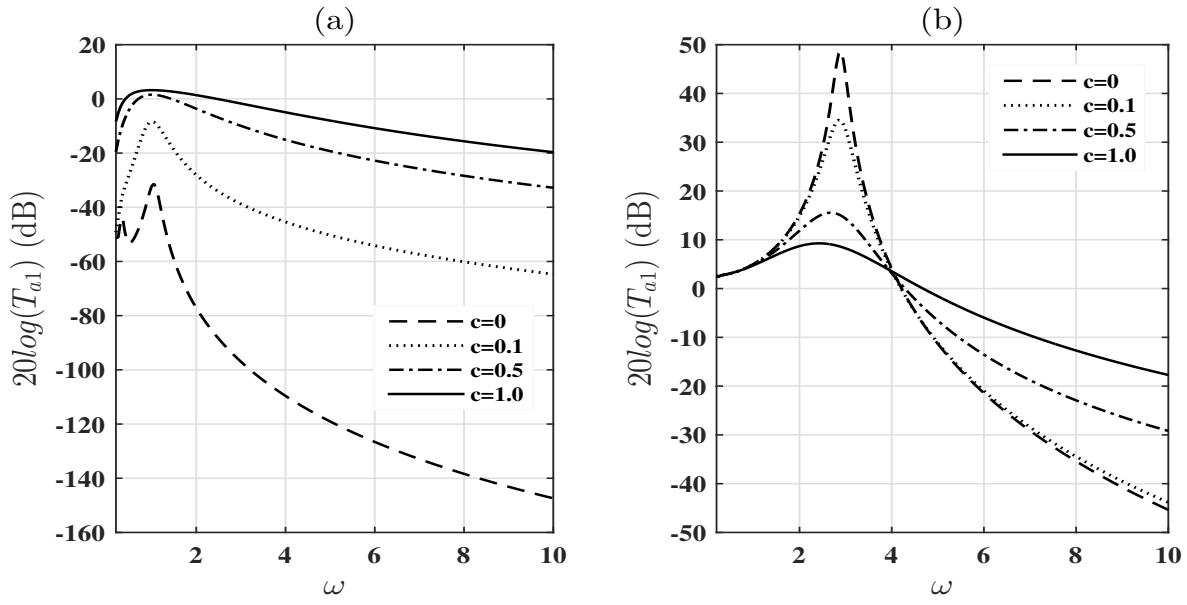

Figure 3.29: Effect of viscosity damping on the absolute transmissibility of the beam bridge (a) under QZS control and (b) under linear viscoelastic control for $c = 0$, $c = 0.1$, $c = 0.5$ and $c = 1.0$

- **Effect of magnitude of the base excitation**

The effect of the base excitation amplitude on the performance of the QZS vibration isolators and the linear viscoelastic isolators is shown in Fig. 3.30. As shown in Fig. 3.30(a), for the QZS vibration isolators, the absolute motion transmissibility increases with the excitation amplitude. Furthermore, for large amplitudes, the steady-states frequency response curve is characterised by a jump phenomenon and the curve presents unstable solutions. In addition, the shift of the resonance peak to the high frequencies can be also observed when the excitation amplitude increase. This means that the use of the QZS vibration isolators is more suitable in the conditions where the vibration excitation is smaller. For linear viscoelastic isolators, the absolute motion transmissibility is unrelated to the excitation amplitude as shown in Fig. 3.30(b).

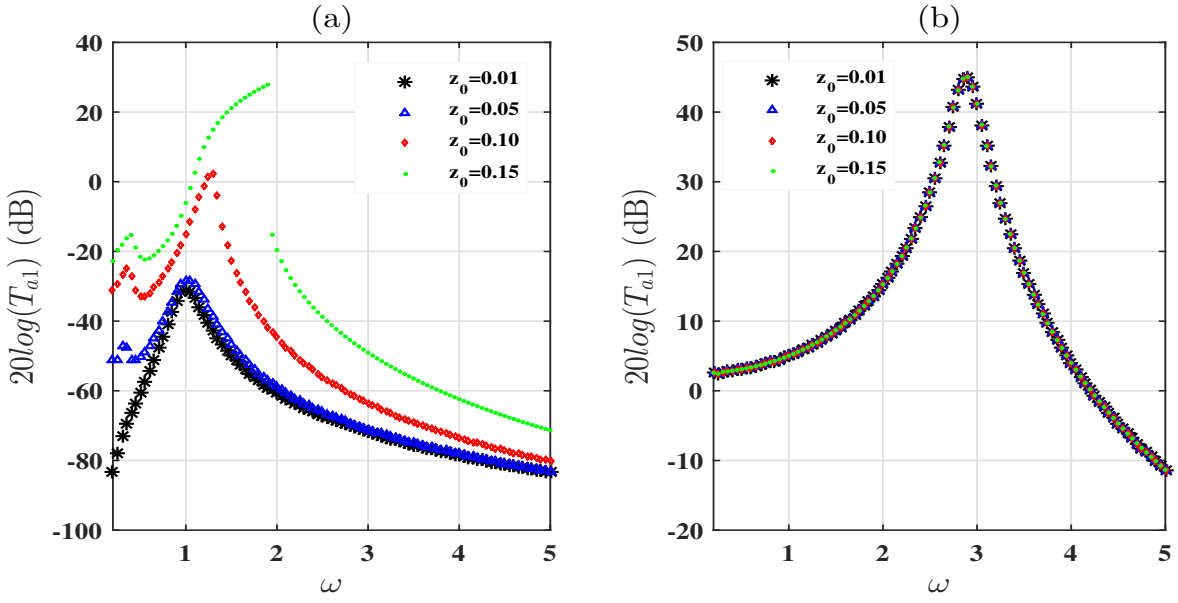

Figure 3.30: Effect of magnitude of base excitation on the absolute transmissibility of the beam bridge (a) under QZS control and (b) under linear viscoelastic control for $z_0 = 0.01$, $z_0 = 0.05$, $z_0 = 0.10$ and $z_0 = 0.15$

3.4 Vibration isolation of a multi-span continuous beam bridge under moving mass using QZS vibration isolators

3.4.1 Model description, modelling and modal equations of the bridge-QZS vibration isolators coupled system

a) Model description and modelling

In order to point out the effectiveness of QZS vibration isolators on the dynamics of a multi-span continuous beam bridge subjected to a single moving load with a constant speed v, let's consider the beam bridge-QZS vibration isolators coupled system shown in Fig. 3.31. Let X and T denote the independent spatial and time variables, respectively. It is assumed that the mass travels from left to right in the direction X at the constant speed v and the beam vibrates only in the Y direction.

The multi-span continuous beam bridge is modeled as a single simply supported span resting on intermediate QZS vibrations isolators placed on each pier of the bridge. The bridge is considered as a damped linear elastic Euler-Bernoulli beam of length L, density ρ, cross-sectional area S, Young's modulus E, second moment of inertia with respect to the neutral axis I, and supported by N QZS vibration isolators located above the piers at positions X_j $(j = 1, ..., N)$ as shown in Fig. 3.31.

The governing equation of motion of the bridge-QZS vibration isolators coupled system under the action of the moving mass M can be written as

$$\rho S\frac{\partial^2 Y}{\partial T^2} + C_b\frac{\partial Y}{\partial T} + EI\frac{\partial^4 Y}{\partial X^4} = \zeta\left(T\right)F_{mov}\left(X,T\right) + \sum_{j=1}^{N} F_{j\_QZS}\left(X,T\right), \tag{3.60}$$

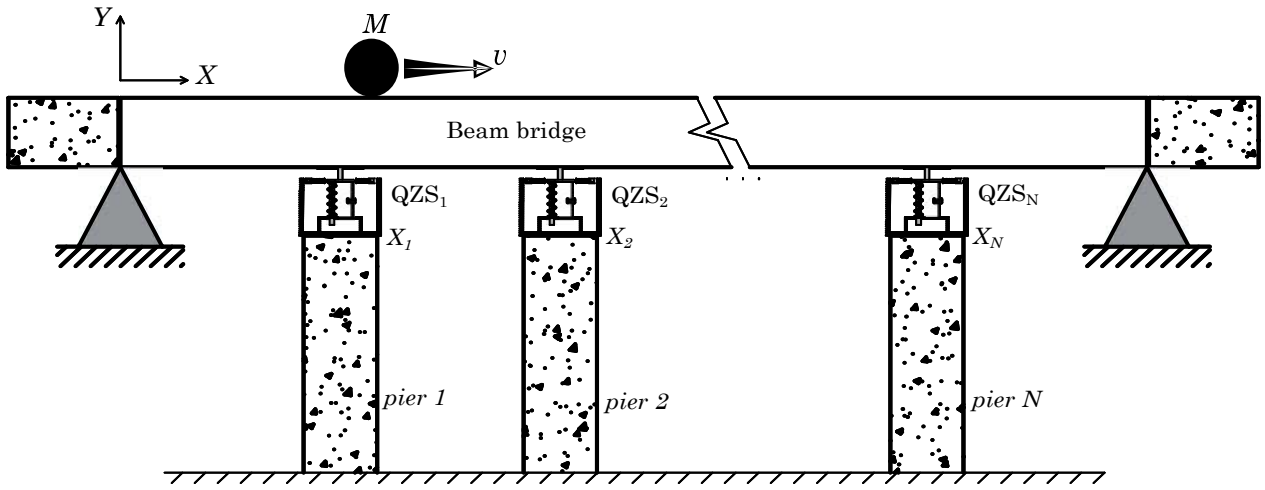

Figure 3.31: Mechanical model of a beam bridge under QZS isolators

with

$$\zeta(T) = \mathrm{H}(vT) - \mathrm{H}(vT - L), \tag{3.61}$$

where $\mathrm{H}(\cdot)$ is the Heaviside step function that defines the time periods during which the moving mass just comes onto and leaves the beam, $Y(X,T)$ is the transverse motion at position X and time T, ρS is the mass per unit of length, EI is the bending stiffness, C_b is the damping coefficient of beam bridge, $F_{j\_QZS}(X,T)$ is the external force due to the QZS isolator under the jth pier of the bridge approximated by Eq. (3.62) and $F_{mov}(X,T)$ is the moving load defined by Eq. (3.63) [168–171] as follows

$$F_{j\_QZS}(X,T) = -\left(C\frac{\partial Y}{\partial T} + \frac{\alpha_{QZS}}{a_0^3}k_v L_0 Y^3\right)\delta(X - X_j), \tag{3.62}$$

$$F_{mov}(X,T) = \left[Mg - M\left(\frac{\partial^2 Y}{\partial T^2} + 2v\frac{\partial^2 Y}{\partial T \partial X} + v^2\frac{\partial^2 Y}{\partial X^2}\right)\right]\delta(X - vT), \tag{3.63}$$

where g is the gravitational acceleration, $\delta(\cdot)$ is the Dirac delta function, C is the damping coefficient of the QZS isolator and α_{QZS} is the geometric ratio of the QZS system defined as

$$\alpha_{QZS} = \frac{a_0}{2(L_0 - a_0)}. \tag{3.64}$$

So, the equation of motion (Eq. (3.60)) can be rewritten as follow

$$\begin{array}{c}\rho S\frac{\partial^2 Y}{\partial T^2}+C_b\frac{\partial Y}{\partial T}+EI\frac{\partial^4 Y}{\partial X^4}+\sum_{j=1}^{N}\left(C\frac{\partial Y}{\partial T}+\frac{\alpha_{QZS}}{a_0^3}k_v L_0 Y^3\right)\delta\left(X-X_j\right)= \\ \zeta\left(T\right)\left[Mg-M\left(\frac{\partial^2 Y}{\partial T^2}+2v\frac{\partial^2 Y}{\partial T\partial X}+v^2\frac{\partial^2 Y}{\partial X^2}\right)\right]\delta\left(X-vT\right)\end{array}, \tag{3.65}$$

with the boundary conditions of a simply supported beam given by

$$Y\left(X,T\right)|_{X=0,X=L}=0 \text{ and } \left.\frac{\partial^2 Y\left(X,T\right)}{\partial X^2}\right|_{X=0,X=L}=0. \tag{3.66}$$

In order to investigate the performance of vibration isolation of the QZS isolator on the beam bridge vibration, let us derive the modal equations.

b) Modal equations

It is convenient to introduce the following non-dimensional quantities

$$x=\frac{X}{L},x_j=\frac{X_j}{L},y=\frac{Y}{L_0},a=\frac{a_0}{L_0},\alpha_{QZS}=\frac{a}{2\left(1-a\right)},\tau=\frac{vT}{L}. \tag{3.67}$$

so that the motion equation (Eq. (3.65)) and the boundary conditions given by Eq. (3.66) can be rewritten in their non-dimensional forms as follow

$$\begin{array}{c}\frac{\partial^2 y}{\partial\tau^2}+\frac{C_b L}{\rho S v}\frac{\partial y}{\partial\tau}+\frac{EI}{\rho S L^2 v^2}\frac{\partial^4 y}{\partial x^4}+\sum_{j=1}^{N}\left[\frac{CL}{\rho S v}\frac{\partial y}{\partial\tau}+\frac{\alpha_{QZS}k_v}{a^3}\frac{L^2}{\rho S v^2}y^3\right]\delta\left(x-x_j\right)= \\ \zeta\left(\tau\right)\left[\frac{MgL^2}{\rho S L_0 v^2}-\frac{M}{\rho S}\left(\frac{\partial^2 y}{\partial\tau^2}+2\frac{\partial^2 y}{\partial\tau\partial x}+\frac{\partial^2 y}{\partial x^2}\right)\right]\delta\left(x-\tau\right)\end{array}, \tag{3.68}$$

where

$$\zeta\left(\tau\right)=\mathrm{H}\left(\tau\right)-\mathrm{H}\left(\tau-1\right)=\begin{cases}1,\ \tau\leq 1\\ \\ 0,\ \tau>1\end{cases}, \tag{3.69}$$

with boundary conditions rewritten as follows

$$y\left(x,\tau\right)|_{x=0,x=1}=0 \text{ and } \left.\frac{\partial^2 y\left(x,\tau\right)}{\partial x^2}\right|_{x=0,x=1}=0. \tag{3.70}$$

To obtain the modal equations, the MS method is applied. This method suggests the solution of the equation of motion (Eq. (3.68)) into the following form

$$y\left(x,\tau\right)=\sum_{n=1}^{\infty}\phi_n\left(x\right)q_n\left(\tau\right), \tag{3.71}$$

where $\phi_n(x)$ are the mode shapes, given in accordance with the boundary conditions of the problem by

$$\phi_n(x) = \sin(n\pi x), \tag{3.72}$$

and $q_n(\tau)$ is the amplitude of the nth mode of vibration. Substituting Eq. (3.72) into Eq. (3.68), multiplying by $\phi_m(x) = \sin(m\pi x)$, integrating over the beam length $[0, L]$ and using the orthogonality condition, leads to the modal equations

$$\begin{aligned}\ddot{q}_m + c_b\dot{q}_m + \omega_m^2 q_m + \sum_{j=1}^{N}\left[c\sum_{n=1}^{\infty}\dot{q}_n\phi_n(x_j) + \frac{2L}{\rho S v^2}\kappa_{QZS}\left(\sum_{n=1}^{\infty}q_n\phi_n(x_j)\right)^3\right]\phi_m(x_j) = \\ 2\varepsilon\left[P - \left(\sum_{n=1}^{\infty}\ddot{q}_n\phi_n(\tau) + 2\sum_{n=1}^{\infty}(n\pi)\dot{q}_n\cos(n\pi\tau) - \sum_{n=1}^{\infty}(n\pi)^2 q_n\phi_n(\tau)\right)\right]\phi_m(\tau)\zeta(\tau)\end{aligned} \tag{3.73}$$

In Eq. (3.73), dots stand for derivatives with respect to the non-dimensional time τ and

$$c_b = \frac{C_b L}{\rho S v}, c = \frac{2C}{\rho S v}, \kappa_{QZS} = \frac{\alpha_{QZS}k_v}{a^3}, P = \frac{gL^2}{L_0 v^2}. \tag{3.74}$$

$$\varepsilon = \frac{M}{\rho S L} \tag{3.75}$$

is the non-dimensional parameter describing the ratio of the moving mass M to the mass of the beam bridge given by ρSL. ω_m is the mth beam natural frequency nondimensionalized with respect to frequency of moving load. Thus $\omega_m = \varpi_m\frac{L}{v}$, with $\varpi_m = \left(\frac{m\pi}{L}\right)^2\sqrt{\frac{EI}{\rho S}}$ the natural frequency of the mth mode of vibration of the beam bridge.

We will focus our attention on the efficiency of vibration reduction due to the QZS vibration isolators. As most of the energy of the beam bridge is concentrated in the first mode [106, 171, 172], a single mode model will be adopted. Hence, modal equation (Eq. (3.73)) can be rewritten in the following form

$$\begin{aligned}\ddot{q} + \omega_1^2 q = -2\varepsilon\eta\omega_1\dot{q} - 2\varepsilon\beta\kappa_{QZS}q^3 + 2\varepsilon P\sin(\pi\tau)\zeta(\tau) \\ - 2\varepsilon\left[\ddot{q}\sin^2(\pi\tau) + 2\pi\dot{q}\cos(\pi\tau)\sin(\pi\tau) - \pi^2 q\sin^2(\pi\tau)\right]\zeta(\tau)\end{aligned}, \tag{3.76}$$

where $q(\tau)$ is the amplitude of the first mode,

$$\omega_1 = \varpi_1\frac{L}{v}, \tag{3.77}$$

with

$$\varpi_1 = \left(\frac{\pi}{L}\right)^2 \sqrt{\frac{EI}{\rho S}}, \tag{3.78}$$

$$2\eta\varepsilon\omega_1 = c_b + c\sum_{j=1}^{N} \sin^2(\pi x_j), \tag{3.79}$$

$$\varepsilon\beta = \frac{L}{\rho S v^2}\sum_{j=1}^{N} \sin^4(\pi x_j). \tag{3.80}$$

From Eq. (3.76), it is obvious that when $\pi = \omega_1$, the constant force term on the right-hand side of Eq. (3.76) behaves like a harmonic excitation with the frequency of the excitation corresponding to a natural frequency of the beam, and therefore even a constant moving force can excite the structure into resonance under these conditions. The resonant speed [55], called critical speed, is defined as

$$v_c = \frac{L\varpi_1}{\pi}. \tag{3.81}$$

Eq. (3.76) is a differential equation with time-dependent periodic coefficients. As such, there is no exact solution [55]. Nevertheless, approximate analytic methods and often numerical methods are used.

3.4.2 Analytical formulation and parametric resonance

If the parameter ε is small, a perturbation method known as method of multiple scales can be used to find approximate analytic solution of Eq. (3.76) for $\tau \leq 1$ (i.e. for $\zeta(\tau) = 1$). Accordingly, this solution is expressed in terms of different time scales as

$$q(\tau, \varepsilon) = q_0(\tau_0, \tau_1) + \varepsilon q_1(\tau_0, \tau_1) + \ldots, \tag{3.82}$$

where τ_m represents different independent time scales given by

$$\tau_m = \varepsilon^m \tau, m = 0, 1, ... \tag{3.83}$$

So, $\tau_0 = \tau$ and $\tau_1 = \varepsilon\tau$. Substituting Eq. (3.82) in Eq. (3.76) and noting that

$$\frac{d}{d\tau} = D_0 + \varepsilon D_1 + \ldots \quad \text{and} \quad \frac{d^2}{d\tau^2} = D_0^2 + 2\varepsilon D_0 D_1 + \ldots, \tag{3.84}$$

where

$$D_m = \frac{\partial}{\partial \tau_m}, \quad \text{i.e.} \quad D_0 = \frac{\partial}{\partial \tau_0} \quad \text{and} \quad D_1 = \frac{\partial}{\partial \tau_1}. \tag{3.85}$$

The following sets of linear ODEs result

$$\varepsilon^0 : D_0^2 q_0 + \omega_1^2 q_0 = 0, \tag{3.86a}$$

$$\begin{gathered} \varepsilon^1 : D_0^2 q_1 + \omega_1^2 q_1 = -2D_0 D_1 q_0 - 2\eta\omega_1 D_0 q_0 - 2\beta\kappa_{QZS} q_0^3 + 2P\sin(\pi\tau_0) \\ - 2\left[D_0^2 q_0 \sin^2(\pi\tau) + 2\pi D_0 q_0 \cos(\pi\tau)\sin(\pi\tau) - \pi^2 q_0 \sin^2(\pi\tau)\right] \\ \text{et cetera.} \end{gathered}, \tag{3.86b}$$

The solution of Eq. (3.86a) reads

$$q_0 = A_1 \exp(i\omega_1\tau_0) + \text{c.c.}, \tag{3.87}$$

where A_1 is a complex amplitude to be determined, c.c. stands for the complex conjugate and $i = (-1)^{1/2}$. The substitution of q_0 in Eq. (3.86b) results in

$$\begin{aligned} D_0^2 q_1 + \omega_1^2 q_1 = & -2\omega_1 \left[iD_1 A_1 \exp(i\omega_1\tau_0) + \text{c.c.}\right] - 2\eta\omega_1^2 \left[iA_1 \exp(i\omega_1\tau_0) + \text{c.c.}\right] \\ & - 2\beta\kappa_{QZS}\left[A_1^3 \exp(3i\omega_1\tau_0) + 3A_1^2 \bar{A}_1 \exp(i\omega_1\tau_0) + \text{c.c.}\right] \\ & - P\left[i\exp(i\pi\tau_0) + \text{c.c.}\right] \\ & - \tfrac{1}{2}\left[\begin{array}{l} -2(\omega_1^2 + \pi^2) A_1 \exp(i\omega_1\tau_0) + (\omega_1 + \pi)^2 A_1 \exp(i(\omega_1 + 2\pi)\tau_0) \\ + (\omega_1 - \pi)^2 \bar{A}_1 \exp(i(-\omega_1 + 2\pi)\tau_0) + \text{c.c.} \end{array}\right] \end{aligned} . \tag{3.88}$$

It can be seen from the terms on the right-hand side of Eq. (3.88) that the moving load inertial effect is manifested in the form of parametric resonance when ω_1 approaches π. Furthermore, when ω_1 approaches π, secular terms develop. The complex amplitude A_1 is now obtained from the condition that these terms are to be eliminated from of Eq. (3.88).

Let's introduce a detuning parameter λ to quantify the deviation of ω_1 from π in the form

$$\pi = \omega_1 + \varepsilon\lambda. \tag{3.89}$$

Equating the secular terms to zero leads to the condition on the complex amplitude A_1 given by

$$\begin{aligned} 2i\omega_1 D_1 A_1 = &-2i\eta\omega_1^2 A_1 + \left(\omega_1^2 + \pi^2\right) A_1 - \tfrac{1}{2}\left(\omega_1 - \pi\right)^2 \bar{A}_1 \exp\left(2i\varepsilon\lambda\tau_0\right) \\ &- 6\beta\kappa_{QZS} A_1^2 \bar{A}_1 - iP\exp\left(i\varepsilon\lambda\tau_0\right) \end{aligned}, \tag{3.90a}$$

$$\begin{aligned} D_0^2 q_1 + \omega_1^2 q_1 = &-\tfrac{1}{2}\left(\omega_1 + \pi\right)^2 \left[A_1 \exp\left(i\left(3\omega_1 + 2\varepsilon\lambda\right)\tau_0\right) + \text{c.c.}\right] \\ &- 2\beta\kappa_{QZS}\left[A_1^3 \exp\left(3i\omega_1\tau_0\right) + \text{c.c.}\right] \end{aligned}. \tag{3.90b}$$

Noting that the complex amplitude A_1 is independent of τ_0 and assuming A_1 to be of the form

$$A_1 = \frac{1}{2} a_1 \exp\left(i\theta\right), \tag{3.91}$$

with amplitude $a_1 = a_1\left(\tau_1\right)$ and phase $\theta = \theta\left(\tau_1\right)$, Eq. (3.90a) results in the following two first-order differential equations for the amplitude and the transformed phase $\varphi = \varepsilon\lambda\tau_0 - \theta$,

$$\omega_1 \dot{a}_1 = -\varepsilon\eta\omega_1^2 a_1 - 0.25\varepsilon\left(\omega_1 - \pi\right)^2 a_1 \sin 2\varphi - \varepsilon P\cos\varphi, \tag{3.92a}$$

$$\omega_1 a_1 \dot{\varphi} = \varepsilon\omega_1\lambda a_1 - 0.25\varepsilon\left(\omega_1 - \pi\right)^2 a_1 \cos 2\varphi + 0.5\varepsilon\left(\omega_1^2 + \pi^2\right) a_1 - \varepsilon\frac{3}{4}\beta\kappa_{QZS} a_1^3 + \varepsilon P\sin\varphi. \tag{3.92b}$$

Eqs. (3.92) can be directly integrated to obtain a_1 and φ for the modal response in the transient period. The transient solution of the first mode valid up to the order of ε is obtained by combining Eqs. (3.82), (3.87) and the solution q_1 from Eq. (3.90b). It is given by

$$q\left(\tau,\varepsilon\right) = a_1\cos\left(\pi\tau - \varphi\right) + \varepsilon\left[\frac{\left(\omega_1 + \pi\right) a_1}{8\pi}\cos\left(3\pi\tau - \varphi\right) + \frac{\beta\kappa_{QZS} a_1^3}{16\omega_1^2}\cos\left(3\pi\tau - 3\varphi\right)\right]. \tag{3.93}$$

By substituting Eq. (3.93) in Eq. (3.71), the non-dimensional beam deflection can be obtained at each point of the beam bridge as

$$y\left(X,\tau\right) = q\left(\tau,\varepsilon\right)\sin\left(\frac{\pi X}{L}\right). \tag{3.94}$$

In the next subsection, we will explore the dynamical response of the beam bridge using numerical simulation of governing equations.

3.4.3 Numerical simulation

In this work, Eqs. (3.76) and (3.92) are numerically solved by a RK4 algorithm in order to generate the numerical and the semi-analytical transverse responses of the beam in presence and in absence of QZS control. The initial values for the first calculations are set as $q = 0$, $\dot{q} = 0$, $a_1 = 0$, and $\varphi = 0$.

Table 3.3 presents the physical and geometrical parameter values of a beam bridge [29, 173]. In the following study, the parameter values are assigned as listed in Table 3.3 if there is no special mention.

Some important parameters are obtained by calculation on the base of Eqs. (3.67), (3.74), (3.75), (3.78), (3.79) and (3.81) as

$\kappa_{QZS} = 20000$ N/m, $\varepsilon = 0.3$, $\varpi_1 = 17.89$ rad/s, $\eta = 0.17$, $v_c = 8.5$ m/s.

a) Validation of analytical study and effectiveness of the QZS isolation

Semi-analytical and numerical non-dimensional maximum deflection versus mass ratio at the critical speed $v_c = 8.5$ m/s are plotted on the same graph in Fig. 3.32. It appears from this figure that the curves obtained from numerical and semi-analytical methods coincide only for very small values of mass ratio ε ($\varepsilon < 0.01$ approximately). The larger ε, the greater the gap between the two curves, reflecting the divergence of the semi-analytical solution to the numerical solution. Therefore, the method of multiple scales used to determine the semi-analytical solution can only be used to determine only an approximate analytical solution whose deviation to the exact solution is even lower than when the value of ε is small. As $\varepsilon = 0.3$ in this work, let us use only the numerical solution in the following to highlight the

Table 3.3: Physical and geometric parameters of a wooden beam bridge

Description	**Parameter**	**Value**
Bending stiffness	EI	3.66 N.m^2
Mass per unit length	ρS	0.22 kg/m
Length of the beam	L	1.5 m
External damping of the beam	C_b	0.001 N.s/m^2
Viscosity damping of the spring	C	0.1 N.s/m
Mass of the moving load	M	0.1 kg
Initial length of the horizontal spring	L_0	0.1 m
Horizontal length of the horizontal spring	a_0	0.05 m
Horizontal spring linear stiffness	k_0	2500 N/m
Vertical spring stiffness	k_v	5000 N/m
Number of piers	N	6
Positions of the piers	X_j	$X_j = 0.133 + 0.247 \times (j-1)$ m

effectiveness of the QZS control used in reducing vibrations of the beam bridge subjected to moving mass.

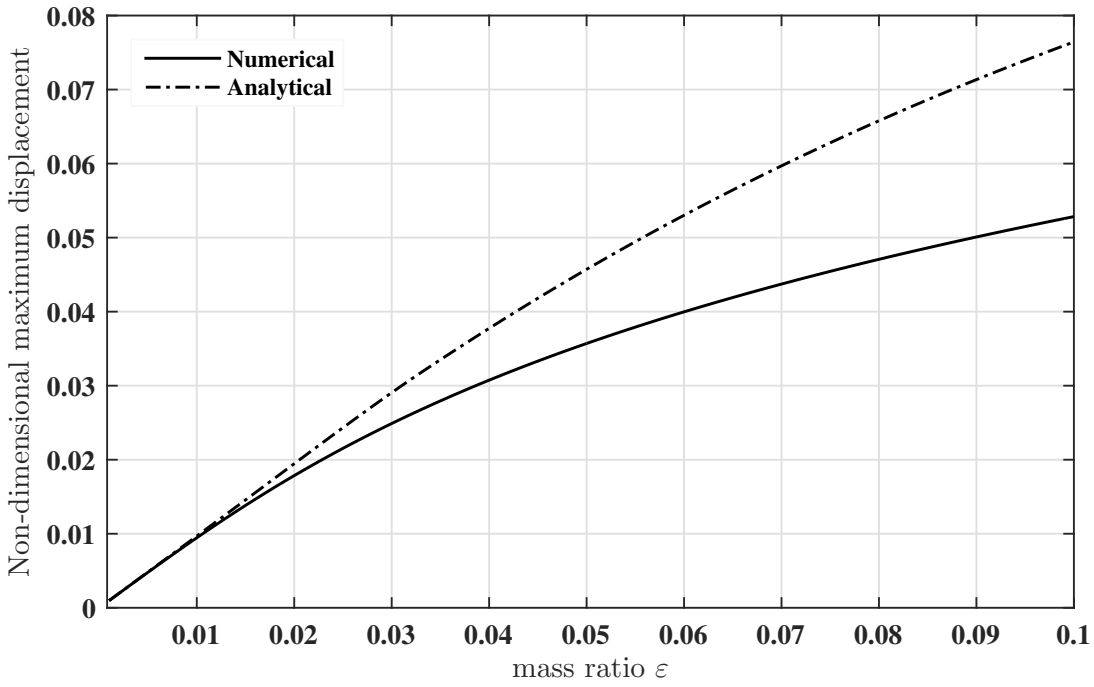

Figure 3.32: Comparison between numerical and semi-analytical non-dimensional maximum deflection versus mass ratio ε under the moving mass at the critical speed $v = v_c = 8.5$ m/s

Fig. 3.33 presents numerical non-dimensional maximum deflection versus moving mass velocity in the presence of QZS control and without control. It can easily be seen that in the presence of QZS vibration isolators, the vibration amplitudes are considerably reduced at low speed of the moving mass and around the resonance peak. However, for high speeds ($v > 30$ m/s), this reduction is less seen, the QZS vibration isolators have less effect. It can be seen from the curves of Fig. 3.33 that QZS isolators are more effective for vibrations produced at low speed, around the critical speed than those of high speeds after the critical speed. The QZS isolators are therefore effective in reducing the vibration of bridges subjected to moving mass. However, for a judicious choice of QZS isolators parameters that are the

nonlinear term κ_{QZS} and the damping coefficient C, better results can be obtained in the reduction of bridge vibrations as shown in Figs. 3.34 to 3.37.

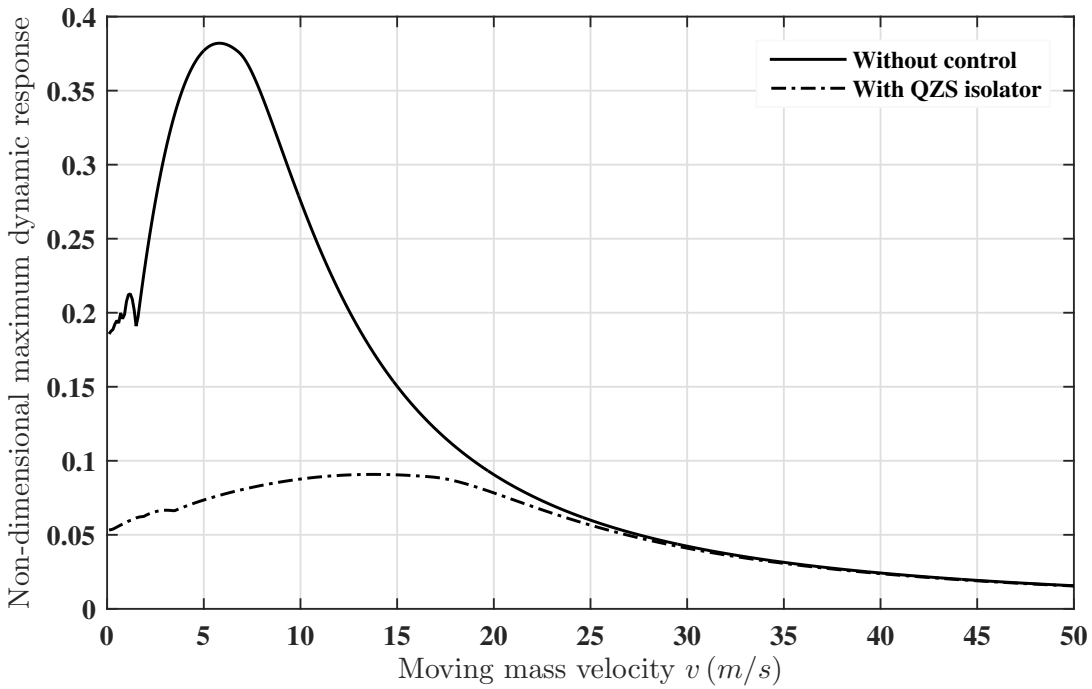

Figure 3.33: Numerical non-dimensional maximum deflection versus moving mass velocity for $\varepsilon = 0.3$ in presence of QZS isolator and without control

b) Effects of the nonlinear term and the viscosity damping of QZS isolator

Figs. 3.34 and 3.35 show the mid-span deflection time histories plotted for two moving mass velocity, one before the critical speed ($v < v_c$) and the other after the critical speed ($v > v_c$) for different values of nonlinear term κ_{QZS} and damping coefficient C of the QZS vibration isolators and when the moving mass is onto ($\tau \leq 1$) and out of ($\tau > 1$) the beam bridge. Figs. 3.34(a) and 3.35(a) show that when the speed of the moving mass is set as $v = 5$ m/s $< v_c$ before the resonance peak, during and after its passage on the beam bridge, the vibrations are more and more reduced as the nonlinear term and the damping coefficient increase. However, this reduction is more felt after the passage of the moving mass when

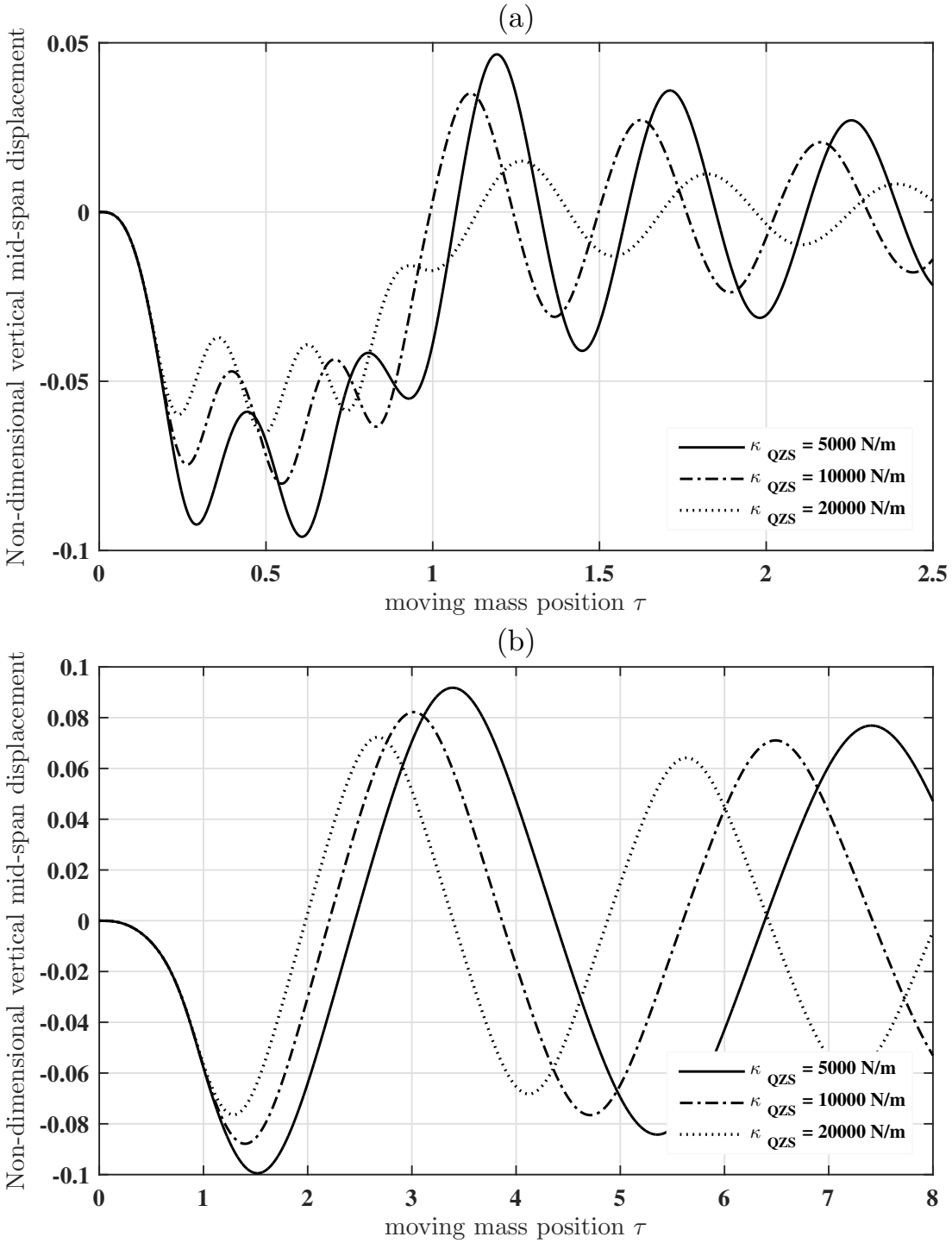

Figure 3.34: Effects of nonlinear term of QZS isolator on the beam bridge mid-span deflection time histories when the moving mass is onto ($\tau \leq 1$) and out of ($\tau > 1$) the beam bridge for $\varepsilon = 0.3$ (a) $v = 5$ m/s ($v < v_c$) and (b) $v = 50$ m/s ($v > v_c$)

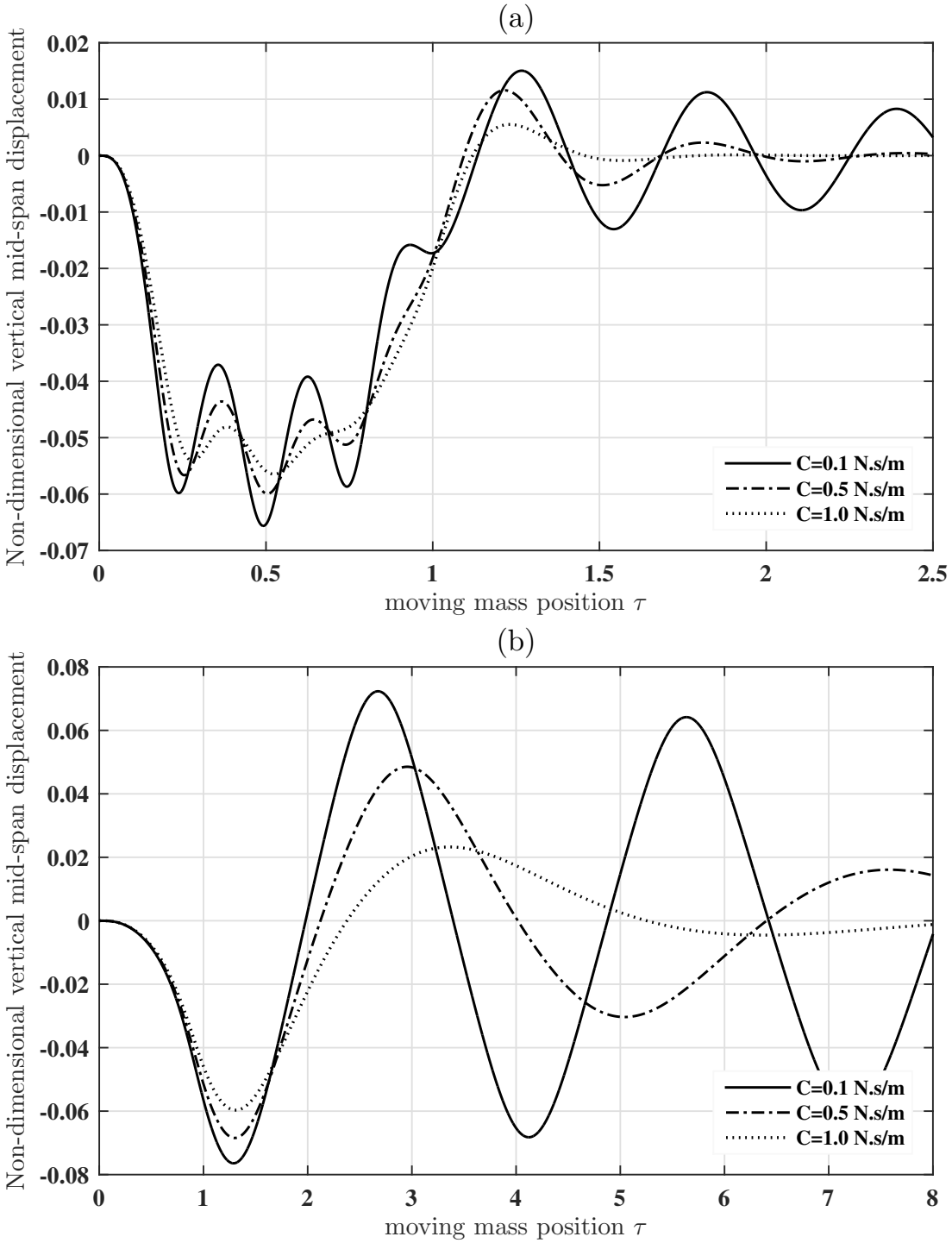

Figure 3.35: Effects of damping coefficient of QZS isolator on the beam bridge mid-span deflection time histories when the moving mass is onto ($\tau \leq 1$) and out of ($\tau > 1$) the beam bridge for $\varepsilon = 0.3$ (a) $v = 5$ m/s ($v < v_c$) and (b) $v = 50$ m/s ($v > v_c$)

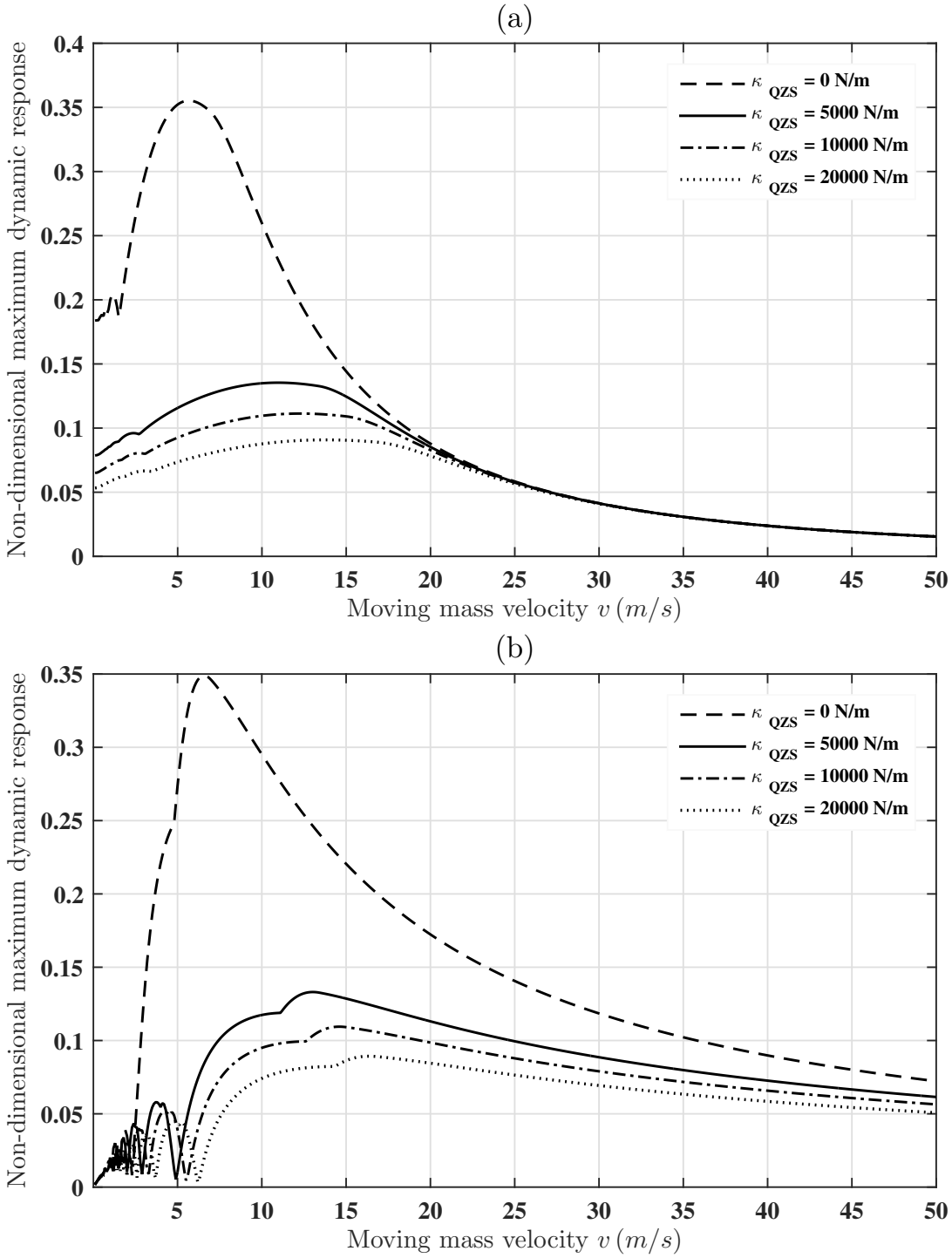

Figure 3.36: Effects of nonlinear term of QZS isolator on the beam bridge non-dimensional maximum dynamic response versus moving mass velocity for $\varepsilon = 0.3$ when the moving mass is (a) onto the beam ($\tau \leq 1$) and (b) out of the beam ($\tau > 1$)

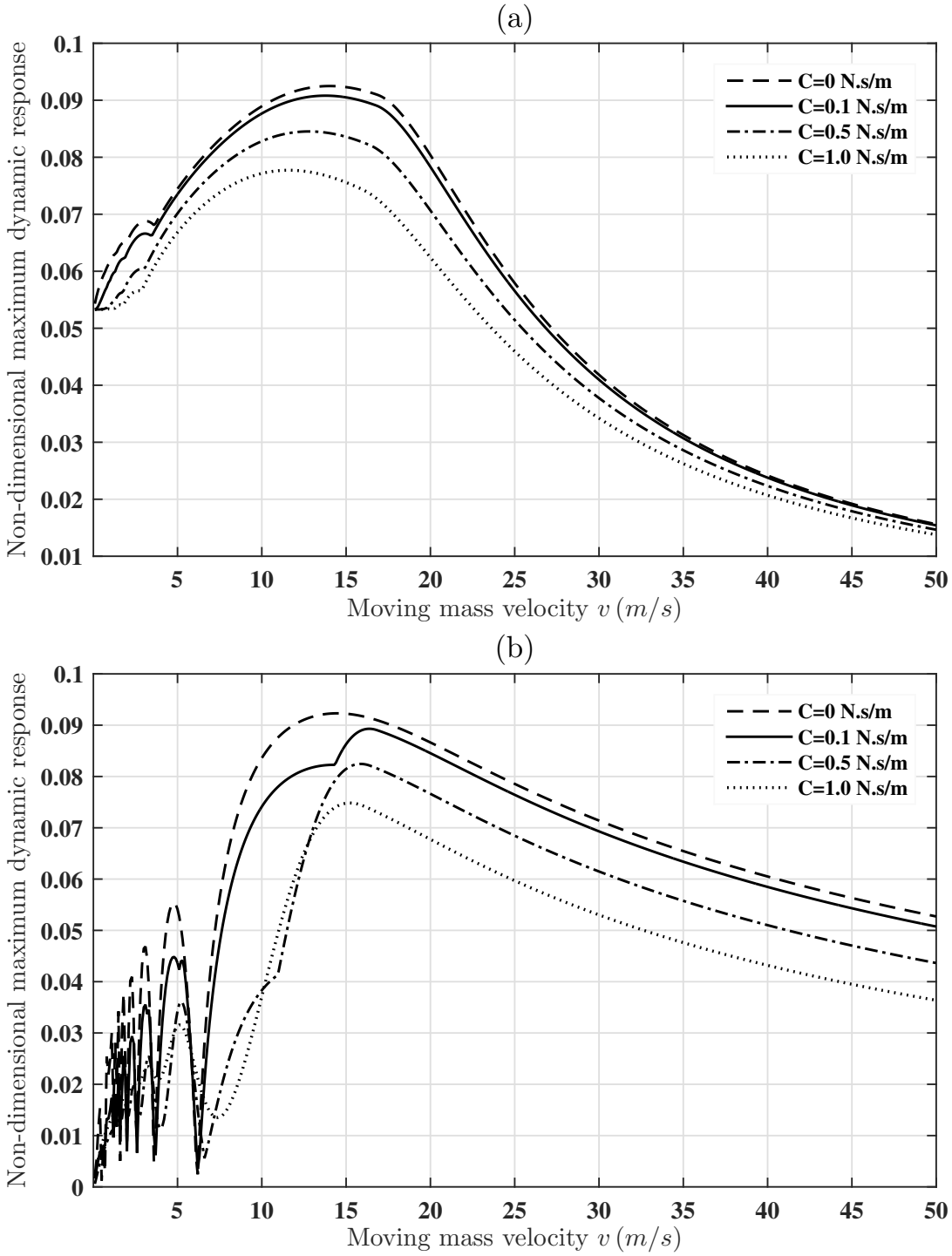

Figure 3.37: Effects of damping coefficient of QZS isolator on the beam bridge non-dimensional maximum dynamic response versus moving mass velocity for $\varepsilon = 0.3$ when the moving mass is (a) onto the beam ($\tau \leq 1$) and (b) out of the beam ($\tau > 1$)

the damping coefficient increases as shown in Fig. 3.35(a). For the speed $v = 50$ m/s $> v_c$ after resonance peak, the same observations are made as the damping coefficient increases as shown in Fig. 3.35(b). But when the nonlinear term of the QZS vibration isolators increases, its effect is noticeable until the moving mass has left the beam bridge as shown in Fig. 3.34(b). When the moving mass is still on the beam bridge, no decrease in amplitude is observed due to the presence of the QZS vibration isolators. The results obtained are found and confirmed for other velocity values through the amplitude curves plotted as a function of the moving mass velocity in Figs. 3.36 and 3.37.

All these results observed for singular values of speed lower and higher than the critical speed are confirmed for a greater number of velocity values by the plot of non-dimensional dynamical response of the beam bridge versus moving mass velocity in Figs. 3.36 and 3.37. Figs. 3.37(a) and 3.37(b) show that the vibration amplitudes of the beam bridge do indeed decrease when the damping coefficient increases whatever the moving mass velocity. After the moving mass has left the beam bridge, similar observations are made by increasing the nonlinear term as shown in Fig. 3.36(b). On the other hand, this observation is only valid for the low speeds and those around the resonance peak when the nonlinear term increases during the passage of the moving mass on the beam bridge. But for high speeds after the resonance peak ($v > 30$ m/s), the nonlinear term has no effect on beam bridge vibrations as shown in Fig. 3.36(a).

It follows that the combined effects of the nonlinear term and damping coefficient give to QZS vibration isolators great efficiency in reducing the vibrations of beam bridges subjected to a moving mass.

3.5 Conclusion

The present chapter has presented the results obtained in our thesis. First of all, a theoretical model of two bridges coupled via their close environment is developed and validated by lab experiments. Analytical, numerical and experimental studies of the dynamical responses of the two coupled beam bridges are carried out in the cases where one of the coupled bridges is subjected to a combination of sinusoidal excitation and periodic impulsive force. The effects of the close environment and the distance between the two coupled bridges on the dynamical responses of each of them is pointed out. Secondly, after a QZS vibration isolator being designed and modelled, it is then placed between a beam bridge structure and its piers to reduce its vibrations due to base excitation of the piers on one hand and to a moving mass on the other hand. The nonlinear intergro-partial differential governing equations of the elastic beam bridge, in different cases of study are derived considering the geometric nonlinearity. Based on the modal analysis of the controlled beam bridge, the Galerkin method is used to discretize and solve the governing equation. Finally, the efficiency of the QZS vibration isolators on the transverse vibration of multi-span continuous beam bridges is studied. It rises that QZS vibration isolators can extend the service life of a multi-span continuous beam bridge by significantly reducing its vibrations.

General Conclusion

The experimental studies of the interactions of coupled bridges are relatively much fewer than the theoretical studies of this problem in the literature. Therefore, it is essential to combine the theoretical and experimental studies of this problem in order to gain knowledges on bridge interactions. Analytical, numerical and experimental studies of the dynamical responses and quasi-zero stiffness vibration isolation of two seven-span continuous beam bridges indirectly coupled via their close environment are carried out in this thesis. Main conclusions are presented below and future works are proposed.

Firstly, the experimental and theoretical studies are carried out on a model of two seven-span continuous beam bridges indirectly coupled via their close environment. It appears that when one of the coupled bridges is excited, the amplitudes of vibration of each coupled bridges depend on the mechanical characteristics of the coupling close environment and the distance between the bridges. The experimental and theoretical results show that the transverse displacements of the coupled bridges increase when the distance between them decreases. Another information related to this work is that, the close environment made up of the ground under the piers of the coupled bridges really acts like a viscoelastic Winkler foundation. Therefore, the experimental scale model built in the laboratory give rise to the validation of the theoretical modelling qualitatively. Secondly, the efficiency of a QZS vibration isolation on the transverse vibration of the two multi-span continuous coupled beam bridges is studied when the beam bridge is subjected to pier base vibrating excitation on one hand, and to moving mass on other hand.

For the beam bridge subjected to pier base vibrating excitation, the performance of the quasi-zero stiffness vibration isolator and the equivalent linear viscoelastic isolator are evaluated through steady-state response and absolute motion transmissibility of the beam bridge. The following conclusions are drawn:

(1) The quasi-zero stiffness vibration isolator and the linear viscoelastic isolator are both

effective for high frequencies but only the quasi-zero stiffness vibration isolator is able to reduce low frequency vibrations.

(2) The linear viscoelastic isolator strongly change the natural frequencies of the beam bridge compared to the quasi-zero stiffness vibration isolator.

(3) The quasi-zero stiffness vibration control is more efficient than the linear viscoelastic control.

(4) A curious and original result observed in the presence of quasi-zero stiffness vibration isolation shows that the increase of the viscous damping leads to an increase of the absolute motion transmissibility by sacrificing the performance of nonlinear isolation.

(5) The quasi-zero stiffness vibration isolator is more powerful that nonlinear geometric term, vertical spring stiffness, viscous damping and magnitude of base excitation are small. So, to build a quasi-zero stiffness vibration isolator with better performance, the damper must be removed and its vertical spring must be designed to have the lowest possible stiffness leading to achieve a quasi-zero stiffness behavior.

For the beam bridge subjected to a moving mass, the method of multiple scales and the fourth-order Runge-Kutta algorithm are used for analytical and numerical solutions of these equations, respectively. The research has been focused on the analysis of the effectiveness of a quasi-zero stiffness vibration isolator. The influence of different parameters on the dynamical responses of the beam bridge is investigated and a particular attention is paid to the effects of the nonlinear term and the damping coefficient of the QZS vibration isolator. Hence, from the analysis and results presented in this thesis, the following conclusions are pointed out:

(6) The method of multiple scales analysis presented in this thesis is able to capture the parametric resonance phenomenon that leads in moving mass problems.

(7) The influence of the moving mass inertia is manifested in the modal equations in the form of the mass ratio parameter. This parameter is used in the perturbation analysis to bring out

the semi-analytical solution of the beam bridge response. It appears from the results that the semi-analytical solution is closed to the numerical solution only for very small values of mass ratio.

(8) quasi-zero stiffness vibration isolators can significantly reduce the vibration of the multi-span continuous beam bridge subjected to moving masses.

In summary, this thesis demonstrates the superiority of the quasi-zero stiffness vibration isolation in comparison of the corresponding linear isolation. A quasi-zero stiffness vibration isolator with suitable parameters has the advantage of more effectively isolating unwanted vibrations transmitted from the foundation to the deck of the bridge, as it can achieve excellent low-frequency isolation performance including low initial isolation frequency and wide isolation frequency band. The application of the quasi-zero stiffness mechanism on the design and development of novel earthquake-resistant systems can improve seismic performance of buildings and bridge structures.

This work leads to perspectives which firstly go in the direction of improving its results and secondly in the direction of the realization of such structures. The bridges studied in this thesis are uniform girders that are different from many real bridges whose cross-section is not uniform, such as continuous bridges, suspension bridges and cable-stayed bridges. In addition, a real bridge for a high-speed railway line is normally made of prestressed concrete with a sophisticated track system. Thus, an idea for future work is to build a more realistic bridge specimen and study it theoretically and experimentally in the laboratory. Field tests on real bridges could also be carried out in the future should such an opportunity arise.

Bibliography

Bibliography

[1] P. Paultre, O. Chaallal and J. Proulx, (1992), Bridge dynamics and dynamic amplification factors-a review of analytical and experimental findings, *Canadian Journal of Civil Engineering 19: 260-278.*

[2] J. Meng, H. Ghasemi and E.M. Lui, (2004), Analytical and experimental study of a skew bridge model, *Engineering Structures 26: 1127-1142.*

[3] K. Liu, E. Reynders, G. De Roeck and G. Lombaert, (2009), Experimental and numerical analysis of a composite bridge for high-speed trains, *Journal of Sound and Vibration 320: 201-220.*

[4] R.K. Chatterjee, T.K. Datta and C.S. Surana, (1994), Vibration of continuous bridges under moving vehicles, *Journal of Sound and Vibration 169: 619-632.*

[5] S.Yang, X. Fang, J. Zhang and D. Wang, (2016), Dynamic behavior of bridge-erecting machine subjected to moving mass suspended by wire ropes, *Journal of Applied Mathematics and Mechanics 36: 741-748.*

[6] E. Bozdag, E. Sunbuloglu and H. Ersoy, (2006), Vibration analysis of new Galata Bridge: experimental and numerical results, *Computers and Structures 84: 283-292.*

[7] O.B. Mekki, (2007), Amortissement Semi-actif des Structures Flexibles: Application au Contrôle des Grands Ponts. *XXVemes Rencontres Universitaires de Génie Civil, PRIX RENE HOUPERT.*

[8] P. Fokou Sighano and J.M. Ndindjock, (2012), Conception et dimensionnement du tablier d?un pont caisson en béton précontraint : cas du second pont sur le Wouri. *Master thesis in civil engineering, Faculty of Industrial Engineering, University of Douala.*

[9] G.S. Paddan and M.J. Griffin, (2002), Evaluation of whole-body vibration in vehicles, *Journal of Sound and Vibration 253(1): 195-213.*

[10] X. Sun, J. Xu, X. Jing and L. Cheng, (2014), Beneficial performance of a quasi-zero-stiffness vibration isolator with time-delayed active control, *International Journal of Mechanical Sciences 82: 32-40.*

[11] M.C. Kunde and R.S. Jangid, (2003), Seismic behavior of isolated bridges: A-state-of-the-art review, *Electronic Journal of Structural Engineering 3(3).*

[12] S. Iwnicki, (2006), Handbook of Railway Vehicle Dynamics, *Boca Raton, CRC Press.*

[13] B. Yan, (2007), Active vibration isolation with a distributed parameter isolator, *Ph.D. thesis, University of Southampton, Faculty of Engineering, Science and Mathematics, Institute of Sound and Vibration Research.*

[14] A. Carrella, (2008), Passive Vibration Isolators with High-Static-Low-DynamicStiffness, *Ph.D. thesis, University of Southampton, Institute of Sound and Vibration Research.*

[15] F. Naeim and J. Kelly, (1999), Design of seismic isolated structures: from theory to practice, *New York, Wiley.*

[16] C. Bedon and A. Morassi, (2014), Dynamic testing and parameter identification of a base-isolated bridge, *Engineering Structures 60(2): 85-99.*

[17] C.M. Harris and A.G. Piersol, (2002), Shock and vibration handbook, *McGraw-Hill, New York.*

[18] X. Huang, X. Liu and H. Hua, (2014), On the characteristics of an ultra-low frequency nonlinear isolator using sliding beam as negative stiffness, *Journal of Mechanical Science and Technology 28(3), 813-822.*

[19] W.S. Robertson, M.R.F. Kidner, B.S. Cazzolato, and A.C. Zander, (2009), Theoretical design parameters for a quasi-zero stiffness magnetic spring for vibration isolation, *Journal of Sound and Vibration 326, 88-103.*

[20] Z.F. Hao, Q.J. Cao and M. Wiercigroch, (2017), Nonlinear dynamics of the quasi-zero-stiffness SD oscillator based upon the local and global bifurcation analyses, *Nonlinear Dynamics 87, 987-1014.*

[21] C. Cheng, S.M. Li, Y. Wang and X.X. Jiang, (2018), Resonance of a quasi-zero stiffness vibration system under base excitation with load mismatch, *International Journal of Structural Stability and Dynamics 18, 1850002.*

[22] T.D. Le, M.T.N. Bui and K.K. Ahn, (2016), Improvement of vibration isolation performance of isolation system using negative stiffness structure, *IEEE-ASME Transactions on Mechatronics 21, 1561-1571.*

[23] Chen Wai-Fah, (1999), Structural Engineering Handbook, *Boca Raton: CRC Press LLC.*

[24] B.R. Nana Nbendjo and P. Woafo, (2006), Modelling, Control by Sandwich of the Dynamics and Optimization in a Strongly Nonlinear Beam, *Far East Journal of Dynamical Systems 8: 267-283.*

[25] Q. Zhang and B.Z. Guo, (2004), Stabilization of an Elastic Plate with Viscoelastic Boundary Conditions, *Journal of Optimization Theory and Application 122(3): 669-690.*

[26] H.P. Niu, Y.H. Zhang, X.H. Zhang and S.L. Xie, (2010), Active Vibration Control of Plates Using Electro-Magnetic Constrained Layer Damping, *International Journal of Applied Electromagnetics and Mechanics 33(1): 831-837.*

[27] T. Aida, K. Kawazoe and S. Toda, (1995), Vibration Control of Plates by Plate-Type Dynamics Vibration Absorber, *Journal of Vibration and Acoustics 117(3): 332-338.*

[28] T. Aida, S. Toda, S.N. Ogowa and Y. Simada, (1992), Vibration Control of Beams by Beam Type Dynamics Vibrations Absorber, *ASCE Journal of Engineering Mechanics 118(2): 163-175.*

[29] H. Sonfack Bouna and B.R. Nana Nbendjo, (2012), Vibration control of a plate subjected to impulsive force by plate-type dynamic vibration absorbers, *World Journal Mechanics 2: 143-151.*

[30] R. Lobet, (2017), Modelling of the Shear Behaviour of Coupling Beams with Fibre Reinforced Concrete, *Master thesis, Faculty of Applied Sciences, University of Liège.*

[31] S.M. Han, H.B. and T. Wan, (1999), Dynamics of transversely vibrating beams using four engineering theories, *Journal of Sound and Vibration 225(5): 935-988.*

[32] X. Xiao, X. Jin, Z. Wen, M. Zhu and W. Zhang, (2010), Effect of tangent track buckle on vehicle derailment, *Multibody System Dynamics, 25: 1-41.*

[33] A.D. Kerr, (1964), Elastic and Viscoelastic Foundation Models, *Journal of Applied Mechanics, 31(3): 491-498.*

[34] M. Hetényi, (1964), Beams on Elastic Foundation: Theory with Applications in the Fields of Civil and Mechanical Engineering, *University of Michigan Press, Ann Arbor, Michigan.*

[35] W. Huang and Y. Zou, (1994), The dynamic response of a viscoelastic Winkler foundation-supported elastic beam impacted by a low velocity projectile, *Computers and Structures 52: 431-436.*

[36] S. Lu and D. Xuejun, (1998), Dynamic analysis to infinite beam under a moving line load with uniform velocity, *Journal of Applied Mathematics and Mechanics 19: 368-373.*

[37] C. Johansson, (2013), Simplified dynamic analysis of railway bridges under high-speed trains, *Licentiate Thesis, KTH Royal Institute of Technology, Stockholm, Sweden.*

[38] F. Deckner, K. Viking and S. Hintze, (2012), Ground vibrations due to pile and sheet pile driving-prediction models of today, *To be published in Proceedings of the European Young Geotechnical Engineers Conference, Gothenburg.*

[39] R. Holmberg, P.W. Arnberg, O. Bennerhult, L. Forssblad, L. Gereben, L. Hellman, K. Olsson, G. Rundquist, C. Sjöberg, K. Sjökvist and G. Wallmark,(1984),Vibrations generated by traffic and building construction activities, *Swedish Council for Building Research, Stockholm.*

[40] R.D. Woods, (1997), Dynamic Effects of Pile Installations on Adjacent Structures, *National Academy Press, Washington D.C.*

[41] M.R. Svinkin, (2008), Soil and Structure Vibrations From Construction and Industrial Sources, *The 6th International Conference on Case Histories in Geotechnical Engineering, Arlington, Virginia.*

[42] J.F. Semblat, L. Lenti, D. Jacqueline and J.J. Leblond, (2011), Railway vibrations induced into the soil: experiments, modelling and isolation, *Revue Française de Géotechnique 23-36: 134-135.*

[43] J.F. Semblat, (1998), Amortissement et dispersion des ondes: points de vue physique et numérique, *Revue française de génie civil 2: 91-111.*

[44] J.M. Biggs, (1965), Structural Dynamics, *McGraw- Hill, New York.*

[45] R.R. Craig, (1981), Structural Dynamics, *John Wiley, New York, New Civil Engineer, magazine of the Institution of Civil Engineers, 1 Great George Street, London, twenty five biweekly issues per year.*

[46] K.J. Bathe, (1982), Finite Element Procedures in Engineering Analysis, *Prentice-Hall, Englewood Cliffs, NJ.*

[47] R. Clough and J. Penzien, (1993), Dynamics of Structures, *2nd Edn, McGraw- Hill, New York.*

[48] N.M. Newmark and E. Rosenblueth, (1971), Fundamentals of Earthquake Engineering, *Prentice-Hall, Englewood Cliffs, NJ.*

[49] M. Paz, (1997), Structural Dynamics, *4th Edn, Van Nostrand- Reinhold, New York.*

[50] I. Argyris and H.P. Mlejnek, (1991), Dynamics of Structures, *North-Holland, Amsterdam.*

[51] A.K. Chopra, (1995), Dynamics of Structures: Theory and Applications to Earthquake Engineering, *Prentice-Hall, Englewood Cliffs, NJ.*

[52] B. Ravindra and A.K. Mallik, (1994), Performance of non-linear vibration isolators under harmonic excitation, *Journal of Sound and Vibration, 170(3): 325-337.*

[53] H. Ding and L-Q. Chen, (2019), Nonlinear vibration of a slightly curved beam with quasi-zero-stiffness isolators, *Nonlinear Dynamics 95: 2367-2382.*

[54] S. Lenci and G. Rega, (2000), Periodic Solutions and Bifurcations in an Impact Inverted Pendulum under Impulsive Excitation, *Chaos, Solitons and Fractals, 11(15): 2453-2472.*

[55] H. Ouyang, (2011), Moving-load dynamic problems: a tutorial (with a brief overview), *Mechanical Systems and Signal Processing 25: 2039-2060.*

[56] S.P. Timoshenko, (1953), History of Strength of Materials: With a Brief Account of the History of Theory of Elasticity and Theory of Structures, *McGraw-Hill, New York.*

[57] L. Fryba, (1972), Vibration of Solids and Structures under Moving Loads, *Noordhoff International, Groningen.*

[58] L. Fryba, (1999), Vibration of Solids and Structures under Moving Loads, *Prague, Thomas Telford.*

[59] F.Y. Cheng, H. Jiang, and K. Lou, (2010), Smart structures: innovative systems for seismic response control, *CRC Press.*

[60] S.T. De la Cruz, (2003), Contribution to the assessment of the efficiency of friction dissipators for seismic protection of buildings, *PhD thesis, PhD Dissertation, Technical University of Catalonia, Barcelona.*

[61] M.C. Constantinou, T.T. Soong and G.F. Dargush, (1998), Passive energy dissipation systems for structural design and retrofit, *Multidisciplinary Center for Earthquake Engineering Research Buffalo, New York.*

[62] R.E. Christenson, (2001), Semiactive control of civil structures for natural hazard mitigation: Analytical and experimental studies, *PhD thesis, University of Notre Dame.*

[63] J. Marko, (2006), Influence of damping systems on building structures subject to seismic effects, *PhD thesis, Queensland University of Technology.*

[64] M.D. Symans, F.A. Charney, A.S. Whittaker, M.C. Constantinou, C.A. Kircher, M.W. Johnson, and R.J. McNamara, (2008), Energy dissipation systems for seismic applications: current practice and recent developments, *Journal of Structural Engineering, 134(1): 3-21.*

[65] George William Housner, L A Bergman, TK Caughey, AG Chassiakos, RO Claus, SF Masri, RE Skelton, TT Soong, BF Spencer, and James TP Yao. Structural control: past, present, and future, *Journal of engineering mechanics, 123(9):897-971, 1997.*

[66] B.F. Spencer Jr. and S. Nagarajaiah, (2003), State of the art of structural control, *Journal of structural engineering, 129(7):,845-856.*

[67] T.T. Soong and M.C. Constantinou, (1994), Passive and Active Structural Vibration Control in Civil Engineering, *Springer, New York.*

[68] M.D. Symans and M.C. Constantinou, (1999), Semi-activ e control systems for seismic protection of structures: a state-of-the-art review, *Engineering Structures 21: 469-487.*

[69] H. Yoshioka, J.C. Ramallo and B.F. Spencer Jr., (2002), "Smart" base isolation strategies employing magneto-rheological dampers, *Journal of Engineering Mechanics ASCE 128: 540-551.*

[70] H. Lemura and M.H. Pradono, (2002), Passive and semi-active seismic response control of a cable-stayed bridge, *Journal of Structural Control 9: 189-204.*

[71] K. Park, I. Lee, H. Jung and J. Park, (2003), Integrated passive?active system for seismic protection of a cable-stayed bridge, *Earthquake Engineering and Structural Dynamics 7: 615-633.*

[72] J.C. Ramallo, E.A. Johnson and B.F. Spencer Jr., (2002), Smart base isolation systems, *Journal of Engineering Mechanics ASCE 128: 1088-1100.*

[73] N. Makris and S. Chang, (2000), Effect of viscous, viscoplastic and friction damping on the response of seismic isolated structures, *Earthquake Engineering and Structural Dynamics 29: 85-107.*

[74] B.B. Soneji and R.S. Jangid, (2007), Passive hybrid systems for earthquake protection of cable-stayed bridge, *Engineering Structures 29: 57-70.*

[75] W. Yan, W. Xu, J. Wang and Y. Chen, (2014), Experimental research on the effects of a tuned particle damper on a viaduct system under seismic loads. *Journal of Bridge Engineering, 19(3): 4013004.*

[76] L.F.F. Miguel and R.H.A. Lopez, (2015), firefly algorithm for the design of force and placement of friction dampers for control of man-induced vibrations in footbridges, *Optimization and Engineering, 16(3): 633-661.*

[77] J. Chou and A. Pham, (2015), Smart artificial firefly colon y algorithm-based support vector regression for enhanced forecasting in civil engineering, *Computer-Aided Civil and Infrastructure Engineering, 30(9): 715-732.*

[78] K. Takeya, E. Sasaki and Y. Kobayashi, (2016), Design and parametric study on energy harvesting from bridge vibration using tuned dual-mass damper systems, *Journal of Sound and Vibration, 361: 50-65.*

[79] L.F.F. Miguel, R.H. Lopez, A.J. Torii and A.T. Beck, (2016), Robust design optimization of TMDs in vehicle-bridge coupled vibration problems, *Engineering Structures, 126: 703-711.*

[80] A. Camara, R. Cristantielli, M.A. Astiz and C. Málaga-Chuquitaype, (2017), Design of hysteretic dampers with optimal ductility for the transverse seismic control of cable-stayed bridges, *Earthquake Engineering and Structural Dynamics, 46(11): 1811-1833.*

[81] N. Attary, M. Symans, S. Nagarajaiah, A.M. Reinhorn, M.C. Constantinou, A.A. Sarlis, D.T.R. Pasala and D.P. Taylor, (2015), Experimental shake table testing of an adaptive passive negative stiffness device within a highway bridge model, *Earthquake Spectra, 31(4): 2163-2194.*

[82] N. Attary, M. Symans, S. Nagarajaiah, A.M. Reinhorn, M.C. Constantinou, A.A. Sarlis, D.T.R. Pasala and D.P. Taylor, (2015), Performance evaluation of negative stiffness devices for seismic response control of bridge structures via experimental shake table tests, *Journal of Earthquake Engineering, 19(2): 249-276.*

[83] E.I. Rivin, (2003), Passive vibration isolation, *New York, ASME Press.*

[84] J. Den Hartog, (1934), Mechanical Vibrations, *McGraw - Hill, New-York.*

[85] H. Frahm, (1909), Device for damping vibrations of bodies, *Technical representative, US No. Patent 989958.*

[86] J. Ormondroyd and J. Den Hartog, (1928), The theory of the dynamic vibration absorber, *Transactions of ASME 50: 9-22.*

[87] T. Asami, O. Nishihara and A. Baz, (2002), Analytical solutions to H? and H2 optimization of dynamic vibration absorbers attached to damped linear systems, *Journal of Vibration and Acoustics 124 (2): 284-295.*

[88] M. Zilletti, S. Elliott and E. Rustighi, (2012), Optimisation of dynamic vibration absorbers to minimise kinetic energy and maximise internal power dissipation, *Journal of Sound and Vibration 331(18): 4093-4100.*

[89] Y. Fujino and M. Abe, (1993), Design formulas for tuned mass dampers based on a perturbation technique, *Earthquake Engineering and Structural Dynamics 22(10): 833-854.*

[90] S. Krenk, (2005), Frequency analysis of the tuned mass damper, *Journal of Applied Mechanics 72(6): 936-942.*

[91] M. Hadi and Y. Arfiadi, (1998), Optimum design of absorber for MDOF structures, *Journal of Structural Engineering 124(11): 1272-1280.*

[92] R. Rana and T. Soong, (1998), Parametric study and simplified design of tuned mass dampers, *Engineering Structures 20(3): 193-204.*

[93] F. Sadek, B. Mohraz, A. Taylor and R. Chung, (1997), A method of estimating the parameters of tuned mass dampers for seismic applications, *Earthquake Engineering and Structural Dynamics 26(6): 617-636.*

[94] C. Lee, Y. Chen, L. Chung and Y. Wang, (2006), Optimal design theories and applications of tuned mass dampers, *Engineering Structures 28(1) 43-53.*

[95] G. Bekda and S. Nigdeli, (2011), Estimating optimum parameters of tuned mass dampers using harmony search, *Engineering Structures 33(9): 2716-2723.*

[96] B. Ebrahimi, M. Khamesee and M. Golnaraghi, (2008), Design and modeling of a magnetic shock absorber based on eddy current damping effect, *Journal of Sound and Vibration 315(4 - 5): 875-889.*

[97] Z. Wang, Z. Chen and J. Wang, (2012), Feasibility study of a large-scale tuned mass damper with eddy current damping mechanism, *Earthquake Engineering and Engineering Vibration 11(3): 391-401.*

[98] X. Lu, B. Huang, Q. Zhang, X. Lu, (2018), Experimental and analytical study on vibration control effects of eddy-current tuned mass dampers under seismic excitations, *Journal of Sound and Vibration 421: 153-165.*

[99] S. Krenk and J. Hogsberg, (2014), Tuned mass absorber on a flexible structure, *Journal of Sound and Vibration, 333: 1577-1595.*

[100] F. Bourquin, G. Caruso, M. Peigney and D. Siegert, (2014), Magnetically tuned mass dampers for optimal vibration damping of large structures, *Smart Materials and Structures 23(8): 085009.*

[101] H. Yu, F. Gillot and M. Ichchou, (2013), Reliability based robust design optimization for tuned mass damper in passive vibration control of deterministic/uncertain structures, *Journal of Sound and Vibration 332(9): 2222-2238.*

[102] R.A. Ibrahim, (2008), Recent advances in nonlinear passive vibration isolators, *Journal of Sound and Vibration, 314(3): 371-452.*

[103] J.E. Ruzicka and T.F. Derby, (1971), Influence of damping in vibration isolation. 1st Edn, Washington, *The Shock And Vibration Information Center, Naval Research Laboratory.*

[104] H. Ding, Z-Q. Lu and L-Q. Chen, (2018), Nonlinear isolation of transverse vibration of pre-pressure beams, *Journal of Sound and Vibration 442: 738-751.*

[105] L. Meng, J. Sun and W. Wu, (2015), Theoretical Design and Characteristics Analysis of a Quasi-Zero Stiffness Isolator Using a Disk Spring as Negative Stiffness Element, *Shock and Vibration 813763.*

[106] E.I. Rivin, (2001), Passive Vibration Isolation, *ASME Press, NewYork, NY, USA.*

[107] A. Carrella, M.J. Brennan and T.P. Waters, (2007), Optimization of a quasi-zerostiffness isolator, *Journal of Mechanical Science and Technology 21: 946-949.*

[108] A. Carrella, M.J. Brennan and T.P. Waters, (2007), Static analysis of a passive vibration isolator with quasi-zero-stiffness characteristic, *Journal of Sound and Vibration 301: 678-689.*

[109] A. Carrella, M.J. Brennan and I. Kovacic, T.P. Waters, (2009), On the force transmissibility of a vibration isolator with quasi-zero-stiffness, *Journal of Sound and Vibration 322: 707-717.*

[110] T. Zhu, B. Cazzolato, W.S.P. Robertson et al., (2015), Vibration isolation using six degreeof-freedom quasizero-stiffness magnetic levitation, *Journal of Sound and Vibration 358: 48-73.*

[111] K. Chai, Q-C. Yang and J-J. Lou, (2016), Dynamic characteristic analysis of two-stage quasi-zero stiffness vibration isolation system, *Vibroengineering Procedia 10.*

[112] X. Sun and X. Jing, (2015), Multi-direction vibration isolation with quasi-zero stiffness by employing geometrical nonlinearity, *Mechanical Systems and Signal Processing 62-63: 149-163.*

[113] P. Alabuzhev, A. Gritchin, L. Kim, G. Migirenko, V. Chon and P. Stepanov, (1989), Vibration Protecting and Measuring Systems with Quasi-Zero Stiffness, *Hemisphere Publishing, New York, USA.*

[114] R.M.D. Arafat, S.T. Park and C.B. Sajal, (2010), Design of a vehicle suspension system with negative stiffness system, *IST Transaction of Mechanical System Theoretic and Application 1(2): 17.*

[115] T.D. Le and K.K. Ahn, (2011), A vibration isolation system in low frequency excitation region using negative stiffness structure for vehicle seat, *Journal of Sound and Vibration 330(26): 6311-6335.*

[116] T.D. Le and K.K. Ahn, (2013), Experimental investigation of a vibration isolation system using negative stiffness structure, *International Journal of Mechanical Sciences 70: 99-112.*

[117] X.T. Liu, X.C. Huang and H.X. Hua, (2013), On the characteristics of a quasi-zero stiffness isolator using Euler buckled beam as negative stiffness corrector, *Journal of Sound and Vibration 332(14): 3359-3376.*

[118] X.C. Huang, X.T. Liu, J.Y. Sun, Z.Y. Zhang and H.X. Hua, (2014), Vibration isolation characteristics of a nonlinear isolator using Euler buckled beam as negative stiffness corrector: A theoretical and experimental study, *Journal of Sound and Vibration 333: 1132-1148.*

[119] B.A. Fulcher, D.W. Shahan, M.R. Haberman, C.C. Seepersad and P.S. Wilson, (2014), Analytical and experimental investigation of buckled beams as negative stiffness elements for passive vibration and shock isolation systems, *Journal of Vibration and Acoustics 136: 031009.*

[120] D.L. Platus, (1992), Negative stiffness-mechanism vibration isolation systems, *Vibration Control in Microelectronics, Optics, and Metrology 1619: 44-54.*

[121] A. Carrella, M.J. Brennan, T.P. Waters and Jr.V. Lopes, (2012), Force and displacement transmissibility of a nonlinear isolator with high-static-low-dynamic-stiffness, *International Journal of Mechanical Sciences 55(1): 2229.*

[122] Y.L. Li and D.L. Xu, (2017), Vibration attenuation of high dimensional quasi-zero stiffness floating raft system, *International Journal of Mechanical Sciences 126: 186-195.*

[123] X.L. Wang, J.X. Zhou, D.L. Xu, H.J. Ouyang and Y. Duan, (2017), Force transmissibility of a two-stage vibration isolation system with quasi-zero stiffness, *Nonlinear Dynamics 87: 633-646.*

[124] Y. Wang, S.M. Li, S. Neild and J.S.Z. Jiang, (2017), Comparison of the dynamic performance of nonlinear one and two degree-of-freedom vibration isolators with quasizero stiffness, *Nonlinear Dynamics 88: 635-654.*

[125] Z.J. Fan, J.H. Lee, K.H. Kang and K.J. Kim, (1998), The forced vibration of a beam with viscoelastic boundary supports, *Journal of Sound and Vibration 210(5): 673-682.*

[126] B.L. Lv, W.Y. Li and H.J. Ouyang, (2015) Moving force-induced vibration of a rotating beam with elastic boundary conditions, *International Journal of Structural Stability and Dynamics 15(1): 1450035.*

[127] T. Zhang, H. Ouyang, Y.O. Zhang and B.L. Lv, (2016), Nonlinear dynamics of straight fluid-conveying pipes with general boundary conditions and additional springs and masses, *Applied Mathematical Modelling 40(17-18): 7880-7900.*

[128] Y.R. Wang and Z.W. Fang, (2015), Vibrations in an elastic beam with nonlinear supports at both ends, *Journal of Applied Mechanics and Technical Physics 56(2): 337-346.*

[129] X.Y. Mao, H. Ding and L.Q. Chen, (2017) Vibration of flexible structures under nonlinear boundary conditions, *Journal of Applied Mechanics 84(11): 111006.*

[130] H. Ding, S. Wang and Y-W. Zhang, (2018), Free and forced nonlinear vibration of a transporting belt with pulley support ends, *Nonlinear Dynamics 92(4): 2037-2048.*

[131] H. Ding, C.W. Lim and L.Q. Chen, (2018), Nonlinear vibration of a traveling belt with non-homogeneous boundaries, *Journal of Sound and Vibration 424(4): 78-93.*

[132] J.E. Mottershead, and M.I. Friswell, (1993), Model up dating in structural dynamics: A survey, *Journal of Sound and Vibration, 167: 347-375.*

[133] M.F. Green, and D. Cebon, (1994), Dynamic response of highway bridges to heavy vehicle loads: theory and experimental validation, *Journal of Sound and Vibration, 170: 51-78.*

[134] M.F. Green, (1990), Dynamic response of short-span highway bridges to heavy vehicle loads, *PhD thesis, University of Cambridge.*

[135] J.W. Kwark, E.S. Choi, Y.J. Kim, B.S. Kim and S.I. Kim, (2004), Dynamic behavior of two-span continuous concrete bridges under moving high-speed train, *Computers and Structures, 82: 463-474.*

[136] S-Y. Lee and S-S. Yhim, (2005), Dynamic behavior of long-span box girder bridges subjected to moving loads: Numerical analysis and experimental verification, *International Journal of Solids and Structures, 42: 5021-5035.*

[137] P. Koziol, (2016), Experimental validation of waveletbased solution for dynamic response of railway track subjected to a moving train, *Mechanical Systems and Signal Processing, 79: 174-181.*

[138] P. Paultre, J. Proulx and M. Talbot, (1995), Dynamic testing procedures for highway bridges using traffic loads, *Journal of Structural Engineering, 121: 362-376.*

[139] C.S. Huang, Y.B. Yang, L.Y. Lu and C.H. Chen, (1999), Dynamic testing and system identification of a multi?span highway bridge, *Earthquake engineering and structural dynamics, 28: 857-878.*

[140] A. Gonzalez, E.J. Obrien, D. Cantero, Y. Li, J. Dowling and A. Znidaric, (2010), Critical speed for the dynamics of truck events on bridges with a smooth road surface, *Journal of Sound and Vibration, 329: 2127-2146.*

[141] E-T. Lee, H-C. Eun, Y-J. Choi, Y-J. Ahn, S-G. Lee and S-W. Park, (2016), Structural performance experiment by moving cart tomount measurement sensors, *Journal of Vibroengineering, 18: 1157-1166.*

[142] C. Bilello, L.A. Bergman and D. Kuchma, (2004), Experimental investigation of a small-scale bridge model under a moving mass, *Journal of Structural Engineering, 130: 799-804.*

[143] D. Stancioiu, H. Ouyang, J.E. Mottershead and S. James, (2011), Experimental investigations of a multi-span flexible structure subjected to moving masses, *Journal of Sound and Vibration, 330: 2004-2016.*

[144] X. Bian, H. Jiang, C. Cheng, Y. Chen, R. Chen and J. Jiang, (2014), Full-scale model testing on a ballastless high-speed railway under simulated train moving loads, *Soil Dynamics and Earthquake Engineering, 66: 368-384.*

[145] T.H.T. Chan and D.B. Ashebo, (2006), Moving axle load from multi-span continuous bridge: laboratory study, *Journal of Vibration and Acoustics, 128: 521-526.*

[146] P.J. Mcgetrick, C.W. Kim, A. Gonzalez and E.J.O. Brien, (2015), Experimental validation of a drive-by stiffness identification method for bridge monitoring, *Structural Health Monitoring, 14: 317-331.*

[147] C.W. Kim, S. Inoue, K. Sugiura, P.J. Mcgetrick and M. Kawatani, (2016), Extracting bridge frequencies from dynamic responses of two passing vehicles, *In: ZINGONI, A., Edn. Insights and Innovations in Structural Engineering, Mechanics and Computation:*

Proceedngs of the Sixth International Conference on Structural Engineering, Mechanics and Computation, Cape Town, South Africa, CRC Press, 1858-1864.

[148] A.H Nayfeh and D.T. Mook, (1995), Nonlinear Oscillations, *John Wiley and Sons, 2nd Edn.*

[149] A.H. Nayfeh, (1973), Perturbation Methods, *John Wiley and Sons.*

[150] D.W. Jordan and P. Smith, (1999), Nonlinear Ordinary Differential Equations, *Oxford, 3th Edn.*

[151] J.J. Thomsen, (1997), Vibration and Stability - Order and Chaos, *McGraw Hill.*

[152] L. Meirovitch, (1986), Elements of Vibration Analysis, *McGraw Hill, International Edn.*

[153] A. Rand, (2005), Lecture Notes on Nonlinear Vibration, *Wiley.*

[154] C. Hayashi, (1964), Nonlinear Oscillations in Physical Systems, *McGraw Hill.*

[155] B.G. Galerkin, (1915), Series solution of some problems of elastic equilibrium of rods and plates, *Vestn. Inzh. Tekh19: 897-908.*

[156] D. Xu, Y. Zhang, J. Zhou and J. Lou, (2014), On the analytical and experimental assessment of the performance of a quasi-zero-stiffness isolator, *Journal of Vibration and Control 20(15): 2314-2325.*

[157] W.S. Clarence, (2005), Vibration and Shock Handbook, *Taylor and Francis Group, Boca Raton.*

[158] P. Paultre, O. Chaallal and J. Proulx, (1992), Bridge dynamics and dynamic amplification factors-a review of analytical and experimental findings, *Canadian Journal of Civil Engineering 19: 260-278.*

[159] R.K. Chatterjee, T.K. Datta and C.S. Surana, (1994), Vibration of continuous bridges under moving vehicles, *Journal of Sound and Vibration 169: 619-632.*

[160] C. Johansson, C. Pacoste and R. Karoumi, (2013), Closed-form for the mode superposition analysis of the vibration in muti-span beam bridges caused by concentrated moving loads, *Computers and Structures 119:,85-94.*

[161] S. Marchesiello, A. Fasana, L. Garibaldi and B.A.D. Piombo, (1999), Dynamics of multi-span continuous straight bridges subject to multi-degrees of freedom moving vehicle excitation, *Journal of Sound and Vibration 224: 541-561.*

[162] A.A.N. Djanan, B.R.N. Nbendjo and P. Woafo, (2011), Control of vibration on a hinged-hinged beamunder a non-ideal excitation using RLC circuit with variable capacitance, *Nonlinear Dynamics 63: 477-489.*

[163] W. Huang and Y. Zou, (1994), The dynamic response of a viscoelastic Winkler foundation-supported elastic beam impacted by a low velocity projectile, *Computers and Structures 52: 431-436.*

[164] S. Lu and D. Xuejun, (1998), Dynamic analysis to infinite beam under a moving line load with uniform velocity, *Journal of Applied Mathematics and Mechanics 19: 368-373.*

[165] T.G. Gutowsky and C.L. Dym, (1976), Propagation of ground vibration: a review, *Journal of Sound and Vibration 49: 179-193.*

[166] L.M.A. Tabejieu, B.R.N. Nbendjo and G. Filatrella, (2019), Effect of the fractional foundation on the response of beam structure submitted to moving and wind loads, *Chaos, Soliton and Fractals 127: 178-188.*

[167] Q. Meng, X. Yang, W. Li, E. Lu and L. Sheng, (2017), Research and Analysis of Quasi-Zero-Stiffness Isolator with Geometric Nonlinear Damping, *Shock and Vibration 6719054.*

[168] N.Z.A. Elkasem, M.A.N. Abdel-Mooty and S.A. Murad, (2009), Dynamic Response of Highway Bridges to Moving Vehicles Considering Higher Modes, *Journal of Engineering and Applied Sciences 56: 21-38.*

[169] Y. Khadri, S. Tekili, E.M. Daya, A. Daouadji, M. Guenfoud and B. Merzoug, (2009), Analysis of the Dynamic Response of Bridges Under Moving Load, *International Review of Mechanical Engineering 3: 91-99.*

[170] Y. Pi and H. Ouyang, (2016), Vibration control of beams subjected to a moving mass using a successively combined control method, *Applied Mathematical Modelling 40: 4002-4015.*

[171] R. Tian, X. Yang, Q. Zhang and X. Guo, (2016), Vibration reduction in beam bridge under moving loads using nonlinear smooth and discontinuous oscillator, *Advances in Mechanical Engineering 8: 1-12.*

[172] Y. Wang, S. Li, C. Cheng and X. Jiang, (2016), Dynamic Analysis of a High-Static-Low-Dynamic-Stiffness Vibration Isolator with Time-Delayed Feedback Control, *Shock and Vibration 40: 4002-4015.*

[173] Y. Pi and H. Ouyang, (2017), Lyapunov-based boundary control of a multi-span beam subjected to moving masses, *Journal of Vibration and Control 23: 2221-2234.*

List of Publications

1- **H. Sonfack Bouna**, B.R. Nana Nbendjo and P. Woafo, (2018), On the dynamics of two multi-span continuous beam bridges model coupled by their close environment, *International Journal of Dynamics and Control 6: 29-40.*

2- **H. Sonfack Bouna**, B.R. Nana Nbendjo and P. Woafo, (2020), Isolation performance of a quasi-zero stiffness isolator in vibration isolation of a multi-span continuous beam bridge under pier base vibrating excitation, *Nonlinear Dynamics 100: 1125-1141.*

Other publications

1- **H. Sonfack Bouna** and B.R. Nana Nbendjo, (2012), Vibration control of a plate subjected to impulsive force by plate-type dynamic vibration absorbers, *World Journal Mechanics 2: 143-151.*

Int. J. Dynam. Control
DOI 10.1007/s40435-016-0293-3

On the dynamics of two multi-span continuous beam bridges model coupled by their close environment

H. Sonfack Bouna[1] · **B. R. Nana Nbendjo**[1] · **P. Woafo**[1]

Received: 17 June 2016 / Revised: 1 December 2016 / Accepted: 7 December 2016

Abstract In this paper, we sought to develop a valid theoretical model of two bridges coupled via their dynamic environment modelled as a linear viscoelastic Winkler foundation. Analytical, numerical and experimental study of the dynamic response of the two bridges are explored in the cases where they are submitted to sinusoidal excitation and periodic impulsive force. The effects of the close environment and the distance between the two bridges on the amplitude of vibration of each beam bridge is pointed out.

Keywords Coupled bridges · Sinusoidal excitation · Periodic impulsive force · Vibration reduction · Winkler foundation

1 Introduction

The experimental study of the vibration characteristics of structural systems is an important element in our efforts to understand and control many vibration phenomena encountered in design. Very often, tests are performed on a complex structure with the objective of obtaining an empirical description of its dynamic behavior, or providing verification for an analytical or a numerical structural model [1–5]. To quantify the dynamic response of a given structure, the determination of its intrinsic dynamic properties such as natural frequencies, vibration modes and damping, etc., is of particular importance. These structural characteristics can be determined using a modal test [6]. Performing a modal test on a structure allows an analyst to validate results generated using a finite element, analytical or numerical model, and so more confidence can be placed on the structural model to provide meaningful analysis results.

Over the years, dynamic tests of highway bridges have been performed by many researchers and engineers. However, most of the tests are in-field dynamic tests [7]. Lab-based dynamic tests of full assemblage bridge models under a controlled environment are rather scanty. Regardless of whether the tests were performed on the field or in the laboratory, these tests were focused essentially on single bridges [8]. Despite the existence of many bridges coupled on beds of multiple rivers, dynamic tests on bridges coupled by their close environment are rarely performed. It is therefore of interest to investigate these coupled bridges from a dynamic test setting.

The present study consists of a dynamic test which aims at developing a enough complete descriptive theoretical model of indirect coupled bridges. After several dynamic tests performed on a scale model built in the laboratory, a mathematical modelling of the device is then proposed. We analyze analytically and numerically the effectiveness of this modelling.

The work is organized as follows. In Sect. 2, the experimental device is presented and the mathematical modelling of the system is carried out. Section 3 is devoted to the theoretical analysis of the dynamic response of system on the basis of the resulting modal equations using direct numerical simulations and analytical explanation. Section 4 is devoted to some experimental investigation. Section 5 gives some concluding remarks.

✉ B. R. Nana Nbendjo
nananbendjo@yahoo.com

[1] Laboratory of Modelling and Simulation in Engineering, Biomimetics and Prototypes, Faculty of Science, University of Yaoundé I, P.O. Box 812, Yaoundé, Cameroon

Published online: 26 December 2016

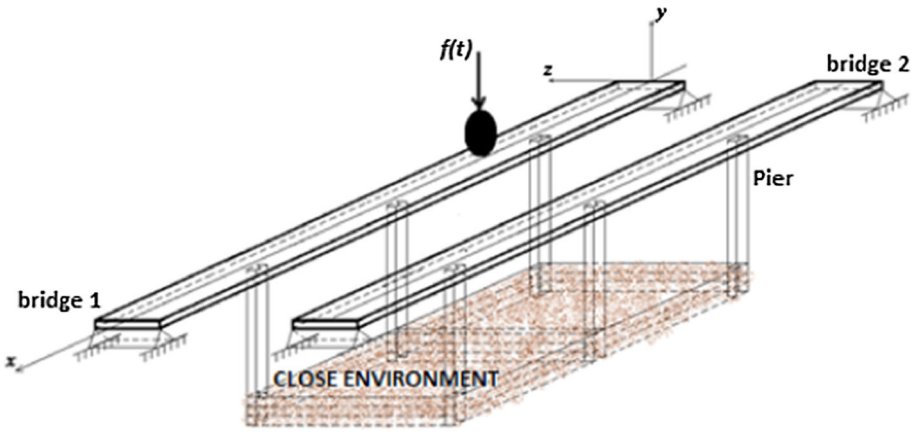

Fig. 1 Schematic of the experimental device

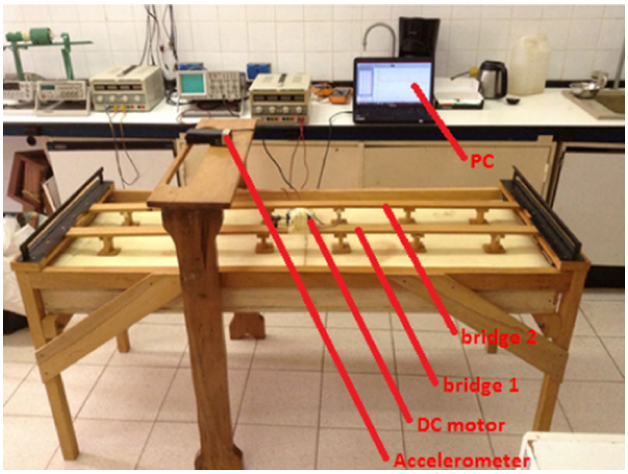

Fig. 2 Photograph of the experimental set up

2 Description of the experimental devices and general mathematical formalism

2.1 Experimental set up

The experimental device under study is a model of two coupled bridges, on one of which exerts a localized combination of sinusoidal load and periodic impulsive load. As shown in the Fig. 1, the bridges are indirectly coupled via their close environment (soil support) through their pier. The bridge model of the experimental device consists of two wooden beams (see Fig. 2) whose dimensions are compiled in the Table 1.

In the scale model, the two bridges are represented by two wooden beams of dimensions specified in the Table 1. In addition, a polyurethane (PU) mattress plays the role of the close environment and an universal motor attached to one of the beam bridges (bridge 1) imposes its vibrations on it as both sinusoidal and periodic impulsive loads. Vibrations are sensed by DE-ACCM2G accelerometers incorporated to the structure and then processed by appropriate computer software. Let us note that the DE-ACCM2G is an off the shelf 2 axis 2g accelerometer solution with analog outputs. It features integrated op amp buffers for direct connection to a micro controller's analog inputs, or for driving heavier loads.

Table 1 Dimensions of the experimental set up elements

	Model
Length	1.5 m
Height	45 mm
Width	12 mm
Thickness	1 mm
Pier length	60 mm
Span length	13.25 and 24.7 cm

2.2 General mathematical formalism

2.2.1 Model of the bridge and soil support

The transverse equation of motion for a homogeneous, isotropic and uniform elastic beam subjected to a time-varying load is taken as the governing Euler–Bernoulli equation [9–11], i.e.

$$\rho S \frac{\partial^2 y^*}{\partial t^{*2}} + \delta \frac{\partial y^*}{\partial t^*} + EI \frac{\partial^4 y^*}{\partial x^{*4}} = f\left(x^*, t^*\right), \tag{1}$$

where $y^* = y^*(x^*, t^*)$ is the transverse deflection of the beam, E the Young's modulus, I the inertia moment with respect to the neutral axis, S the beam cross-section, ρ the density of the beam, δ the vertical viscous damping coefficient and $f(x^*, t^*)$ is all the external load per unit length.

The external excitation brought by the motor is supposed to be both sinusoidal and impulsive and localized at the point x_0 of bridge 1. So, it can be described as follows

$$f\left(x^*, t^*\right) = \left[f_{\sin}\left(x^*, t^*\right) + f_{imp}\left(x^*, t^*\right)\right] \delta\left(x^* - x_0^*\right), \tag{2}$$

where $\delta(x)$ is the Dirac delta function which reflects the local nature of excitation on the bridge, $f_{\sin}(x^*, t^*)$ the sinusoidal load and $f_{imp}(x^*, t^*)$ the periodic impulsive force occurring at regular intervals of time T [12], given by expressions (3) and (4), respectively.

$$f_{\sin}\left(x^*, t^*\right) = f_0 \cos \omega^* t^*, \tag{3}$$

$$f_{imp}\left(x^*, t^*\right) = I_0 \sum_{i=1}^{N} \left\{H\left(t^* - iT^*\right) - H\left[t^* - \left(iT^* + \Delta T^*\right)\right]\right\}, \tag{4}$$

where f_0 is the amplitude of the sinusoidal load and ω^* its frequency. I_0 is the amplitude of each impulsion, N stand for the total number of impulsions while ΔT represents the duration of the impact. $H(x)$ is the Heaviside function defined as follows

$$H(x) = \begin{cases} 1 \text{ if } x \geq 0 \\ 0 \text{ if } x < 0 \end{cases} \tag{5}$$

The coupling between the two bridges is an indirect coupling via an environment that is primarily the ground under their piers that can be modelled as a linear viscoelastic Winkler foundation [13,14] (Kelvin–Voigt model of soil [3]). Thus, for this system, each bridge suffers from environmental coupling (soil support), external restoring forces $F_j(x, t)$ located under the piers and given as follows

$$F_j\left(x^*, t^*\right) = -\left[k_s y^*\left(x^*, t^*\right) + c_s \frac{\partial y^*\left(x^*, t^*\right)}{\partial t^*}\right] \delta\left(x^* - x_j^*\right), \tag{6}$$

where k_s and c_s are the two coupling parameters characterizing the strength and the damping of the soil, respectively. x_j^* are the positions of the piers under the considered bridge and $\delta(x)$ is the Dirac delta function which reflects the local nature of piers positions.

2.2.2 Modelling the propagation of vibration in the soil

Let $a(z_\alpha, \omega)$ the acceleration in the soil at the distance z_α from the source. It was shown that the acceleration $a\left(z_\beta, \omega\right)$ at the distance z_β can be estimated in the frequency domain [15,16] as a function of $a(z_\alpha, \omega)$ as follows

$$a\left(z_\beta, \omega\right) = a\left(z_\alpha, \omega\right) \exp\left[ik^*(\omega) d_{\alpha\beta}\right], \tag{7}$$

where $d_{\alpha\beta} = \left|z_\beta - z_\alpha\right|$ is the distance between the two points z_α and z_β and $k^*(\omega)$ the complex wave number defined by:

$$k^*(\omega) = k(\omega) + i\lambda(\omega), \tag{8}$$

where $k(\omega) = \frac{2\pi c}{\omega}$ is the real wave number; with c the wave velocity in the ground. $\lambda(\omega)$ is the vibration attenuation factor defined by the viscoelastic model considered to model the close environment.

But a more simplest model used to describe the propagation of the vibration into the soil is given by [17] as follows

$$a\left(z_\beta, \omega\right) = a\left(z_\alpha, \omega\right) \exp\left[-\lambda(\omega) d_{\alpha\beta}\right]. \tag{9}$$

Let set $\gamma_{\alpha\beta} = exp\left[-\lambda(\omega) d_{\alpha\beta}\right]$ the coefficient reflecting the vibration transfer from point z_α to point z_β; which decreases with the distance $d_{\alpha\beta}$. This coefficient reflects the vibration propagation from one to another point. Thus, the expression (9) can be rewritten as follows

$$a\left(z_\beta, \omega\right) = \gamma_{\alpha\beta} a\left(z_\alpha, \omega\right). \tag{10}$$

It comes out that a pier of index-number α of acceleration $a(z_\alpha, \omega)$ induces on each neighboring pier of index-number β, some vibration translated by the inertia force given by the following equation

$$f_\beta(t) = -m_\beta a\left(z_\beta, \omega\right) = -m_\beta \gamma_{\alpha\beta} a\left(z_\alpha, \omega\right), \tag{11}$$

where m_β is the mass of the neighboring pier of index-number β.

2.2.3 Modelling the coupled bridges system

Taking into account the above considerations, the system which consists of a bridge under localized universal motor excitation coupled to a second one by their close environment is governed by the following set of equations

$$\begin{cases} \rho_1 S_1 \frac{\partial^2 y_1^*}{\partial t^{*2}} + \delta_1 \frac{\partial y_1^*}{\partial t^*} + E_1 I_1 \frac{\partial^4 y_1^*}{\partial x^{*4}} \\ + \sum_{\alpha=1}^{N_1} \left[c_s \frac{\partial y_1^*}{\partial t^*} + k_s y_1^*\right] \delta\left(x^* - x_{1\alpha}^*\right) \\ + \sum_{\alpha=1}^{N_1} m_{1\alpha} \sum_{\beta=1}^{N_2} \gamma_{\alpha\beta} \frac{\partial^2 y_2^*}{\partial t^{*2}} \delta\left(x^* - x_{2\beta}^*\right) \\ = \left[f_{\sin}\left(x^*, t^*\right) + f_{imp}\left(x^*, t^*\right)\right] \delta\left(x^* - x_0^*\right), \\ \rho_2 S_2 \frac{\partial^2 y_2^*}{\partial t^{*2}} + \delta_2 \frac{\partial y_2^*}{\partial t^*} + E_2 I_2 \frac{\partial^4 y_2^*}{\partial x^{*4}} \\ + \sum_{\alpha=1}^{N_2} \left[c_s \frac{\partial y_2^*}{\partial t^*} + k_s y_2^*\right] \delta\left(x^* - x_{2\alpha}^*\right) \\ + \sum_{\alpha=1}^{N_2} m_{2\alpha} \sum_{\beta=1}^{N_1} \gamma_{\alpha\beta} \frac{\partial^2 y_1^*}{\partial t^{*2}} \delta\left(x^* - x_{1\beta}^*\right) = 0, \end{cases} \tag{12}$$

where $y_j^* = y_j^*(x^*, t^*)$ is the transverse displacement of the bridge of index-number j, N_1 and N_2, $m_{1\alpha}$ and $m_{2\alpha}$, and $x_{1\alpha}^*$ and $x_{2\alpha}^*$ are the numbers of piers, masses and positions of the piers under the bridge 1 and the bridge 2, respectively. As the two beam bridges are hinged–hinged one, the boundary conditions of the problem are given by:

$$y_1^*(x^*,t^*)\big|_{x^*=0,x^*=L}=0,\quad y_2^*(x^*,t^*)\big|_{x^*=0,x^*=L}=0,$$
$$\frac{\partial^2 y_1^*(x^*,t^*)}{\partial^2 x^*}\Big|_{x^*=0,x^*=L}=0,\quad \frac{\partial^2 y_2^*(x^*,t^*)}{\partial^2 x^*}\Big|_{x^*=0,x^*=L}=0.$$

Let consider the dimensionless variables defined as $x=\frac{x^*}{L}$, $y_1=\frac{y_1^*}{L}$, $y_2=\frac{y_2^*}{L}$, $t=t^*\omega_0$; where $\omega_0=\frac{1}{L^2}\sqrt{\frac{E_1I_1}{\rho_1S_1}}$. Then, the dimensionless problem is given by the following set of equations

$$\begin{cases}\frac{\partial^2 y_1}{\partial t^2}+\lambda_1\frac{\partial y_1}{\partial t}+\omega_1^2\frac{\partial^4 y_1}{\partial x^4}+\sum_{\alpha=1}^{N_1}\left[c_{s1}\frac{\partial y_1}{\partial t}+k_{s1}y_1\right]\delta(x-x_{1\alpha})\\ \quad+\sum_{\alpha=1}^{N_1}\sum_{\beta=1}^{N_2}\gamma_{\alpha\beta1}\frac{\partial^2 y_2}{\partial t^2}\delta(x-x_{2\beta})=F(t)\,\delta(x-x_0)\\ \frac{\partial^2 y_2}{\partial t^2}+\lambda_2\frac{\partial y_2}{\partial t}+\omega_2^2\frac{\partial^4 y_2}{\partial x^4}+\sum_{\alpha=1}^{N_2}\left[c_{s2}\frac{\partial y_2}{\partial t}+k_{s2}y_2\right]\delta(x-x_{2\alpha})\\ \quad+\sum_{\alpha=1}^{N_2}\sum_{\beta=1}^{N_1}\gamma_{\alpha\beta2}\frac{\partial^2 y_1}{\partial t^2}\delta(x-x_{1\beta})=0,\end{cases}\tag{13}$$

where

$$M_1=\rho_1S_1,\ M_2=\rho_2S_2,\ \mu=\frac{M_1}{M_2},\ \varepsilon=\frac{E_1I_1}{E_2I_2}$$
$$\omega_1^2=\frac{1}{L^4}\frac{E_1I_1}{M_1\omega_0^2}=1,$$
$$\omega_2^2=\frac{1}{L^4}\frac{E_2I_2}{M_2\omega_0^2}=\frac{\mu}{\varepsilon}\omega_1^2=\frac{\mu}{\varepsilon},\ \omega=\frac{\omega^*}{\omega_0}$$
$$\lambda_1=\frac{\delta_1}{M_1\omega_0},\ \lambda_2=\frac{\delta_2}{M_2\omega_0},\ c_{s1}=\frac{c_s}{M_1\omega_0},$$
$$c_{s2}=\frac{c_s}{M_2\omega_0}=\mu c_{s1}$$
$$k_{s1}=\frac{k_s}{M_1\omega_0^2},\ k_{s2}=\frac{k_s}{M_2\omega_0^2}=\mu k_{s1}$$
$$\gamma_{\alpha\beta1}=\frac{m_{1\alpha}}{M_1}\gamma_{\alpha\beta},\ \gamma_{\alpha\beta2}=\frac{m_{2\alpha}}{M_2}\gamma_{\alpha\beta},$$
$$F(t)=\frac{L^3}{E_1I_1}\left[f_{\sin}(x,t)+f_{imp}(x,t)\right]$$

The system (13) is the dimensionless equations of coupled bridges resting on a linear viscoelastic Winkler foundation. In index notation, this system is put in the following combined form

$$\frac{\partial^2 y_i}{\partial t^2}+\lambda_i\frac{\partial y_i}{\partial t}+\omega_i^2\frac{\partial^4 y_i}{\partial x^4}+\sum_{\alpha=1}^{N_i}\left[c_{si}\frac{\partial y_i}{\partial t}+k_{si}y_i\right]\delta(x-x_{i\alpha})$$
$$+\sum_{\alpha=1}^{N_i}\sum_{\beta=1}^{N_j}\gamma_{\alpha\beta i}\frac{\partial^2 y_j}{\partial t^2}\delta\left(x-x_{j\beta}\right)=F_i(t)\,\delta(x-x_0),$$
$$i,j=1,2\ \text{ and }\ j\neq i,\tag{14}$$

with

$$F_i(t)=\begin{cases}F(t) & \text{if } i=1\\ 0 & \text{if } i=2\end{cases}\tag{15}$$

In the following sections we will deal with Eq. (14).

3 Analytical explanation of the model

The method of separation of variables suggests the solutions of the system (14) into the following form

$$y_i(x,t)=\sum_{n=1}^{\infty}\phi_n(x)\,q_{in}(t),\tag{16}$$

where $\phi_n(x)$ are the mode shapes, given in accordance with the boundary conditions of the problem by the expression (17).

$$\phi_n(x)=\sin(n\pi x)\tag{17}$$

$q_{in}(t)$ are time functions determined by the modal equations which are obtained by substituting the transverse displacements by their expressions (16) in Eq. (14) governing the dynamics of the system, multiplying by $\phi_m(x)$, and integrating over the length of the beam bridge. Applying the orthogonality property of spatial functions and with some mathematical calculations and arrangements, the modal equations are obtained below written in index notation

$$\ddot{q}_{in}+2\lambda_{in}\dot{q}_{in}+\omega_{in}^2q_{in}+C_{ji}\ddot{q}_{jn}=2F_i(t)\sin(n\pi x_0),\tag{18}$$

where $i,j=1,2$ and $j\neq i$, $n=1,\ldots,\infty$ characterizing the different modes of vibration and

$$2\lambda_{in}=\lambda_i+2c_{si}\sum_{\alpha=1}^{N_i}\sin^2(n\pi x_{i\alpha}),\tag{19}$$

$$\omega_{in}^2=\omega_i^2(n\pi)^4+2k_{si}\sum_{\alpha=1}^{N_i}\sin^2(n\pi x_{i\alpha}),\tag{20}$$

$$C_{ji}=2\sum_{\alpha=1}^{N_i}\sum_{\beta=1}^{N_j}\gamma_{\alpha\beta i}\sin^2\left(n\pi x_{j\beta}\right).\tag{21}$$

For the bridge of index-number i, ω_{in} is the frequency of the vibration mode n. The term C_{ji} given by expression (21) is the coupling term reflecting the impact of the bridge of

index-number j on the bridge of index-number i. It depends on the vibration transfer coefficient $\gamma_{\alpha\beta}$; and therefore on the distance between the two bridges with respect of which it decreases. System (18) can be rewritten as follows

$$\begin{cases} \ddot{q}_{1n} + 2\lambda_{1n}\dot{q}_{1n} + \omega_{1n}^2 q_{1n} + C_{21}\ddot{q}_{2n} = 2F\,(t)\sin\,(n\pi x_0) \\ \ddot{q}_{2n} + 2\lambda_{2n}\dot{q}_{2n} + \omega_{2n}^2 q_{2n} + C_{12}\ddot{q}_{1n} = 0 \end{cases} \tag{22}$$

An analytical solution of this system of modal equations is given in the following subsections in the cases of sinusoidal excitation and periodic impulsive load.

3.1 Analytical solution of the modal equations for sinusoidal excitation

In this case, system (22) can be rewritten as follow

$$\begin{cases} \ddot{q}_{1n} + 2\lambda_{1n}\dot{q}_{1n} + \omega_{1n}^2 q_{1n} + C_{21}\ddot{q}_{2n} = F_{0n}\cos\omega t, \\ \ddot{q}_{2n} + 2\lambda_{2n}\dot{q}_{2n} + \omega_{2n}^2 q_{2n} + C_{12}\ddot{q}_{1n} = 0, \end{cases} \tag{23}$$

where $F_{0n} = \frac{2L^3}{E_1 I_1} f_0 \sin\,(n\pi x_0)$

To solve this system, let us use the harmonic balance method. Let set

$$\begin{cases} q_{1n} = A_n \cos\,(\omega t + \varphi_1)\,, \\ q_{2n} = B_n \cos\,(\omega t + \varphi_2)\,. \end{cases} \tag{24}$$

Substituting Eq. (24) into Eq. (23), we obtain after some algebraic manipulations the following amplitude equations

$$\begin{cases} A_n = F_{0n}\sqrt{\frac{\eta_1^2+\eta_2^2}{\eta^2}} \\ B_n = F_{0n}\sqrt{\frac{\eta_3^2+\eta_4^2}{\eta^2}}, \end{cases} \tag{25}$$

where

$$\begin{cases} \eta = \left(\omega_{1n}^2-\omega^2\right)^2\left(\omega_{2n}^2-\omega^2\right)^2 - 2\omega^4 C_{12}C_{21}\left(\omega_{1n}^2-\omega^2\right)\left(\omega_{2n}^2-\omega^2\right) - 4\omega^2\lambda_{1n}^2\left(\omega_{2n}^2-\omega^2\right)^2 \\ -4\omega^2\lambda_{2n}^2\left(\omega_{1n}^2-\omega^2\right)^2 + 16\omega^4\lambda_{1n}^2\lambda_{2n}^2 - 8\omega^6 C_{12}C_{21}\lambda_{1n}\lambda_{2n} + \omega^8 C_{12}^2 C_{21}^2 \\ \eta_1 = \left(\omega_{1n}^2-\omega^2\right)^2\left(\omega_{2n}^2-\omega^2\right) - \omega^4 C_{12}C_{21}\left(\omega_{2n}^2-\omega^2\right) - 2\omega^2\lambda_{2n}\left(\omega_{1n}^2-\omega^2\right) \\ \eta_2 = 2\omega\lambda_{1n}\left(\omega_{2n}^2-\omega^2\right)^2 + 2\omega^5 C_{12}C_{21}\lambda_{2n} - 8\omega^3\lambda_{1n}\lambda_{2n}^2 \\ \eta_3 = \omega^2 C_{12}\left[\left(\omega_{1n}^2-\omega^2\right)\left(\omega_{2n}^2-\omega^2\right) + 4\omega^2\lambda_{1n}\lambda_{2n} + \omega^4 C_{21}\right] \\ \eta_4 = 2\omega^3 C_{12}\left[\lambda_{1n}\left(\omega_{2n}^2-\omega^2\right) + \lambda_{2n}\left(\omega_{1n}^2-\omega^2\right)\right] \end{cases} \tag{26}$$

The last two expressions of this system show as might be expected that the vibrations of the unexcited coupled bridge 2 strongly depend on the vibration transfer coefficient C_{12} from the main bridge 1 to the second one.

3.2 Analytical solution of the modal equations for periodic impulsive excitation

In this case, system (22) can be rewritten as follows

$$\begin{cases} \ddot{q}_{1n} + 2\lambda_{1n}\dot{q}_{1n} + \omega_{1n}^2 q_{1n} + C_{21}\ddot{q}_{2n} \\ = F_{0n}\sum_{i=1}^{N}\{H\,(t - iT_0) - H\,[t - (iT_0 + \tau)]\}, \\ \ddot{q}_{2n} + 2\lambda_{2n}\dot{q}_{2n} + \omega_{2n}^2 q_{2n} + C_{12}\ddot{q}_{1n} = 0, \end{cases} \tag{27}$$

where $F_{0n} = \frac{2L^3}{E_1 I_1} I_0 \sin\,(n\pi x_0)$, T_0 and τ are respectively dimensionless period and duration of the impact of the periodic impulsive excitation. They are define as $T_0 = T\omega_0$, $\tau = \Delta T\omega_0$.

As the analytical resolution of equations of system (27) is not quite evident, let us look at the case of two identical beam bridges whose modal equations are given by (28).

$$\begin{cases} \ddot{q}_{1n} + 2\lambda_n\dot{q}_{1n} + \omega_n^2 q_{1n} + C\ddot{q}_{2n} \\ = F_{0n}\sum_{i=1}^{N}\{H\,(t - iT_0) - H\,[t - (iT_0 + \tau)]\}, \\ \ddot{q}_{2n} + 2\lambda_n\dot{q}_{2n} + \omega_n^2 q_{2n} + C\ddot{q}_{1n} = 0, \end{cases} \tag{28}$$

where $\lambda_n = \lambda_{1n} = \lambda_{2n}$, $\omega_n^2 = \omega_{1n}^2 = \omega_{2n}^2$, $C = C_{12} = C_{21}$.

To solve these new equations, it useful to assume new variables as follows

$$q_+ = q_{1n} + q_{2n}, \tag{29}$$

$$q_- = q_{1n} - q_{2n}, \tag{30}$$

each of them is solution of following differential equation (31) below

$$\ddot{q}_{\pm} + 2\lambda_{\pm}\dot{q}_{\pm} + \omega_{\pm}^2 q_{\pm} = F_{0\pm} \sum_{i=1}^{N} \{H\,(t - iT_0) - H\,[t - (iT_0 + \tau)]\} \tag{31}$$

equations respectively obtain by adding and Subtracting the two set of Eq. (28) and where $\lambda_{\pm} = \frac{\lambda_n}{1\pm C}$, $\omega_{\pm}^2 = \frac{\omega_n^2}{1\pm C}$, $F_{0\pm} = \frac{F_{0n}}{1\pm C}$.

The solutions of system (28) are then obtain from new variable parameters as follows

$$\begin{cases} q_{1n} = \frac{q_+ + q_-}{2}, \\ q_{2n} = \frac{q_+ - q_-}{2}. \end{cases} \tag{32}$$

For each modes ($n = 1, 2, \ldots \infty$), the solutions of Eq. (31) can be expressed as the sum of a homogeneous solution and a particular solution, i.e.

$$q_{\pm}\,(t) = q_{\pm}^{H}\,(t) + q_{\pm}^{P}\,(t)\,, \tag{33}$$

where

$$q_{\pm}^{H}\,(t) = \left[A_{\pm}\cos\Omega_{\pm}t + B_{\pm}\sin\Omega_{\pm}t\right]e^{-\lambda_{\pm}t} \tag{34}$$

is the homogeneous solution, where $\Omega_{\pm} = \sqrt{\omega_{\pm}^2 - \lambda_{\pm}^2}$.

The form of the external excitation of Eq. (31) suggests a treatment per intervals in order to determine its particular solutions $q_{\pm}^{P}\,(t)$. To do so, let us subdivide time in two great time domains according to instant where the impacts occur. These two great time domains correspond one to intervals of time before the impact sequence i and after the last impact sequence N and another to intervals of time during the impact sequence i.

Before the impact sequence i i.e. $\forall t \in [(i-1)T_0 + \tau; iT_0$ $[; i = 1, \ldots, N$ and after the last impact sequence N i.e. $\forall t \in [NT_0 + \tau; +\infty[$, $H(t - iT_0) - H[t - (iT_0 + \tau)] = 0$ and therefore a particular solution can be $q_{\pm}^{P}(t) = 0$.

During the impact sequence i i.e. $\forall t \in [iT_0;\ iT_0 + \tau$ $[;\ i = 1, \ldots, N$, $H\,(t - iT_0) - H[t - (iT_0 + \tau)] = 1$ and therefore a particular solution can be $q_{\pm}^{P}(t) = \frac{F_{0\pm}}{\omega_{\pm}^2}$. So, general solution of the problem can be written

$$q_{\pm}\,(t) = \begin{cases} q_{\pm}^{(i)}\,(t_1) \\ = \left[A_{\pm}^{(i)}\cos\Omega_{\pm}t_1 + B_{\pm}^{(i)}\sin\Omega_{\pm}t_1\right]e^{-\lambda_{\pm}t_1} \\ \text{For}\quad (i-1)\,T_0 + \tau \le t < iT_0 \quad \text{or} \quad t > NT_0, \\ \tilde{q}_{\pm}^{(i)}\,(t_2) \\ = \left[C_{\pm}^{(i)}\cos\Omega_{\pm}t_2 + D_{\pm}^{(i)}\sin\Omega_{\pm}t_2\right]e^{-\lambda_{\pm}t_1} \\ \quad + \frac{F_{0\pm}}{\omega_{\pm}^2}\ \text{For}\ \ iT_0 \le t < iT_0 + \tau, \end{cases} \tag{35}$$

where $i = 1, \ldots, N$, $t_1 = t - [(i-1)\,T_0 + \tau]$ the initial instant just after the impact sequence $i-1$ and $t_2 = t - iT_0$ the initial instant of the impact sequence i. Taking into account the Eqs. (29) and (30), the final solutions of the modal Eq. (28) are given per intervals as follows:

– Before the impact sequence i i.e. $\forall t \in [(i-1)\,T_0 + \tau; iT_0[; i = 1, \ldots, N$ and after the last impact sequence N i.e. $\forall t \in [NT_0 + \tau; +\infty[$

$$\begin{cases} q_{1n}\,(t) = q_{1n}^{(i)}\,(t_1) \\ = \frac{1}{2}\left\{\left[A_{+}^{(i)}\cos\Omega_{+}t_1 + B_{+}^{(i)}\sin\Omega_{+}t_1\right]e^{-\lambda_{+}t_1}\right. \\ \quad \left. + \left[A_{-}^{(i)}\cos\Omega_{-}t_1 + B_{-}^{(i)}\sin\Omega_{-}t_1\right]e^{-\lambda_{-}t_1}\right\}, \\ q_{2n}\,(t) = q_{2n}^{(i)}\,(t_1) \\ = \frac{1}{2}\left\{\left[A_{+}^{(i)}\cos\Omega_{+}t_1 + B_{+}^{(i)}\sin\Omega_{+}t_1\right]e^{-\lambda_{+}t_1}\right. \\ \quad \left. - \left[A_{-}^{(i)}\cos\Omega_{-}t_1 + B_{-}^{(i)}\sin\Omega_{-}t_1\right]e^{-\lambda_{-}t_1}\right\}, \end{cases} \tag{36}$$

– During the impact sequence i i.e. $\forall t \in [iT_0;\ iT_0 + \tau$ $[;\ i = 1, \ldots, N$

$$\begin{cases} q_{1n}\,(t) = \tilde{q}_{1n}^{(i)}\,(t_2) \\ = \frac{1}{2}\left\{\left[C_{+}^{(i)}\cos\Omega_{+}t_2 + D_{+}^{(i)}\sin\Omega_{+}t_2\right]e^{-\lambda_{+}t_2}\right. \\ \quad \left. + \left[C_{-}^{(i)}\cos\Omega_{-}t_2 + D_{-}^{(i)}\sin\Omega_{-}t_2\right]e^{-\lambda_{-}t_2}\right\} + \frac{F_{0n}}{\omega_n^2}, \\ q_{2n}\,(t) = \tilde{q}_{2n}^{(i)}\,(t_2) \\ = \frac{1}{2}\left\{\left[C_{+}^{(i)}\cos\Omega_{+}t_2 + D_{+}^{(i)}\sin\Omega_{+}t_2\right]e^{-\lambda_{+}t_2}\right. \\ \quad \left. - \left[C_{-}^{(i)}\cos\Omega_{-}t_2 + D_{-}^{(i)}\sin\Omega_{-}t_2\right]e^{-\lambda_{-}t_2}\right\}, \end{cases} \tag{37}$$

where unknown integration constants $A_{\pm}^{(i)}$, $B_{\pm}^{(i)}$, $C_{\pm}^{(i)}$ and $D_{\pm}^{(i)}$ are determined from the initial conditions of the problem which correspond to the final conditions of the previous phases of the movement.

4 Dynamical investigation

In this section, we present the results of numerical simulations of the proposed model of coupled bridges. Subsequently, we compare the theoretical results with experimental results obtained on the scale model built in the laboratory to assess the efficiency of the proposed theoretical model. In our simulations, we limit only on the first mode of vibration ($n = 1$) and the numerical method used is the fourth-order Runge–Kutta method.

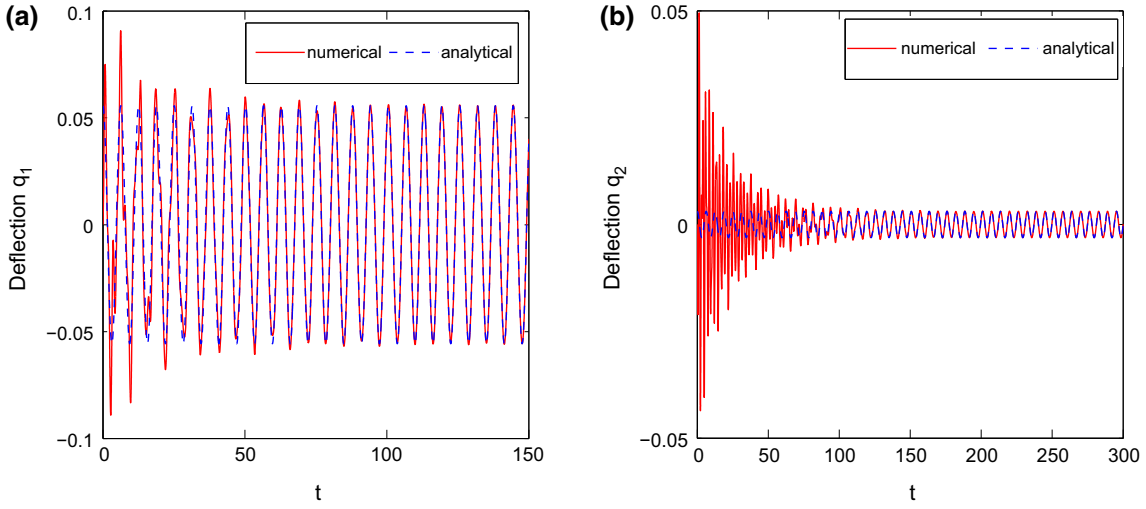

Fig. 3 Comparison of numerically and analytically deflections obtained for sinusoidal excitation: **a** bridge 1; **b** bridge 2

4.1 Dynamic response of coupled bridges: validation of analytical study

Numerical solutions of the coupled system subjected to each kind of excitation (sinusoidal and impulsive) is found and displayed in the same graph with the corresponding analytical solutions. The curves of Figs. 3 and 4 are obtained for the given set of dimensionless parameters:

– For sinusoidal excitation:

$$\lambda_1 = \lambda_2 = 0.05, \quad \omega_1 = \omega_2 = 10, \quad C_{12} = C_{21} = 0.5, \quad \omega = 1, \quad F_0 = 0.5$$

– For train of 3 impulsions:

$$\lambda_1 = \lambda_2 = 0.05, \quad \omega_1 = \omega_2 = 1, \quad C_{12} = C_{21} = 0.5, \quad T_0 = 50; \quad \tau = 0.1, \quad F_0 = 0.5$$

The coincidence between the numerical and analytical curves after the initial transient regime for the two bridges in Figs. 3 and 4 shows that the proposed analytical solutions are quite good.

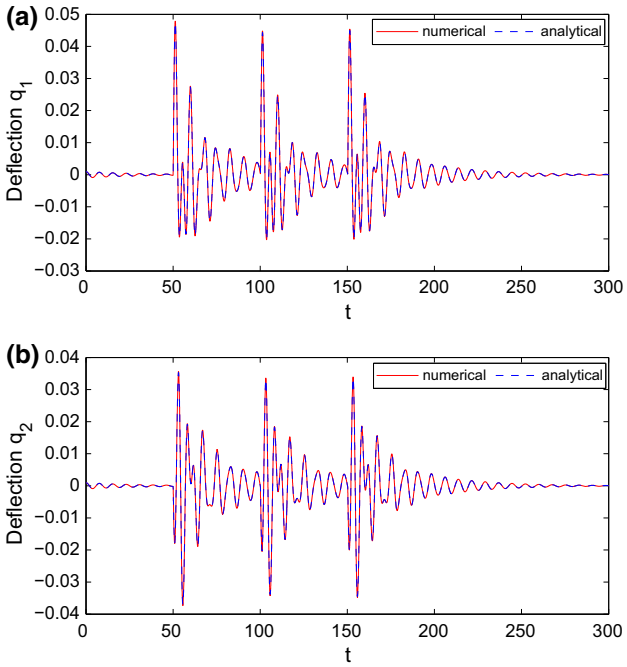

Fig. 4 Comparison of numerically and analytically deflections obtained for periodic impulsive excitation: **a** bridge 1; **b** bridge 2

4.2 Resonant response

The amplitude curves are plotted versus the excitation frequency ω of the sinusoidal excitation on the one hand and the period T_0 of the periodic impulsive excitation on the other hand. the different curves obtained are presented and discussed below for set of dimensionless parameters $\lambda_1 = \lambda_2 = 0.05$, $C_{12} = C_{21} = 0.5$, $F_0 = 0.5$.

– For sinusoidal excitation

Each of the amplitude curves corresponding to the dynamic response of the two coupled bridges to a sinusoidal excitation present, four resonances in two pairs with very close peaks. The two pairs are separated by many antiresonances which the most significant antiresonance which is located at the frequency ω_2 of bridge 2 (Fig. 5). As shown in Figs. 5 and 6, the two bridges present their resonance pairs approximately at the same positions on either side of the antiresonance frequency ω_2. However, these positions vary depending on the frequencies ω_1 and ω_2 of the bridges 1 and

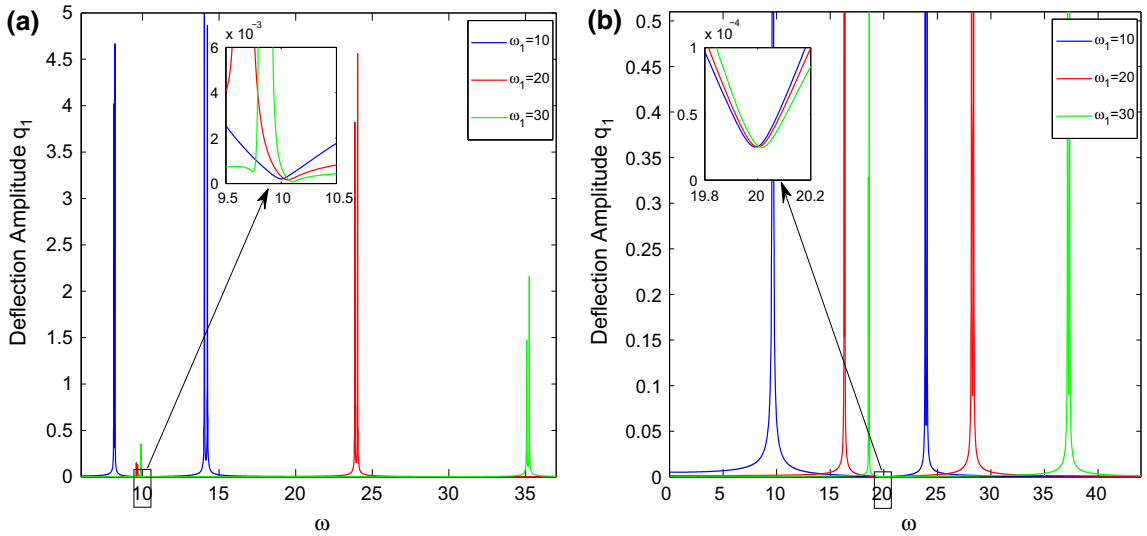

Fig. 5 Amplitude curves of bridge 1 versus the frequency ω of the sinusoidal excitation for **a** $\omega_2 = 10$; **b** $\omega_2 = 20$

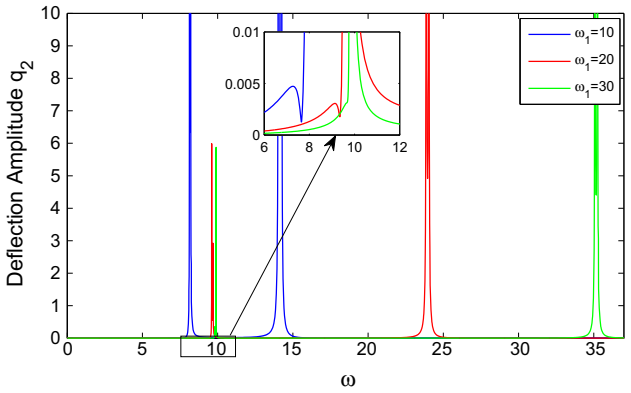

Fig. 6 Amplitude curves of bridge 2 versus the frequency ω of the sinusoidal excitation for $\omega_2 = 10$

2 respectively; one gradually become closer to the antiresonance frequency ω_2 while the other move away when ω_1 increases (Fig. 6).

The antiresonance frequency ω_2 pointed out here for which the vibration amplitudes of bridge 1 become almost zero can be an interesting result in vibration control of the dynamics of beams. It will be then a good issue to consider the control of the vibration of a beam by another beam dimensioned at the excitation frequency range of this later.

– For periodic impulsive excitation

In this case, all the amplitude curves of bridges present an infinite number of resonances of lesser importance. The intensities of these resonances decrease with respect to the period T_0 of the impulsive excitation (i.e. increase with respect to its frequency) and with respect to the frequencies ω_1 and ω_2 of the two bridges; and their value tend asymptotically to a given limit (Figs. 7, 8). But we can notice from Fig. 8a that the change in the frequency ω_2 of Bridge 2 does not have significant effect on the dynamics of bridge 1.

It is therefore clear from this study that it would be more beneficial to the structure to have great natural frequencies of vibration in order to present small amplitude responses.

4.3 Effects of some parameters on the dynamics of coupled bridges

In this section we present the influence of various parameters on the dynamic responses of the two coupled bridges. This is in order to point out the influences of the viscoelastic coupling of the soil and the effect of the distance between the two bridges. Figures 9, 10 and 11 show the amplitude of the two bridges versus the dimensionless parameters involving the viscoelastic coupling the distance between the bridges.

– Effects of viscoelastic coupling of the Winkler foundation

The dimensionless parameters reflecting the effects of the viscoelastic coupling are the frequencies ω_1 and ω_2 of the two bridges and the damping coefficients λ_1 and λ_2. The frequencies ω_1 and ω_2 depict the stiffness of the soil through the terms k_{si} of expression (20) while λ_1 and λ_2 depict its viscosity through the terms c_{si} of expression (19). So, the study of the effects of viscoelastic coupling is close to the study of the effects of these four parameters on the dynamic responses of the two bridges.

The study of the effect of the frequencies ω_1 and ω_2 was made in the previous paragraph. Figures 7 and 8 for periodic impulsive excitation, show that the amplitudes of vibration of the two bridges decrease with these frequencies so with the

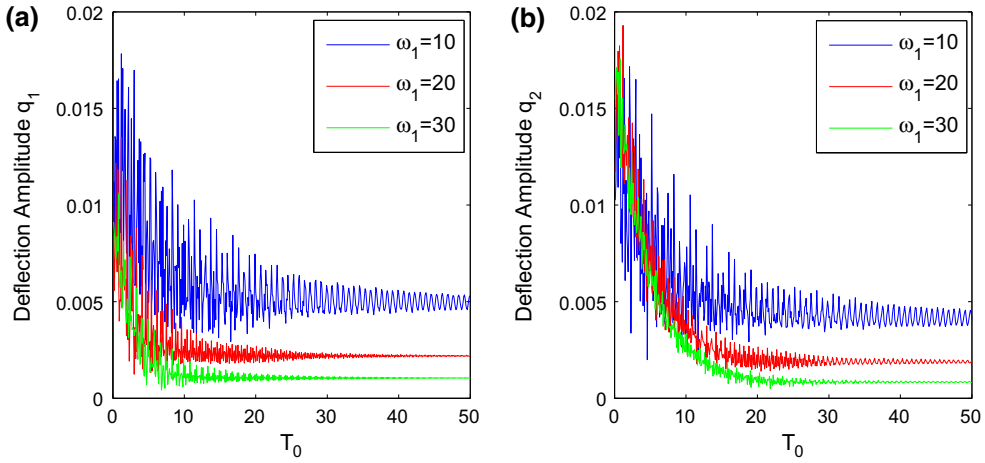

Fig. 7 Amplitude curves versus the period T_0 of the periodical impulsive excitation for several values of ω_1 **a** bridge 1; **b** bridge 2

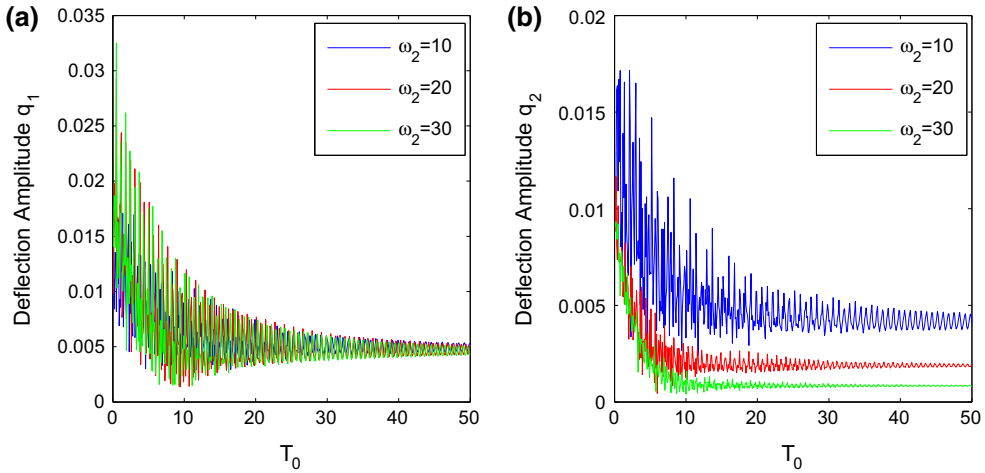

Fig. 8 Amplitude curves versus the period T_0 of the periodical impulsive excitation for several values of ω_2 **a** bridge 1; **b** bridge 2

rigidity k_s of the Winkler foundation, according to the definition of the dimensionless parameters of Eq. (13). But the behavior is more unclear in the case of a sinusoidal excitation (Figs. 5, 6).

As regards the effect of the damping coefficients λ_1 and λ_2, for the dimensionless quantities $\omega_1 = \omega_2 = 10$, $\omega = 1$, $C_{12} = C_{21} = 0.5$, $T_0 = 50$; $\tau = 0.1$, $F_0 = 0.5$, one obtain the amplitude curves of Figs. 9 and 10. The curves of Fig. 9 shows that deflection amplitudes of the two bridges increases with respect to the damping coefficients λ_1 and λ_2 in the case of sinusoidal excitation. However, the behavior vary in the case of periodic impulsive excitation (Fig. 10).

It come out from this study that the viscoelastic coupling of the soil presents various effects on the dynamics of the two beams bridges.

– Effects of the distance between the two bridges

The dimensionless parameters that depicts the effect of distance on the dynamics of the experimental device are the coupling coefficients C_{12} and C_{21} between the two modal equations of system (22). According to Eqs. (9) and (21), C_{12} and C_{21} are decreasing function of the distance between the bridges. Studying the effects of the distance between the two bridges comes down now to study the effect of the parameters C_{12} and C_{21} on their dynamic responses. To this end, the curves of Fig. 11 is plotted for the given values of dimensionless parameters:

$$\lambda_1 = \lambda_2 = 0.05, \quad \omega_1 = \omega_2 = 10, \quad \omega = 1,$$
$$T_0 = 50; \quad \tau = 0.1, \quad F_0 = 0.5$$

Figure 11 shows that for a sinusoidal excitation, the deflection amplitudes of the bridges increase with most values of the coupling parameters C_{12} and C_{21}; i.e. when the distance between the two bridges decreases. This is however not

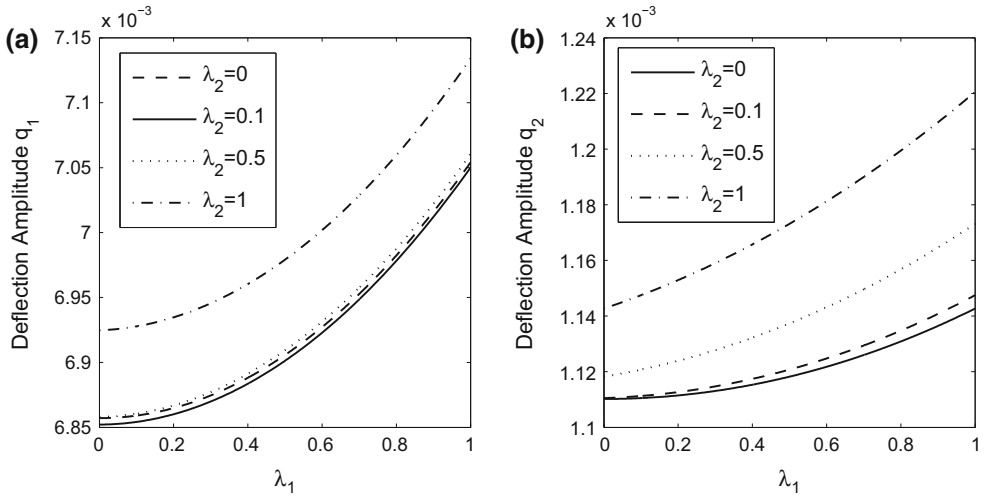

Fig. 9 Amplitude curves versus the damping coefficient λ_1 for sinusoidal excitation: **a** bridge 1; **b** bridge 2

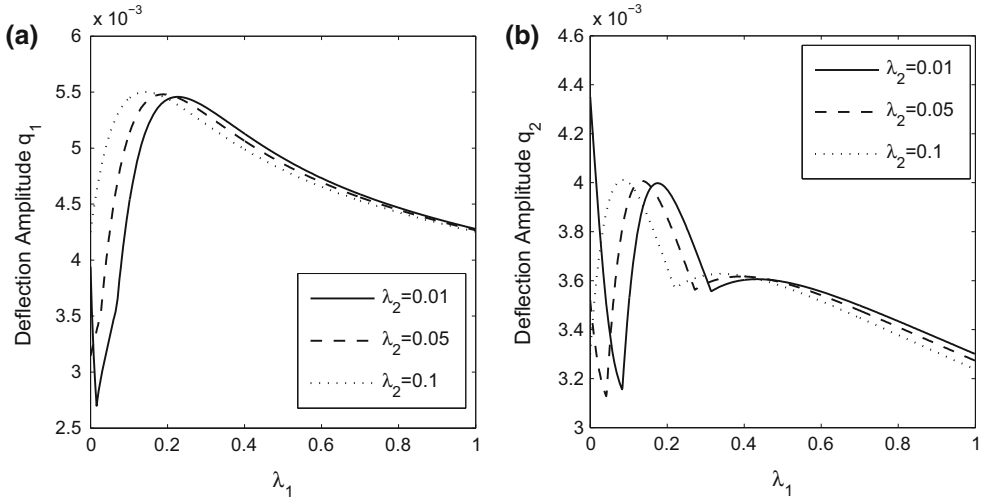

Fig. 10 Amplitude curves versus the damping coefficient λ_1 for periodical impulsive excitation: **a** bridge 1; **b** bridge 2

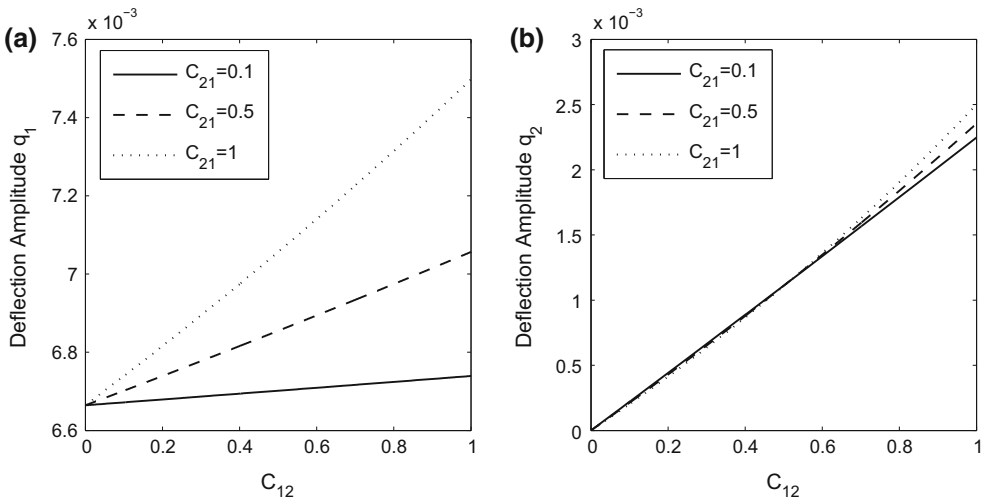

Fig. 11 Amplitude curves versus the coupling coefficient C_{12} for sinusoidal excitation: **a** bridge 1; **b** bridge 2

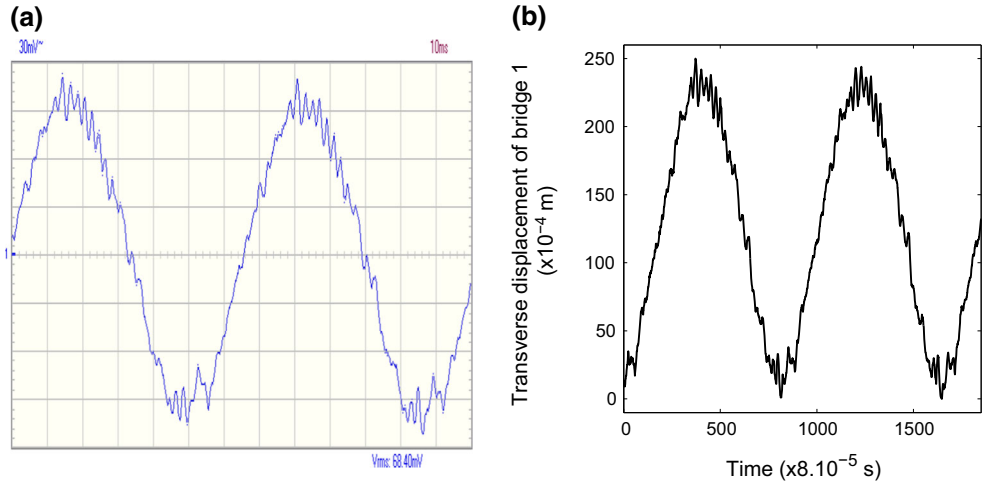

Fig. 12 Transversal displacements of bride 1 for excitation motor excite at the voltage $U = 23V$: **a** screen of the digital oscilloscope; **b** plotted in Matlab software

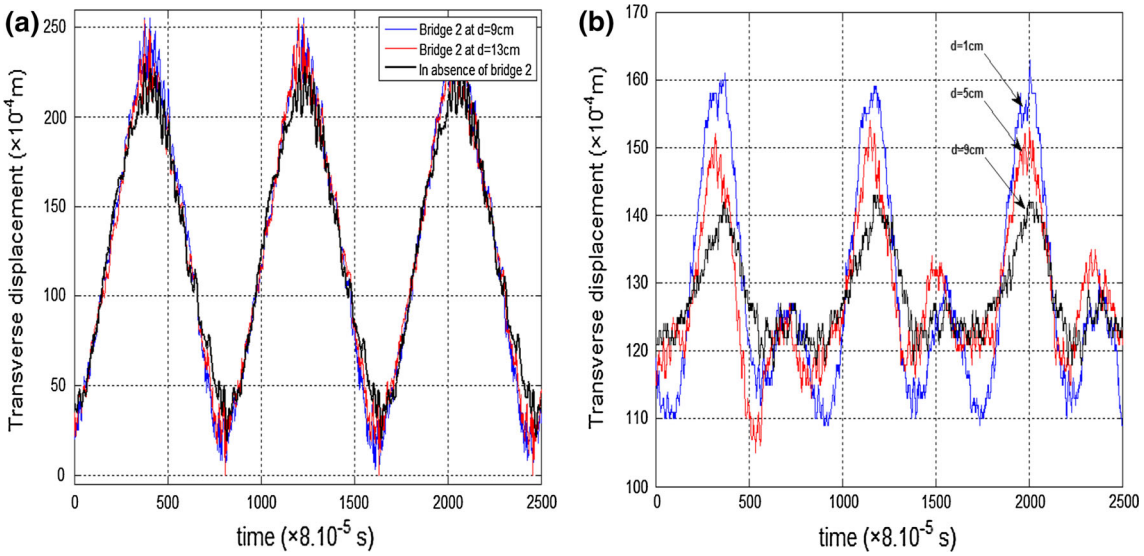

Fig. 13 Experimental transverse displacement for several distances between the two bridges: **a** bridge 1; **b** bridge 2

checked for certain values for bridge 2 from a certain value of C_{12} around 0.5. Before this value, the amplitudes increase with C_{12} but decrease with C_{21}.

For a periodic impulsive excitation, complex behaviors are observed with variation of amplitudes around a given values. Bridge 2 nevertheless has a lesser disordered response than bridge 1 with the amplitudes that tend to decrease while C_{12} and C_{21} increase.

4.4 Experimental validation of the theoretical analysis

In this subsection, we compare of the experimental results obtained from the model built in the laboratory is done with some results of previous theoretical study.

4.4.1 Transverse displacements of the coupled bridges

The transverse displacements of bridge 1 in the presence of the outer exciter universal motor are captured using the miniaturized accelerometer DE-ACCM2G incorporated into the structure and the results are shown in the Fig. 12.

Figure 12 shows a perfect similarity between the curves displayed in the portable digital oscilloscope and those drawn in Matlab software from the experimental data file.

4.4.2 Effect of environmental coupling

To highlight experimentally the effects of coupling, the transverse displacements are captured for different distances between the two coupled bridges. The data obtain are then

plotted in Fig. 13 and compared to the results of numerical simulations of the developed model.

The experimental results in Fig. 13 show that the transverse displacements of bridge 1 (subject to universal motor excitation) and the bridge 2 (free of excitation) increases when the distance between them decreases. This result has indeed been obtained theoretically on the curve of the Fig. 11 for which the deflection amplitudes of the bridges increase with coupling parameters C_{12} and C_{21}; i.e. when the distance between the two bridges decreases. We can therefore conclude once again that the mathematical model we have developed is qualitatively valid.

We have shown in these previous two paragraphs that the proposed coupled bridgemathematical model is qualitatively satisfactory.

5 Conclusion

An analytical, numerical and experimental study to predict the dynamics response of two bridges indirectly coupled via their ground support were done. It appears from this study that, when the structure are excited, the amplitude of vibration of each structure depends on the nature of the soil and the distance between the bridges. Another information related to this work is that, the ground support of the bridges really acts like a viscoelastic membrane on their piers. Furthermore, it is the support of propagation of the vibrations between the two bridges. Therefore, the experimental scale model built in the laboratory give rise to the validation of the theoretical modelling and explanation.

Acknowledgements Part of this work was completed during a research visit of Prof Nana Nbendjo at the University of Kassel in Germany. He is grateful to the Alexander von Humboldt Foundation for financial support within the Georg Forster Fellowship. Prof Woafo acknowledge the support of the Humboldt Foundation (Germany) through the equipment Grant.

References

1. Paultre P, Chaallal O, Proulx J (1992) Bridge dynamics and dynamic amplification factors—a review of analytical and experimental findings. Can J Civ Eng 19:260–278
2. Meng J, Ghasemi H, Lui EM (2004) Analytical and experimental study of a skew bridge model. Eng Struct 26:1127–1142
3. Liu K, Reynders E, De Roeck G, Lombaert G (2009) Experimental and numerical analysis of a composite bridge for high-speed trains. J Sound Vib 320:201–220
4. Chatterjee RK, Datta TK, Surana CS (1994) Vibration of continuous bridges under moving vehicles. J Sound Vib 169:619–632
5. Yang S, Fang X, Zhang J, Wang D (2016) Dynamic behavior of bridge-erecting machine subjected to moving mass suspended by wire ropes. J Appl Math Mech 36:741–748
6. Johansson C, Pacoste C, Karoumi R (2013) Closed-form for the mode superposition analysis of the vibration in muti-span beam bridges caused by concentrated moving loads. Comput Struct 119:85–94
7. Bozdag E, Sunbuloglu E, Ersoy H (2006) Vibration analysis of new Galata Bridge: experimental and numerical results. Comput Struct 84:283–292
8. Mekki OB (2007) Amortissement Semi-actif des Structures Flexibles: Application au Contrôle des Grands Ponts. XXVemes Rencontres Universitaires de Génie Civil—PRIX RENE HOUPERT
9. Green MF, Cebon D (1994) Dynamic response of highway bridges to heavy vehicle loads: theory and experimental validation. J Sound Vib 170:51–78
10. Marchesiello S, Fasana A, Garibaldi L, Piombo BAD (1999) Dynamics of multi-span continuous straight bridges subject to multi-degrees of freedom moving vehicle excitation. J Sound Vib 224:541–561
11. Djanan AAN, Nbendjo BRN, Woafo P (2011) Control of vibration on a hinged-hinged beamunder a non-ideal excitation using RLC circuit with variable capacitance. Nonlinear Dyn 63:477–489
12. Bouna HS, Nbendjo BRN (2012) Vibration control of a plate subjected to impulsive force by plate-type dynamic vibration absorbers. World J Mech 2:143–151
13. Huang W, Zou Y (1994) The dynamic response of a viscoelastic Winkler foundation-supported elastic beam impacted by a low velocity projectile. Comput Struct 52:431–436
14. Lu S, Xuejun D (1998) Dynamic analysis to infinite beam under a moving line load with uniform velocity. J Appl Math Mech 19: 368–373
15. Semblat JF, Lenti L, Jacqueline D, Leblond JJ (2011) Railway vibrations induced into the soil: experiments, modelling and isolation. Revue Française de Géotechnique 23–36:134–135
16. Semblat JF (1998) Amortissement et dispersion des ondes: points de vue physique et numérique. Revue française de génie civil 2: 91–111
17. Gutowsky TG, Dym CL (1976) Propagation of ground vibration: a review. J Sound Vib 49:179–193

Isolation performance of a quasi-zero stiffness isolator in vibration isolation of a multi-span continuous beam bridge under pier base vibrating excitation

H. Sonfack Bouna, B. R. Nana Nbendjo & P. Woafo

Nonlinear Dynamics
An International Journal of Nonlinear Dynamics and Chaos in Engineering Systems

ISSN 0924-090X
Volume 100
Number 2

Nonlinear Dyn (2020) 100:1125-1141
DOI 10.1007/s11071-020-05580-z

Springer

Nonlinear Dyn (2020) 100:1125–1141
https://doi.org/10.1007/s11071-020-05580-z

ORIGINAL PAPER

Isolation performance of a quasi-zero stiffness isolator in vibration isolation of a multi-span continuous beam bridge under pier base vibrating excitation

H. Sonfack Bouna · B. R. Nana Nbendjo · P. Woafo

Received: 12 August 2019 / Accepted: 17 March 2020 / Published online: 1 April 2020

Abstract This paper considers a vibration control problem for a multi-span beam bridge under pier base vibrating excitation by using nonlinear quasi-zero stiffness (QZS) vibration isolators. Three linear springs are needed to construct a nonlinear vibration isolator with quasi-zero stiffness. The vibration of the multi-span beam bridge under control and without control is governed by partial differential equation and several ordinary differential equations which are derived from Galerkin method. Modal superposition method with numerical modes of the structure and an iterative method are combined to predict the vibration response of the structure under pier base excitation. The influence of the quasi-zero stiffness vibration isolators on isolation of multimodal vibration of beam bridge is studied. The absolute motion transmissibility is proposed to evaluate the performance of the quasi-zero stiffness vibration isolator and is compared with an equivalent linear viscoelastic vibration isolator. The results demonstrate the effectiveness of the these two potential control method as well as a good control performance in suppressing vibration for high frequencies. But at low frequencies, only the quasi-zero stiffness vibration isolator can reduce the vibration amplitude of the beam bridge around the resonance frequency region. The effects of each control parameter on the absolute motion transmissibility of steady-state behaviors are investigated for a better isolation performance.

Keywords Multi-span beam bridge · Base vibrating excitation · Quasi-zero stiffness vibration isolator · Galerkin method · Absolute motion transmissibility · Linear viscoelastic vibration isolator

H. S. Bouna · B. R. N. Nbendjo (✉)· P. Woafo
Laboratory of Modelling and Simulation in Engineering, Biomimetics and Prototypes, University of Yaoundé I, P. O. Box 812, Yaoundé, Cameroon
e-mail: nananbendjo@yahoo.com

1 Introduction

Unsuitable vibrations are a problem that affects many engineering structures. Structure damages, such as fatigue and failure induced by vibrations, often occur at a low excitation frequency in practical engineering [1,2]. Active and passive methods are then the main control strategies that are widely used by researchers and engineers to suppress vibrations. Some researchers have recently used the inertia-free attitude control methods for flexible spacecraft with active vibration suppression [3,4]. However, in most of engineering applications, passive vibration isolations are usually the first solution to the problem of vibration suppression. This is mainly due to the fact that they offer high performance and stability, are quite simple to design and do not require any external power source or computer controls as in the case of active controls. Vibration isolators are therefore widely used to subdue vibrations in order to lengthen the service life of equipments and structures also to provide a more comfortable and safe condition for human beings. For instance, the case of bridges

which act as an important link in surface transportation network. The collapse of bridges during a seismic event will seriously hamper the relief and rehabilitation work. Due to their structural easiness and as the fundamental vibrational period of most bridges ranges from 0.2 to 1.2 s [5], bridges are particularly vulnerable to damages and sometimes collapse when subjected to earthquakes and other external excitation such as moving and wind loads [6–9].

In recent years, base vibration isolation has become an increasingly applied structural design technique to protect bridges from severe loads. The main goal of base vibration isolation is to produce a substantial decoupling of the superstructure from the substructure resting on the vibrating ground by using vibration isolators [10,11]. Vibration isolator is a device placed between a vibration source and an isolated object considered to be protected [12,13]. However, vibration isolation is still an important problem, especially the low-frequency vibration isolation. This method has been widely used in engineering. Its most important characteristics are its natural frequency and load bearing capacity. As it is well known, a linear vibration isolator often faces a difficult choice situation that arises between these two characteristics. For traditional passive linear vibration isolators, a smaller stiffness is needed to achieve a smaller natural frequency so that it can reduce low frequency vibrations [14]. In this case, a larger static deflection is unavoidable in practical applications. To overcome the limitation between the isolation frequency range and the load bearing capacity of linear vibration isolators, many nonlinear vibration isolators such as nonlinear energy sink and nonlinear vibration isolators using quasi-zero stiffness (QZS). A nonlinear energy sink which refers to a lightweight nonlinear device that is attached to a primary linear or weakly nonlinear system, is increasingly used for mitigation the vibrations of discrete and continuous structures [15,16]. A QZS vibration isolator has been proposed to obtain a high static stiffness resulting in a small static deflection and a low dynamic stiffness resulting in a small natural frequency [17–21].

QZS vibration isolators have been proved to offer one of the best passive approach for achieving low vibration environments [22,23]. Because they can meet the needs of isolating low frequency vibration, even ultralow frequency vibration, various forms of negative stiffness mechanisms have been designed to obtain negative stiffness and combine with the positive stiffness structures to construct QZS vibration isolators. Recent years, several types of vibration isolators using QZS mechanisms have been developed and applied to improve working environment for users in many engineering fields, such as vibration resonance test of aircraft, vibration isolation of precision instruments, sensor, energy harvest, suspensions and seats of vehicles and protection of motors. Many different prototypes of QZS vibration isolators were proposed by Alabuzhev et al. [24] and more detailed information about their technical design and their applications was recapitulated by Ibrahim [25]. A vehicle suspension using the negative stiffness mechanism combined with a positive stiffness support was designed by Arafat et al. [26]. A prototype of QZS vibration isolator composed of a pair of bars linked with a pair of horizontal linear springs to improve the vibration isolation performance of vehicle seats under low excitation frequencies was studied theoretically and experimentally by Le and Ahn [27,28]. Liu et al., Huang et al. and Fulcher et al. [29–31] built a QZS vibration isolator by using Euler buckled beams as negative stiffness correctors and explored the isolation performance theoretically and experimentally. In these studies, the isolation starting frequency of the nonlinear isolator were found to be lower than that of the linear one with the same support capacity. Platus [32] developed a nonlinear vibration isolator using two axially loaded beams to achieve the QZS property for horizontal vibration isolation. Carrella et al. [33,34] built a QZS vibration isolator comprised of a vertical spring acting in parallel with two inclined linear springs used as negative stiffness correctors, and investigated the force and motion transmissibilities theoretically. The results demonstrated that the QZS vibration isolator outperforms the linear counterpart in some aspects. Meng et al. [35] proposed a QZS vibration isolator using a disc spring as negative stiffness corrector and investigated its isolation performance considering a mistuned mass. All the researches mentioned above indicate that the effectiveness of the QZS vibration isolator is superior to the linear counterpart when the excitation amplitude is relatively small. However, increasing the excitation amplitude leads to the increase in response and deteriorates the isolation performance of the QZS vibration isolator due to the existence of cubic nonlinear stiffness. The transmissibility of vibration isolators with high dimensional quasi-zero stiffness has also been studied by Li et al. and Wang et al. [36–38]. The results show that quasi-zero stiffness vibration isolators have the low

force transmissibility and the low frequency band for vibration isolation.

From the review of the literature presented, it emerges that both academic and industrial establishments have a particular interest in vibration isolators with a QZS characteristic. However, in all the above-mentioned studies related to nonlinear vibration isolation using QZS mechanism, isolated structures have usually been treated as discrete systems of concentrated masses. The bending vibration of the isolated main structure itself has been neglected. Therefore, it is not understood how multimode bending vibration of isolated structures changes isolation efficiency of a nonlinear QZS vibration isolator. In order to study the performance of a nonlinear QZS vibration isolator on the multimodal elastic vibration of a continuous structure, dynamics and nonlinear isolation of the transverse vibration of a multi-span continuous beam bridge subjected to pier base vibrating excitation are presented in this study. It should be noted that although there are many research papers on bending vibrations and vibration isolation of beams containing linear elastic boundaries and supports [39–41], to the best of the authors' knowledge, there are not many research papers on beams with nonlinear boundaries and supports [42–47]. Presently, there is a lack of methods for studying the bending vibration of beams with nonlinear supports. In addition, the dynamic response and the vibration isolation of a single span beam subjected to different kind of dynamic loads has drawn much research attention, but relatively smaller amount of research work has been done for dynamics and vibration isolation of multi-span beams under base vibrating excitation.

The paper is organized as follows. The structure of the QZS vibration isolator, mathematical modeling of the beam bridge under QZS control, linear viscoelastic control and without control are conducted in Sect. 2. Then, dynamic analysis and modal equations of the beam bridge are carried out in Sect. 3. The comparisons of the nonlinear QZS vibration isolation and the linear counterpart isolation are presented in Sect. 4 where the isolation performance of the QZS vibration isolator related to isolator parameters are also discussed. Section 5 carries out conclusions.

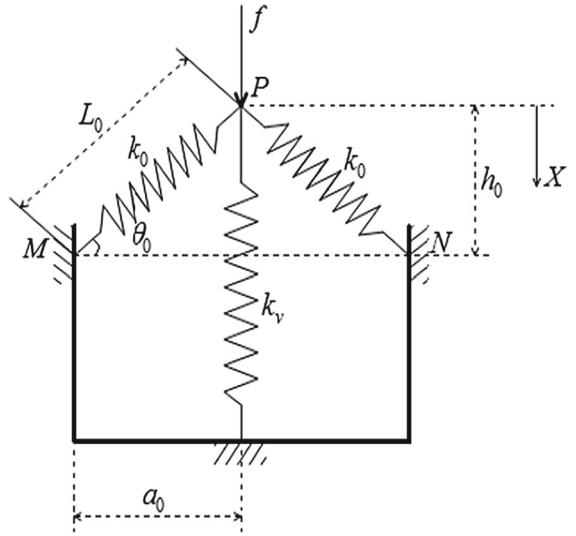

Fig. 1 Schematic representation of an isolator with QZS characteristic

2 Mathematical modelling

2.1 Mechanical model of the QZS vibration isolator

The QZS mechanism under consideration is schematically shown in Fig. 1, where the device to be isolated is not included. The system comprises a vertical spring with linear stiffness k_v which is connected at point P with two linear springs with identical stiffness k_0 and initial length L_0 mounted obliquely. The two springs are initially inclined with a slope of an angle θ_0 from the horizontal plane and hinged at points M and N respectively. Consider a loading force f at point P downwards. The loading point P is initially located at height h_0 above the points M, N and at horizontal distance a_0 apart from these points respectively. It is assumed that $L_0 \geq a_0$. The application of the force f causes a vertical displacement Y_0 and when the system is loaded with a suitably force, the springs are compressed from the initial unloaded position P to the equilibrium position O where the oblique springs are compressed in the horizontal position and the static load is only supported by the vertical spring. When k_v and k_0 match, the positive stiffness of the vertical spring and negative stiffness formed by the oblique springs will cancel with each other to achieve zero stiffness at the equilibrium position. In this way the system is developed into a QZS system.

The geometry of the system is defined by the parameters a_0 and h_0. Provided the coordinate Y_0 defines the displacement from the initial unloaded position, a loading force f given by the following equation, leads to a resulting displacement Y_0 [18,33,48]

$$f = f_v + f_0, \tag{1}$$

where

$$f_v = k_v Y_0, \tag{2}$$

and

$$f_0 = 2k_0 (h_0 - Y_0) \left(\frac{L_0}{\sqrt{a_0^2 + (h_0 - Y_0)^2}} - 1 \right). \tag{3}$$

The term f_v in Eq. (1) denotes the contribution from the vertical spring and the term f_0 denotes the contribution from the two oblique springs. If the variable Y defines the downward displacement of the slider from the equilibrium position, when the oblique springs are placed horizontally after applying the loading force f, Eq. (1) can be rewritten as

$$f = k_v Y - 2k_0 Y \left(\frac{L_0}{\sqrt{a_0^2 + Y^2}} - 1 \right) + k_v h_0. \tag{4}$$

For clarity of analysis, the following non-dimensional parameters are introduced

$$y = Y/L_0, \quad a = a_0/L_0 = \cos\theta_0, \quad h = h_0/L_0,$$
$$\alpha = k_0/k_v, \quad F = \frac{f}{k_v L_0} - h = \left(\frac{f}{k_v} - h_0 \right) / L_0, \tag{5}$$

so that Eq. (4) can be recast in its non-dimensional form as

$$F = y - 2\alpha y \left(\frac{1}{\sqrt{a^2 + y^2}} - 1 \right). \tag{6}$$

According to the definition of stiffness, differentiating Eq. (6) with respect to y gives the non-dimensional stiffness of the QZS system as

$$K = 1 + 2\alpha \left(1 - \frac{a^2}{(a^2 + y^2)^{3/2}} \right). \tag{7}$$

Substituting zero for y and setting Eq. (7) equal to zero, we derive the condition for zero stiffness as

$$\alpha_{QZS} = \frac{a}{2(1-a)} = \frac{\cos\theta_0}{2(1-\cos\theta_0)}. \tag{8}$$

The parameter α denotes the stiffness ratio and α_{QZS} denotes the geometric ratio. When α_{QZS} and α are equal, zero stiffness is achieved [48].

The non-dimensional force and the non-dimensional stiffness as a function of the non-dimensional displacement respectively are plotted in Fig. 2 for the stiffness ratio α equal to the geometric ratio α_{QZS} and when $a = 0.67$.

From Fig. 2, it can be seen that if the stiffness ratio and the geometric ratio are equal ($\alpha = \alpha_{QZS}$), zero stiffness can be obtained at the static equilibrium position. In this case, the negative stiffness provided by the oblique springs exactly counteracts the positive stiffness of the vertical spring in the vertical direction, and as a result, the system is developed into a QZS system. From Fig. 2a, it can also be seen that the relationship between force and displacement given in Eq. (6) is similar to that of a cubic function [18,48]. Therefore, to simplify subsequent dynamic analysis of the QZS system, an approximate cubic expression of the force is sought using a Taylor series expansion at the static equilibrium position $y = 0$ as

$$F(y) \approx F(0) + \sum_{n=1}^{3} \frac{F^n(0)}{n!} y^n = \frac{\alpha_{QZS}}{a^3} y^3. \tag{9}$$

Differentiating Eq. (9) with respect to y gives an approximate expression for the stiffness as

$$K \approx \frac{3\alpha_{QZS}}{a^3} y^2. \tag{10}$$

The approximations defined by Eqs. (9) and (10) are plotted in Fig. 3 in comparison with the exact expressions. It can be seen (Fig. 3b) that the QZS system has a very small stiffness in the neighborhood of the static equilibrium position. Furthermore, there is a very good correlation between the exact curves and the approximate curves for relatively small displacements from the equilibrium position ($\pm$ 0.2 excursion range). Clearly, higher amplitudes of oscillation would invalidate the approximation of the cubic force and the quadratic stiffness [18].

Let's consider this approximation of a QZS system modelling in motion modelling of the dynamics of a beam bridge under QZS vibration isolators driven by a pier base harmonic vibrating displacement.

2.2 Governing equation of a beam bridge with and without control

The mechanical model of transverse vibration of a multi-span continuous beam bridge under QZS vibra-

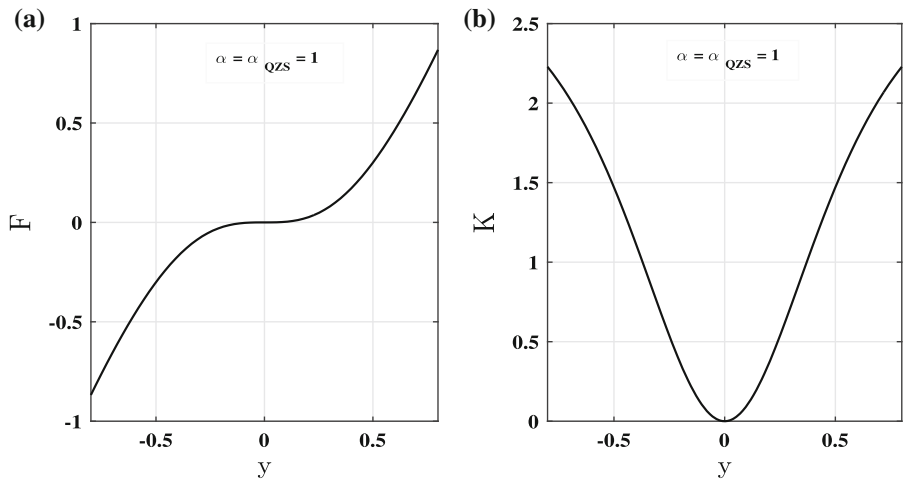

Fig. 2 **a** Force-displacement characteristic and **b** non-dimensional stiffness of the system when $a = 0.67$

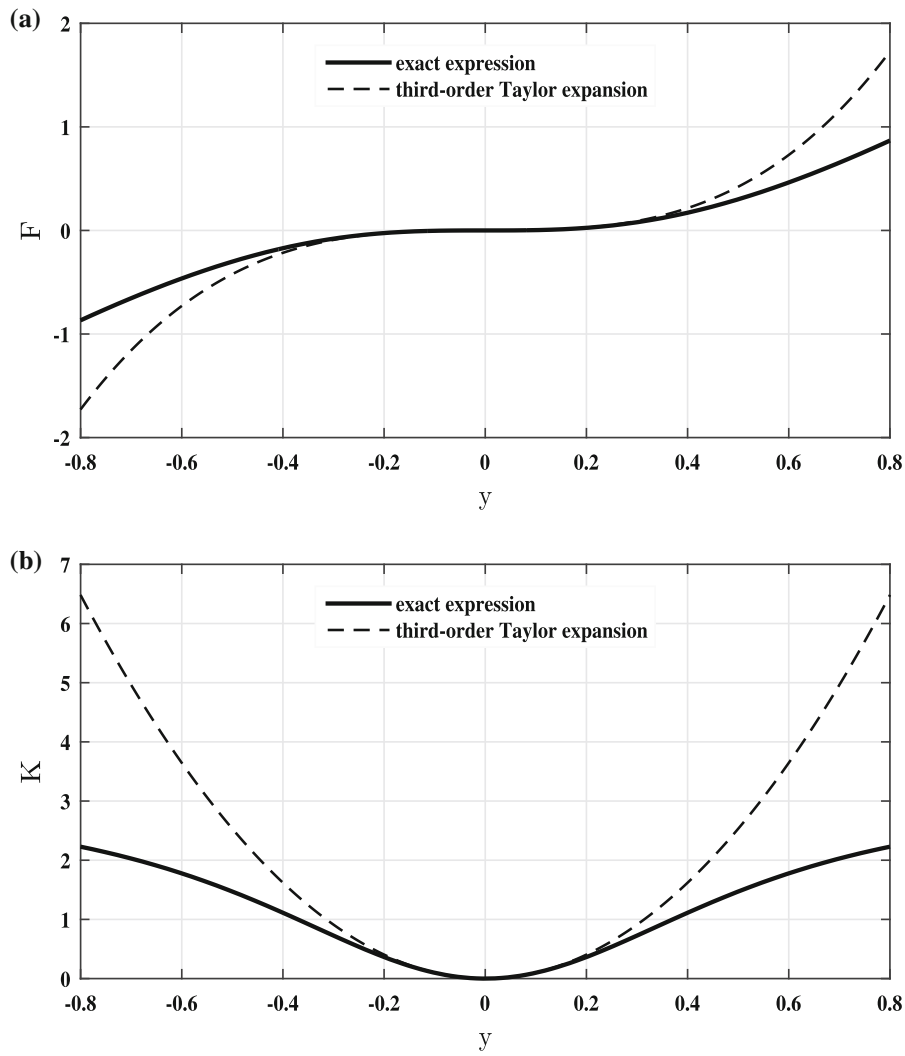

Fig. 3 Non-dimensional **a** force-displacement characteristic and **b** stiffness of the quasi-zero-stiffness system when $a = 0.67$

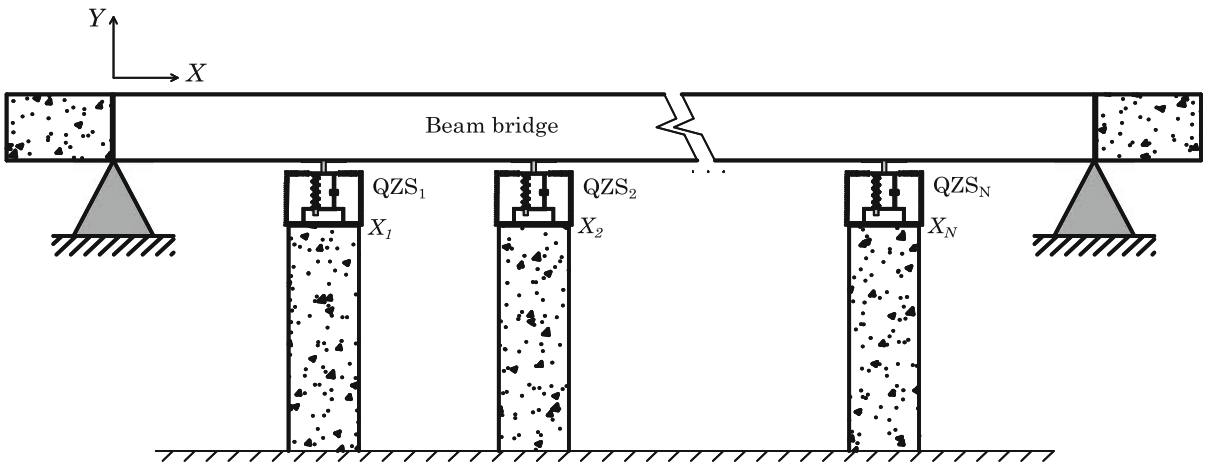

Fig. 4 Mechanical model of the beam bridge with the QZS vibration isolators

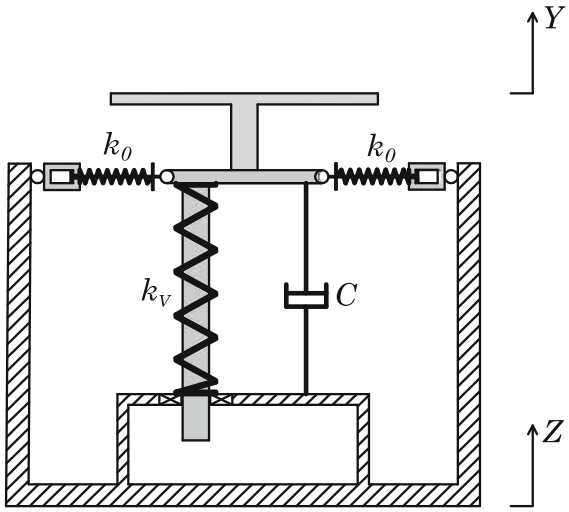

Fig. 5 Schematic of the dynamic model of the QZS vibration isolator

tion isolators is shown in Fig. 4 where each QZS vibration isolator is made up of a QZS system connected in parallel with a viscous damper of damping coefficient C as shown in Fig. 5. Both boundaries of the bridge are simply supported and isolation is achieved by including the QZS vibration isolators under each pier of the bridge located at the positions X_j. L represents the length of the bridge, T and X are the time and the axial coordinate of the bridge, respectively.

The transverse motion of a homogeneous, isotropic and uniform elastic beam bridge subjected to a time varying load is described by the well-known Euler–Bernoulli equation [9] given by

$$\rho S\frac{\partial^2 Y}{\partial T^2}+C_b\frac{\partial Y}{\partial T}+EI\frac{\partial^4 Y}{\partial X^4}=F\left(X,T\right), \tag{11}$$

where $Y\left(X,T\right)$ is the transverse deflection of the beam bridge, ρ and E are the density of the beam and Young's modulus of the beam, respectively; S and I are the area and second moment of area of beam's cross section, C_b is the external viscous damping coefficient of the beam and $F\left(X,T\right)$ represents all the external loads including the external forces due to the QZS vibration isolators under each pier of the beam bridge. The approximate expression of each of these forces is obtained from Eqs. (9) and (5) as follows

$$F_{QZS}=-C\frac{\partial Y}{\partial T}-\frac{\alpha_{QZS}}{a_0^3}k_v L_0 Y^3. \tag{12}$$

Given that the beam bridge is simply supported, the boundary conditions of the problem are given by [6,49]

$$Y\left(X,T\right)|_{X=0,X=L}=0 \quad \text{and} \quad \left.\frac{\partial^2 Y\left(X,T\right)}{\partial X^2}\right|_{X=0,X=L}=0. \tag{13}$$

To investigate the performance of the QZS vibration isolation on bridge vibration, let's consider a sinusoidal base vibrating excitation $Z=Z_0\cos\Omega T$, so the dynamical equations of the beam bridge can be derived as following, where $\delta\left(\cdot\right)$ is the Dirac function, N and X_j are the number and the positions of the QZS vibration isolators located under the piers of the beam bridge, respectively.

2.2.1 With QZS vibration isolators

The dynamical equation of a beam bridge with the N QZS vibration isolators can be obtained as

$$\rho S\frac{\partial^2 Y}{\partial T^2}+C_b\frac{\partial Y}{\partial T}+EI\frac{\partial^4 Y}{\partial X^4}+\sum_{j=1}^{N}\left(C\frac{\partial\left(Y-Z\right)}{\partial T}+\frac{\alpha_{QZS}}{a_0^3}k_vL_0\left(Y-Z\right)^3\right)\delta\left(X-X_j\right)=0. \quad (14)$$

2.2.2 Without QZS control

The dynamical equation of a beam bridge without QZS control can be obtained as

$$\rho S\frac{\partial^2 Y}{\partial T^2}+C_b\frac{\partial Y}{\partial T}+EI\frac{\partial^4 Y}{\partial X^4}=-\frac{\rho S}{N}\ddot{Z}\sum_{j=1}^{N}\delta\left(X-X_j\right), \quad (15)$$

where $\ddot{Z}=-\Omega^2 Z_0\cos\Omega T$. So, Eq. (15) can be rewritten as

$$\rho S\frac{\partial^2 Y}{\partial T^2}+C_b\frac{\partial Y}{\partial T}+EI\frac{\partial^4 Y}{\partial X^4}=\frac{\rho S\Omega^2 Z_0}{N}\sum_{j=1}^{N}\delta\left(X-X_j\right)\cos\Omega T. \quad (16)$$

2.2.3 With linear viscoelastic isolators

For a linear viscoelastic isolator, Eq. (12) giving the external force due to the nonlinear isolator can be rewritten as

$$F_{Linear}=-C\frac{\partial Y}{\partial T}-k_vY. \quad (17)$$

So, the dynamical equation of a beam bridge with the N linear viscoelastic isolators can be obtained as

$$\rho S\frac{\partial^2 Y}{\partial T^2}+C_b\frac{\partial Y}{\partial T}+EI\frac{\partial^4 Y}{\partial X^4}+\sum_{j=1}^{N}\left(C\frac{\partial\left(Y-Z\right)}{\partial T}+k_v\left(Y-Z\right)\right)\delta\left(X-X_j\right)=0. \quad (18)$$

3 Dynamical analysis

Let's introduce the following non-dimensional parameters

$$y=\frac{Y}{L_0},\quad z=\frac{Z}{L_0},\quad z_0=\frac{Z_0}{L_0},\quad x=\frac{X}{L},\quad x_j=\frac{X_j}{L}, \quad (19)$$

$$a=\frac{a_0}{L_0},\quad \alpha_{QZS}=\frac{a}{2\left(1-a\right)},\quad \gamma_{QZS}=\frac{\alpha_{QZS}}{a^3}=\frac{1}{2a^2\left(1-a\right)}, \quad (20)$$

$$t=T\omega_0,\quad \omega_0=\frac{\pi^2}{L^2}\sqrt{\frac{EI}{\rho S}},\quad c_b=\frac{C_b}{\rho S\omega_0},\quad c=\frac{2C}{\rho SL\omega_0},\quad k=\frac{2k_v}{\rho SL\omega_0^2},\quad \omega=\frac{\Omega}{\omega_0}, \quad (21)$$

so that the motion equations Eqs. (14), (16) and (18) can be rewritten in their non-dimensional form given by Eqs. (22), (23) and (24), respectively.

$$\frac{\partial^2 y}{\partial t^2}+c_b\frac{\partial y}{\partial t}+\frac{1}{\pi^4}\frac{\partial^4 y}{\partial x^4}+\frac{L}{2}\sum_{j=1}^{N}\left[c\left(\frac{\partial y}{\partial t}-\frac{\mathrm{d}z}{\mathrm{d}t}\right)+\gamma_{QZS}k\left(y-z\right)^3\right]\delta\left(x-x_j\right)=0, \quad (22)$$

$$\frac{\partial^2 y}{\partial t^2}+c_b\frac{\partial y}{\partial t}+\frac{1}{\pi^4}\frac{\partial^4 y}{\partial x^4}=\frac{z_0\omega^2}{N}\sum_{j=1}^{N}\delta\left(x-x_j\right)\cos\omega t, \quad (23)$$

$$\frac{\partial^2 y}{\partial t^2}+c_b\frac{\partial y}{\partial t}+\frac{1}{\pi^4}\frac{\partial^4 y}{\partial x^4}+\frac{L}{2}\sum_{j=1}^{N}\left[c\left(\frac{\partial y}{\partial t}-\frac{\mathrm{d}z}{\mathrm{d}t}\right)+k\left(y-z\right)\right]\delta\left(x-x_j\right)=0, \quad (24)$$

with boundary conditions

$$y\left(x,t\right)|_{x=0,x=1}=0\quad\text{and}\quad\left.\frac{\partial^2 y\left(x,t\right)}{\partial x^2}\right|_{x=0,x=1}=0. \quad (25)$$

3.1 Resonance responses

In order to obtain the modal equations, the Galerkin method is applied. This method of separation of variables suggests the solutions of the equations of motion [Eqs. (22), (23) and (24)] into the following form

$$y\left(x,t\right)=\sum_{n=1}^{N_{\max}}\phi_n\left(x\right)q_n\left(t\right), \quad (26)$$

where $N_{\max}$ is an integer greater than 1, $q_n\left(t\right)$ is the amplitude of the nth mode of vibration and $\phi_n\left(x\right)$ are the mode shapes, given in accordance with the boundaries conditions of the problem by

$$\phi_n\left(x\right)=\sin\left(n\pi x\right). \quad (27)$$

By applying the Galerkin method, the modal ordinary differential equations (28), (29) and (30) can be derived for the motion partial differential equations (22), (23) and (24), respectively as

$$\ddot{q}_m + c_b\dot{q}_m + \omega_m^2 q_m + c\sum_{j=1}^{N}\sin\left(m\pi x_j\right) \times\left[\sum_{n=1}^{N_{\max}}\dot{q}_n\sin\left(n\pi x_j\right) + z_0\omega\sin\omega t\right] + \gamma_{QZS}k\sum_{j=1}^{N}\sin\left(m\pi x_j\right) \times\left[\sum_{n=1}^{N_{\max}} q_n\sin\left(n\pi x_j\right) - z_0\cos\omega t\right]^3 = 0, \quad (28)$$

$$\ddot{q}_m + c_b\dot{q}_m + \omega_m^2 q_m = \frac{2z_0\omega^2}{NL}\sum_{j=1}^{N}\sin\left(m\pi x_j\right)\cos\omega t, \quad (29)$$

$$\ddot{q}_m + c_b\dot{q}_m + \omega_m^2 q_m + c\sum_{j=1}^{N}\sin\left(m\pi x_j\right) \times\left[\sum_{n=1}^{N_{\max}}\dot{q}_n\sin\left(n\pi x_j\right) + z_0\omega\sin\omega t\right] + k\sum_{j=1}^{N}\sin\left(m\pi x_j\right) \times\left[\sum_{n=1}^{N_{\max}} q_n\sin\left(n\pi x_j\right) - z_0\cos\omega t\right] = 0, \quad (30)$$

where $\omega_m = m^2$ is the non-dimensional natural frequency of the mth mode of the beam bridge, with $m = 1, 2, \ldots, N_{\max}$.

3.2 Absolute motion transmissibility

A more valuable parameter for the assessment of the isolation properties of the QZS vibration isolators is the absolute motion transmissibility which is defined as the ratio between the displacement of the beam bridge at a given point and that of the pier base. So, when the steady-state response occurs for the mth mode, the absolute motion transmissibility of the QZS vibration isolators can be defined as follow

$$T_{am} = \frac{|y_m|_{\max}}{|z|_{\max}} = \frac{|q_m|_{\max}\sin\left(m\pi x\right)}{z_0} = \frac{A_{\mathrm{m}}\sin\left(m\pi x\right)}{z_0}, \quad (31)$$

where A_{m} is the response amplitude of the mth shape mode of the beam bridge, z_0 is the magnitude of the base excitation and $\sin\left(m\pi x\right)$ is the shape function of the mth mode of vibration. This expression of absolute motion transmissibility [Eq. (31)] have the same forms as the linear viscoelastic isolators. The next section aims to show the benefits of employing a QZS isolation mount. This is done by comparing the absolute motion transmissibility of the QZS vibration isolators with that of the equivalent linear viscoelastic supports.

4 Dynamical explanation

In this paper, the number of vibration modes is set as $N_{\max} = 4$. Eqs. (28), (29) and (30) are numerically solved by using the fourth-order Runge–Kutta method in other to generate the transverse response of the beam bridge in the presence of QZS vibration isolators, without a QZS control and in the presence of linear vicoelastic isolators, respectively. The initial values for the first calculations are set as $q_1 = 0.01$ (i.e. $Y_1 = 0.01L_0$), $\dot{q}_1 = 0$, $q_n = 0$, $\dot{q}_n = 0$ for $n = 2, 3, 4$ and the non-dimensional magnitude of the base excitation is $z_0 = 0.05$ (i.e. $Z_0 = 0.05L_0$). Table 1 presents the physical and geometrical parameter values of the QZS vibration isolators used under a seven-span beam bridge with wood material [9,46,49]. In the following study, the parameter values are assigned as listed in Table 1 if there is no special mention.

The non-dimensional parameters are obtained by calculation on the basis of Eqs. (20) and (21) as $a = 0.67$, $\gamma_{QZS} = 3.375$, $\omega_0 = 79.69$ rad/s, $c_b = 0.290$, $c = 0.019$, $k = 2.43$.

So, the first four natural frequencies of the corresponding beam bridge are determined as $\Omega_1 = 79.69$ rad/s ($f_1 = 12.68$ Hz), $\Omega_2 = 318.74$ rad/s ($f_2 = 50.73$ Hz), $\Omega_3 = 717.16$ rad/s ($f_3 = 114.14$ Hz) and Ω_4=1274.95 rad/s (f_4=202.92 Hz). Moreover, the corresponding mode functions of the transverse vibration can be obtained. The fourth-order Runge–Kutta algorithm is used to compute the numerical solutions of Eqs. (28), (29) and (30) for the above non-dimensional parameters.

Table 1 Physical and geometric parameters of the wooden beam bridge and the QZS vibration isolators

Item	Notation	Value
Young's modulus of the beam	E	5.5 GPa
Density of the beam	ρ	800 Kg/m^3
Length of the beam	L	1.5 m
Width of the beam	b	0.045 m
Height of the beam	h_b	0.012 m
External damping of the beam	C_b	10 N.s/m^2
Viscosity damping of the spring	C	0.5 N.s/m
Initial length of the horizontal spring	L_0	0.1 m
Horizontal length of the horizontal spring	a_0	0.067 m
Horizontal spring linear stiffness	k_0	5000 N/m
Vertical spring stiffness	k_v	5000 N/m
Number of piers	N	6
Positions of the piers	X_j	$X_j = 0.133 + 0.247 \times (j-1)$ m

4.1 Resonant vibration without and with control

In this subsection, amplitude and motion transmissibility curves are plotted versus the excitation frequencies ω of the sinusoidal base excitation. The steady-state amplitude A_m and the absolute motion transmissibility T_{am} are plotted in Figs. 6, 7, 8 and 9 for the first four modal primary resonances ($m = 1, 2, 3$ and 4) of the beam bridge in the following cases, firstly in the presence of QZS vibration isolators, then without a QZS control and finally in the presence of linear viscoelastic isolators.

It can be argued that there are two indices that allow measuring the effectiveness of a vibration isolator: the first one is the bandwidth of the isolation region, which is the frequency region within which the transmitted motion amplitude becomes smaller than the base excitation amplitude, that is when $T_{am} < 1$ [i.e. $20\log(T_{am}) < 0$ dB]; the other is the peak-transmissibility, which is the maximum amplitude of the transmitted motion for a given amplitude of the base excitation. Figures 6, 7, 8 and 9 show that for all the first four modes of vibration,

(a) linear and QZS vibration control methods are both effective for high frequencies after resonance but only QZS vibration isolators are able of attenuating low frequency vibrations;
(b) linear viscoelastic isolators change the natural frequencies of the beam bridge while QZS vibration isolators keep them constant;
(c) in the presence of the control, the vibration amplitudes of the first-order mode are very large compared to those of the other three modes, confirming that most of the energy of the beam bridge is concentrated in the first mode [6,49].

In order to confirm the effectiveness of the two control methods, the dynamic responses of the vibration first four modes of the beam bridge when the exciter vibrates at their resonance frequencies have been plotted in Fig. 10.

This figure clearly shows that the QZS control method is more efficient than the linear viscoelastic control method for the first four modes of vibration.

4.2 Evaluation of the vibration isolation performance of the QZS control

The vibration isolators are sometimes used to isolate the displacement excitation transmitted from the base to the working equipment. In this subsection, the effects of some parameters on the absolute transmissibility of steady-state behaviors are investigated, including geometrical arrangement ratio γ_{QZS}, vertical spring stiffness k of the QZS vibrations isolators and for the corresponding linear viscoelastic isolators, damping coefficient c and excitation magnitude z_0. The absolute motion transmissibility curves of the system for these different parameters are plotted in Figs. 14, 15 and 16 for the beam bridge, (a) under QZS control and (b)

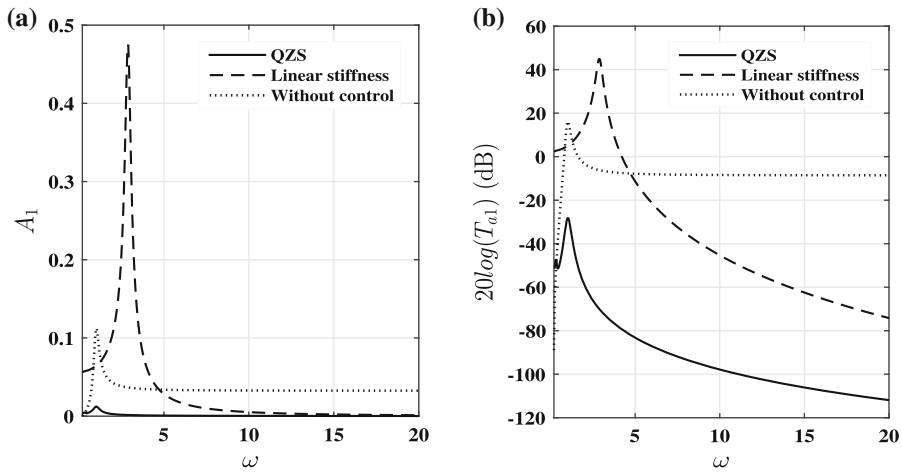

Fig. 6 The steady-state amplitude (**a**) and the absolute motion transmissibility (**b**) for first-order primary resonance of the beam bridge without and with control (QZS and linear viscoelastic controls)

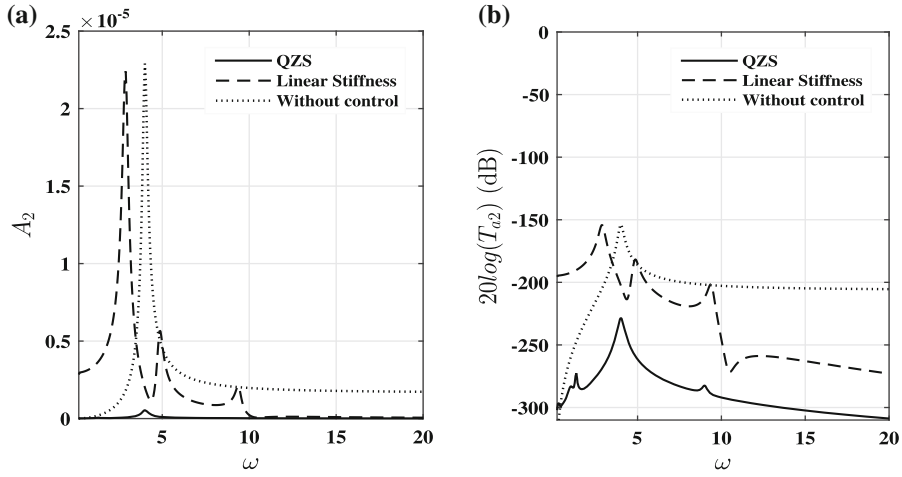

Fig. 7 The steady-state amplitude (**a**) and the absolute motion transmissibility (**b**) for second-order primary resonance of the beam bridge without and with control (QZS and linear viscoelastic controls)

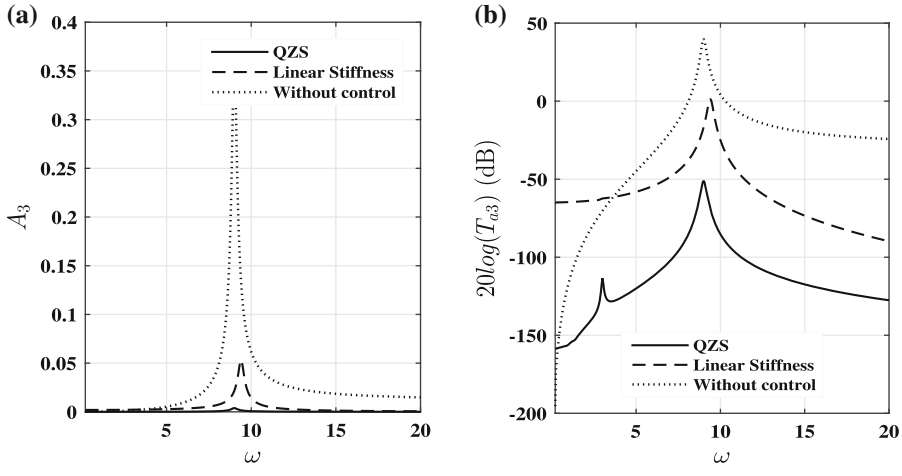

Fig. 8 The steady-state amplitude (**a**) and the absolute motion transmissibility (**b**) for third-order primary resonance of the beam bridge without and with control (QZS and linear viscoelastic controls)

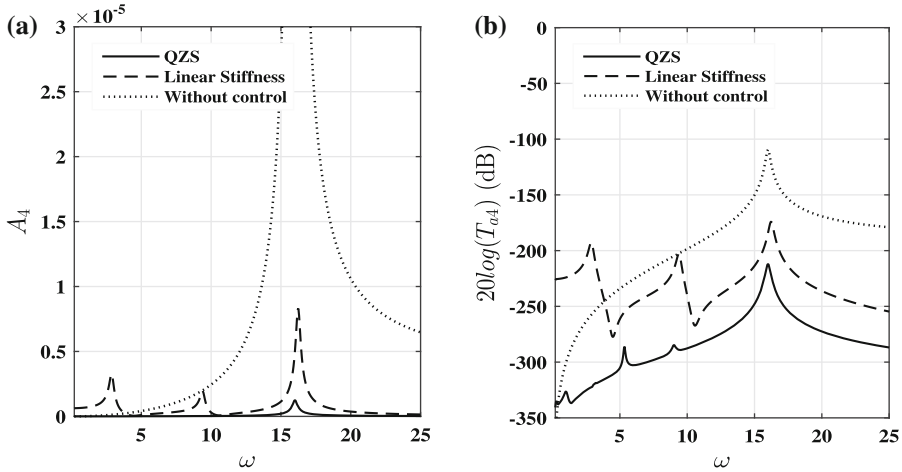

Fig. 9 The steady-state amplitude (**a**) and the absolute motion transmissibility (**b**) for fourth-order primary resonance of the beam bridge without and with control (QZS and linear viscoelastic controls)

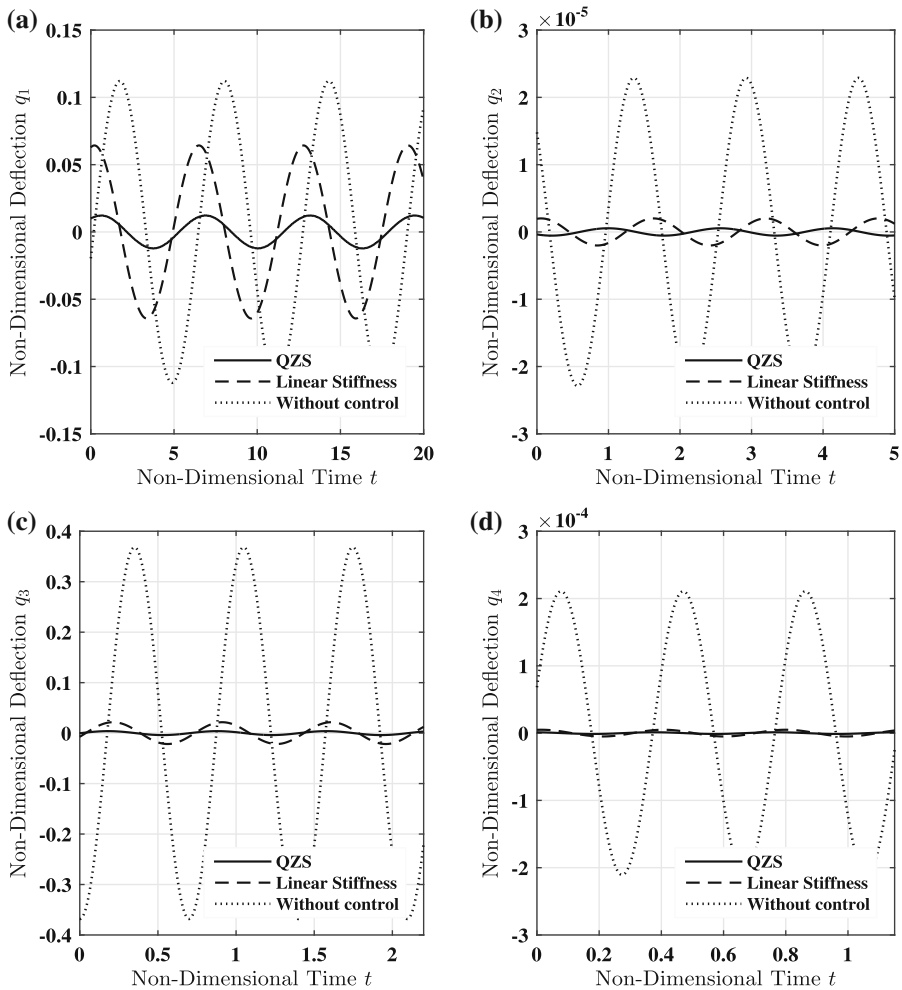

Fig. 10 Times histories of the first four primary resonances of the beam bridge: **a** first-order with $\omega = \omega_1 = 1$, **b** second-order with $\omega = \omega_2 = 4$, **c** third-order with $\omega = \omega_3 = 9$ and **d** fourth-order with $\omega = \omega_4 = 16$

under linear viscoelastic control. Then, the benefit of QZS isolators is verified when some conditions are satisfied, by comparing the absolute motion transmissibility of the QZS vibration isolators with that of the corresponding linear viscoelastic isolators without the horizontal auxiliary springs. The analysis is limited to the first mode of vibration of the midspan of the beam bridge where $\sin(m\pi x) = 1$, insofar as the first mode is expected to carry most of the energy, and therefore one hopes that it could suffice to obtain a first estimate of the system behavior.

4.2.1 *Effect of the nonlinear term of the QZS vibration isolator*

The geometric ratio α_{QZS} is given by Eq. (8) as

$$\alpha_{QZS} = \frac{a}{2(1-a)}. \tag{32}$$

So, for a given value of a, there is only one value of the stiffness ratio α that ensures QZS behavior. Equivalently, the value a_{QZS} that gives quasi-zero stiffness for a given value of the stiffness ratio α is

$$a_{QZS} = \frac{2\alpha}{2\alpha+1}. \tag{33}$$

The subscript QZS on either α or a is used to denote that the other parameter is not independent, but has been chosen in accordance with Eqs. (32) and (33) so as to achieve stable QZS. The combinations of stiffness ratio α and geometric ratio a that give rise to stable QZS are shown in graphical form in Fig. 11. This Fig. 11 shows that for small initial angles ($a \approx 1$, i.e. $\theta_0 \approx 0°$) and according to the expression of the parameter α given in Eq. (5), the order of magnitude of the stiffness of the inclined springs needs to be larger than this of the vertical spring. Furthermore, for moderate initial angle of inclination ($0.4 < a < 0.8$, i.e. $\theta_0 \approx 36°-66°$), then vertical and inclined springs of similar stiffnesses can be used. The combinations of nonlinear geometric parameter γ_{QZS} and geometric ratio a that give rise to stable QZS have been plotted in Fig. 12. This figure shows that for great initial angle of inclination ($a < 0.2$, i.e. $\theta_0 \approx 78°-90°$), the nonlinear geometric parameter γ_{QZS} presents very large values which means that the isolation system involves a strong nonlinearity. The smallest values of control parameter γ_{QZS} ($\gamma_{QZS} = 3.375$) is obtained for $a = 0.67$, corresponding to the initial angle of inclination $\theta_0 = 48°$. Then, the steady-state amplitude and the absolute motion transmissibility for the first mode of the beam bridge for different values of the nonlinear geometric parameter γ_{QZS} are studied and plotted in Fig. 13. This figure shows that the vibration amplitude and the absolute motion transmissibility increase gradually with the nonlinear term of the system, and the bend of the curve is more and more obvious. Furthermore, for strong nonlinearities ($\gamma_{QZS} = 26.1$ and $\gamma_{QZS} = 55.6$), the resonance frequency is shifted to the high-frequency region and a jump phenomenon occurs. Therefore, geometric nonlinearity is not beneficial for the vibration isolation.

4.2.2 *Effect of the vertical spring stiffness*

The absolute motion transmissibility of the first mode of vibration of the beam bridge for different values of the vertical spring stiffness (a) under QZS control and (b) under linear viscoelastic control are plotted in Fig. 14 in order to study the effect of the vertical spring stiffness on the performance of the two types vibration isolators. Figure 14a shows that the vertical spring stiffness presents similar effects on the dynamics of the beam bridge as those observed with the nonlinear term of the QZS vibration isolators. It can be seen that smaller stiffness yields smaller motion transmissibility, i.e. better isolation performance of the QZS vibration isolators. On the other hand, Fig. 14b shows that the motion transmissibility depends strongly on the value of the vertical spring stiffness k of the linear viscoelastic isolators with which it increases, as well as the isolation frequency band. In addition, the frequency of resonance is also shifted to the high frequency region while k increases. Therefore, vertical spring stiffness is not beneficial for the vibration isolation both for QZS vibration isolator and its equivalent linear viscoelastic isolator. But it can be seen that, QZS vibration isolator could have a remarkable benefit in isolation performance compared to linear viscoelastic isolator.

4.2.3 *Effect of the viscosity damping of the QZS vibration isolator*

Figure 15 shows the absolute displacement transmissibility of the QZS vibration isolators and linear viscoelastic isolators for various values of the damping coefficient c. The performance of the linear viscoelastic isolation with respect to its damping is firstly studied. Figure 15b shows that increasing the viscous damping

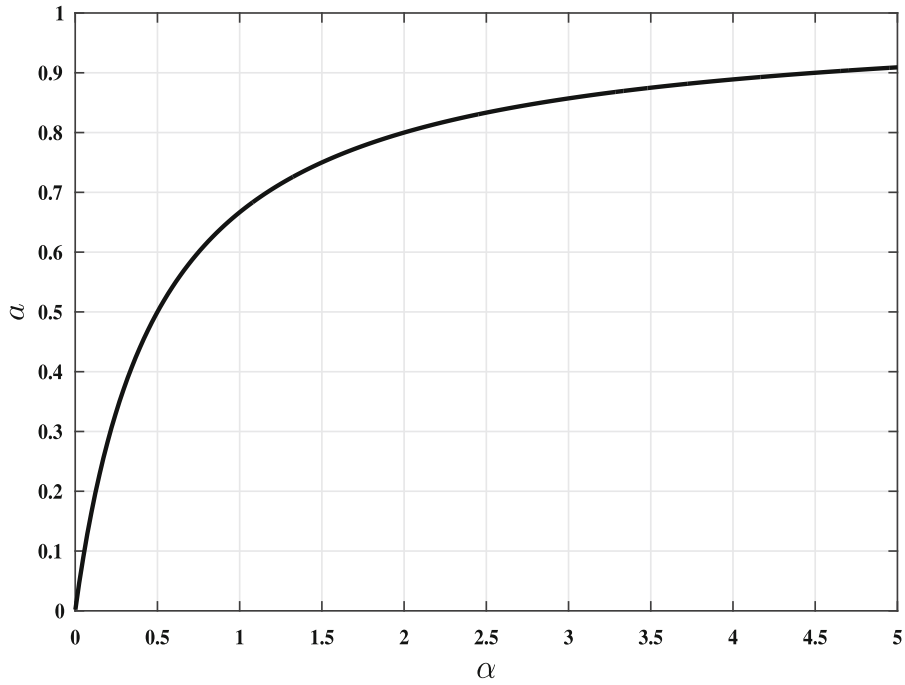

Fig. 11 Combinations of geometric ratio a and stiffness ratio α that yield QZS

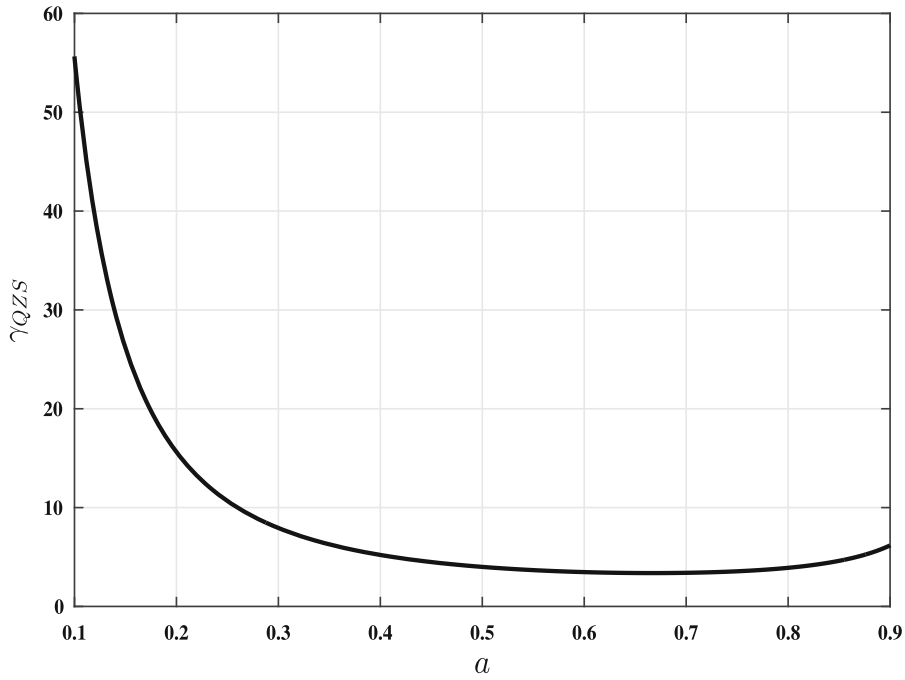

Fig. 12 Combinations of geometric ratio a and nonlinear geometric parameter γ_{QZS} that yield QZS

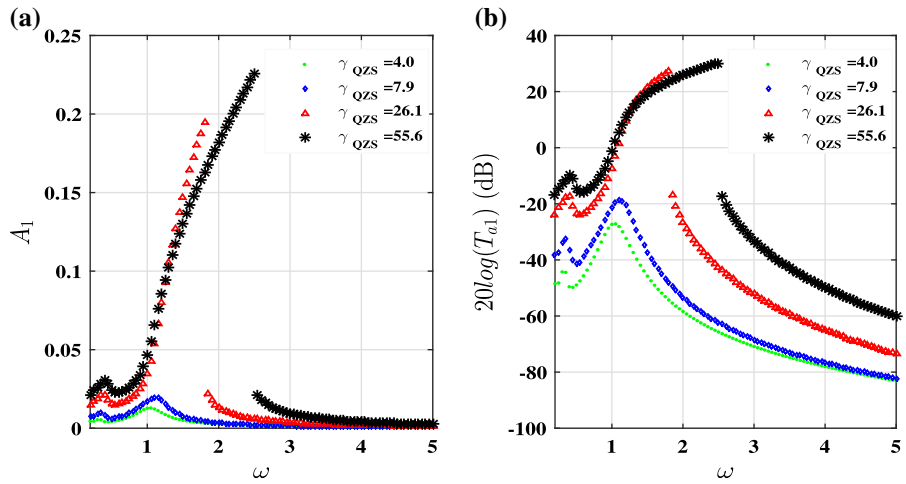

Fig. 13 Effect of the nonlinear geometric parameter γ_{QZS} on **a** the steady-state amplitude and **b** the absolute transmissibility of the beam bridge for $\gamma_{QZS} = 4.0$ ($a = 0.50$), $\gamma_{QZS} = 7.9$ ($a = 0.30$), $\gamma_{QZS} = 26.1$ ($a = 0.15$) and $\gamma_{QZS} = 55.6$ ($a = 0.10$)

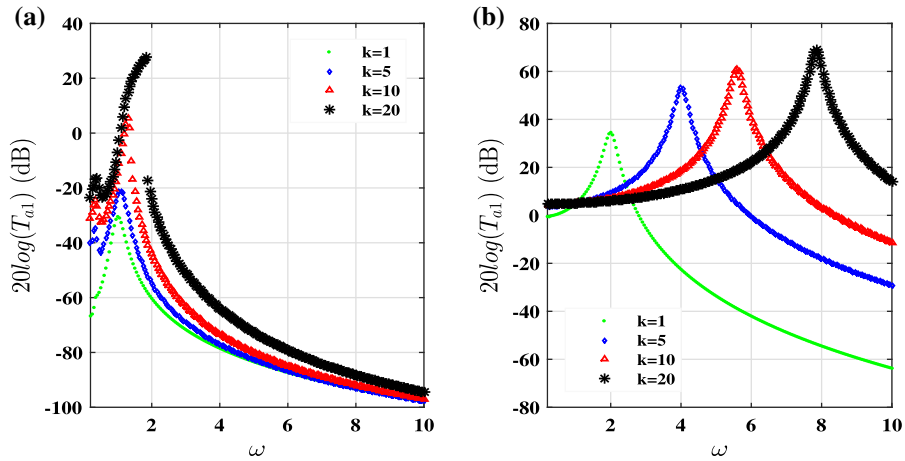

Fig. 14 Effect of the vertical spring stiffness on the absolute transmissibility of the beam bridge **a** under QZS control and **b** under linear viscoelastic control for $k = 1$, $k = 5$, $k = 10$ and $k = 20$

decreases the absolute transmissibility in the resonant frequency range but deteriorates the vibration attenuation rate for high frequencies. Turn to the QZS vibration isolation, the effect of viscous damping on the performance of the nonlinear isolator is given in Fig. 15a. By observing this figure, one can conclude that the increase of viscous damping results in the increase of the absolute transmissibility with sacrificing the performance of the nonlinear isolators. This result is too original in this case of base vibration control of a beam bridge with QZS vibration isolators. Since in most of the cases where QZS vibration isolator is applied for discrete structures, the absolute transmissibility undergoes a reduction as the damping increases [48,50,51], similarly to the case of damping effect on linear viscoelastic isolator. From the above analysis, it can be concluded that, QZS vibration isolator could have a remarkable benefit in isolation performance for relatively low damping or without damping.

4.2.4 Effect of magnitude of the base excitation

The effect of the base excitation amplitude on the performance of the QZS vibration isolators and the linear viscoelastic isolators is shown in Fig. 16. The absolute motion transmissibility of the linear viscoelastic isolators is unrelated to the excitation amplitude as shown in Fig. 16b. As shown in Fig. 16a, for the QZS vibration isolators, the absolute motion transmissibility increases with the excitation amplitude. Furthermore, for large amplitudes, the steady-states frequency response curve is characterised by a jump phenomenon and the curve presentes unstable solution. In addition, the shift of the resonance peak to the high frequencies can be also observed when the excitation amplitude increase. This

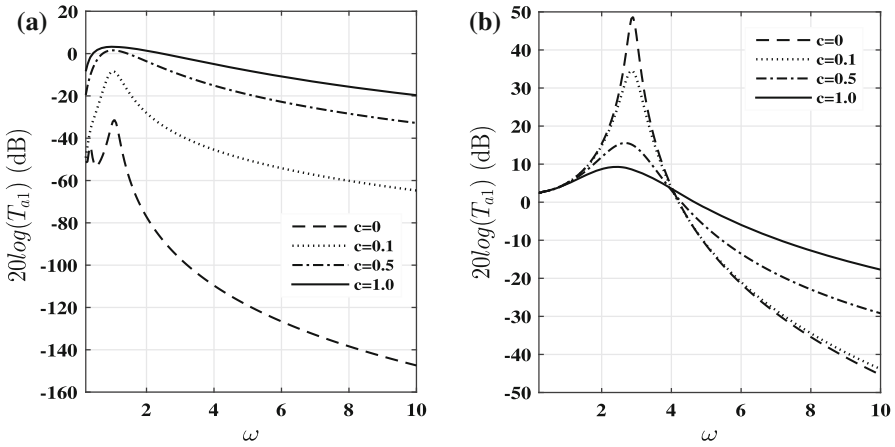

Fig. 15 Effect of viscosity damping on the absolute transmissibility of the beam bridge **a** under QZS control and **b** under linear viscoelastic control for $c = 0$, $c = 0.1$, $c = 0.5$ and $c = 1.0$

means that the use of the QZS isolator is more suitable in the conditions where the vibration excitation is smaller.

5 Conclusion

In this paper, the effectiveness of a QZS vibration isolator on the transverse vibrations of a multi-span continuous beam bridge under pier base vibrating excitation is demonstrated. After being designed and modeled, the QZS vibration isolator is placed between the beam bridge structure and its piers to reduce its vibration due to the excitation of the base of the piers. A nonlinear integro-partial differential governing equation of the elastic beam bridge is derived by considering the geometrical nonlinearity. Based on the modal analysis of the controlled beam bridge, the Galerkin method is used to discretize the governing equation. The performance of the QZS vibration isolator and the equivalent linear viscoelastic isolator are evaluated by the steady-state response and absolute motion transmissibility of the beam bridge. The following conclusions are drawn. (a) The QZS vibration isolator and the linear viscoelastic isolator are both effective for high frequencies but only the QZS vibration isolator is able to reduce low frequency vibrations. (b) The linear viscoelastic isolator strongly change the natural frequencies of the beam bridge compared to the QZS vibration isolator. (c) The QZS vibration control is more efficient than the linear viscoelastic control. (d) A curious and original result observed in the presence of QZS vibration isolation shows that the increase of the viscous damping leads to an increase of the absolute motion transmissibility by sacrificing the performance of nonlinear isolation. (e) The QZS vibration isolator is more powerful that nonlinear geometric term, vertical spring stiffness, viscous damping and magnitude of base excitation are small. So, to build a QZS vibration isolator with better performance, the damper must be removed and its vertical spring must be designed to have the lowest possible stiffness leading to achieve a QZS behavior. In summary, this paper demonstrates the superiority of the QZS vibration isolation. The QZS vibration isolator with suitable parameters has the advantage of more effectively isolating unwanted vibrations transmitted from the foundation to the continuous payload, as it can achieve excellent low-frequency isolation performance including low initial isolation frequency and wide isolation frequency band. The application of the QZS type mechanism on the design and development of novel earthquake-resistant systems can improve seismic performance of building and bridge structures.

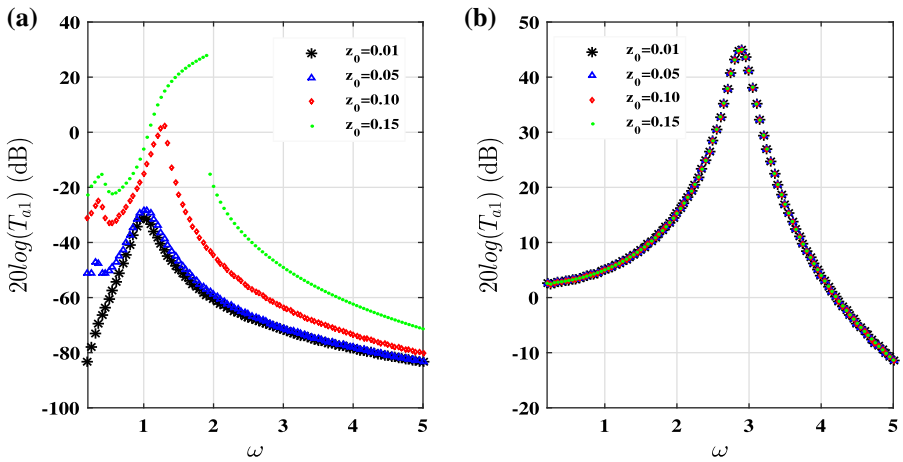

Fig. 16 Effect of magnitude of base excitation on the absolute transmissibility of the beam bridge **a** under QZS control and **b** under linear viscoelastic control for $z_0 = 0.01$, $z_0 = 0.05$, $z_0 = 0.10$ and $z_0 = 0.15$

Acknowledgements Part of this work was completed during a research visit of Prof. Nana Nbendjo at the University of Kassel in Germany. He is grateful to the Alexander von Humboldt Foundation for financial support.

Compliance with ethical standards

Conflict of interest The authors declare that they have no conflict of interest.

References

1. Paddan, G.S., Griffin, M.J.: Evaluation of whole-body vibration in vehicles. J. Sound Vib. **253**(1), 195–213 (2002)
2. Sun, X., Xu, J., Jing, X., Cheng, L.: Beneficial performance of a quasi-zero-stiffness vibration isolator with time-delayed active control. Int. J. Mech. Sci. **82**, 32–40 (2014)
3. Liu, C., Yue, X., Shi, K., Sun, Z.: Inertia-free attitude stabilization for flexible spacecraft with active vibration suppression. Int. J. Robust Nonlinear Control **29**(18), 6311–6336 (2019)
4. Yan, R., Wu, Z.: Attitude stabilization of flexible spacecraft via extended disturbance observer based controller. Acta Astronaut. **133**, 73–80 (2017)
5. Kunde, M.C., Jangid, R.S.: Seismic behavior of isolated bridges: a-state-of-the-art review. Electron. J. Struct. Eng. **3**(3) (2003)
6. Tabejieu, L.M.A., Nbendjo, B.R.N., Filatrella, G.: Effect of the fractional foundation on the response of beam structure submitted to moving and wind loads. Chaos Soliton Fract. **127**, 178–188 (2019)
7. Atmaca, B., Yurdakul, M., Ates, S.: Nonlinear dynamic analysis of base isolated cable-stayed bridge under earthquake excitations. Soil Dyn. Earthq. Eng. **66**, 314–318 (2014)
8. Ghaedi, K., Ibrahim, Z., Adeli, H., Javanmardi, A.: Invited review: recent developments in vibration control of building and bridge structures. J. VibroEng. **19**(5), 1392–8716 (2017)
9. Bouna, H.S., Nbendjo, B.R.N., Woafo, P.: On the dynamics of two multi-span continuous beam bridges model coupled by their close environment. Int. J. Dyn. Control **6**, 29–40 (2018)
10. Naeim, F., Kelly, J.: Design of Seismic Isolated Structures: from Theory to Practice. Wiley, New York (1999)
11. Bedon, C., Morassi, A.: Dynamic testing and parameter identification of a base-isolated bridge. Eng. Struct. **60**(2), 85–99 (2014)
12. Rivin, E.I.: Passive Vibration Isolation. ASME Press, New York (2001)
13. Wang, Y., Li, S., Jiang, X., Cheng, C.: Resonance and performance analysis of a harmonically forced quasi-zero-stiffness vibration isolator considering the effect of mistuned mass. J. Vib. Eng. Technol. **5**(1) (2017)
14. Harris, C.M., Piersol, A.G.: Shock and Vibrations Handbook. McGraw-Hill, New York (2002)
15. Kong, X., Li, H., Wu, C.: Dynamics of 1-dof and 2-dof energy sink with geometrically nonlinear damping: application to vibration suppression. Nonlinear Dyn. **91**(3) (2017)
16. Zhang, Y.W., Yuan, B., Fang, B., et al.: Reducing thermal shock-induced vibration of an axially moving beam via a nonlinear energy sink. Nonlinear Dyn. **87**(2), 1159–1167 (2017)
17. Huang, X., Liu, X., Hua, H.: On the characteristics of an ultra-low frequency nonlinear isolator using sliding beam as negative stiffness. J. Mech. Sci. Technol. **28**(3), 813–822 (2014)
18. Carrella, A.: Passive Vibration Isolators with High-Static-Low-Dynamic-Stiffness. Ph.D. thesis, University of Southampton, Institute of Sound and Vibration Research (2008)
19. Robertson, W.S., Kidner, M.R.F., Cazzolato, B.S., Zander, A.C.: Theoretical design parameters for a quasi-zero stiffness magnetic spring for vibration isolation. J. Sound Vib. **326**, 88–103 (2009)
20. Hao, Z.F., Cao, Q.J., Wiercigroch, M.: Nonlinear dynamics of the quasi-zero-stiffness SD oscillator based upon the local and global bifurcation analyses. Nonlinear Dyn. **87**, 987–1014 (2017)
21. Cheng, C., Li, S.M., Wang, Y., Jiang, X.X.: Resonance of a quasi-zero stiffness vibration system under base excitation

with load mismatch. Int. J. Struct. Stab. Dyn. **18**, 1850002 (2018)
22. Le, T.D., Bui, M.T.N., Ahn, K.K.: Improvement of vibration isolation performance of isolation system using negative stiffness structure. IEEE-ASME Trans. Mech. **21**, 1561–1571 (2016)
23. Dai, H.H., Jing, X.J., Wang, Y., Yue, X.K., Yuan, J.P.: Post-capture vibration suppression of spacecraft via a bio-inspired isolation system. Mech. Syst. Signal Process. **105**, 214–240 (2018)
24. Alabuzhev, P., Gritchin, A., Kim, L., Migirenko, G., Chon, V., Stepanov, P.: Vibration Protecting and Measuring System with Quasi-zero Stiffness. Hemisphere Publishing, New York (1989)
25. Ibrahim, R.A.: Recent advances in nonlinear passive vibration isolators. J. Sound Vib. **314**(3–5), 371–452 (2008)
26. Arafat, R.M.D., Park, S.T., Sajal, C.B.: Design of a vehicle suspension system with negative stiffness system. IST Trans. Mech. Syst. Theor. Appl. **1**(2), 1–7 (2010)
27. Le, T.D., Ahn, K.K.: A vibration isolation system in low frequency excitation region using negative stiffness structure for vehicle seat. J. Sound Vib. **330**(26), 6311–6335 (2011)
28. Le, T.D., Ahn, K.K.: Experimental investigation of a vibration isolation system using negative stiffness structure. Int. J. Mech. Sci. **70**, 99–112 (2013)
29. Liu, X.T., Huang, X.C., Hua, H.X.: On the characteristics of a quasi-zero stiffness isolator using Euler buckled beam as negative stiffness corrector. J. Sound Vib. **332**(14), 3359–3376 (2013)
30. Huang, X.C., Liu, X.T., Sun, J.Y., Zhang, Z.Y., Hua, H.X.: Vibration isolation characteristics of a nonlinear isolator using Euler buckled beam as negative stiffness corrector: a theoretical and experimental study. J. Sound Vib. **333**, 1132–1148 (2014)
31. Fulcher, B.A., Shahan, D.W., Haberman, M.R., Seepersad, C.C., Wilson, P.S.: Analytical and experimental investigation of buckled beams as negative stiffness elements for passive vibration and shock isolation systems. J. Vib. Acoust. **136**, 031009 (2014)
32. Platus, D.L.: Negative stiffness-mechanism vibration isolation systems. Vib. Control Microelectron. Opt. Metrol. **1619**, 44–54 (1992)
33. Carrella, A., Brennan, M.J., Waters, T.P.: Static analysis of a passive vibration isolator with quasi-zero-stiffness characteristic. J. Sound Vib. **301**(3–5), 678–689 (2007)
34. Carrella, A., Brennan, M.J., Waters, T.P., Lopes Jr., V.: Force and displacement transmissibility of a nonlinear isolator with high-static-low-dynamic-stiffness. Int. J. Mech. Sci. **55**(1), 22–29 (2012)
35. Meng, L., Sun, J., Wu, W.: Theoretical design and characteristics analysis of a quasi-zero stiffness isolator using a disk spring as negative stiffness element. Shock Vib. **813763** (2015)
36. Li, Y.L., Xu, D.L.: Vibration attenuation of high dimensional quasi-zero stiffness floating raft system. Int. J. Mech. Sci. **126**, 186–195 (2017)
37. Wang, X.L., Zhou, J.X., Xu, D.L., Ouyang, H.J., Duan, Y.: Force transmissibility of a two-stage vibration isolation system with quasi-zero stiffness. Nonlinear Dyn. **87**, 633–646 (2017)
38. Wang, Y., Li, S.M., Neild, S., Jiang, J.S.Z.: Comparison of the dynamic performance of nonlinear one and two degree-of-freedom vibration isolators with quasi-zero stiffness. Nonlinear Dyn. **88**, 635–654 (2017)
39. Fan, Z.J., Lee, J.H., Kang, K.H., Kim, K.J.: The forced vibration of a beam with viscoelastic boundary supports. J. Sound Vib. **210**(5), 673–682 (1998)
40. Lv, B.L., Li, W.Y., Ouyang, H.J.: Moving force-induced vibration of a rotating beam with elastic boundary conditions. Int. J. Struct. Stab. Dyn. **15**(1), 1450035 (2015)
41. Zhang, T., Ouyang, H., Zhang, Y.O., Lv, B.L.: Nonlinear dynamics of straight fluid-conveying pipes with general boundary conditions and additional springs and masses. Appl. Math. Model. **40**(17–18), 7880–7900 (2016)
42. Wang, Y.R., Fang, Z.W.: Vibrations in an elastic beam with nonlinear supports at both ends. J. Appl. Mech. Tech. Phys. **56**(2), 337–346 (2015)
43. Mao, X.Y., Ding, H., Chen, L.Q.: Vibration of flexible structures under nonlinear boundary conditions. J. Appl. Mech. **84**(11), 111006 (2017)
44. Ding, H., Wang, S., Zhang, Y.-W.: Free and forced nonlinear vibration of a transporting belt with pulley support ends. Nonlinear Dyn. **92**(4), 2037–2048 (2018)
45. Ding, H., Lim, C.W., Chen, L.Q.: Nonlinear vibration of a traveling belt with non-homogeneous boundaries. J. Sound Vib. **424**(4), 78–93 (2018)
46. Ding, H., Lu, Z.-Q., Chen, L.-Q.: Nonlinear isolation of transverse vibration of pre-pressure beams. J. Sound Vib. **442**, 738–751 (2018)
47. Ding, H., Chen, L.-Q.: Nonlinear vibration of a slightly curved beam with quasi-zero-stiffness isolators. Nonlinear Dyn. **95**, 2367–2382 (2019)
48. Xu, D., Zhang, Y., Zhou, J., Lou, J.: On the analytical and experimental assessment of the performance of a quasi-zero-stiffness isolator. J. Vib. Control **20**(15), 2314–2325 (2014)
49. Bouna, H.S., Nbendjo, B.R.N.: Vibration control of a plate subjected to impulsive force by plate-type dynamic vibration absorbers. World J. Mech. **2**, 143–151 (2012)
50. Chai, K., Yang, Q.-C., Lou, J.-J.: Dynamic characteristic analysis of two-stage quasi-zero stiffness vibration isolation system. Vibroeng. Procedia **10** (2016)
51. Meng, Q., Yang, X., Li, W., Lu, E., Sheng, L.: Research and analysis of quasi-zero-stiffness isolator with geometric nonlinear damping. Shock Vib. **6719054** (2017)